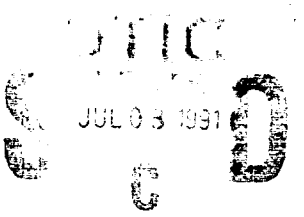

(2)

UNSTEADY TURBULENT FLOWS IN CHANNELS WITH PARALLEL OR DIVERGING WALLS

Final Technical Report

G. BINDER, S.TARDU, R.F. BLACKWELDER,
M.Q. FENG, R.D. MAESTRI

APRIL 1991

United States Army

EUROPEAN RESEARCH OFFICE OF THE U.S. ARMY

London England

Contract Number DAJA 45-87-C-0015

INSTITUT DE MECANIQUE DE GRENOBLE

ASSOCIATION POUR LE DEVELOPPEMENT DE LA RECHERCHE

UNSTEADY TURBULENT FLOWS IN CHANNELS WITH PARALLEL OR DIVERGING WALLS

Final Technical Report

G. BINDER, S.TARDU, R.F. BLACKWELDER,
M.Q. FENG, R.D. MAESTRI

APRIL 1991

United States Army

EUROPEAN RESEARCH OFFICE OF THE U.S. ARMY

London England

Contract Number DAJA 45-87-C-0015

INSTITUT DE MECANIQUE DE GRENOBLE

ASSOCIATION POUR LE DEVELOPPEMENT DE LA RECHERCHE

SECURITY CLASSIFICATION OF THIS PAGE (When Data Entered)

REPORT DOCUMENTATION PAGE		READ INSTRUCTIONS BEFORE COMPLETING FORM
1. REPORT NUMBER SEVEN	2. GOVT ACCESSION NO.	3. RECIPIENT'S CATALOG NUMBER
4. TITLE (and Subtitle) UNSTEADY TURBULENT FLOWS IN CHANNELS WITH PARALLEL OR DIVERGING WALLS		5. TYPE OF REPORT & PERIOD COVERED Final Technical Report 6. PERFORMING ORG. REPORT NUMBER 26 June 1987-26 Aug.1991
7. AUTHOR(s) G. BINDER, S. TARDU, R. F. BLACKWELDER, M. Q. FENG, R. D. MAESTRI		8. CONTRACT OR GRANT NUMBER(s) DAJA 45-87-C-0015
9. PERFORMING ORGANIZATION NAME AND ADDRESS Association pour le Développement de la Recherche Institut de Mécanique de Grenoble 155 cours Berriat, 38000 Grenoble, FRANCE		10. PROGRAM ELEMENT, PROJECT, TASK AREA & WORK UNIT NUMBERS R&D 49 22 - AN -01
11. CONTROLLING OFFICE NAME AND ADDRESS U.S. Army Research, Development & Stand. Group, UK 233 Old Marylebone Road, London NW 1 STH, ENGLAND		12. REPORT DATE April 1991 13. NUMBER OF PAGES 263
14. MONITORING AGENCY NAME & ADDRESS(if different from Controlling Office)		15. SECURITY CLASS. (of this report) 15a. DECLASSIFICATION/DOWNGRADING SCHEDULE
16. DISTRIBUTION STATEMENT (of this Report) APPROVED FOR PUBLIC RELEASE; DISTRIBUTION UNLIMITED		
17. DISTRIBUTION STATEMENT (of the abstract entered in Block 20, if different from Report)		
18. SUPPLEMENTARY NOTES		
19. KEY WORDS (Continue on reverse side if necessary and identify by block number) Unsteady flow; Turbulence; Boundary Layers; Adverse Pressure Gradient; Water ; L.D.A.; Hot film Anemometer; Streak Visualisations.		

20. ABSTRACT (Continue on reverse side if necessary and identify by block number)

Turbulent flows subjected to imposed velocity oscillations have been studied experimentally in a water channel. A wide range of forcing conditions have been covered (amplitudes: 10% do 70%, frequencies: $\omega+ = 0{,}0005$ to 0.25). Velocities u have been measured with LDA and hot-film anemometer. The wall shear-stress τ has been measured with flush mounted hot-films gages calibrated in situ with the LDA. Near wall dye-streak visualisations have also been performed. The phase average of any quantity q (e.g. $q=u$, $q=u'u'$, $q=\tau$, $q=\tau'\tau'$, etc..) is decomposed into a time-mean $\overline{q}$ and a modulation $\tilde{q}$: $\langle q \rangle = \overline{q} + \tilde{q}$.

DD FORM 1 JAN 73 1473 EDITION OF 1 NOV 68 IS OBSOLETE UNCLASSIFIED

SECURITY CLASSIFICATION OF THIS PAGE (When Data Entered)

Block 20. ABSTRACT Continued

It has been confirmed that the time-mean statistical characteristics of the channel flow (between parallel walls unless otherwise specified) are essentially not affected by the imposed oscillations even when these have amplitudes of 64%.

It has been shown that the appropriate similarity parameter of the oscillating quantities u and τ is the non-dimensional Stokes length l_s^+ (or the frequency $\omega^+=2/l_s^{+2}$). In the regime of high frequency forcing ($l_s^+<10$) the oscillating flow is governed by purely viscous shear forces although the time-mean flow is fully turbulent. At lower frequencies, the oscillating flow is influenced by the turbulence, in particular the amplitude of τ increases with respect to the Stokes value and becomes proportional to l_s^+. This behaviour is explained by the fact that when $l_s^+<10$, the oscillating flow in confined in the near wall layer where viscous forces are dominant. The relative amplitudes of the modulations of the turbulent intensities u'u' and $\tau'\tau'$ decrease sharply with increasing forcing frequency once $\omega^+>0.003$. This decay of the turbulence response is faster for the wall sher-stress. For forcing frequencies such that $\omega^+<0.014$, these modulations lag behind u and τ respectively by about 75 and 130 viscous time units. At very high forcing frequencies ($\omega^+>0.045$), however, the oscillating flow departs from the Stokes solution and the modulations of the turbulent intensities increase again with increasing ω^+ while their time lags with respect to $\tilde{u}$ and $\tilde{\tau}$ decrease. This paradoxical behaviour is unexplained thus far.

Ejections and burts in the near wall region in pulsatile flow have been investigated by means of hot film measurements of u' at $y^+=15$ and of τ' as well as by visualizations. Four single point detection schemes were used and compared. The phase modulations of the ejection detection parameters, especially those of the VITA scheme, and of the the grouping criteria of ejections into burts have been analysed. The results obtained with probe detection have to a fair extent been confirmed by the visualizations. It has been shown that the time-mean frequency of the ejections decreases with ω^+ in the high frequency regime. The amplitude and phase shift of the ejection frequency modulation depend strongly on ω^+. In particular, the amplitude decreases with ω^+ when it approaches the time-mean bursting frequency. It has been established that the single ejection burts (SEBs) and multiple ejection burts (MEBs) react quite differently to imposed oscillations : the MEBs (as the characteristics of ejections) scale with the modulation of the wall shear-stress but not the SEBs. The frequency of the latter vary more strongly with ω^+. The modulation of some phase averaged conditional averages are also discussed.

Wall shear-stress measurements have been performed at four different stations in flows in diverging channels (divergence angles of 2.4 and 6°) forced at amplitudes of 20 and 40° and at six different frequencies (l_s^+=7; 9; 13; 18; 27; 36 at the channel entrance). Important differences with the behaviour in constant area channels have been observed: the time-mean values $\overline{\tau}$ and $\overline{\tau'\tau'}$ may be considerably increased (by nearly a factor two) in the wide angle diffusor with large

Block 20. ABSTRACT Continued

amplitude and high frequency forcing; the $\tilde{\tau}$- oscillations, on the contrary, have smaller amplitudes in the wide angle diffusor (less than one half) and the increase with ω^+ is not observed. The phase shifts of $\tilde{\tau}$ do no longer follow the Stokes solution at high forcing frequency. Changes in $\widetilde{\tau'\tau'}$ are also observed. It seems that the l_s^+ parameter similarity does no longer hold in time-mean adverse pressure gradient flows.

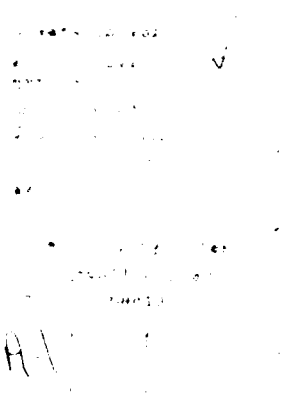

Acknowledgements

The authors wish to thank European Rearch Office of the US ARmy for providing financial support under the contract DAJA 45-87-C-0015. The present investigation is part of long rang program which is aimed at developing an understanding of unsteady turbulent boundary layer flows.The contract monitors during the period of this study were Dr F.H. Oertel and Dr R.E. Reichenbach. The authors would like to express their appreciation to Dr F.H. Oertel and Dr R.E. Reichenbach for their encouragement during the course of this wotk.

Presentation of the Report

Unsteady turbulent flows occur in many practical situations. In aerodynamics the classical, but by no means the sole, example is the helicopter blade in forward flight. The various flows related to the internal combustion engine - the fuel-air supply to the cylinders, the flow inside the cylinders and the exhaust - an all unsteady to various degrees. Aero-acoustics turbomachinery and biological flows also provide many examples. All transient flows are, of course, unsteady. One example of immense importance is the transient flow and heat transfer in a nuclear power plant faced with partial pump failure in the primary circuit.

Reliable predictions of such unsteady turbulent flows, either for design or safety purposes, would evidently be of great usefulness but are not within reach at the present time because nearly all turbulence models have been devised for and tested on steady flows. All unsteady turbulent flow computations carried out so far have simply extended steady closures by making the transport equations time dependent, except for the recent and notable attempt of J. T. L. Liu and R. R. Mankbadi (Wall Layer Response in Unsteady Turbulent Flow, EUROMECH Colloquium 272, "Response of Shear Flows to Imposed Unsteadiness", Aussois, France, Jan. 14-18, 1991). Truly unsteady modelling would have to take time delays of the various mechanisms, such as the pressure velocity correlations or the dissipation, into account for instance when the characteristic time of forcing becomes comparable to one of the turbulence time scales . The main obstacle to the development of closures for non-stationary turbulence is the lack of understanding of the underlying physics.

The experimental research described in this report is part of a long range effort aiming at elucidating the mechanisms of the turbulence response to imposed unsteadiness and at building up a data base against which models can be tested. In order to determine the progressive departure of the turbulence from the steady state conditions and to gain physical insight it is important to cover a wide range of unsteady flow conditions. This has been a constant concern in this investigation.

In the Part One, the response of channel flow to imposed unsteadiness is investigated. The time-mean and oscillating characteristics of the longitudinal velocity and of the wall shear-stress as well as of their turbulent fluctuations have been measured. Somme properties of small scales of turbulence as the Taylor time scale, the skewness and flatness factors of $\partial u'/\partial t$ have also been determined. Some of the physis of the turbulence response are analysed. The applicability of the quasi-steady approximation to various quantities is also examined. The data which has been collected should prove useful for the testing of models. It has actually been proposed to the "Collaborative Testing of Turbulence Modles" project sponsored jointly by the US Air Force OSR, the US Army RO, NASA and the US Office of Naval Research and streered by Profs P. Bradshaw (Stantord), B. Launder (Manchester) and J. Lumley (Cornell).

The extension of the previous work to higher frequencies is described in Part Two.This was prompted by the findings of Finnicum and Hanratty (PCH Physics-Chemical Hydrodynamics, vol 10,1988) showing that the amplitude of the turbulence response increases again when the forcing frequency approaches and exceeds the time-mean bursting frequency. This paradoxical and, as yet unexplained behaviour, has been confirmed by the present measurements.

In Part Three, a step further into the physics is made by investigating the response of turbulent coherent structures in the vicinity of the wall to forced oscillations. Much effort is devoted to the analysis and adaptation of various ejection detection schemes to the unsteady regime and similarly with the grouping of the ejections into bursts.

Since single probe dectetions of coherent structures are not fully devoid of arbitrariness, the previous study has been partly repeated by detecting the ejections via dye visualizations. Thus a completely independent set of results on the modulation of the ejection and the burst frequencies has been obtained. This study is reported in Part Four.

Finally in Part Five, the families of pulsed turbulent flows in two diverging channels are investigated. The imposition of a time-mean adverse pressure gradient increases the flow complexity by one more degree and brings it closer to practical situations as those encountered on lifting airfoils. The main purpose was find out how adverse pressure gradients modify the response of the flow to imposed unsteadiness with respect to flows in zero pressure gradient or in constant area ducts. The data collected in these conditions should make a good and probably difficult test for turbulence models.

Table of contents

PART ONE. TURBULENT CHANNEL FLOW WITH LARGE AMPLITUDE VELOCITY OSCILLATIONS

List of Figures

l_s^+=12; a_{uc}=0.70; U_c=18.5cm/s

a) Wall shear stress <τ>

b) Intensity of the turbulent wall shear stress fluctuations <τ'τ'>.

Figure 4) Expampls of phase averages

LDA measurements:y^+=4.86; l_s^+=8.1; U_c=17.5cm/s; a_{uc}=0.64

a) Velocity <u> ; b) Intensity of turbulent velocity fluctuations <u'u'>

Figure 5) Mean velocity profiles in steady and unsteady flow. For legend see Table 2

Figure 6) Mean turbulent intensity profiles in steady and unsteady flow. For legend see figure 5

Figure 7) Ratio of unsteady to steady time mean wall shear stress. For legend see Table 3

Figure 8) Time mean r.m.s. values of the turbulent wall shear stress fluctuations. For legend see Table 3

Figure 9) Evolution of the periodic streamwise velocity oscillations with distance from the wall

a) Amplitude profils

_____ : Viscous Stokes solution (For legend see Table 2)

b) Phase shift with respect to the centerline velocity oscillations.

Figure 10) Instanteous velocity profils in the presence of reverse flow.

l_s^+=8.1; U_c=16.9cm/s; a_{uc}=0.64

Figure 11) Observations of reverse flow compared with the Binder-Kueny criterion given by the straight line.

Figure 12) Oscillation of the wall shear stress vs frequency parameter l_s^+

For legend see Table 3

a) Amplitude normalized by the Stkes value

b) Phase shift with respect to the centerline velocity oscillations

Figure 13) Oscillation of the wall shear stress measured with the Houdevill-Cousteix gage

a) Amplitude; b) Phase shift

Figure 14) Amplitude profils of the modulation of the loggitudinal turbulent intensity

For legend see Table 2.

a) Valus scaled with constant time mean shear velocity

b) Intensity with respect to local velocity oscillations

c) Ratio of relative amplitudes of turbulent velocity fluctuations and local velocity oscillations

Figure 15) Variation of the phase of the turbulent velocity fluctuation modulation with distance from the wall. For legend see Table 2

a) Phase shift with respect to the centerline velocity oscillations

b) Time lag

Figure 16) Modulation of the turbulent fluctuations of the wall shear stress(For legend see Figure 7)

a) Amplitude

b) Phase shift

Figure 17) Modulation of the turbulent intensities of the velocity at $y^+=15$ and of the wall shear stress vs focing frequency.

a) Ratio of relative amplitudes

b) Ratio with respect to the quasi-steady values.

c) Phase shift

Figure 18) Examples of phase averages $y^+=15$; $a_{uc}=0.20$; $l_s^+=9.5$

a) Taylor time micro-scale

b) Liepmanne time-scale

c) Skewness factor of $\partial u'/\partial t$

d) Flatness factor of $\partial u'/\partial t$

Figure 19) Time mean of the zero crossing period and time mean Taylor scale vs Frequency parameter. +: $1/N_0^+$; x : $1 / 2 p 1^+$ ($y^+=15$)

Figure 20) Amplitudes of the modulations of the Liepmanne and of the Taylor scale vs frequency parameter

a) Relative amplitudes

b) Relative amplitudes scaled with the amplitude of the wall shear stress.

c) Phase shift with respect to th eoscillation of the wall shear stress

Figure 21) Time mean values of skewness and flatness of velocity time derivative .($y^+=15$) vs frequency parameter

Figure 22) Relative amplitude of the modulation of the skewness and flatness of the velocity time derivative.

PART TWO. WALL SHEAR STRESS MODULATION IN UNSTEADY TURBULENT CHANNEL FLOW WITH HIGH IMPOSED FREQUENCIES

List of Figures

PART THREE. RESPONSE OF BURSTING TO IMPOSED VELOCITY OSCILLATIONS

List of Figures

PART FOUR. COHERENT STRUCTURES IN UNSTEADY WALL FLOW VISUALIZATION RESULTS

List of Figures

Figure 9. Phase average of ejection height.T=16.0s.
a) a_{uc}=0.20; b) a_{uc}=0.13

Figure 10. Phase average of ejection height. T=34.0s.
a) a_{uc}=0.20; b) a_{uc}=0.13

Figure 11. Phase average of ejection lift-up over distance ΔX^+=100. T=2.6s.
a) a_{uc}=0.2; b) a_{uc}=0.13

Figure 12. Phase average of ejection lift-up over distance ΔX^+=100.T=5.3s.
a) a_{uc}=0.20; b) a_{uc}=0.13

Figure 13. Phase average of ejection lift-up over distance ΔX^+=100. T=7.0s.
a) a_{uc}=0.20; b) a_{uc}=0.13

Figure 14. Phase average of ejection lift-up over distance ΔX^+=100.T=16.0s
a) a_{uc}=0.20; b) a_{uc}=0.13

Figure 15. Phase average of ejection lift-up over distance ΔX^+=100. T=34.0s.
a) a_{uc}=0.20; b) a_{uc}=0.1355

Figure 16. Phase average of burst frequency. T=2.6s, a_{uc}=0.20.
a) single ejection bursts; b) multipl ejection bursts. Time of occurence based on first ejection; c) multipl ejection bursts. Time of occurence based on last ejection.

Figure 17. Phase average of burst frequency. T=5.3s, a_{uc}=0.20.
a) single ejection bursts; b) multipl ejection bursts. Time of occurence based on first ejection; c) multipl ejection bursts. Time of occurence based on last ejection.

Figure 18. Phase average of burst frequency. T=7.0s, a_{uc}=0.20.
a) single ejection bursts; b) multipl ejection bursts. Time of occurence based on first ejection; c) multipl ejection bursts. Time of occurence based on last ejection.

Figure 19. Phase average of burst frequency. T=16.0s, a_{uc}=0.20.
a) single ejection bursts; b) multipl ejection bursts. Time of occurence based on first ejection;c) multipl ejection bursts. Time of occurence based on last ejection.

Figure 20. Phase average of burst frequency. T=34.0s, a_{uc}=0.20.
a) single ejection bursts; b) multipl ejection bursts. Time of occurence

PART FIVE. WALL-SHEAR STRESS MEASUREMENTS IN UNSTEADY FLOWS IN DIVERGING CHANNELS

List of Figures

Figure 15. Amplitude of the wall shear-stress with respect to the Stokes value vs $ls+$. $\theta=2.4°$.

a) $(a_{uc})_o=0.10$; b) 0.20; c) 0.40

Figure 16. Amplitude of the wall shear-stress with respect to the Stokes value vs ls^+. $\theta=6.0°$.

a) $(a_{uc})_o=0.10$; b) 0.20; c) 0.40

Figure 17. Phase shift of wall shear-stress oscillation with respect to centerline velocity oscillation. $\theta=2.4°$.

a) $(a_{uc})_o=0.10$; b) 0.20; c) 0.40

Figure 18. Phase shift of wall shear-stress oscillation with respect to centerline velocity oscillation. $\theta=6.0°$.

a) $(a_{uc})_o=0.10$; b) 0.20; c) 0.40

Figure 19. Relative amplitude of the modulation of the turbulent fluctuation intensity referred to the relative amplitude of the oscillation of the wall shear stress vs ls^+. $\theta=2.4°$.

a) $(a_{uc})_o=0.10$; b) 0.20; c) 0.40

Figure 20. Relative amplitude of the modulation of the turbulent fluctuation intensity referred to the relative amplitude of the oscillation of the wall shear stress vs ls^+. $\theta=6.0°$.

a) $(a_{uc})_o=0.10$; b) 0.20; c) 0.40

Figure 21. Relative amplitude of the modulation of the turbulent fluctuation intensity referred to the relative amplitude of the oscillation of the wall shear stress vs ω^+. $\theta=2.4°$.

a) $(a_{uc})_o=0.10$; b) 0.20; c) 0.40

Figure 22. Relative amplitude of the modulation of the turbulent fluctuation intensity referred to the relative amplitude of the oscillation of the wall shear stress vs ω^+. θ=6.0°.

a) $(a_{uc})_o$=0.10; b) 0.20; c) 0.40

Figure 23. Relative amplitude of turbulent wall shear stress fluctuation modulation referred to the relative amplitude of velocity oscillation in the centerline vs ls^+. θ=2.4°.

a) $(a_{uc})_o$=0.10; b) 0.20; c) 0.40

Figure 24. Relative amplitude of turbulent wall shear stress fluctuation modulation referred to the relative amplitude of velocity oscillation in the centerline vs ls^+. θ=6.0.

a) $(a_{uc})_o$=0.10; b) 0.20; c) 0.40

Figure 25. Relative amplitude of turbulent wall shear stress fluctuation modulation referred to the relative amplitude of velocity oscillation in the centerline vs ω^+. θ=2.4°.

a) $(a_{uc})_o$=0.10; b) 0.20; c) 0.40

Figure 26. Relative amplitude of turbulent wall shear stress fluctuation modulation referred to the relative amplitude of velocity oscillation in the centerline vs ω^+. θ=6.0°.

a) $(a_{uc})_o$=0.10; b) 0.20; c) 0.40

Nomenclature

Roman Symbols

$A_{\tilde{q}}$	Amplitude of q.
$a_{\tilde{q}}=A_q/\overline{q}$	Relative amplitude of q.
f	Frequency of foced oscillation.
f_e	Ejection frequency.
f_b	Burst frequency.
h	Half channel width.
h	Ejection height.
$\Delta h=h(x_2)-h(x_1)$	Lift of ejection.
l	Length.
$l_s=\sqrt{2\nu}/\omega$	Stokes length.
p	Presseure.
q	Unspecified quantity.
t	Time.
$T=1/f$	Period of forced oscillation.
u,v	Velocities in x,y direction;
u_τ	Shear velocity.

Greek symbols

δ^*	Displacement thickness.
$\beta=(\delta^*/\tau)(\partial p/\partial x)$	Clauser parameter.
θ	Total diffuser angle.
$\omega=2\pi f$	Angular velocity.
τ	Wall shear stress.

Indices

$()_o$	Quantity at inlet of diffuser.
$()_v$	Interne variables.
$()_c$	Quantity in the centerline.

$()^+$	Quantity normalized by interne variables.

Other Symbols

$\overline{()}$	Time mean Average.
$\widetilde{()}$	Periodic oscillation.
$()'$	Turbulent fluctuation.
$< >$	Average perfomed at the same phase in each of a series of periodic events.

PART ONE

TURBULENT CHANNEL FLOW WITH LARGE AMPLITUDE VELOCITY OSCILLATIONS

Submitted to the J.Fluid Mechanics

TURBULENT CHANNEL FLOW WITH LARGE AMPLITUDE VELOCITY OSCILLATIONS

Sedat F. TARDU, Gilbert BINDER

Institut de Mécanique de Grenoble
BP 53-X
38041, Grenoble, Cédex-France

Ron F. BLACKWELDER

Department of Aerospace Engineering, University of Southern California, Los Angeles, California, 90089-1454,U.S.A

Abstract

Measurements in turbulent channel flow with forced oscillations covering a wide range of frequencies (ω^+=0.03 - 0.0005) and amplitudes (10-70% of centerline velocity) are presented and discussed. Phase averages of the velocity <u>, across the flow and of the wall shear stress <τ>, as well as of the turbulent fluctuations <u'u'> and <τ'τ'> are obtained with LDA and hot film techniques. The time mean quantities, except $\bar{u}'^2$, are not affected by the imposed oscillations whatever their frequency and amplitude. It is shown that the appropriate similarity parameter for the oscillating quantities $\tilde{u}$ and $\tilde{\tau}$ is the non-dimensionnal Stokes length l_s^+ (or the frequency $\omega^+ = 2/ l_s^{+2}$). In the regime of high frequency forcing ($l_s^+ < 10$) the oscillating flow $\tilde{u}$ and $\tilde{\tau}$ is governed by purely viscous shear forces although the time-mean flow is fully turbulent. This behaviour may be explained by the physical significance of l_s^+. At lower frequency $l_s^+ > 10$, the oscillating flow is influenced by the turbulence, in particular the amplitude of $\tilde{\tau}$ increases with respect to the Stokes amplitude and becomes proportionnel to l_s^+. The relative amplitudes of <u'u'> and <τ'τ'> decreases sharply with increasing forcing frequency

once $l_s^+ < 25$. This decay of the turbulence response is faster for the wall shear stress. For forcing frequencies such that $l_s^+ > 12$, $\langle u'u' \rangle$ and $\langle \tau'\tau' \rangle$ lag behind $\langle u \rangle$ and $\langle \tau \rangle$ respectively by about 75 and 130 viscous time units. These lags decrease by a factor two at higher forcing frequencies. It is shown that in the log-layer, the turbulence modulation diffuses away from the wall with a diffusivity equal to that of the time mean turbulence. The imposed oscillations are felt down to the small scales of the turbulence as may be evidenced from the cyclic modulation of the Taylor-microscale, the skewness ans the flatness factors of $\partial u'/\partial t$. The modulations of the skewness and the flatness go through a maximum around $l_s^+ \approx 12$.

1. Introduction

Unsteadiness imposed on a turbulent shear flow by means of time dependent boundary conditions greatly increases its complexity owing to the facts that time must be added to the independent space variables and that the forcing introduces an amplitude and a time scale.Starting from a single steady flow, one type of forcing generates, thus, an entire two parameters family of unsteady flows. In addition several types of forcing are generally not only possible but relevant to practical situations.

A classical example is the flow around an airfoil rendered unsteady by either oscillations of the angle of attack or of the free-stream velocity or of a combination of these two boundary conditions as on helicopter blades.Somewhat simpler situations derived from this practical case, are the unsteady flat plate turbulent boundary layer or turbulent channel flow driven by oscillations of the free stream - or the center line - velocity about a mean value.

The complexity of these unsteady wall flows is reflected in the diffuculty in establishing which similarity parameters are physically the most relevant.Thus, for the non-dimensional frequency or Strouhal number Cousteix et al (1977) have used $\omega X/\bar{U}_e$ (where $\omega = 2\pi f$ is the frequency of imposed oscillations, X is the distance from the leading edge of the flat plate and where $\bar{U}_e$ is the time mean free stream velocity) to present their data.Arguing that the imposed oscillations should interact most strongly with the turbulence when their frequencies are comparable, Ramaprian and Tu (1983) have proposed $\omega\delta/\bar{u}_\tau$ where $\bar{u}_\tau$ is the friction velocity based on the time mean wall shear stress. Since as a rough approximation $\bar{u}_\tau \propto \bar{U}_e$ and for the flat plate $\delta \propto X$, there is a kinship betwen these two frequency parameters.

A similarity parameter of a different kind, namely $l_s^+ = l_s \bar{u}_\tau / \nu$ ($l_s = \sqrt{2\nu/\omega}$ being the thickness of the viscous Stokes layer) was introduced by Ronneberger & Ahrens (1977) and independently later by our own group (Binder & Kueny 1981).An appropriate name for this parameter could be "Stokes-Reynolds number". The introduction, a priori rather surprising of the viscous Stokes thickness, was based in both studies on observations that the oscillating flow near the wall followed closely the viscous Stokes solution when the forcing frequency was high enough. It may be interesting to note that these observations pertained to quite different physical experiments since the first authors investigated air flow in a pipe with acoustic forcing and measured the oscillating wall shear stress, while our group investigated pulsed flow in a 2D water channel and measured the oscillating velocity by means of LDA with the point closest to the wall at $y^+ = 3$.In order to explain the viscous behaviour of the oscillating flow at high forcing frequencies, both groups linked two facts together: one, that in this case viscosity alone diffuses the oscillating wall shear stress to a distance of the order of l_s which varies like $1/\sqrt{\omega}$ and two, that the turbulent flow near the wall in the steady regime is dominated by viscous effects up to $y^+ \cong 12$ since below this distance the Reynolds stress is smaller than the viscous stress. Consequently, if the frequency is high enough so that $l_s^+ < 12$, the shear wave from the wall will reach the asymptotic outer values before the turbulence can play an appreciable role in the momentum transfer. This may be defined as the high frequency regime. The oscillating flow as shown by these experiments departs progressively from the viscous Stokes solution at larger values of l_s^+.

It may easily be seen that the forcing frequency scaled with inner variables is related to l_s^+ by the simple formula $\omega^+ = 2/l_s^{+2}$ .It is also interesting to note that the Strouhal number based on l_s and u_τ is inversely proportional to l_s^+ :

$$\omega l_s / \bar{u}_\tau = \sqrt{2}\, \omega^+ = 2 / l_s^+$$

In the two experiments mentioned above which have lead to the definition of l_s^+ , the amplitudes of the imposed oscillations were small, 5% or less. In other experiments with larger amplitudes (Cousteix et al. 1981; Ramaprian and Tu 1983; Parikh et al 1981), on the other hand, measurements could only be made in the more accessible outer regions of the shear flow and could not be made in the lower logarithmic region or below. Yet, it is in this latter region where 50% of the mean velocity variations occur and up to 100% of the change in

oscillating velocity at medium or high forcing frequencies. The questions of the role of the amplitude on unsteady effects and on the relevance of the l_s^+ parameter under high amplitude forcing could, therefore, not be answered with the existing data.

The research reported here was specifically designed to investigate the velocity field in the logarithmic and the wall region with a wide range of imposed amplitudes and frequencies.Particular attention has been paid to study the response of the turbulence to imposed amplitudes as high as 65 % of the free stream velocity with imposed frequencies reaching the mean bursting frequency. Detailed measurements of the wall shear stress and of the streamwise velocity modulations are reported. The effect of the imposed unsteadiness on the small and intermediate scales of the turbulence is studied through the measurements of the modulation of the zero-crossing frequency and moments of the fluctuating streamwise velocity time derivative.

The notations q, $\tilde{q}$ and q' are used to designate the time-mean, periodic and random turbulent part of the quantity q so that in established flow

$$q(y,t;T)=\bar{q}(y)+\tilde{q}(y,t/T)+q'(y,t)$$

The braquet < > designates the ensemble or phase average:

$$<q(y,t/T)>=\bar{q}(y)+\tilde{q}(y,t/T)=\lim_{N\to\infty}\left(\sum_{i=1}^{N} q(t+iT)\right)$$

It follows that: $<q'>=0$ and $<q^2>=(<q>)^2+<q'q'>$.

$<q'q'>$ is a function of t/T and in keeping with the expression of <q>, it is convenient to write $<q'q'>(t/T)= \overline{q'q'} + \tilde{q'q'}\ (t/T)$ where $\tilde{q'q'}$ is the "modulation" of the variance about the time mean value $\overline{q'q'}$. $\tilde{q}$ or $\tilde{q'q'}$ are not necessarily pure sine-functions and are most conveniently described by the amplitudes and phases of the successive terms of the Fourier series. In the present results the fundamental mode is generally dominant although higher harmonics may in some instances be substantial especially in the turbulence modulations. An adequate description of the modulation is then given by the amplitude and phase of the fundamental mode, designated by $A_{(\tilde{})}$ and $\Phi_{(\tilde{})}$ where the index is the quantity under consideration as for example, $A_{\tilde{q}}$ and $\Phi_{\tilde{q}}$ or $A_{\tilde{q'q'}}$ and $\Phi_{\tilde{q'q'}}$. Finally the relative modulation, i.e. the amplitude of the modulation with respect to the time-mean value of the same quantity $A_{(\tilde{})}/(\bar{})$ will be designated by the lower case letter $a_{(\tilde{})}$, as for example $a_{\tilde{q}}=A_{\tilde{q}}/\bar{q}$ or $a_{\tilde{q'q'}}=A_{\tilde{q'q'}}/\overline{q'q'}$.

2. Experimental Facilities

2.1 The flow loop apparatus

The main elements of the flow loop are: a constant head tank with a large free surface in order to minimize variations in the total head when flow is pulsed, the pulsator, a control valve, a settling chamber with screens and a honey comb, a converging section with a 10/1 contraction, the test channel, a large free surface tank (1*2*4.5 m^3) and the pump (Figure 1). The last meter of the channel is immersed in this tank.A divergence up to 30° can be imposed on this section to set up a time mean pressure gradient. The return flow to the pump is via a free surface flow in order to limit the elements of the loop subjected to large unsteady pressure forces.

The dimensions of the test channel are: width=100 mm, length=2600 mm, span=1000 mm. The boundary layer at the channel entrance is tripped by tridimensional 5 mm high crenel type roughnesses.

Oscillations in the flow rate are produced by the following device: the inflow pipe to the pulsator terminates in a cylinder having 24 longitudinal 5*200 mm slots machined in its surface (Figure 1).The end of the cylinder was capped so the water had to exit through the slots.A moveable sleeve was tightly fitted around the cylinder so the sleeve covered some,all or none of length of the slots.This apparatus was housed in a larger cylinder which collected the water exiting through the slots and allowed it to continue into the settling chamber.The oscillation frequency of the sleeve was controlled by a variable speed motor through an eccentric bearing.The eccentricity was adjustable to control the amplitude of the oscillation.The mean flow was controlled by adjusting the length of the connecting arm between the eccentric bearing and the sleeve.These three variables were easily changed in a continuous manner and allowed great flexibility in adjusting the flow conditions.The amplitude could be varied from 0 to 80% of the mean flow and the period from 2.5 sec to infinity,although the largest period studied was 132 sec.The time period was repeatable within 0.1%.

The flow loop provided very stable and repeatable mean and periodic flow conditions for a given setting of the pulsator.These conditions varied less than 0.5 % from one day to another. The pulsator proved to be very convenient for the in situ calibration of hot films.

2.2) Flow characteristics

The mean centerline velocity $\bar{U}_c$ can be varied from 0 to 50 cm/s. The corresponding maximum Reynolds number based on the half height h of the channel is $(Re_h)_{max}=25*10^3$ and the corresponding value of Re_θ is $Re_\theta \equiv 2500$. Measurements show that the flow is fully turbulent at the measuring station when $\bar{U}_c > 6$ cm/s . For most of the data presented here $\bar{U}_c$=17.5 cm/s and Re_h=8500. Even with a centerline amplitude of 64% the flow was then still turbulent under static conditions when the flow rate was minimum, avoiding thus undesirable complications which could be produced by periodic transitions. On the other hand, with $\bar{U}_c$=17.5 cm/s the value of the friction velocity was $\bar{u}_\tau$ = 0.89 cm/s , so that the inner scale $l_v = \nu/\bar{u}_\tau$ was $l_v \equiv 0.126$ mm which made it possible to make LDA velocity measurements down to y^+=3 despite the large span of the channel and to explore the inner layer.

The variations of the centerline velocity in the spanwise direction were less than 2 % . This was expected on account of the large 10/1 aspect ratio of the channel.The symmetry of the mean and of the periodic flow with respect to the center plane was also checked.

Because of space limitations the channel length is only 52h and the measurement station was at a distance 42h from the entrance. This length is somewhat short to insure fully developped turbulent flow despite the rather large height of the entrance trip, since this length should be about 90h at Re_h = 25000 (Comte-Bellot, 1965). Development length of the turbulent flow is, however, neither uniform across the channel nor the same for different quantities: it is faster near the wall than in the core and its rate decreases with the order of the moment considered. Since the transverse gradients of the oscillating field are entirely or, at very low forcing frequencies, almost entirely confined within the inner layer, as shown by previous measurements and confirmed by present ones, the requirement on the channel length can, therefore, be relaxed without putting undue restrictions on the generality of the results. This conclusion is supported by the following facts: the measured time-mean velocity and longitudinal turbulent intensity are the same at the measuring station and 6h further downstream and are in good agreement with previously published data. Furthermore, the time mean and periodic characteristics of the wall shear stress were measured at four stations located rrespectively at x/h=32 ; 38.3 ; 44.6 and 50.8 from the channel entrance. The results for four typical cases are given in Table 1. It is seen in these conditions with the centerline

velocity of 9.54 cm/s , the characteristics of the mean values and of the modulations of the wall shear stress and of its turbulent fluctuations are the same at these four locations within experimental accuracy. It may, therefore, be concluded that the flow is sufficiently well established at x/h=42 for the type of measurements reported here.

2.3 Wall deflections

If the periodic pressure variations $\tilde{p}$ which drive the oscillating flow produces wall deflections $\tilde{d}$ a probe which does not move with the wall will see a parasitic velocity oscillation $\tilde{u_d}$ due to its displacement across the mean velocity profile. Since the maximum velocity gradient is $\bar{u}_\tau^2/\nu$ in the viscous sublayer:

$$\tilde{u_d} \leq \frac{u_\tau^2}{\nu}\,\tilde{d}$$

and:

$$A_{\tilde{u}d} \leq \frac{u_\tau^2}{\nu}\,A_{\tilde{d}}$$

So that

$$\frac{A_{\tilde{u}d}}{A_{\tilde{u}}} < \frac{u_\tau^2}{\nu}\,\frac{A_{\tilde{d}}}{A_{\tilde{u}}} = \frac{A_{\tilde{d}}^{+}}{A_{\tilde{u}}^{+}}$$

where $(\,)^+$ designates the quantity scaled with inner variables as usual. Hence, the relative error on the measured velocity amplitude is of order of $A_{\tilde{d}}^{+} / A_{\tilde{u}}^{+}$. Under given forcing conditions the error is proportionnally worse as the wall is approchad since $A_{\tilde{u}}^{+}$ tends to zero and it is likely to be more severe when the viscous length scale $\nu/\bar{u}_\tau$ is smaller. It is possible that such wall deflections were sufficiently important in the experiment of Acharya (1975) to account for the surprizing shape of the $A_{\tilde{u}}$ and $\Phi_{\tilde{u}}$ profiles of this author in the high frequency case.

In order to check the magnitude of the periodic displacement of the wall, measurements were made with an ultrasonic depth gauge having a sensitivity of 1μm have been used (figure 2). If the imposed frequency is small compared to the resonance frequency of the structure as is the case here, the amplitude of the displacement should be proportional to the

driving force $\tilde{p}$ and, therefore, to $\omega A_{\tilde{u}c}$.It is seen from figure 2 that indeed $A_{\tilde{d}}(\mu m)=2f(Hz)A_{\tilde{u}c}(cm/s)$.This gives a maximum error less than 10% in the most unfavourable case corresponding to f=0.4 Hz.

3.) Instrumentation; data acquisition and reduction

3.1) Instrumentation

LDA measurements

The streamwise velocity in the channel flow was measured by a one component 25 mW laser Doppler anemometer (Binder et al, 1985).The dimensions of the measuring volume were 0.3 and 1.5 mm (2.3 * 12 l_v). These dimensions could be reduced by a factor of 5 by use of a 5X-beam expander. Measurements as close as 0.25 mm ≅ 2.5 l_v (for $\bar{U}_c$=17.5 cm/s) were then possible, but not without difficulty because the signal quality very close to the wall is poor and the sampling rate is quite small (a few samples/s).

The period of the Doppler signal was determined by a home made counter (Tardu et al,1986).The Doppler signal was frequency shifted with a Pockel cell in order to make measurements in reverse flow. Mclaughin&Tiederman's correction (Mclaughin&Tiederman, 1973) was applied in order to eliminate the statistical bias due to the proportionnality between sampling rate and velocity when the processor is not saturated as was the case here. Incidently, this can simply be done by determining the average Doppler period as well as the average Doppler frequency. Indeed, consider a population of measured velocities over which averages are determined. On the histogram of this population, let n_i be the number of samples of the class u_i. If the concentration of scattering particles is homogeneous, the number of measurement is proportional to the flux of particles through the probe volume i.e. $n_i=ku_i$. Then the measured (index "m") moment of order p is:

$$(\overline{u^p})_m = \frac{\sum_i n_i u_i^p}{\sum_i n_i} = \frac{\sum_i u_i^{p+1}}{\sum_i u_i} = \frac{\overline{u^{p+1}}}{\bar{u}}$$

where $\overline{u^{p+1}}$ is the true moment of order p+1 . Let d_f be the fringe spacing, f_D and t_D be the

measured Doppler frequency and period, so that $u_i = d_f f_{Di} = d_f / t_{Di}$. For p=1, by substituting u=u+u' in the above formula, one obtains

$$(\bar{u})_m = d_f (\overline{f_D})_m = \frac{\overline{u^2}}{\bar{u}} = \bar{u} \left(1 + \frac{\overline{u'^2}}{\bar{u}^2}\right)$$

The average Doppler frequency yields, thus, a biased value of the mean velocity as shown by Mclaughin&Tiederman. For p=-1, however:

$$\overline{\left(\frac{1}{u_m}\right)} = \frac{\overline{(t_D)_m}}{d_f} = \frac{1}{\bar{u}} \qquad \text{or} \qquad \bar{u} = \frac{d_f}{\overline{(t_D)_m}}$$

which shows that the true unbiased mean velocity may simply be obtained from the average Doppler period. This is especially interesting because counters actually determine the Doppler period.

The mean velocity and turbulent intensity were, thus, computed from the average Doppler period and frequency according to the two relations:

$$\bar{u} = \frac{d_f}{\overline{(t_D)_m}}$$

$$\overline{u^2} = \bar{u}^2 + \overline{u'^2} = d_f^2 \frac{\overline{(f_D)_m}}{\overline{(t_D)_m}}$$

Similar relations apply to the ensemble or phase averages.

Hot film measurements:

The wall shear stress τ was measured with DANTEC 55R46 or TSI 126^R W flush mounted hot-film probes (sensing surfaces 0.2*0.75 mm (1.6*6 l_v) and 0.127*1mm (1*8 l_v) respectively). They were operated at overheat ratios between 3 to 8 % with DISA 55MO1 or DANTEC 56C01 constant temperature anemometers. Bucking amplifiers or a digital to analog converter were used to suppress the DC anemometer output at zero velocity, so that the signal could be amplified before A/D conversion. This conversion was mostly performed with an ANALOG-DEVICE RTI-800 board (accuracy: 11 bit+sign ; 8 channels) installed in a OLIVETTI 240 PC computer.

The hot film gages were calibrated in situ by determining the velocity gradient at

the wall with the LDA. To do this properly requires several measuring points within the viscous sublayer ($y^+ < 5$) and the precise determination of the y-position, two requirements which come up against great practical difficulties. As already mentioned above measurements are not possible here below $y^+=2.5$ and they are difficult for $2.5<y^+<5$, because of the low sampling rate which combined with the high turbulence level requires extremely long integration times (2 hours or more) . The y-positions are known accurately only to within an additive y_0 because the exact position of the wall cannot be determined. In order to be able to use some points beyond $y^+=5$ and to reduce the uncertainty about the exact location of the wall, $\bar{u}_\tau$ and y_0 are both obtained from a least square fit of the measured profile with the empirical relation $\bar{u}^+=14.5 \tanh (y^+/14.5)$ for $y^+<14.5$. This law differs from Eckelmann's data (Eckelmann 1974 ; originally tabulated data kindly provided by the authors) by less than 2% over the range of y^+ from 0 to 14.5) .

The mean wall shear stress determined with this method was aptly correlated by the Blasius formula: $\bar{\tau} = 0.048\ Re_h^{-1/4}\ (\rho \bar{U}_c^2/2)$. This empirical relation was subsequently used to determine $\bar{\tau}$ from the measurement of $\bar{U}_c$. The exponent in the heat transfer law: $E^2 = A+B\ \tau^n$ where E is the output from the hot wire set, was always found to be between 0.33 and 0.35 . Consequently, the theoretical value 1/3 of the Lévêque solution consistent with the results of Spence & Brown (1968) was used. The calibration constants A and B were usually determined from five couples (E,τ) .

At large amplitudes,reverse flow was encountered at the wall.Figure 3 shows the phase average of the modulation of the wall shear stress $<\tau>$ in such a case.Pedley (1975) has shown that the response of the thermal boundary layer in reversing flow depends on the frequency parameter $\omega^* = \omega^+ (L_f^{+2}\ Pr)^{1/3}$ where ω^+ and L_f^+ are respectively the angular frequency and the streamwise length of the sensor in wall units and Pr is the molecular Prandtl number of the fluid. In our case $\omega^+<0.06$ and the response of the thermal boundary layer may be considered as quasi-steady. On the other hand when flow reversal occurs,the heat transfer rate does not reach zero because of diffusion effects.The heat transfer rate measured at $<\tau>=0$ is three times greater than the value given by the boundary layer analysis of Pedley (1975) and the numerical solutions of Kaiping(1983) which neglects the axial diffusion. Since this diffusion is important in our case on account of the small value of the time mean Péclet number

Pr L_f^{+2} a complete numerical solution of the whole thermal elliptical equation was carried out. The numerical solutions are in good agreement with the measurements (Tardu 1988). Since the response of the boundary layer is quasi-steady, the film output during flow reversal has been rectified by taking the symmetry with respect to zero (figure 3).

Some measurements were also performed with a single fiber hot-film probe (model DANTEC 55R11, sensing element: 70μm=0.6 l_v in diameter and 1.25 mm= 11 l_v long) mainly for velocity time derivative and zero crossing frequency measurements. The calibration of this probe was done in the channel with the LDA by a least square fit to the relation $E^2 = A+Bu^n$. n was found to be between 0.45 and 0.5 . For these measurements a 15 bit + sign PRESTON A/D converter was used with a ampling frequency of 500 Hz (i.e. 4.2 to 8 $\bar{u}_\tau^2$ / ν) after preiiltering the signal by a KROHN-HITE filter. The total duration of the record used was $2.2*10^5$ ν / $\bar{u}_\tau^2$.

The calibration of the hot films was checked before and after each measurement. Because of the low overheat ratio used in water, the hot film measurements are quite sensitive to temperature drifts. The temperature of the water was continuously monitored. In order to minimize temperature variations, the water of the flow loop is cooled by a heat exchanger supplied with tap water. In the best conditions, the temperature change was less than 0.1°C per hour. When the integration time exceedeed 15 mn, the film response was corrected for the temperature drift by assuming linear variation over the time interval.

3.2) Data reduction

The phase locked ensemble averages <q> and <q'q'> necessary to determine $\bar{q}$, $\tilde{q}$ (t/T) and <q'q'> (t/T) were obtained by dividing the cycle into bins of equal width (generally 50) and the desired quantity was averaged in each bin. The beginning of each cycle was provided by a pulse from a photo electric cell triggered by the pulsator. Errors on long time averages due to slow drifts in the forcing period were thus avoided.

Examples of phase averages are shown on figure 4. Fourier analysis was applied to these phase averages in the folowing form:

$$<\Phi> = \bar{q} + A_{\tilde{q}} \cos(\omega t + \Phi_{\tilde{q}}) + \sum_{n=2}^{\infty} A_{\tilde{q}\,n} \cos(n\omega t + \Phi_{\tilde{q}\,n})$$

and similarly for <q'q'> . The coefficients of the first ten modes were systematically computed

and recorded.

Statistical convergence of the phase averages was checked by inspecting the data points. The truncated Fourier series limited to the first or to the first three modes was drawn through the data points as shown on the example of Fig. 4. Poor convergence was revealed by large scatter of the data points with respect to the smooth Fourier series. In most cases an integration time of $10^5 \nu / \bar{u}_\tau^2$ ($\cong$ 15-25 mn) was sufficient to insure satisfactory statistical convergence of the phase averages.

4.) Results and Discussion

The complete profiles of $\bar{u}$, $\tilde{u}$ and $\widetilde{u'u'}$ of unsteady flows forced at four different frequencies such that l_s^+=8.1, 16, 23, 34 (see Table 2) and with a centerline amplitude of 64% have been measured with LDA. The flow with high frequency forcing l_s^+=8.1 but with a centerline amplitude of 30% has also been investigated.

The properties of $\bar{\tau}$, $\tilde{\tau}$ and $\widetilde{\tau'\tau'}$ measured with the flush mounted hot film gage have been determined by varying the period of the imposed oscillations from 2.6 to 132s, i.e. l_s^+=8.1 to 64, for centerline amplitudes between 10 to 70% (Table 3). Since the frequency parameter $l_s^+ = \sqrt{2}\ \bar{u}_\tau / \sqrt{\nu\omega}$ depends also upon $\bar{u}_\tau$ which is roughly proportionnal to the centerline velocity measurements have also been performed with different centerline velocities. In one case case with 60% centerline amplitude, the velocity was varried between 16 and 26 cm/s.

4.1) The time mean characteristics

4.1.1 The mean velocity

The mean velocity distributions $\bar{u}(y)$ are shown on figure 5 for steady and unsteady flow conditions. The time mean unsteady velocities are compared with the mean velocities at the same y^+ position for the same value of $\bar{U}_c$.The steady flow measurements compare well with Eckelmann's (1974) data at a similar Reynolds number.The closest measurement point to the

wall is at $y^+=4$ and the exploration of the flow field is performed from the viscous sublayer into the logarithmic layer.The unsteady profiles obtained with two different amplitudes and four different frequencies are shown on the same figure.Clearly there is no effect of the imposed unsteadiness on the time mean velocity profiles despite the large forced amplitudes. These results are significant since for $l_s^+=8.1$ and $a_{\tilde{u}c}=0.64$, the amplitude of the velocity oscillations becomes greater than the local mean velocity near the wall and periodic flow reversal occurs. They confirm the findings of Karlsson (1959) , Cousteix et al.(1981) and Binder and Kueny (1981) obtained however for smaller values of the imposed amplitude.

Mizushina et al.(1973-75) and Ramaprian and Tu (1983) have suggested that the insensitivity of the mean flow to imposed oscillations may only be true at low amplitudes and low frequencies, i.e. at frequencies significantly below the bursting frequency. The bursting frequency reported by Blackwelder and Haritonidis(1984) is $\bar{f}_b^+=0.0035$ and the value given more recently by Coughran and Bogard (1987) is $\bar{f}_b^+=0.0062$. Since $f^+=(\pi\, l_s^{+2})^{-1}$, it is seen that the highest frequency of the present experiments is $f^+=0.005$ which is close to the values given above and, yet, the mean flow remains unaltered even for imposed amplitudes as high as $0.64\ \bar{U}_c$.

The oscillating flow may interact with the mean flow directly via the oscillating part of the Reynolds stress $\widetilde{uv}$, or indirectly via $\overline{u'v'}$ since the Reynolds equation for the mean flow is:

$$u_j\frac{\partial \bar{u}_i}{\partial x_j} = -\frac{1}{\rho}\frac{\partial \bar{p}}{\partial x_i} + \frac{\partial}{\partial x_j}\left[\frac{1}{2}\nu\left(\frac{\partial \bar{u}_i}{\partial x_j}+\frac{\partial \bar{u}_j}{\partial x_i}\right) - \overline{u'_i u'_j} - \widetilde{u_i u_j}\right]$$

The results presented in this paragraph suggest that, $\widetilde{uv}$ is negligible and that the mean Reynolds stress is unaltered by imposed velocity oscillations.Although order of magnitude analysis must be used with caution in unsteady flows because of the phase shifts between the oscillating terms, it may still be noted that in an unsteady boundary layer without adverse pressure gradient $\partial\tilde{u}/\partial x \equiv 0$ and by continuity $\tilde{v}\equiv 0$ so that $\widetilde{uv}\equiv 0$ and this is a fortiori true in channel flow.

4.1.2 The longitudinal turbulent intensity

The dominating impression from figure 6 which shows the profiles of the time mean longitudinal turbulent intensity $\sqrt{\overline{u'u'}}/\bar{u}_\tau$ is that the unsteadiness has no dramatic effect on this quantity even in these cases of large amplitude forcing and the classical profiles are found in steady and unstaedy flows with a maximum at $y^+ = 12$ (Coles 1978). The observed differences between the various flows on this graph must be viewed in remembering that the measured $\sqrt{\overline{u'u'}}/\bar{u}_\tau$ vs y^+ distributions in steady flow vary somewhat with Reynolds number (Wei & Willmarth, 1989) and from one experiment to another. Notwithstanding these differences between steady flows, there is a systematic increase in the turbulent intensity in the forced flows at low frequency : thus in the case $l_s^+ = 34$, the maximum value at approximatly $y^+ = 12$ is about 15 % higher and further away from the wall the intensity is about 30 % higher than in steady flow.

These results do not agree with the earlier measurements of Mizushima et al (1975) who found an increase of the mean turbulent intensity at high forcing frequencies which they interpreted as a sort of resonnance between the turbulence and the imposed oscillations in these conditions. Such trends were also found by Ramaprian and Tu (1983), who adopted a similar point of view.

The production term in the transport equation of $\overline{u'u'}$ is:

$$-\overline{\langle u'v' \rangle \frac{\partial \langle u \rangle}{\partial y}} = -\overline{u'v'}\frac{\partial \bar{u}}{\partial y} - \overline{\tilde{u}\tilde{v}}\frac{\partial \tilde{u}}{\partial y}$$

since by definition $\tilde{u} = 0$ and $\overline{\tilde{u}\tilde{v}} = 0$. The relative insensitivity of the $\overline{u'u'}$ profiles indicates that the production by the interaction with the oscillating velocity gradient $\overline{u'v'\partial\tilde{u}/\partial y}$ is small compared with $\overline{u'v'}\partial\bar{u}/\partial y$ unless $\overline{u'v'}$ is itself affected by the imposed unsteadiness or that the other mechanisms, namely turbulent transport and dissipation, exactly counter balance the increased production which is an unlikely eventuality. The production of the oscillating terms could only be appreciable if the terms $\overline{\tilde{u}\tilde{v}}$ and $\partial\tilde{u}/\partial y$ were comparable in amplitude to the corresponding mean values in overlapping intervals and if they were nearly in phase. The absence of effects on the mean turbulent intensity at high forcing frequencies, say $l_s^+ \leq 8$, observed here is coherent with the measurements of the oscillating velocity $\tilde{u}$ analysed in the

next section which show that $\partial\tilde{u}/\partial y$ is essentially confined in a layer of thickness l_s^+ in this case.The contribution of the oscillating flow $\overline{\tilde{u}'\tilde{v}'\partial\tilde{u}/\partial y}$ to the total turbulent production $-\overline{\langle u'v'\rangle\,\partial\langle u\rangle/\partial y}$ could, therefore, be locally appreciable only in the unlikely situation where the modulation $-\overline{\tilde{u}'\tilde{v}'}$ could reach large values between $y^+=0$ and l_s^+ and, even then, there would be an excess production in a thin layer so that its contribution to the production integrated over the whole boundary layer would still be small. Conversely, when l_s^+ and the forcing amplitude are large enough as in the present case for $l_s^+=34$, the oscillating flow can appreciably contribute to the total production and raise the turbulence level as observed here.

4.1.3 The wall shear stress

Figure 7 shows the ratio of the unsteady to the steady mean wall shear stress corresponding to the same mean velocity vs. l_s^+. These measurements were performed by changing the imposed frequency by a factor of 40 and the imposed amplitude by a factor of 7, but also by modifying the mean Reynolds number while the oscillation period was kept constant, in order to proof the validity of the similitude parameter l_s^+. It is seen that within a scatter of +-9% the time mean wall shear stress is not affected by the oscillations. This is a priori surprizing because of the non-linear relationship between the wall shear stress and the centerline velocity in turbulent flow. It will be shown below that, at low frequencies ($l_s^+>20$) the wall shear stress is in phase with the centerline velocity as may be expected in the quasi-steady flow (qs). The Blasius formula may then be assumed to hold at any instant of the cycle so that

$$\langle\tau\rangle_{qs}=C/2\ (\langle U_c\rangle h/\nu)^{-1/4}\ \rho\langle U_c\rangle^2$$

If $\bar{\tau}_{steady}$ is the shear stress corresponding to the mean velocity

$$\bar{\tau}_{steady} = C\left(\frac{\overline{U_c}\,h}{\nu}\right)^{-1/4}\frac{1}{2}\rho\,\overline{U_c}^2$$

We write $\langle U_c\rangle=\overline{U_c}\,(1+a_{\tilde{U}c}\cos\omega t)$

Then upon expanding and in retaining two terms, yields:

$$<\tau>_{qs} = \bar{\tau}_{steady} \left(1 + \frac{7}{4} a_{\tilde{uc}} \cos\omega t + \frac{21}{32} a_{\tilde{uc}}^2 \cos^2\omega t\right)$$

Hence

$$\bar{\tau}_{qs} = \bar{\tau}_{steady} \left(1 + \frac{21}{64} a_{\tilde{uc}}^2\right)$$

For the largest amplitude $a_{\tilde{uc}}$=0.7 the result is: $\bar{\tau}_{qs} = 1.16\ \bar{\tau}_{steady}$.

The predicted increase in $\bar{\tau}$ due to non linear effects is also at most 16% in the present experiments and is nearly barried in the experimental scatter. One may note the tendancy of the full squares corresponding to 70% amplitude to lie on the average above the value one.

4.1.4 The turbulent wall shear stress fluctuations

The time mean RMS of the turbulent fluctuations of the unsteady wall shear stress is plotted on figure 8. $\sqrt{\overline{\tau'\tau'}}$ is 0.26 to 0.45 times $\bar{\tau}_{steady}$ with a mean value of 0.34 .In spite of the difficulty in making such measurements--for instance, values as low as 0.06 have been reported in the litterature (Chambers et al. 1982)-- the results agree well with the steady values of Sandborn(1979).The mean value of 0.34 compares well with 0.36 found from the direct simulation data of Kim et al. (1987).No trend was observed as the frequency varied suggesting that the rms value of the fluctuating shear stress $\sqrt{\overline{\tau'\tau'}}$ is unaffected as was found approximatively for $\overline{u'u'}$.

These results are remarkable when it is considered that in some regions, the amplitude of the oscillations was greater than 100% of the local mean flow, so that reverse flow occured over 25% of the cycle. At these large forcing amplitudes $A_{\tilde{uc}}/\tilde{u}_\tau$=15 and the energy in the periodic flow is at least 25 times greater than in the turbulent fluctuations.In spite of this there is no apparent change in the statistics of the mean flow implying that the mean flow is essentially decoupled from the large amplitude oscillations.

4.2 The characteristics of the cyclic variation

All the oscillating quantities $\tilde{u}$, $\tilde{\tau}$, $\widetilde{u'u'}$ and $\widetilde{\tau'\tau'}$ are functions of t/T. The full representation of these time functions for all the points across the flow and all the values of the forcing amplitude and forcing frequency would be very cumbersome. Therefore, as alluded to earlier only the amplitude and phase of the fundamental Fourier mode are retained. The description of an entire function by only two numbers is acceptable in as much as the higher modes are comparatively small. This is always the case here eventhough the forcing amplitudes were large enough to generate non-linear effects. Conversely, in order to bear a fair judgement on the importance of the oscillating flow data it should be kept in mind that every point on the amplitude and phase plots summarizes an entire time dependent phase average curve.

4.2.1 Amplitude and Phase Shifts of the Velocity Oscillations

The results concerning the oscillating part of the velocity field are presented as a function of $y_S=y/l_S$. This scaling serves to emphasize coincidences with and departures of the oscillating velocity from the viscous Stokes solution. In unsteady turbulent boundary layers, the usual lenght scales as l_ν or δ would only be appropriate for the similarity of quasi-steady properties of the flow. The parameter $l_S^+=l_S/l_\nu$, however, indicates how far the viscous Stokes layer would penetrate into the turbulent boundary layer if it were unaffected by the turbulence.

The profiles of the amplitude and of the phase shift of the fundamental mode of the velocity oscillations $\tilde{u}$ for the five different forcing conditions are presented in figures 9-a and 9-b. Only the fundamental is considered because it contains most of the energy of the oscillations at all y positions. The first harmonic, for instance, is typically less than 5% of the fundamental.

The most striking result on these figures is that for the highest frequency investigated corresponding to $l_S^+=8.1$, both the amplitude and the phase shift are close to the viscous Stokes solution. Thus, a phase shift of +33° has been measured at $y_S=0.6$, while the Stokes solution for this point gives +31° and the extrapolation of the phase-shift to $y_S=0$ falls close to +45° which is characteristic of the Stokes solution.

The explanation of the behaviour of the oscillating velocity $\tilde{u}$ in the high frequency regime lies in the fact that within a distance $y^+=12$ from the wall viscous effects dominate over

turbulence effects. In steady turbulent flow, for instance the ratio of viscous to the turbulent shear stress is larger than one up to $y^+=12$. Now, the purely viscous Stokes layer has a thickness of roughly 2 l_s, since at a distance l_s from the wall the amplitude and phase of $\tilde{u}$ are respectively 85% and 70% of the values at infinity and since beyond 2 l_s the velocity oscillates essentially as a plug flow in which the oscillating vorticity is zero. Thus, when $l_s^+ \leq 6$, $\tilde{u}$ reaches the asymptotic outer values under the (nearly) sole effect molecular viscosity before the turbulence can effectively enhance the diffusion of vorticity. An equivalent argument is to consider that, if molecular viscosity should diffuse the oscillating vorticity to a distance less than 12 l_v during the period T, it is necessary that

$$(12\ l_v)^2/\nu < T$$

i.e. $l_s^+ < 6.8$. This condition is close to the one given above.

Thus, viscous diffusion alone governs the removal of unsteady vorticity from the wall for frequencies such that $l_s^+ \leq 6$. Turbulence does not participate in the diffusion, because at distances from the wall where turbulent diffusion becomes important there is no vorticity left to diffuse. Considering the qualitative nature of these arguments, it is clear that the infered upper limit of l_s^+ of 6 to 7 for purely viscous oscillating flow is only approximate. The present results which show that the viscous behaviour is well verified for $l_s^+=8.1$ as well as other observations presented below indicate that this upper limit is somewhat higher, close to 10.

It follows from the same arguments that the oscilating velocity should progressively depart from the viscous Stokes solution when l_s^+ is increased beyond this critical value. This is well born out by the results on figures 9a and b and it is particularly clear on the phase-shift which appears as a more sensitive parameter than the amplitude. It is seen that the maximum phase lead near the wall progressively decreases with increasing values of l_s^+ and becomes negative, i.e. a phase lag, at the two lowest frequencies corresponding to $l_s^+=23$ and 34. In these two flows the phase shift with respect to the centerline velocity is always less than 10°. This represents less than 3% of the cycle and stresses the need for great care in the measurements.

Although the changes in the amplitude profiles of $\tilde{u}$ are not dramatic in this representation, it is clear that at the lowest frequency for

l_s^+=34, the profile is both steeper near the wall and thicker than the Stokes profile. This is in keeping with the effect of turbulence in steady flows: it increases the shear stress in the wall region and, therefore, the viscous stress at the wall, and at the same time the large scales diffuse the vorticity to greater distances into the flow. It is seen that for l_s^+=34, there is oscillating vorticity to a distance from the wall of approximatively $y^+=y_s l_s^+=8*34=272$ while at the highest frequency of the experiments it extends only to $y^+=2*8=16$.

Eventhough the flows in the present experiments were forced with a centerline velocity amplitude of 64% , the results on the oscillating velocity agree surprizingly well with the earlier measurements (Binder&Kueny, 1981) performed in flows with small oscillation amplitudes ($a_{\tilde{uc}}$=5 or 3%). On figures 9a and 9b, there are also a few points corresponding to a forcing with $a_{\tilde{uc}}$=30 % and l_s^+=8.1. These points are close to those of the flow forced at the same frequency and at larger amplitude. It may, therefore, be concluded that, in the case of channel flow, non-linear effects due to the forcing amplitude are small up to centerline amplitudes as large as 64%. This is not exactly what might be expected at a first glance, especially if it is remembered that at the higher frequencies the local amplitudes become larger than 100% near the wall.

Attention is finally drawn to the fact that the amplitudes in the immediate neighbourhood of the wall are slightly below the Stokes curve at the highest frequencies for l_s^+=8.1 and 16. This is an apparently paradoxical result since it means that the oscillating wall shear-stress is less than the purely viscous value in turbulent channel flow! Experimental inaccuracies were first suspected, especially since near wall measurements are particlarly difficult. These points were, therefore, checked with care and this result was confirmed. This point will be further discussed in the section on the oscillations of the wall shear stress.

4.2.2 Observation of Reverse Flow

One of the more interesting consequences of the Stokes-type flow is that at sufficiently large amplitude,reverse flow without separation can occur near the wall over part of the oscillation cycle. Reverse flow appears at a given point when $\langle u \rangle < 0$ which implies that $A_{\tilde{u}} > \bar{u}$. The instanteneous profiles corresponding to l_s^+=8.1 and $a_{\tilde{uc}}$=0.64 shown on figure 10

demonstrate the existence of negative velocities at some times of the oscillation cycle.

In the near wall region where both $A_{\tilde{u}}$ and $\bar{u}$ vary linearly with y, the condition $A_{\tilde{u}}>\bar{u}$ is equivalent to $A_{\partial\tilde{u}/\partial y}>\partial\bar{u}/\partial y$ and therefore equivalent to $A_{\tilde{\tau}}>\bar{\tau}$. If it is further assumed that the oscillations follow the Stokes solution, i.e. $\tau=\sqrt{2}\,A_{\tilde{uc}}/l_s$, the condition for reverse flow is then

$$\sqrt{2}\,A_{\tilde{uc}}/l_s>\bar{u}_\tau^2/\nu$$

i.e $A_{\tilde{uc}}/\bar{u}_\tau>l_s^+/\sqrt{2}$ or $A_{\tilde{uc}}^+>l_s^+/\sqrt{2}$.

This simple criterion first derived by BK combines the amplitude and the frequency of the oscillation in one formula and shows that the occurrence of reverse flow will depend upon both parameters.

The validity of this criteria for flow reversal is amply confirmed by the experimental observations plotted on Fig. 11. These have been made with three different techniques, a frequency shifted LDA, flush mounted hot-films and flow visualizations with a hydrogene buble wire either parallel or perpendicular to the wall as well as with dye injected through a slot in the wall. It is seen that the values lying above the line $A_{\tilde{uc}}/\bar{u}_\tau=l_s^+/\sqrt{2}$ experience reverse flow as predicted by the above criterion up to $l_s^+=20$. For larger values of l_s^+, the line of separation between flows with and flows without reversal lies below the straight line of the criteria which means that flow reversal will occur for lower amplitudes than those predicted for a given l_s^+. This is consistent with the steepening of the velocity amplitude gradient at the wall produced by the turbulence at the larger values of l_s^+ which is clearly demonstrated by the measurements of the oscillating wall shear stress discussed in the next section.

The earlier observations of reverse flow of Karlsson(1959) and Jarayaman et al.(1982) also plotted on the figure are in agreement with the criteria. The observations of the latter authors are particularly interesting because they were made in a mild adverse pressure gradient and prove thus indirectly that Stokes flow may still occur in such circumstances. We have recently made similar observations in a small angle (2.4°) diffuser.

The flow reversal of the three visual observations on Fig.11 which do not conform with the criteria was probably due to turbulent fluctuations near the minimum velocity. On the other hand, the linear part of $A_{\tilde{u}}$ may extent further into the outer layer than $\overline{u^+}$ which gives an area of negative velocity in the intern part of the flow and this is not foreseeable with the criteria given above.

4. 2. 3. The Oscillation of the Wall Shear Stress

The evolutions of the amplitude $A_{\tilde{\tau}}$ and of the phase shift $\Phi_{\tilde{\tau}} - \Phi_{\tilde{u}c}$ of the oscillating wall shear stress are plotted vs. l_s^+ on figures 12a and 12b.

The amplitude is non-dimensionalized with the amplitude of the viscous Stokes stress at the same frequency i.e. $A_{\tilde{\tau}(Stokes)} = \sqrt{2}\,\mu\, A_{\tilde{u}c}/\, l_s$. The ratio $A_{\tilde{\tau}}/\, A_{\tilde{\tau}(Stokes)}$ involves thus entirely distinct quantities which, moreover, are measured with different techniques: A_τ is measured with the wall hot-film gage while $A_{\tilde{\tau}(Stokes)}$ is determined from the frequency and the centerline amplitude measured by LDA . It is recalled that the data on figure 12 was obtained by varying the frequency and the amplitude of the imposed oscillations respectively by a factor 50 and 7, and by changing the shear velocity via the centerline velocity by a factor 1.6 . It should be stressed that l_s^+ is more sensitive to changes in u_τ i.e. to the Reynolds number than in ω since it is directly proportionnal to $\bar{u}_\tau$ but only inversely proportionnal to the square root of ω. The fairly good collapse of the data points for both the amplitude and the phase shift on single curves is, therefore, physically significant and supports the claim that l_s^+ is the appropriate similarity parameter for the near wall unsteady flow.

At the higher frequencies, $l_s^+ < 10$, the amplitude of $\tilde{\tau}$ is close to the Stokes value and the frequency shift with respect to the outer velocity oscillation approaches 45° as predicted by the Stokes solution. These wall shear stress measurements do also clearly confirm the conclusion drawn from the velocity measurements, namely that in the high frequency regime the oscillating flow ignores the existence of the turbulence.

A neat confirmation of this result was recently provided by the measurements of the acoustic impedance of pneumotachographs to forced oscillations. The method of forced oscillations is a promising non-intrusive technique for the physiological investigation of the lung which does not require the cooperation of the patient who can breathe freely through a supply tube during the test. The method was developped under the restriction that the flow in the supply tube was laminar. B. Louis and D. Isabey (1990) have recently shown that this severe restriction may be relaxed and that the method is still applicable when the flow is turbulent provided that the forcing frequency is high enough to make l_s^+ smaller than 10. Their measurements show that the impedance in turbulent flow departs from the viscous values only once $l_s^+ > 10$.

It is further observed that both the amplitude and the phase shift of τ move rapidly away from the viscous limit as soon as $l_s^+ > 10$. When $l_s^+ = 20$ the phase shift is nearly zero and the amplitude is close to the quasi-steady turbulent value as discussed below.

The phase shift data of Ramaprian and Tu (1983), Mac and Hanratty(1985) of Houdeville et al. (taken in a flat plate boundary layer) is also shown on Fig. 12b. The agreement with the present measurement is quite satisfactory when it is kept in mind that 10° is less than 3% of the cycle. The phase shift vs l_s^+ curve seems thus to have a universal character. It is remarkable that this curve does not depend on the amplitude of the oscillations.

Houdeville et al. (1984) encountered serious difficulties in measuring the wall shear stress oscillations with the flush mounted hot film in air owing to the parasitic heat transfer through the substratewhich produces a considerable reduction in the frequency response. In order to minimize this unwanted transfer these authors developped a probe where a flush mounted hot-wire is placed above a small cavity. The results of these authors quoted above were obtained with such a probe. Our results obtained with a similar probe in water are shown on Fig. 13. The phase shifts measured in this way were systematically higher than those obtained with the flush mounted film. For instance, at the lowest l_s^+, phase shifts as high as 60° were obtained (Fig. 13b). A small change in the wall configuration may thus have noticeable effect on the probe response.

Close inspection of the high frequency data of Fig. 12a reveals that the amplitude ratio is systematically smaller than one at the highest frequencies. There actually is a dip in the curve around $l_s^+ = 15$. This surprizing result of a shear stress smaller than the purely viscous value - consistent with the observation made earlier on the gradient of the amplitude of the oscillating velocity near the wall- was noted before by Ronneberger and Ahrens (1977) in their investigation of pipe flow subjected to small amplitude acoustic forcing. The dip in the amplitude ratio near $l_s^+ = 11$ is unmistakable in their plot owing to the smaller scatter in their data. These authors attempt to explain this behaviour with a model which takes the effective viscosity (the molecular plus the eddy viscosity) with distance from the wall into account. Because of this increase in effective viscosity, the outward diffusing shear wave is partly reflected back towards the wall by the buffer layer and the resulting shear wave is weaker if the interference is destructive. This accounts in a qualitative way for the minimum in the $A_\tau^- / A_{\tau(\text{Stokes})}^-$ data. Indeed, if $l_s^+ < 10$ then the shear wave is already strongly attenuated when

it reaches the buffer layer and the reflected wave is weak. On the other hand, when $l_s^+ > 15$, the shear wave is enhanced by turbulent diffusion and $A_{\tilde{\tau}} > A_{\tilde{\tau}(\text{Stokes})}$. Ronneberger and Ahrens (1977) find fair quantitative agreement with their data by assuming a rigid wall at $y^+ = 15$, i.e. total reflection at this location. With the more realistic assumption of an effective viscosity where the eddy viscosity is based on the Prandtl mixing length and the formula of van Driest, the computed $A_{\tilde{\tau}} / A_{\tilde{\tau}(\text{Stokes})}$ curve does unfortunately not display a minimum. One may speculate that a time dependent eddy viscosity which could in particular be phase shifted with respect to the shear could perhaps account better for these observations.

The amplitude of the oscillating shear stress increases monotonously with l_s^+ and is larger than the Stokes value when $l_s^+ > 20$. In the present experiments values nearly three times larger than the viscous stress at the corresponding frequency have been measured. As pointed out earlier, this is due to turbulent diffusion once the oscillating layer is thick enough to penetrate into the region where turbulent diffusion dominates molecular transport.

From the relationships derived for the quasi-steady limit in section 4.1 one obtains for the amplitude of the fundamental mode:

$$\frac{A_{\tilde{\tau}(qs)}}{A_{\tilde{\tau}(\text{Stokes})}} = \frac{7}{4\sqrt{2}} \frac{1}{1 + \frac{21}{64} a^2_{\tilde{u}\tilde{c}}} \frac{\bar{u}_\tau}{\bar{U}_c} l_s^+$$

Since in the present experiments $u_\tau / U_c = 1/22$, it follows

$$\frac{A_{\tilde{\tau}(qs)}}{A_{\tilde{\tau}(\text{Stokes})}} = \frac{0.056}{1 + \frac{21}{64} a^2_{\tilde{u}\tilde{c}}} l_s^+$$

The lines for $a_{\tilde{u}\tilde{c}} \to 0$, and $a_{\tilde{u}\tilde{c}} = 0.7, 1$ are drawn on Fig. 12a. It is seen that the data is in satisfactory agreement with this simple relationship: the points for the smaller amplitudes are close to the line calculated with $a_{\tilde{u}\tilde{c}} = 0$ while the points of the 70% amplitude case fall -but for one exception- on the line corresponding to $a_{\tilde{u}\tilde{c}} = 0.7$.

4. 2. 4.) The modulation of the longitudinal turbulent intensity

The amplitude profiles of the modulation $\widetilde{u'u'}$ of the longitudinal turbulent intensity for the four flows investigated are plotted in three ways in order to illustrate different features.

The variations in the absolute level of $A_{\widetilde{u'u'}}$ across the flow and with the oscillation frequency ($a_{\widetilde{uc}}$=0.64 in all four cases) are most clearly shown by normalizing the amplitude with the constant mean shear velocity as on Fig. 14a. This representation does also facilitate comparison with the mean turbulent intensity of Fig. 6 and it is seen that amplitude profiles are similar to the mean profiles with a peak around y^+=12-15.

The most important observation is that the higher the oscillation frequency, the smaller the modulation of the turbulence is. Thus, the maximum value of $A_{\widetilde{u'u'}}$ for the highest frequency, l_s^+=8.1 is only half the value for l_s^+=24 or 34 and it tends to zero more rapidly.At the highest frequency $A_{\widetilde{u'u'}}$ is zero as soon as y^+>60 while at the lowest frequency l_s^+=34, $A_{\widetilde{u'u'}}$ is still about $5\bar{u}_\tau^2$ at y^+=100. This behaviour is amply confirmed by the modulation of the turbulent shear stress modulation that will be discussed in the next section.

The interpretation of this observation is that at the higher frequencies the turbulence can no longer follow the imposed oscillation and has an attenuated response. This contradicts some earlier ideas according to which the interaction of the imposed oscillations with the turbulence should be most intense when their frequencies are comparable as it happens when resonance occurs (Mizushina et al. 1973, Ramaprian and Tu 1983). The most energetic turbulent eddies near the wall have a frequency $\omega^+ \cong 0.1$ according to the spectra measured at y^+=15 by Compte-Bellot (1965) while the frequency of the imposed oscillations in the l_s^+=8.1 case is only 0.03. Clearly the response of the turbulence is already attenuated at frequencies lower than that energy containing eddies.

The modulation of the local relative turbulent intensity $\sqrt{A_{\widetilde{u'u'}}} / A_{\widetilde{u}}$ of Fig. 14b is reminiscent of the ratio $\sqrt{u'^2}/\bar{u}$ of the mean values. It is seen that the attenuation of the modulation of the turbulence in the high frequency case is brought out even more clearly in this representation since near the wall there is a factor three difference between the high frequency

values and those of the three other cases. The good collapse of the points of these latter flows up to $y^+=20$ is also noteworthy. There is, hence, a sharp change in the turbulence response between when l_s^+ decreases below the value 16.

Comparison of the modulation of turbulent intensity with the time mean value would be misleading in the representation of Fig. 14b. Indeed, in the quasi-steady limit $\langle u'u'\rangle/\langle u\rangle^2$ should be a function of $\langle y^+\rangle$ only. Indeed the law of the wall $\bar{u}^+=f(y^+)$ and $\sqrt{\bar{u'^2}}/\bar{u}_\tau=g(y^+)$ in steady flow yields to:

$$\frac{\overline{u'^2}}{\bar{u}^2}=\frac{g(y^+)}{f^2(y^+)}=F(y^+)$$

In the quasi steady limit one should have then

$$\frac{\langle u'u'\rangle}{\langle u\rangle^2}\ (qs)=F(\langle y^+\rangle)$$

where $\langle y^+\rangle=\langle u_\tau\rangle y/\nu$. Now F is a slowly varying function of y^+ (Eckelmann, 1974) so that for small amplitude forcing one should have:

$$\frac{\langle u'u'\rangle}{\langle u\rangle^2}\ (qs)\equiv cte$$

Hence

$$\frac{\overline{u'u'}\ (1+\widetilde{u'u'}/\overline{u'u'})}{\bar{u}^2\ (1+2\tilde{u}/\bar{u})}\equiv cte$$

i.e.

$$\frac{\widetilde{u'u'}}{\overline{u'u'}}=2\frac{\tilde{u}}{\bar{u}}$$

i.e. that the turbulence is in phase with the velocity and that

$$\frac{A_{\widetilde{u'u'}}}{\overline{u'u'}}=2\frac{A_{\tilde{u}}}{\bar{u}}\quad\text{or}\quad a_{\widetilde{u'u'}}=2a_{\tilde{u}}$$

In order to compare the turbulent intensities of the periodic and of the mean flow, one should thus consider $A_{\widetilde{u'u'}}/A_{\tilde{u}}$ and $\overline{u'u'}/\bar{u}$ or equivalently the relative amplitudes $a_{\widetilde{u'u'}}$ and $a_{\tilde{u}}$ and not the ratio with the RMS values. The plot of ratio $a_{\widetilde{u'u'}}/2a_{\tilde{u}}$ (Fig. 14c) shows again the sharp difference between high frequency and the other cases: the turbulence drops at least by a factor

and bt as much as a factor four throughout the flow in the high frequency case. It is observed that $a_{\tilde{u}'u'}/2a_{\tilde{u}}$ is closest to one in the neighbourhood of the wall but does quite reach this value. This is not surprizing considering that ONE is the quasi-steady small amplitude limit and that 34% forcing amplitude of these flows is certainly not small. One may, on the contrary, be rather surprized that the value $a_{\tilde{u}'u'}/2a_{\tilde{u}}$ is so close to ONE for such a large amplitude forcing, in other words that the turbulence response does not saturate more rapidly with the forcing amplitude.

The phase shift profiles of u'u' with respect to the velocity oscillation u, drawn on Fig. 15a, show that the modulation of the turbulence always lags behind the modulation of the velocity as in a relation between cause and effect. It is clear from this figure that the lag decreases with l_s^+ at a fixed y_s - the changes would even be sharper in terms of absolute distance or of y^+ - and that it increases with distance from the wall for a given l_s^+ at a rate that varies inversely with l_s^+.

The first feature is expected since one should approach the quasi-steady regime as the imposed frequency is decreased. Yet, that the lag still reaches 50° at $l_s^+=34$ is less evident. By comparison with $\tilde{u}$ and $\tilde{\tau}$ whose phase shifts with respect to the imposed centerline oscillations are quite small when $l_s^+>20$, it is clear that the turbulence is slower to reach the quasi-steady regime. This is somewhat similar to observations on the streamwise development of steady turbulent flows which show that the mean velocity is more rapidly established than the turbulent intensity.

The second feature , i.e. the increase of the phase lag with y^+, suggest to consider the time lag:

$$\Delta t^+ = (\Phi_{\widetilde{u'u'}}-\Phi_{\tilde{u}})\frac{1}{\omega^+} = (\Phi_{\widetilde{u'u'}}-\Phi_{\tilde{u}})l_s^{+2}/2$$

where the Φ's are expressed in radians. The plot of Δt^+ vs y^+ of Fig. 15b shows that, for $y^+>30$, the points for the four forcing frequencies are scattered about a single straight line with a slope $dy^+/d(\Delta t^+)\cong 0.4$. It appears thus, that the modulation of the turbulent intensity is propagated away from the wall with a constant speed of 0.4 wall units. This is equivalent to saying that the maximum (or the minimum) of the turbulent intensity $\widetilde{u'u'}(t/T)$ is transported away from the wall with this speed. Now, $0.5dy^2/dt$ is a diffusivity and, therefore, the

diffusivity with which the maximum/minimum of $\tilde{u}'u'$ diffuses away from the wall is:

$$v^{+}_{\tilde{u}'u'} = \frac{1}{2}\frac{d\,y^{+2}}{dt} = y^{+}\frac{d\,y^{+}}{dt} \equiv 0.4\ y^{+}$$

But this is exactly the value of the momentum eddy diffusivity v_t^+ in the logarithmic layer of the mean velocity profile. Hence $v_{\tilde{u}'u'} \equiv v_t$. Furthermore, in one point closure as the k-ε model, the transport or diffusion term in the equation of the turbulent kinetic energy k is modelled as a gradient diffusion with a diffusivity $v_k = v_t/\sigma_k$, where σ_k is an empirical constant choosen such as to optimize the agreement between experimental data and predictions in some basic shear flows. The standart value of σ_k is $\sigma_k = 1$, i.e. $v_k = v_t$ (Rodi, 1980 pp 28-29). Consequently : $v_{\tilde{u}'u'} \equiv v_k$, i.e. the modulation of the longitudinal turbulent energy in the inertial sublayer diffuses away from the wall with a diffusivity equal to diffusivity of time mean turbulent kinetic energy in the corresponding staedy wall flow. Implied in this conclusion is that most of the production of $\tilde{u}'u'$ occurs near the wall in the layer $y^+ < 30$ and that it is weak beyond. This is quite compatible with the smallness of the oscillating gradient $\partial\tilde{u}/\partial y$ once $y^+ > l_s^+$. Implied is also that the dissipation -which accounts for the decrease of $A_{\tilde{u}'u'}$ with y^+- is either sufficiently small or in phase with $\tilde{u}'u'$.

4.2.5 *Modulation of the turbulent intensity of the wall shear stress*

The data on the amplitude $A_{\tilde{\tau}'\tau'}$ and on the phase shift $\Phi_{\tilde{\tau}'\tau'} - \Phi_{\tilde{u}c}$ of the modulation of the phase averaged turbulent wall shear-stress fluctuations $\langle\tau'\tau'\rangle$ is plotted vs l_s^+ on figures 16a and 16b. Various normalizations were tried for $A_{\tilde{\tau}'\tau'}$. The most satisfactory one is $\bar{\tau}\,A_{\tilde{\tau}}$ applied in Fig. 16a rather than $\bar{\tau}^2$ as previously used by Binder et al. (1985). Indeed

$$\frac{A_{\tilde{\tau}'\tau'}}{\bar{\tau}\,A_{\tilde{\tau}}} = \frac{\overline{\tau'\tau'}}{\bar{\tau}^2}\,\frac{a_{\tilde{\tau}'\tau'}}{a_{\tilde{\tau}}} \equiv (0.35)^2\,\frac{a_{\tilde{\tau}'\tau'}}{a_{\tilde{\tau}}}$$

and $a_{\tilde{\tau}'\tau'}/a_{\tilde{\tau}}$ may be interpreted as the response of the turbulence to the forcing $\bar{\tau}$. In the quasi-steady limit $\langle\tau'\tau'\rangle/\langle\tau\rangle^2$ must be independent of time. This ratio may be written as follows after expanding:

$$\frac{\langle\tau'\tau'\rangle}{\langle\tau\rangle^2} = \frac{\overline{\tau'\tau'}}{\bar{\tau}^2}\cdot\frac{1+\widetilde{\tau'\tau'}/\overline{\tau'\tau'}}{(1+\frac{1}{2}a_{\tilde{\tau}}^2)+2\tilde{\tau}/\bar{\tau}+(\tilde{\tau}^2/\bar{\tau}^2-\frac{1}{2}a_{\tilde{\tau}}^2)}$$

Noting that

$$\overline{\tilde{\tau}^2} = A_{\tilde{\tau}}^2 / 2$$

if higher harmonics are neglected, the term 1/2 $a_{\tilde{\tau}}^2$ is added and substracted in the denominator in order to make the average variation over the cycle zero. If only the first order oscillating terms are retained, this expression becomes:

$$\frac{\langle \tau'\tau' \rangle}{\langle \tau \rangle^2} = \left(\frac{\overline{\tau'\tau'}}{\bar{\tau}^2} \right) \left(\frac{1}{(1 + \frac{1}{2} a_{\tilde{\tau}}^2)} \right) \frac{1 + \widetilde{\tau'\tau'}/\overline{\tau'\tau'}}{1 + \frac{2}{1 + \frac{1}{2} a_{\tilde{\tau}}^2} \tilde{\tau}/\bar{\tau}}$$

Quasi-steadiness of $\langle \tau'\tau' \rangle / \langle \tau \rangle^2$ requires than that the right hand side is independent of time, hence:

$$(\widetilde{\tau'\tau'})_{qs} / \overline{\tau'\tau'} = \frac{2}{1 + \frac{1}{2} a_{\tilde{\tau}}^2} \frac{\tilde{\tau}}{\bar{\tau}}$$

or

$$(a_{\widetilde{\tau'\tau'}})_{qs} / a_{\tilde{\tau}} = \frac{2}{1 + \frac{1}{2} a_{\tilde{\tau}}^2}$$

Thus in the quasi-steady limit i.e. $l_s^+ \dashrightarrow \infty$

$$\frac{(A_{\widetilde{\tau'\tau'}})_{qs}}{\bar{\tau} A_{\tilde{\tau}}} = (0.35)^2 \frac{2}{1 + \frac{1}{2} a_{\tilde{\tau}}^2}$$

Finally if we substitute $(a_{\tilde{\tau}})_{qs} = (7/4) a_{\tilde{u}}$ (see section 4.1), this expression becomes

$$\left(\frac{A_{\widetilde{\tau'\tau'}}}{\bar{\tau} A_{\tilde{\tau}}} \right)_{qs} = \frac{0,24}{1 + \frac{49}{32} a_{\tilde{u}c}^2}$$

The values of this ratio for small amplitudes and for the maximum centerline amplitude $a_{\tilde{u}c}$=0.70 are respectively 0.24 and 0.14. These values are shown on Fig. 16a. It is seen that the experimental results follow these predicted trends. Considering the approximations required and the experimental scatter in these measurement one would not expect better qualitative agreement.

The most striking feature of Fig. 16a is the sharp decline of the amplitude at the lower values of l_s^+, i.e. at the higher forcing frequencies, as was observed on the turbulent velocity fluctuations discussed in the previous section. The attenuation of the modulation of the turbulent wall shear stress fluctuation is, however, sharper than that of the velocity fluctuations: there seems to be a real cut-off at $l_s^+ \cong 10$.

Analysis of the phase shift data showed that the time lag:

$$\Delta t^+_{\tilde{\tau}'\tau'} = -(\Phi_{\tilde{\tau}'\tau'} - \Phi_{\tilde{u}c}) / \omega^+$$

was a constant irrespective of the frequency as well as of the amplitude of forcing. The plot of $(\Phi_{\tilde{\tau}'\tau'} - \Phi_{\tilde{u}c})$ vs ω^+ rather than l_s^+ is, therefore, more appropriate. Fig. 16b shows indeed a good collapse of the data points about a single straight line. The slope of this line corresponds to $\Delta t^+ = 90$. This time is smaller than the relaxation time $T_m^+ = 200$ of the model proposed by Mao and Hanratty (1985). On the other hand, according to this model, the modulation of the turbulence should begin to decrease when $T^+ < T_m^+$ i.e. once $l_s^+ < 8$. The measurements show that the response of the turbulence in the viscous sublayer starts to fall off already at $l_s^+ = 15$ and in some instances at $l_s^+ = 20$ which corresponds to forcing periods $T^+ = 700$ and $T^+ = 1200$ which are quite a bit larger than the relaxation time. This observation points into the same direction as the remark made in the previous section about the damping of $A_{\tilde{u}'u'}$ which begins at frequencies which are larger that the energy containing eddies.

4.2.6 Comparison of the frequency response of the turbulent velocity and wall shear stress fluctuations

The response of the modulation of the turbulence has been further investigated by making hot film measurements at $y^+ = 15$ where the maximum amplitude $A_{\tilde{u}'u'}$ occurs for nine different frequencies and for four amplitudes: $l_s^+ = 7.3$, 8., 9.5, 12, 16, 24, 30, 44, 60; $a_{\tilde{u}c} = 0.1$; 0.2; 0.3; 0.4. At the small values of l_s^+ (7.3 and 8) the data was only gathered at the 20% amplitude because of the mediocre measurement accuracy near or in conditions of flow reversal. Simultaneous velocity and wall shear stress measurements were performed in the 20% amplitude flows.

The responses of the turbulence at $y^+ = 15$ and at $y^+ = 0$ $a_{\tilde{u}'u'}/a_{\tilde{u}}$ and $a_{\tilde{\tau}'\tau'}/a_{\tilde{\tau}}$ is plotted on Fig. 17a. The LDV results for $a_{\tilde{u}c} = 0.64$ discussed earlier (Fig. 14) are also shown on the figure. The decrease of the response with frequency is again clearly demonstrated. Noteworthy is the grouping of the values of $a_{\tilde{u}'u'}/a_{\tilde{u}}$ vs ω^+ for the different amplitudes about a single curve when $\omega^+ > 0.008$ which points to an apparently linear dependance of the turbulence on the *local* value of the velocity oscillation and *not* on the centerline velocity. There is

obviously scatter of the data points about this curve but it should be judged by keeping in mind that the ratio $a_{\tilde{u}'\tilde{u}'}/a_{\tilde{u}}$ involves four different quantities. The larger scatter at low forcing frequencies may indicate a contrario that other factors beside $a_{\tilde{u}}$ influence the modulation of turbulence.

It is seen on Fig. 17a that the response of the turbulent wall shear stress fluctuations differs from that of the turbulent velocity fluctuations at $y^+=15$, namely it begins to decline at lower forcing frequencies and decreases more rapidly with ω^+. In the quasi-steady regime and in the small amplitude approximation one should have:

$$a_{\tilde{\tau}'\tilde{\tau}'} = 2\, a_{\tilde{\tau}}$$

The value $a_{\tilde{\tau}'\tilde{\tau}'}/a_{\tilde{\tau}}=1.75$ at the lowest frequency in the $a_{\tilde{U}C}=0.20$ case is thus close to the quasi-steady limit.

Another representation of the same data is shown on Fig. 17b where the relative amplitudes of the turbulence modulation are normalized with the corresponding quasi-steady values. $a_{\tilde{\tau}'\tilde{\tau}'(qs)}$ has been computed from the relationship developped in the previous section. The relative amplitude of the modulation $a_{\tilde{u}'\tilde{u}'(qs)}$ at the fixed position $y^+=15$ is computed by assuming that the distribution $\langle u'u'\rangle/\langle u_\tau^2\rangle = f(\langle y^+\rangle)$ is independent of time- which implies zero phase shift between $\langle u'u'\rangle$ and $\langle\tau\rangle$- and is the same as in steady flow. For convenience we write $\langle y^+\rangle = y\langle u_\tau\rangle/\nu$. Since $\langle y^+\rangle$ varies during the cycle, $\langle u'u'\rangle$ varies as the product $f(\langle y^+\rangle)\langle u_\tau^2\rangle$. Thus, if during the cycle the representative point stays on a portion of the f vs y^+ curve where f is either an increasing, a constant or a decreasing function of y^+, than $a_{\tilde{u}'\tilde{u}'}$ is either larger, equal or smaller than a_τ. For instance near the wall in the region $y^+<12$ where $\sqrt{\bar{u'u'}}/\bar{u}_\tau \propto y^+$, one obtains if $\langle y^+\rangle < 12$ at all times:

$$\langle u'u'\rangle \propto \langle u_\tau^2\rangle\langle y^{+2}\rangle \propto \langle u_\tau^4\rangle$$

i.e. $a_{\tilde{u}'\tilde{u}'(qs)} \cong 2a_{\tilde{\tau}(qs)}$. On the other hand , about the mean position $y^+=15$ of interest here which is on the decreasing portion of f, $a_{\tilde{u}'\tilde{u}'(qs)} \cong 0.8 a_{\tilde{\tau}(qs)}$. The $\sqrt{\bar{u}'^2}/\bar{u}_\tau$ vs y^+ distribution measured by Alfredsson and Johansson (1982) was used to for the computation of $a_{\tilde{u}'\tilde{u}'(qs)}$. The distribution in the range $0<y^+<50$ was divided into three parts and a least square linear approximation was fitted to each.

The plot of Fig 17b which shows trends very similar to those of Fig. 17a serves to emphasize the fact that the modulation of the turbulence is a monotonously decreasing function of the forcing frequency. Also shown on this figure are the measurements of Finnicum and Hanratty (1988) obtained with the eloctrochemical technique. The values of $A_{\sqrt{<\tau'\tau'>}}/\bar{\tau}$ of these authors have been converted to $a_{\tilde{\tau}'\tilde{\tau}'}/\ a_{\tilde{\tau}'\tilde{\tau}'(qs)}$ by making the linear assumption which yields $a_{\sqrt{<\tau'\tau'>}}=(1/2)a_{\tilde{\tau}'\tilde{\tau}'}$ and the assumption $a_{\tilde{\tau}'\tilde{\tau}'(qs)}=4a_{\tilde{u}_c}$. It is seen that the results of these authors agree remarkably well with the present ones. The small increase in the lower frequency range in a few cases as for a_{uc} are smaller than the experimental uncertainty and therefore not significant. The increase in the modulation of the turbulence observed by Shemer et al.(1985) is, therefore, not confirmed by the present measurements. These authors do, however, qualify their conclusion by pointing out that the absolute differences due to changes with the forcing frequency were always small. The contradiction between the two sets of observations may, hence, be more apparent than real.

The differences in the amplitude response of $<\tau'\tau'>$ and $<u'u'>$ pointed out on Fig. 17a are even more contrasted on Fig. 17b. The lower frequency response of $\tilde{\tau}'\tilde{\tau}'$ with respect to that of $\tilde{u}'\tilde{u}'$ implies a larger relaxation time of the turbulence in the immediate vicinity of the wall as compared to that in the buffer layer. Another manifestation of the relaxation time is the delay between the turbulence modulations and the oscillations of the corresponding quantities which at first sight may be considered as the forcing terms. The time delays inferred from the phase shift data of Fig 17c are coherent with the conclusion drawn from the amplitude response, namely that the time lag of $\tilde{\tau}'\tilde{\tau}'$ with respect to $\tilde{\tau}$ is about twice as large as the lag of $\tilde{u}'\tilde{u}'$ with respect to $\tilde{u}$ at a given frequency. This figure also shows two distinct frequency regimes already alluded to in the previous section (Note that on Fig. 16b the maximum frequency is only $\omega^+=0.02$ and that the phase shift is with respect to $<U_c>$ and not with respect to $<\tau>$ as on Fig. 17c, the difference in the phase shift on the two figures corresponds therefore to the phase lead $\Phi_{\tilde{\tau}}-\ \Phi_{\tilde{u}_c})$ .In the high frequency regime $\omega^+>0.025$, the time lag is roughly half that in the lower one $\omega^+<0.015$.

It may be remarked that the end of this low frequency regime corresponds to $l_s^+=12$ which is close to value $l_s^+=10$ where the oscillating field deviates from the Stokes solution. Even more relevant may be the observation that the beginning of the high frequency regime is close to the average bursting frequency in steady flow $\omega_b^+=2\pi f_b^+=0.036$ (Bogard

& Tiederman, 1986; Coughran & Bogard 1987). It is not really unexpected that the turbulent response changes when the forcing cycle becomes shorter than the interval between the events which are responsible for a large part of the turbulence production.

The reason why the turbulence modulation in the viscous sublayer has a relaxation time that is 2 to 3 times larger than in the buffer layer is an open question. In the present work only the global response of the turbulence has been investigated. Some insight into the question would possibly be gained by analysing the spectral contents of $\langle u'u' \rangle$ and $\langle \tau'\tau' \rangle$ for different forcing frequencies. This could be done by frequency filtering the signal prior to the phase averaging. To perform such an analysis would obviously be an enormous task that is beyond the scope of this paper. As a first step, however, some characteristics of the small turbulent scales have been extracted from the u'(t)- signal. These results are described in the next section.

4.3) Modulation of the small scales

The Taylor micro scale and the zero crossing frequency, the skewness and the flatness factors of the time derivative du'/dt have been determined at $y^+=15$ in flows forced with an amplitude $a_{UC}=20\%$ and at $l_s^+=7.2$, 9.5, 12., 16., 30., 60.

The instanteneous turbulent fluctuation $u'(t)=u(t)-\langle u(t) \rangle$ was computed after $\langle u \rangle$ was obtained, stored on the disk of the NORSK-100 computer and processed in various ways. The time derivative was obtained with a 32 point finite impulse response zero phase shift filter. The cut-off frequency of the digital derivator was set at $f^+=1$ in order to avoid noise contamination of the skewness and flatness factors of du'/dt (Kuo&Corrsin, 1971).

The "dead-band" effect on the zero crossing frequency (due to the presence of noise which produces spurious crossings) was checked in one case by measuring the crossing frequency four increasing levels $L\sqrt{\langle u'u' \rangle}$. This frequency reached a plateau near L=0 showing that the S/N was adequate. The same conclusion was reached by varying the cut-off frequency of the filter.

The phase averages of the zero-crossing frequency $\langle N_0 \rangle$ of the turbulent intensity $\langle u'^2 \rangle$ and of the moments $\langle (du'/dt)^n \rangle$ with n=2,3 and 4 were determined. These phase averages are statistically well converged as shown on the examples on Fig. 18.

For a gaussian signal the time scale based on the zero crossing frequency N_0 : $\langle\Lambda\rangle = 1/(2\pi\langle N_0\rangle)$ is the same as the Taylor micro scale λ: $\langle\lambda^2\rangle = \langle u'^2\rangle / \langle (du'/dt)^2\rangle$ (Liepmann, 1949). It was experimentally established by Liepmann (1949) and Sreenivasan et al.(1983) that the equality $\bar{\lambda}=\bar{\Lambda}$ still holds for near wall turbulence in steady flow despite its non gaussian character. Fig. 19 and 20 show that this is also true in unsteady flow since the time mean values of the amplitudes and of the phase shifts of $\tilde{\Lambda}$ and $\tilde{\lambda}$ remain close when the forcing frequency is varied. This agreement is rather remarkable considering that the methods for determining $\tilde{\lambda}$ and $\tilde{\Lambda}$ are completely independent. It shows that the methods used are basically correct.

It is seen that time mean value of the micro-scale $\tilde{\lambda}$ (Fig. 19) is quite insensitive to the forcing over the investigated frequency range. For the cyclic variations of the micro-scale, it may first be remarked that in the quasi-steady regime the scaled values $\langle\lambda^+\rangle$ should be independent of time i.e. $\langle\lambda^+\rangle=\bar{\lambda}^+$,if the variations due to those of the position $\langle y^+\rangle$ may be neglected. This is in effect the case, because as shown by Sreenivasan et al. (1983) Λ determined from τ' is the same as Λ determined from u' in the buffer layer. Hence if the inner scaling is true:

$$\langle\lambda\rangle=\bar{\lambda}^+\frac{\nu}{\langle\tau/\rho\rangle}=\bar{\lambda}\frac{1}{\langle\tau\rangle/\bar{\tau}}$$

and if the amplitudes are small

$$1+\tilde{\lambda}/\bar{\lambda}=\frac{1}{1+\tilde{\tau}/\bar{\tau}}\cong 1-\tilde{\tau}/\bar{\tau}$$

Hence in the quasi steady small amplitude limit one should have with inner scaling:

$$a_{\tilde{\lambda}}=a_{\tilde{\tau}} \qquad \Phi_{\tilde{\lambda}}-\Phi_{\tilde{\tau}}=180°$$

Figure 20 shows that this is well born out by the measurements - despite the fact $a_{\tilde{\tau}(qs)}=2a_{\tilde{u}c}$ is not very small - when $l_s^+>30$. It is seen that the phase of $\tilde{\lambda}$ remains nearly in opposition with the phase $\tilde{\tau}$ over the whole frequency range. The amplitude ratio $a_{\tilde{\lambda}}/a_{\tilde{\tau}}$, on the contrary decreases sharply when the forcing frequency is increased with a minimum value of about 0.3 at $l_s^+=10$.

The micro-length scale λ_x may be inferred from the time scale by the Taylor hypothesis $\lambda_x = \bar{u}\,\lambda$, assuming that the convection velocity of the small scales is the local mean

velocity. In unsteady flow the Taylor hypothesis should be written with the phase averaged velocity: $dx=-\langle u\rangle\, dt$ so that

$$\left\langle\left(\frac{du'}{dx}\right)^2\right\rangle=\left\langle\left(\frac{du'}{\langle u\rangle dt}\right)^2\right\rangle=\frac{1}{\langle u\rangle^2}\left\langle\left(\frac{du'}{dt}\right)^2\right\rangle$$

and hence $\langle\lambda_x\rangle=\langle u\rangle\langle\lambda\rangle$

Thus

$$\bar{\lambda}_x\left[1+a_{\lambda x}\cos(\omega t+\Phi_{\lambda x}-\Phi_\tau)\right]=\bar{u}\,\bar{\lambda}\left(1+a_u\cos(\omega t+\Phi_u-\Phi_\tau)\right)\left(1+a_\lambda\cos(\omega t+\Phi_\lambda-\Phi_\tau)\right)$$

This shows that $(\bar{\lambda}_x)_{unst}=(\bar{\lambda}_x)_{st}$ since both $\bar{u}$ and $\bar{\lambda}$ are not modified by forcing. Further more, by noticing that at $y^+=15$, $(\Phi_u-\Phi_\tau)$ is generally small and by making the use of the result $\Phi_\lambda-\Phi_\tau\equiv 180°$ and by assuming that the amplitudes are small the above relation simply yields:

$$a_{\lambda x}\equiv|a_\lambda-a_u|$$

The amplitude of the micro length scale varies thus due to the combined effects of the forcing on the micro time scale and of the convection velocity. In order to find out what the relative contribution of each one is, it is best to express both in terms of the centerline amplitude in the high frequency (HF) and low frequency (LF) regime. For a_u, we have at

- HF : $a_u\equiv 2a_{uc}$ since at $y^+=15$ $A_u=A_{uc}$ and $\bar{u}\equiv 1/2\ \bar{U}_c$.

- LF : $a_u\equiv a_{uc}$ since at $y^+=15$ $\langle u\rangle=\langle u_\tau\rangle f(\langle y^+\rangle)\equiv\langle u_\tau\rangle$

(because $f(\langle y^+\rangle)\equiv f(y^+)\left(1+\dfrac{f'(15)}{f(15)}\cdot\dfrac{\tilde{u}_\tau y}{\nu}\right)$

$\dfrac{f'(15)}{f(15)}=\dfrac{0.6}{11}<<1$

For a_λ, we deduct the value from the ratio a_λ/a_τ of Fig. 20b, so we need the relation between a_τ and a_{uc}. At

-HF $\qquad a_\tau=\sqrt{2}\,\dfrac{\bar{U}_c}{u_\tau}\,\dfrac{a_{uc}}{l_s^+}=31\,\dfrac{a_{uc}}{l_s^+}$ (see section 4.2.3)

- LF $a_\tau\equiv(7/4)\ a_{uc}$.

Combining these results yields:

at HF ($l_s^+<10$) $\quad \tilde{a}_{\lambda x} = \left| \frac{31}{l_s^+} \frac{\tilde{a}_\lambda}{\tilde{a}_\tau} - 2 \right| \tilde{a}_{uc}$

at LF ($l_s^+>30$) where $\tilde{a}_\lambda = \tilde{a}_\tau \quad \tilde{a}_{\lambda x} = \frac{3}{4} \tilde{a}_{uc}$

Thus at LF the contribution of $\tilde{a}_\lambda$ to $\tilde{a}_{\lambda x}$ is nearly twice that $\tilde{a}_u$. On the other hand at HF the factor $31\, \tilde{a}_\lambda / \tilde{a}_\tau l_s^+$ which is the contribution of $\tilde{a}_\lambda$ is minimum when $\tilde{a}_\lambda / \tilde{a}_\tau$ is minimum since this ratio increases rapidly when l_s^+ exceeds 10 as shown by Fig. 20b. From the measured values of this figure, it follows that $(31\, \tilde{a}_\lambda / l_s^+ \tilde{a}_\tau)_{ls+=10} \equiv 1$. Thus $(\tilde{a}_\lambda / \tilde{a}_u)_{min} = 1/2$ which means that at $l_s^+ = 10$ the modulation of $\tilde{\lambda}_x$ is mainly due to the convection velocity and $\tilde{a}_{\lambda x} = \tilde{a}_{uc}$. The conclusion is that $\tilde{\lambda}_x$ is mostly modulated with an amplitude which is of the same order as that of the centerline velocity. The forcing is, therefore, felt in the small scales of the turbulence. In short, the modulation of the microscale $\tilde{\lambda}_x$ comes manily from the convection velocity at HF and manily from the microscale λ at LF. In the range $10<l_s^+<30$, there should hence be a frequency when the two contributions to $\tilde{a}_{\lambda x}$ balance and for which $\tilde{\lambda}_x$ should be zero or at least small. One may further remark that when $l_s^+<10$ $\tilde{a}_\lambda / \tilde{a}_u$ will increase again with decreasing l_s^+; actually at $l_s^+=7$ $\tilde{a}_\lambda / \tilde{a}_u = 1.1$, so the $\tilde{a}_{\lambda x}$ is zero again close to $l_s^+=7$. $\tilde{a}_{\lambda x}$ varies thus rapidly in the range l_s^+ (7;30).

Another aspect of the small turbulence scale is represented by the skewness S of du'/dt because it is directly related to the vorticity/ dissipation production which is composed of terms like $(\partial u'/\partial x)^3$. It is indeed easily seen that $<S>(\partial u'/\partial t) = -<S>(\partial u'/\partial x)$ because of the normalization with the variance so that the convection velocity does not intervene. The mean value of <S> is about 0.85 (Fig.21) and compares well with the data of Ueda and Hinze (1975) taken in steady flow. As for other quantities, the time mean skewness is not affected by the forcing.

For the discussion of the modulation of $\tilde{S}$ let us first remark that this is a structure parameter independent of any scaling and that it is independent of the Reynolds number provided this number is large enough (Kuo and Corrsin, 1971). Since at low frequency the forcing affects the phase averages only via the changes of the centerline velocity and the changes of the Reynolds number, and since the profile of S is flat around $y^+=15$ in quasi-steady flow (Ueda and Hinze, 1975), it may be expected that <S> is not modulated in this case. This is well born

out by the measurements, since the amplitude $a_{\tilde{S}}$ is effectively zero when $l_s^+ = 60$ as shown on Fig. 22. The constancy of $\tilde{S}$ during the cycle implies that $\langle(\partial u'/\partial t)^3\rangle$ varies exactly in the same way as $(\langle(\partial u'/\partial t)^2\rangle)^{3/2}$ which is effectively modulated as low frequency as was seen above in the discussion of the micro scale. At high forcing frequencies $a_{\tilde{S}}$ reaches values of the order of 10% i.e. $0.5a_{\tilde{uc}}$. This may appear to be a small modulation at first sight but in view of the preceeding discussion it is quite significant since it reveals a change in the internal structure of the small scale turbulence. The amplitude $a_{\tilde{S}}$ seems to pass through a maximum at $l_s^+ = 12$. With due caution on account of the small number of data points, of the small relative variations of <S> and of the experimental uncertainty, the same critical value of the frequency parameter is found again.

The flatness factor of $\partial u'/\partial t$ is related to a sort of intermittency of the turbulence. It may be seen on Fig. 21 that the time average value is about 6.6 and compares well again with the steady flow data at $y^+ = 15$ of Ueda and Hinze (1975). The modulation amplitude of <F> (Fig. 22) varies in the same manner with the forcing frequency as that of <S>. The remarks made above concerning the low and high frequency behaviour of <S> are also relevant for the flatness factor.

5.)Conclusion

The data on unsteady turbulent channel flow discussed in this paper has been acquired by making use of several experimental techniques and covers a significant range of forcing amplitudes and frequencies. It confirms that all the time mean characteristics -with the sole exception of the turbulent intensity in the inertial sublayer- are not affected by the forcing even when the amplitude and the frequency are high enough to produce periodic flow reversal near the wall. The similarity of the oscillating velocity field u and of the oscillating wall shear stress τ when the non dimensional Stokes length l_s^+ (or equivalently the forcing frequency ω^+ expressed in wall units) is constant is also confirmed. It is shown that these periodic oscillations are affected by the turbulence only when $l_s^+ > 10$.

The turbulence itself is modulated by the forcing as may be evidenced from the phase averages $\langle u'u'\rangle$ and $\langle \tau'\tau'\rangle$. The variations of the turbulence modulation across the flow

show that it diffuses away from the wall with a diffusivity that is very close to the eddy diffusivity in the inertial sublayer. This suggests that a large part of the u'u'-modulation is produced in the buffer layer where also most of the mean turbulence energy is produced. The frequency response of $\widetilde{u'u'}$ at $y^+=15$ and of $\widetilde{\tau'\tau'}$ decays when the forcing frequency increases once $l_s^+<20$. Moreover $\widetilde{\tau'\tau'}$ decays sooner and faster than $\widetilde{u'u'}$, showing that the relaxation time of the turbulence that filters to the wall is about two to three times larger than that in the buffer layer. Similar conclusions are reached from the time lags between the modulation of the random turbulent fluctuations and the oscillations of the corresponding deterministic quantities. These time lags are 75 and 130 wall units respectively for $\widetilde{u'u'}$ and $\widetilde{\tau'\tau'}$ when $\omega^+<0.012$, i.e. $l_s^+>13$. They decrease by nearly a factor two once $\omega^+>0.025$. It may be noted that this value approaches the bursting frequency of the mean flow $\omega_b^+=0.036$.

The forcing propogates to the small scales of the turbulence as may be evidenced from the cyclic variations of the Taylor micro scale and from the skewness factor of $\partial u'/\partial t$.

The evolution of several parameters reveal that critical changes in the turbulence occur in the range $l_s^+=10$ to 13 i.e. $\omega^+=0.012$ to 0.02. As was pointed out this upper frequency approaches the mean bursting frequency. It may also be speculated that there is an optimal interaction of the oscilating flow with the turbulence in the buffer region in this frequency range since at higher frequencies this region oscillates as a plug flow with zero or small oscillating shear and at lower frequencies the quasi-steady regime is approached.

Simple quasi-steady analysis combined with the linearity assumption predicts many low frequency behaviours remarkably well and gives at least the right trend when the forcing amplitudes are large. It allows then to show saturation effects, as on the modulation of $\tau'\tau'$ whose amplitude in the linear quasi-steady limit is four times the centerline amplitude. The quasi-steady regime is reached as soon as l_s^+ exceeds 30.

It must be emphasized that the present results concern unstaedy channel flow while in most practical situations one has to deal with boundary layers and furthermore with boundary layers in pressure gradients. From the agreement of some unsteady boundary layer results with the present data and from the fairly universal character of the turbulent flow near the wall - not withstanding some recent observations to the contrary - one may expect unsteady turbulent boundary layers to behave much as channel flows in the inner layer. This does evidently not preclude the existence of substantial differences in the unsteady behaviours of the

outer flows due to the loss of the streamwise homogeneity, and the intermittency in the wake region where the presence of the wall is felt only weakly.

Acknowledgments

This work was supported in part by the European Office of the U.S. Army Research Development and Standardization Group (contract DAJA 45-87-C-001) and monitored by Dr. R.E. Reichenbach. During part of this work R.F. Blackwelder was on leave from USC and supported as Professeur Associé by the Institut National Ploytechnique de Grenoble. This support is greatfully acknowledged.

References

ACHARYA M., 1975 " Measurements and Predictions of a Fully Developped Turbulent Channel Flow with Imposed Controlled Oscillations, PhD Thesis, Stanford Univ. Dept. Mech. Engineering

BLACKWELDER, R.F.; HARITONIDIS, J.H., 1983 " Scaling of the Bursting Frequency in Turbulent Boundary Layers" J. Fluid Mech., 132, 87

BINDER, G. ; KUENY, J.L. , 1981 "Measurements of the Periodic Velocity Oscillations Near the Wall in Unsteady Turbulent Channel Flow" , Unsteady Turbulent Shear Flows,ed. by Michel et al., Springer Verlag.

BINDER, G. ; TARDU, S. ; BLACKWELDER R.F. ; J.L. , KUENY , 1985 "Etude Expérimentale de Couches Limites Turbulentes Instationnaires Soumises à des Gradients de Pression Moyens Nuls ou Positifs" , Agard Symposium on Unsteady Aerodynamics-Fundamentals and Applications to Aircraft Dynamics; Conference Proceedings No.386

BINDER, G. ; TARDU, S. ; BLACKWELDER R.F. ; J.L. , KUENY , 1985 "Large Amplitude Periodic Oscillations in the Wall Region of a Turbulent Channel Flow",Proceedings of the Fifth Symposium on Turbulent Shear Flows, Cornell University,U.S.A 1985.

BOGARD,D.G.; TIEDERMAN, W.G., 1986 "Burst Detection with Single Point Velocity Measurements" J. Fluid Mech. 162, 389

CARR,L.W. ,1981 "A Review of Unsteady Turbulent Boundary-Layer Experiments" , NASA Technical Memorendum 81297.Also in Unsteady Turbulent Shear Flows,ed. by Michel et al., Springer Verlag.

CHAMBERS, F.W., MURPHY, H.D., McELIGOT, D.M., 1983, " Lateraly Converging Flow Part 2 Temporal Wall Shear Stress", J. Fluid Mech. , 127, 403

COMPTE-BELLOT, G. 1965 "Ecoulement Turbulent entre deux Parois Parallèles" Publications Scientifiques et Techniques de l'Air.

COUGHRAN, M.T.; BOGARD, D.G., 1987 "An Experimental Study of the Burst Structure in a LEBU-Modified Boundary-layer" 10th Symposium on Turbulence, Rolla, Missouri, September 1987, 45-1

COUSTEIX, J. ; HOUDEVILLE, R. ; JAVELLE J. 1977 "Structure and Developpment of a Turbulent Boundary Layer in an Oscillatory External Flow" , Proceedings of the First Symposium on Turbulent Shear Flows, Pennsylvania State University, U.S.A 1977.

COUSTEIX, J. ; JAVELLE, J. ; HOUDEVILLE R. 1981 "Influence of Strouhal Number on the Structure of Flat Plate Turbulent Boundary Layer" ,Proceedings of the Third Symposium on Turbulent Shear Flows,University of California,Davis,U.S.A 1981

COUSTEIX, J. ; HOUDEVILLE, R. 1985 "Turbulence and Skin Friction Evolutions in an Oscillating Boundary Layer" , Proceedings of the Fifth Symposium on Turbulent Shear Flows , Cornell University,U.S.A 1985.

ECKELMANN,H.,1974 "The Structure of the Viscous Sublayer and the Adjacent Wall Region in a Turbulent Channel Flow",J.Fluid Mechanics 132,87.

FINNICUM, D.S. ; HANRATTY T.J. 1988 " Effect of Imposed Sinusoidal Oscillations on Turbulent Flow in a Pipe" PCH PhysicoChemical Hydrodynamics, 10,N° 5/6, 585

HOUDEVILLE R., JULLIEN J.E., COUSTEIX J., 1984 "Mesure du Frottement Pariétal par Jauges à Elements Chauds" La Recherche Aérospatiale, 1984-1

KAIPING P.,1983 "Unsteady Forcrd Convective Heat Transfer from a hot film in Non-reversing and Reversing Shear Flow" Int. J. Heat and Mass Transfer, 26, 4, 545

KARLSSON, K.F. 1959 "An Unsteady Turbulent Boundary Layer" J. Fluid Mechanics, 5 , 622.

KIM J., MOIN, P., MOSER R., 1987 " Turbulence Statistics in Fully Developped Channel Flow at Low Reynolds Number" J. Fluid Mech. 177, 133

KUO, A.Y.S.; CORRSIN, S., 1971, "Experiments on Internal Intermittency and Fine-Structure Distribution Functions in Fully Turbulent Flow" J. Fluid Mech., 50, 285

LIEPMANN, H.W., 1949, "Die Anwendung eines Satzes über die Nullstellen Stochastishcer Funktionen auf Turbulenzmessungen" Helv. Phys. Acta, 22, 119

LOUIS, B. ; ISABEY, D., 1990 "Impedance of Laminar Oscillatory Flow Superimposed on a Continuous Turbulent Flow" , Application to respiratory impedance measurements in Respiratory Biomechanics, Ed. EPSTEIN and LIGAS, pp. 57-64, Springer.

MAO, Z-X.; HANRATTY, T.J., 1986 "Studies of the Wall Shear Stress in a Turbulent Pulsating Pipe Flow" J. Fluid Mech., 170, 545

McLAUGHLIN, D.K.; TIEDERMAN, W.G.,1973, "Biasing Correcting for Individual Realization of Laser Anemometer Measurements in Turbulent Flows", Phys. of Fluids,16, 2082

MIZUSHINA, T. ; MARUYAMA ; SHIOZAKI, Y. 1973 "Pulsating Turbulent Flow in a Tube" J. Chem. Engr. Japan,6, 487.

MIZUSHINA, T. ; MARUYAMA ; HIPASAWA, H. 1975 "Structure of the Turbulence in Pulsating Pipe Flows" J. Chem. Engr. Japan,8, 210.

PARIKH, P.G., REYNOLDS, W.C., JAYARAMAN, R., CARR, L.W. 1981, "Dynamic Behaviour of an Unsteady Turbulent Boundary Layer", Proc.IUTAM Symp. on "Unsteady Turbulent Shear Flows"Toulouse May 5-8, 1981

PEDLEY, T.J., 1976 "Heat Transfer from a Hot Film in Reversing Shear Flow" J. Fluid Mech.,78, 513

RAMAPRIAN,B.R. ; TU, S.W., 1983 , "Fully Developped Periodic Turbulent Pipe Flow", J. Fluid Mechanics,137, 31 .

RODI, W., 1980, "Turbulence Models and their Application in Hydraulics- A State of the Art Review" Int. Association of Hydraulic Research Monograph. Delft, the Netherlands, 1980

RONNEBERGER, D. AHRENS, C.D. , 1977 "Wall Shear Stress Caused by Small Amplitude Perturbations of Turbulent Boundary-Layer Flow:An Experimental Investigation" J. Fluid Mechanics, 83, 433 .

SHEMER, L. ; WYGNASKI, E.K. ; KIT E. ,1985 "Pulsating Flow in a Pipe" J.fluid Mechanics,153, 313.

SPENCE D.A., BROWN G.L., 1968 "Heat transfer to a Quadratic Shear Profile" J. Fluid Mech. 33, 753

SREENIVASAN, K.R.; PRABHU A.; NARASIMHA R., 1983, "Zero-crossings in Turbulent Signals" J. Fluid Mech., 137, 251

TARDU, S.; BINDER G., BLACKWELDER R.F., 1986 " An Experimental Investigation of LDA Bias Using a Large Amplitude Oscillatory Channel Flow" Third International Symposium on Applications of Laser Anemometry to Fluid Mechanics, Lisbon, Portugal

TARDU S., 1988 " Ecoulement Turbulent Instationnaire près d'une paroi; Réponse des Structures Turbulentes", PhD Thesis, Un. Joseph Fourier, Grenoble I.

UEDA, H.; HINZE, J.O., 1975, "Fine-Structure Turbulence in the Wall Region of a Turbulent Boundary Layer" J. Fluid Mech., 67, 125

WEI T., WILLMARTH W.W., 1989 " Reynolds-number Effects on the Structure of a Turbulent Channel Flow" J. Fluid Mech. 204, 57

station	l_s^+	f^+	$\bar{U}_c$	$a_{\tilde{u}c}$	$\bar{\tau}_{unst}/\bar{\tau}_{st}$	$\sqrt{\bar{\tau}'\tau'}/\bar{\tau}$	$a_{\tilde{\tau}'\tilde{\tau}}/a_{\tilde{\tau}}$	$\phi_{\tilde{\tau}}-\phi_{\tilde{u}c}$	$\phi_{\tilde{\tau}'\tilde{\tau}'}-\phi_{\tilde{u}c}$	$a_{\tilde{\tau}}/a_{\tilde{u}c}$
1	17,9	$9{,}9345*10^{-4}$	17,63	0,31	0,92	0,38	1,85	9,12	-25,10	1,82
2	17,9	$9{,}9345*10^{-4}$	17,63	0,31	0,90	0,39	1,90	7,11	-26,05	1,71
3	17,9	9,9345*10-4	17,63	0,31	0,91	0,40	1,90	10,40	-24,82	1,71
4	17,9	9,9345*10-4	17,63	0,31	0,96	0,40	1,78	10,54	-23,36	1,80
1	12,9	1,9069*10-3	9,54	0,08	0,96	0,34	1,89	43,80	-40,70	1,62
2	12,9	1,9069*10-3	9,54	0,08	0,99	0,31	1,74	30,45	-34,27	1,60
3	12,9	1,9069*10-3	9,54	0,08	1,05	0,27	2,15	42,62	-57,72	1,60
4	12,9	1,9069*10-3	9,54	0,08	0,97	0,30	2,31	47,25	-56,45	1,66
1	4,6	1,5043*10-2	15,77	0,40	0,98	0,39	0,36	22,76	-339,55	3,61
2	4,6	1,5043*10-2	15,77	0,40	1,00	0,35	0,37	18,34	-343,03	3,45
3	4,6	1,5043*10-2	15,77	0,40	1,03	0,38	0,32	19,61	-341,87	3,59
4	4,6	1,5043*10-2	15,77	0,40	0,94	0,41	0,31	16,75	-342,58	3,55
1	2,9	3,7849*10-2	13,38	0,67	0,96	0,41	0,34	31,43	-324,4	2,24
2	2,9	3,7849*10-2	13,38	0,67	1,08	0,36	0,37	23,95	-332,48	2,26
3	2,9	3,7849*10-2	13,38	0,67	1,01	0,35	0,36	22,09	-330,76	2,28
4	2,9	3,7849*10-2	13,38	0,67	1,09	0,39	0,38	23,98	-332,87	2,37

Table-1) Flow conditions at four streamwise locations for several imposed frequencies and amplitudes.

	l_s^+	$a_{\widetilde{uc}}$
■	8.1	0.64
◆	8.1	0.30
+	16	0.64
▲	23	0.64
×	34	0.64
□	Steady Flow	
▪	Eckelmann (1972) Steady Channel Flow	

Table 2 Experimental conditions and corresponding symbols. Measurement of velocity and turbulent intensity profiles.

	$\overline{U}_c$(cm/s)	$a_{\widetilde{uc}}$	T (s)
▲	28.5	0.13	2.6-33
×	19.0	0.19	3-31
◆	30.0	0.27	2.6-61
◈	30.0	0.17	2.6-61
□	30.0	0.10	2.6-15
■	18.5	0.70	4-132
▲	16-26	0.60	6
o	Houdeville et al.(1984)		
●	Menendez and Ramaprian(1983)		
▪	Mao and Hanratty(1986)		

Table 3) Measurement of the wall shear stress and its turbulent fluctuations

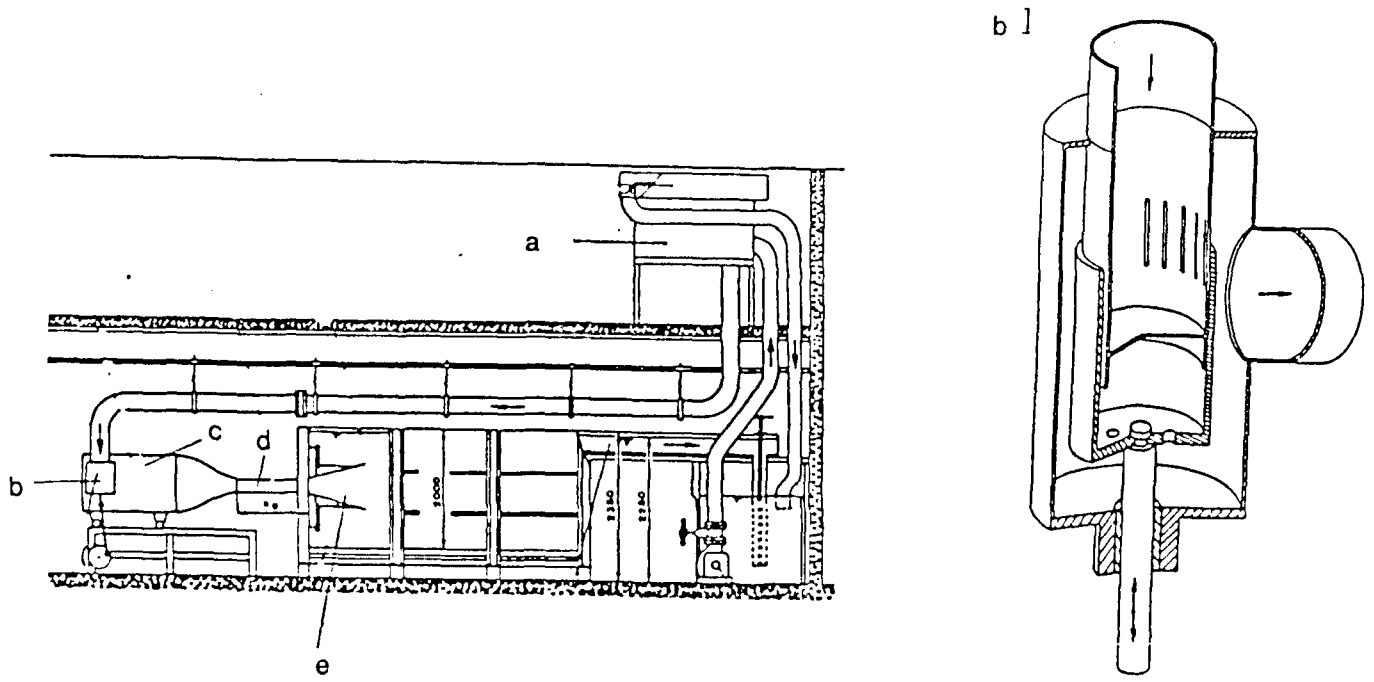

Figure 1 The water channel and pulsating device
a)Constant head tank b) Pulsating device c) Setting chamber d) Channel e) Test section

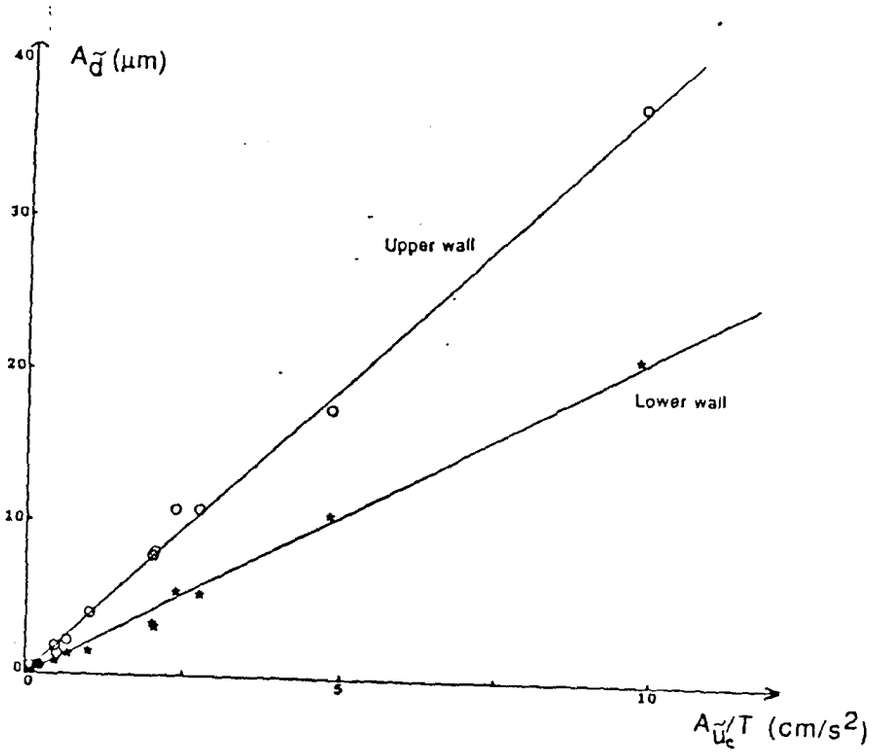

Figure 2 Amplitude of the periodic wall deflections produced by the oscillating pressure

a)

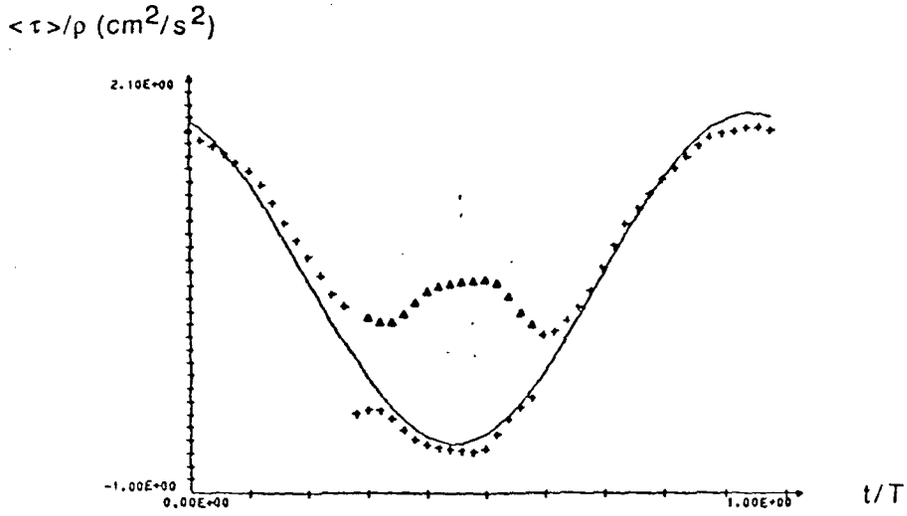

b

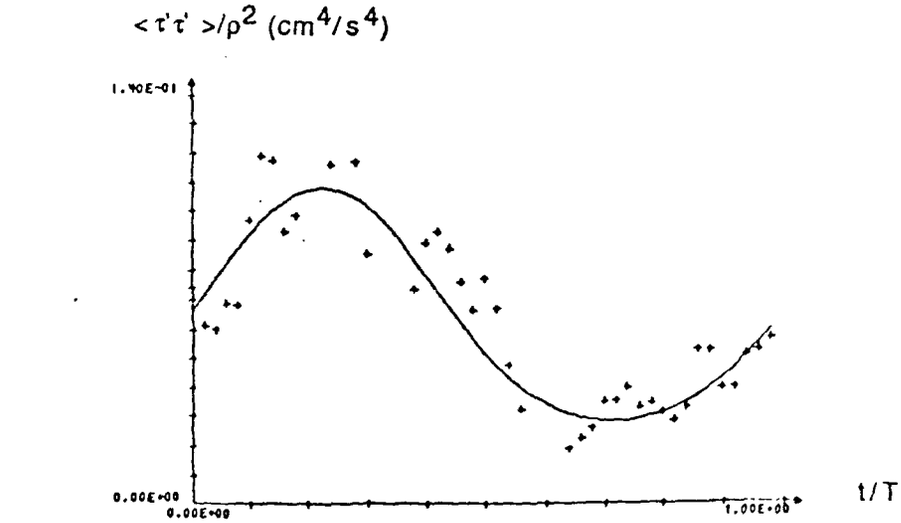

Figure 3 Examples of phase averages in the presence of reverse flow. l_s^+=12, a_{uc}=0.70, U_c=18.5 cm/s.
a) Wall shear stress <τ> ; b) Intensity of the turbulent wall shear stress fluctuations <τ'τ'>

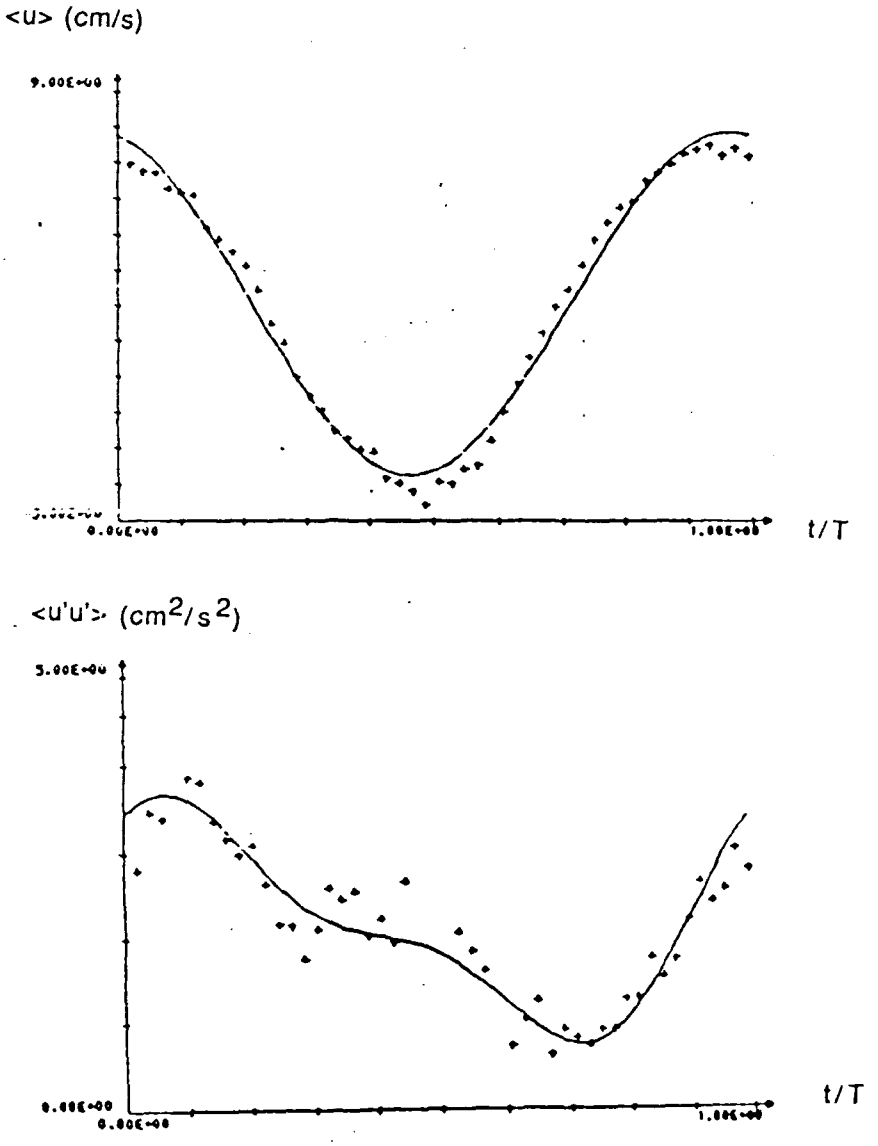

Figure 4 Examples of phase averages
LDA measurements: y^+=4.86, l_s^+=8.1, U_C=17.5 cm/s a_{uc}= 0.64
a) Velocity <u> b) Intensity of turbulent velocity fluctuations <u'u'>

$\bar{U}(y)/\bar{u}_\tau$

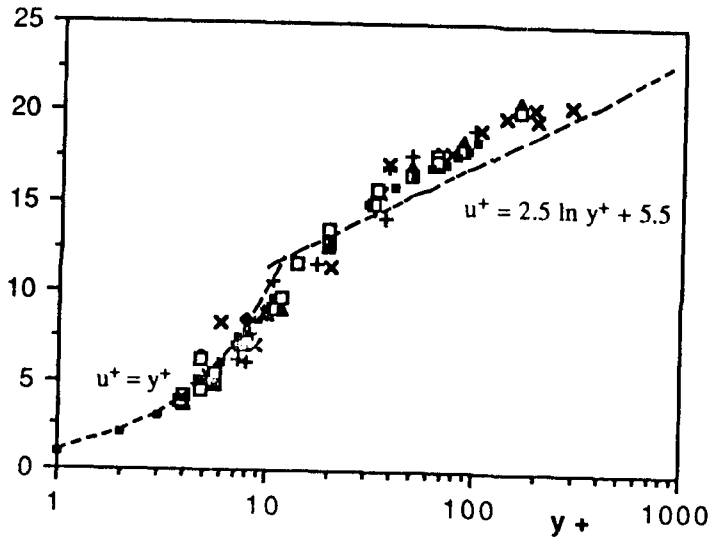

Figure 5 Mean velocity profiles in steady and unsteady flow . For legend see Table 2

$\sqrt{\overline{u'u'}}/\bar{u}_\tau$

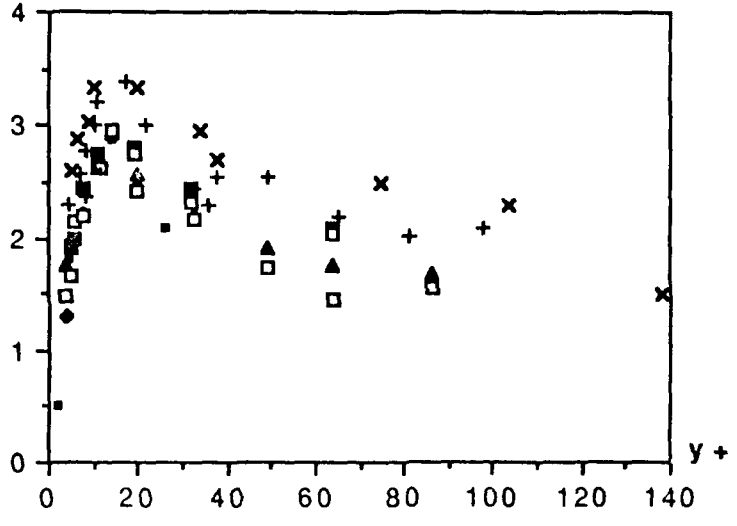

Figure 6 Mean turbulent intensity profiles in steady and unsteady flow. For legend see Table 2.

$\bar{\tau}_{unsteady}/\bar{\tau}_{steady}$

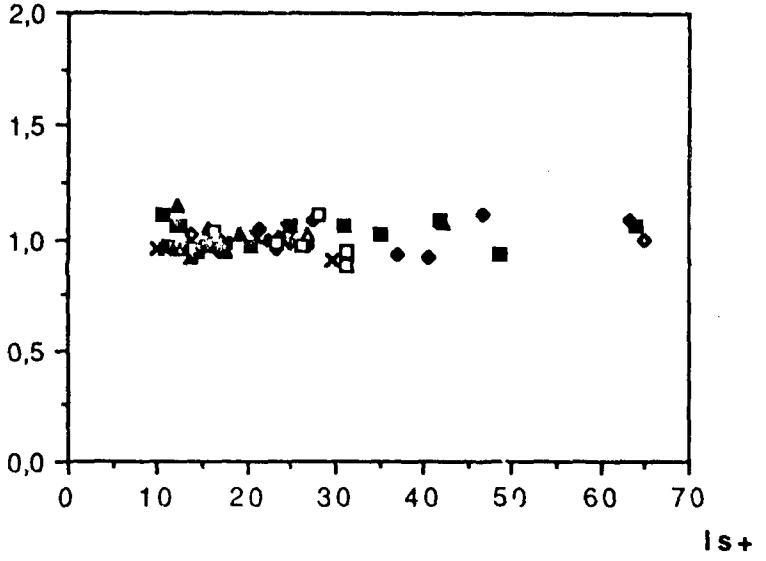

Figure 7 Ratio of unsteady to steady time mean wall shear stress. For legend see Table 3

$\sqrt{\overline{\tau'\tau'}}/\bar{u}_\tau^2$

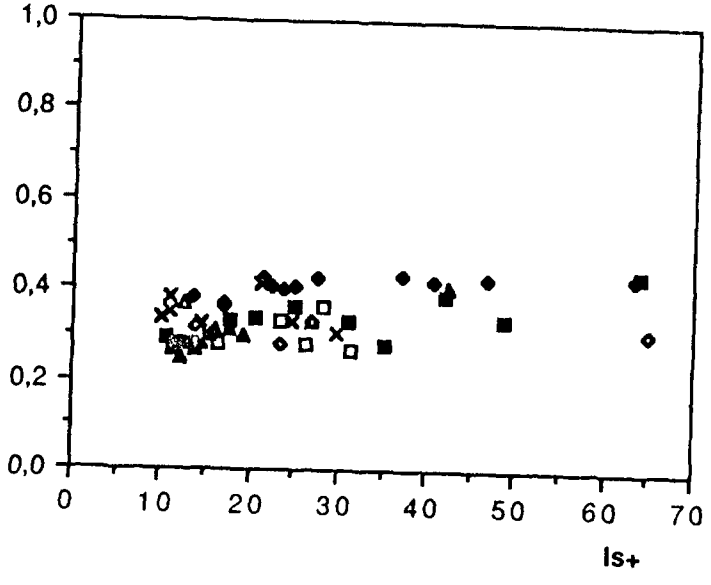

Figure 8 Time mean rms values of the turbulent wall shear stress fluctuations (for legend *see Table 3*)

a)

$A_{\tilde{u}}/A_{\tilde{u}c}$

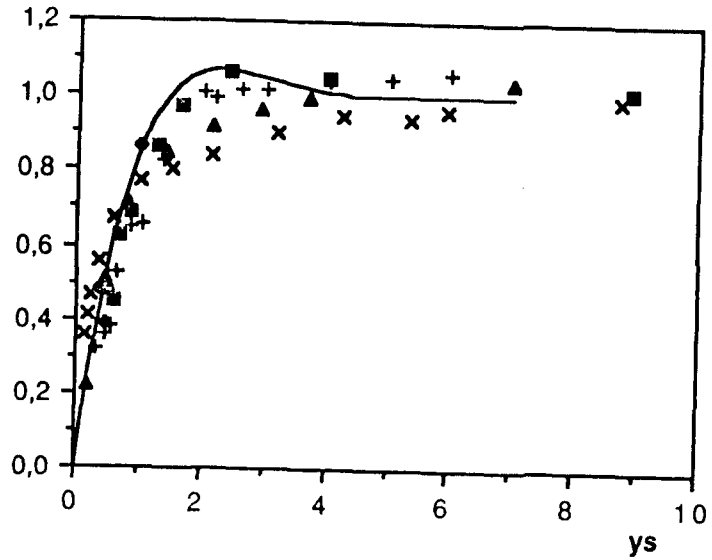

b)

$\Phi_{\tilde{u}} - \Phi_{\tilde{u}c}$

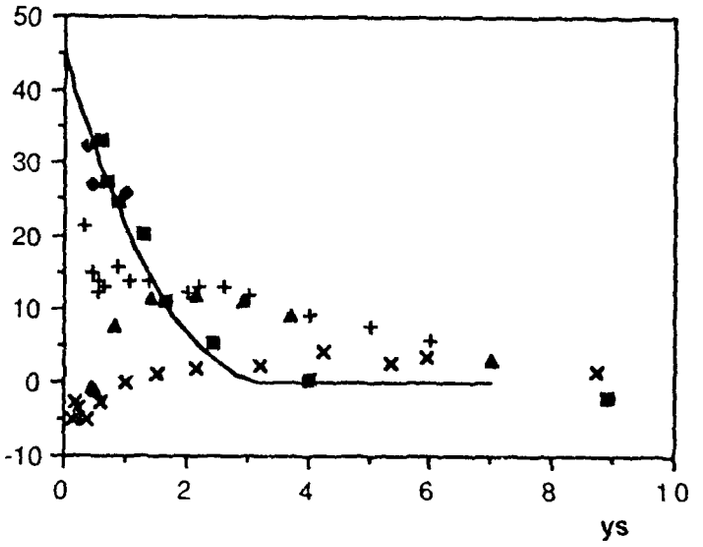

Figure 9 Evolution of the periodic streamwise velocity oscillations with distance from the wall

a) Amplitude profiles

_____ : Viscous Stokes solution (For legend see Table 2)

b) Phase shift profiles with respect to the centreline velocity oscillations.

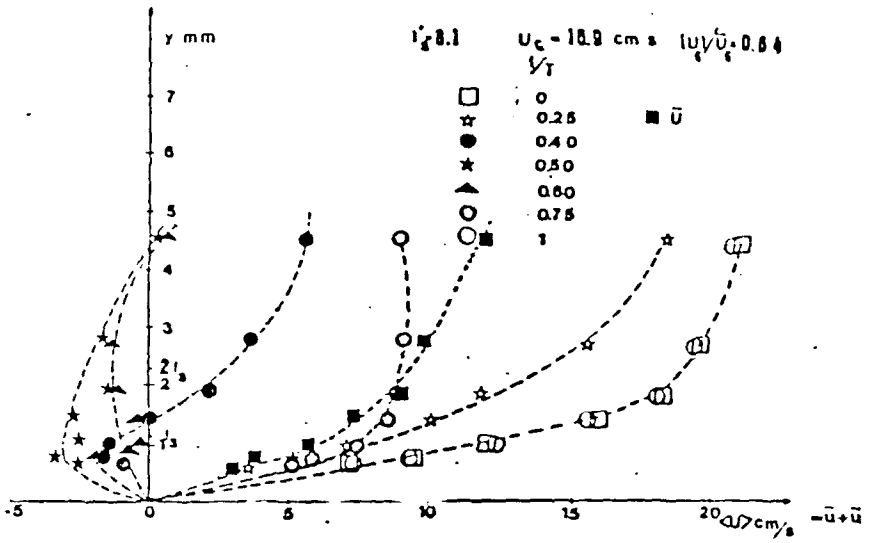

Figure 10) Instanteneous velocity profiles in the presence of reverse flow. U_C=16.9 cm/s ; a_{UC}=0.64 ; l_s^+=8.1

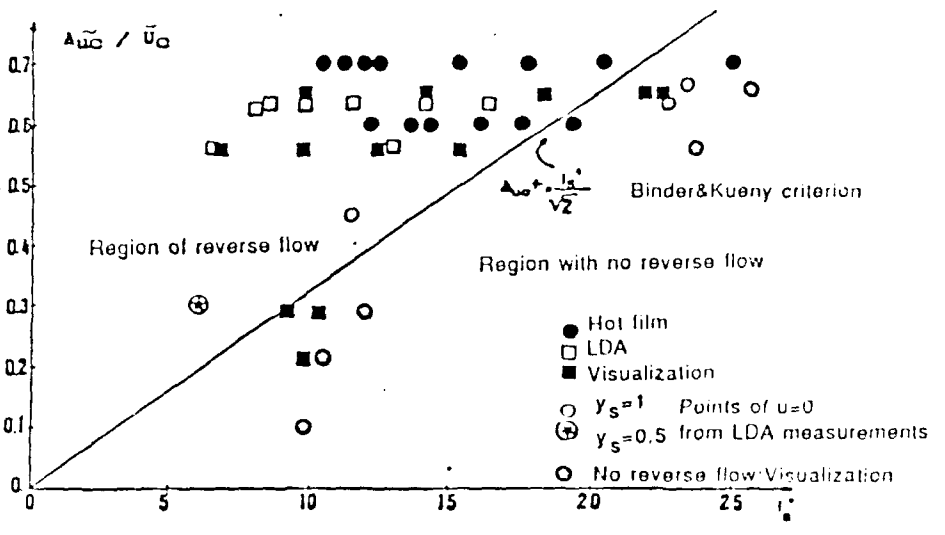

Figure 11)Observations of reverse flow compared with the Binder-Kueny criterion given by the straight line.

a)

$A_{\tilde{\tau}}/A_{\tilde{\tau}(\text{Stokes})}$

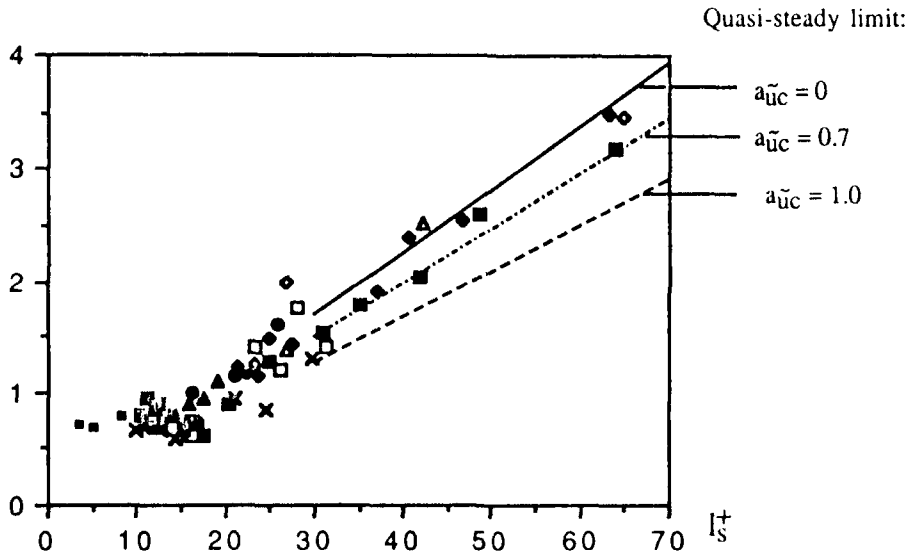

b)

$\Phi_{\tilde{\tau}} - \Phi_{\tilde{u}c}$

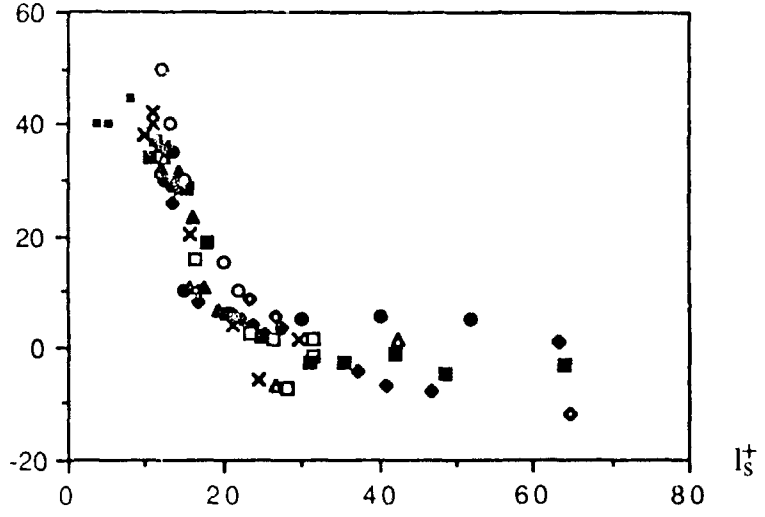

Figure 12 Oscillations of the wall shear stress vs frequency parameter l_s^+ (for legend see Table 3)

a) Amplitude normalized by the Stokes value

b) Phase shift with respect to the centerline velocity oscillations

a)

$A_{\tilde{\tau}}/A_{\tilde{\tau}}(\text{Stokes})$

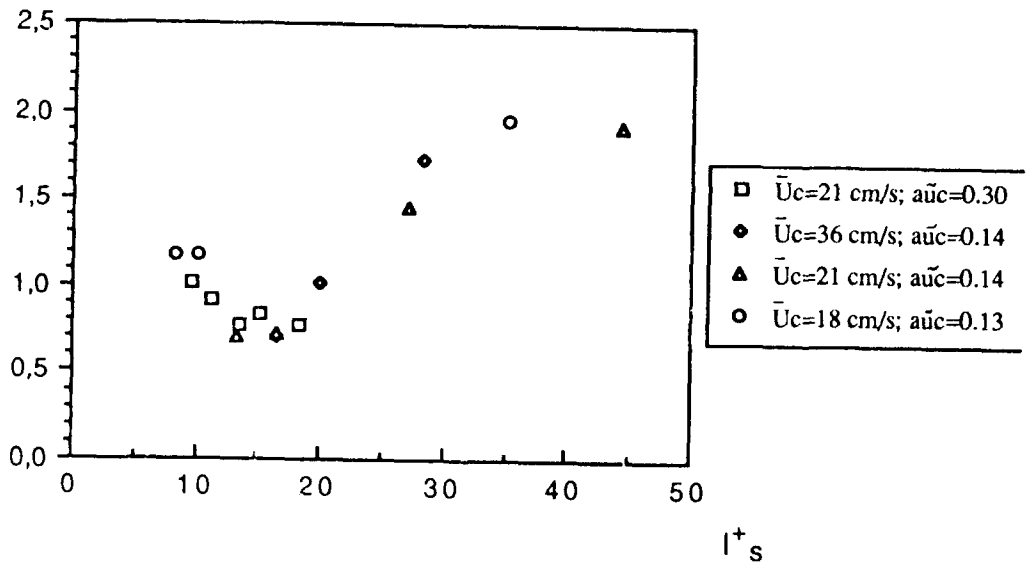

b)

$\Phi_{\tilde{\tau}} - \Phi_{\tilde{uc}}$

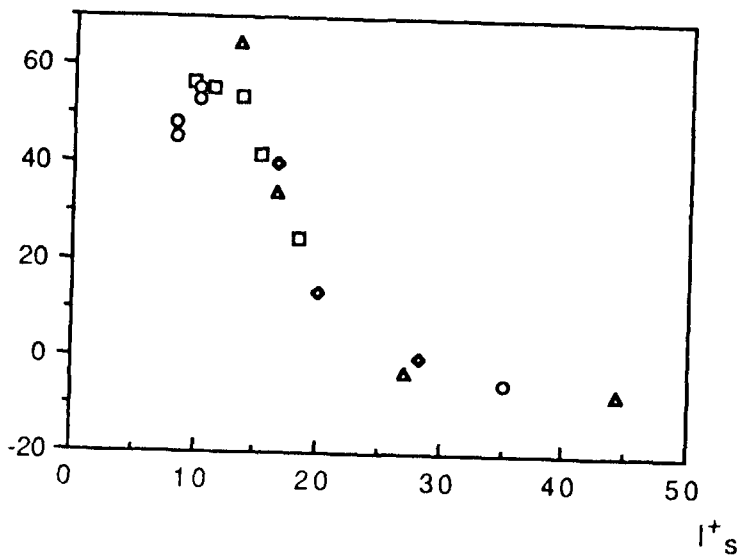

Figure 13 Oscillations of the wall shear stress measured with the Houdeville-Cousteix gage
a) Amplitude
b) Phase shift

a)

$A_{\tilde{u}'u'}/\bar{u}_\tau^2$

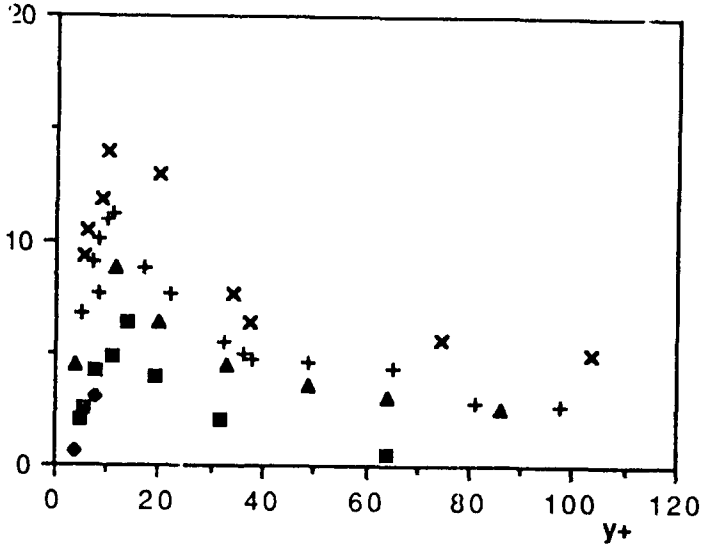

b)

$\sqrt{A_{\widetilde{u'u'}}} / A_{\tilde{u}}$

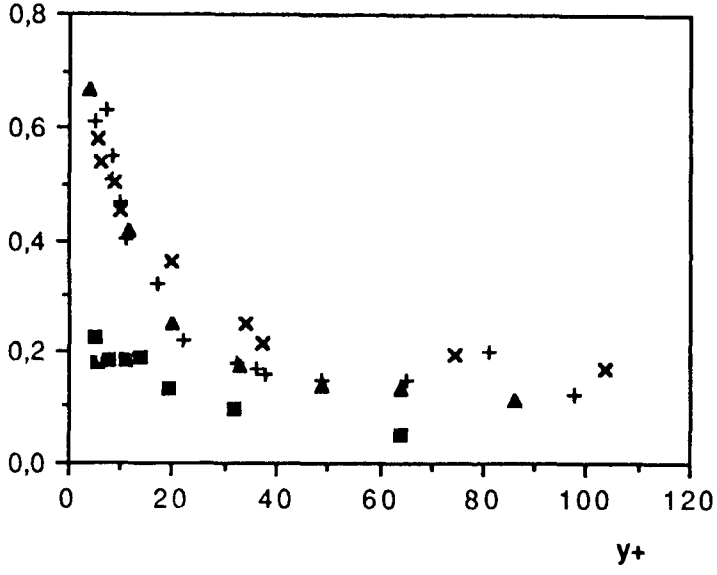

c)

$a_{\tilde{u}'u'}/2a_{\tilde{u}}$

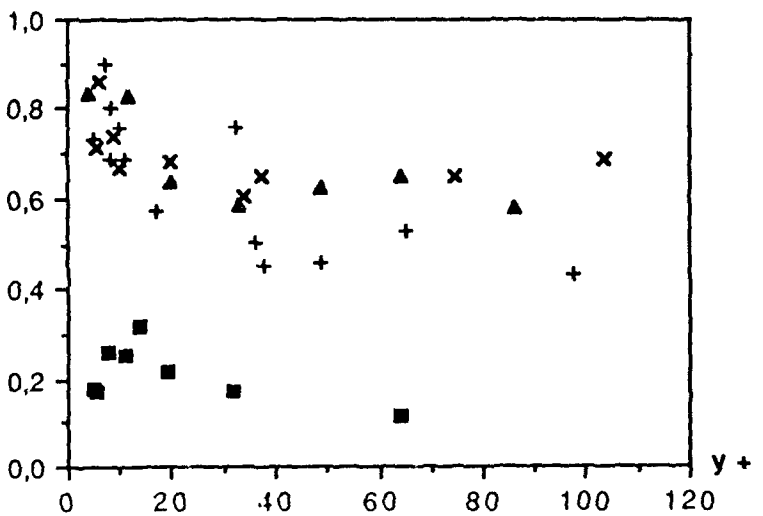

Figure 14 Amplitude profiles of the modulation of the longitudinal turbulent intensity . For legend see Table 2.

a) Values scaled with constant time mean shear velocity

b) Intensity with respect to local velocity oscillations

c) Ratio of relative amplitudes of turbulent fluctuations and local velocity oscillations

a)

$\Phi_{\tilde{u}'u'} - \Phi_{\tilde{u}\tilde{c}}$

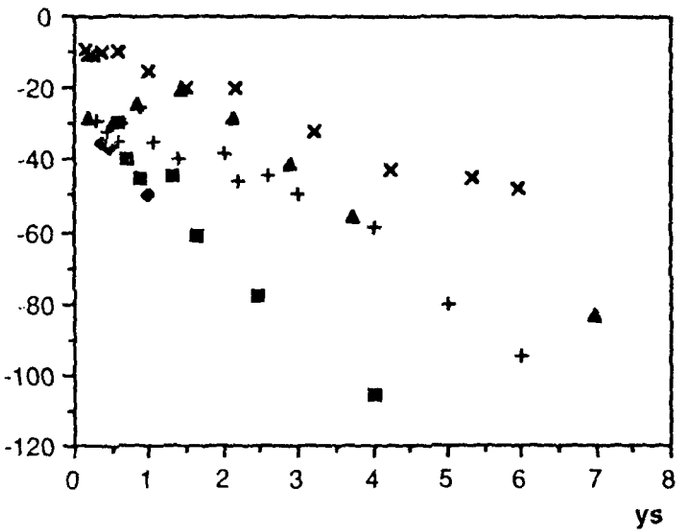

b)

$$\Delta t^{+} = (\Phi_{\tilde{u}'u'} - \Phi_{\tilde{u}\tilde{c}})\, i_s^{+2}/2$$

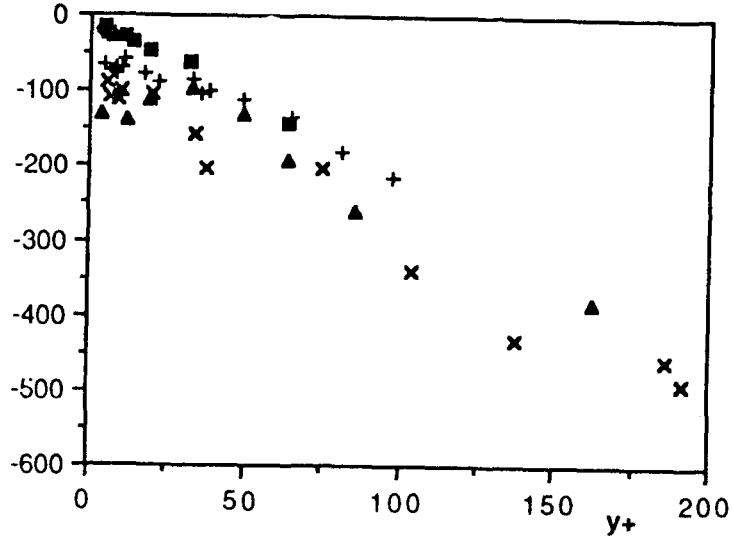

Figure 15 Variations of the phase of the turbulent velocity fluctuation modulation with distance from the wall. For legend see Table 2

a) Phase shift with respect to the centreline oscillations

b) Time lag

a)

$A_{\widetilde{\tau'}\widetilde{\tau'}} / \bar{\tau}\, A_{\tilde{\tau}}$

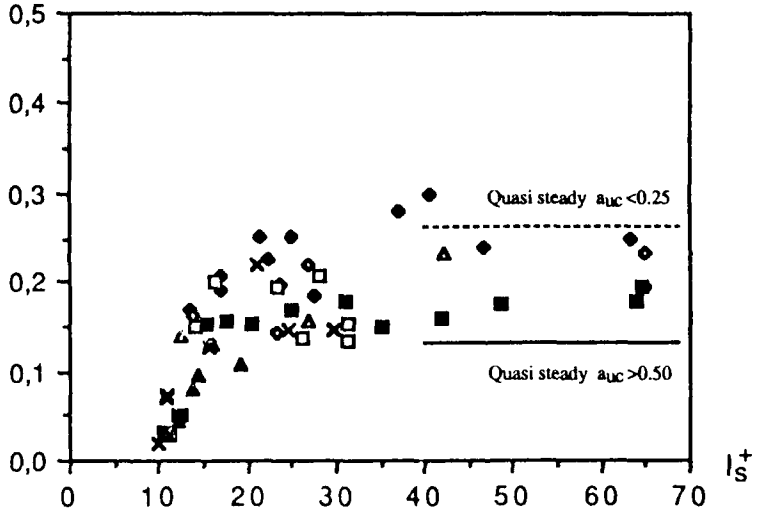

b)

$\Phi_{\tilde{\tau}'\tau'} - \Phi_{\tilde{u}c}$

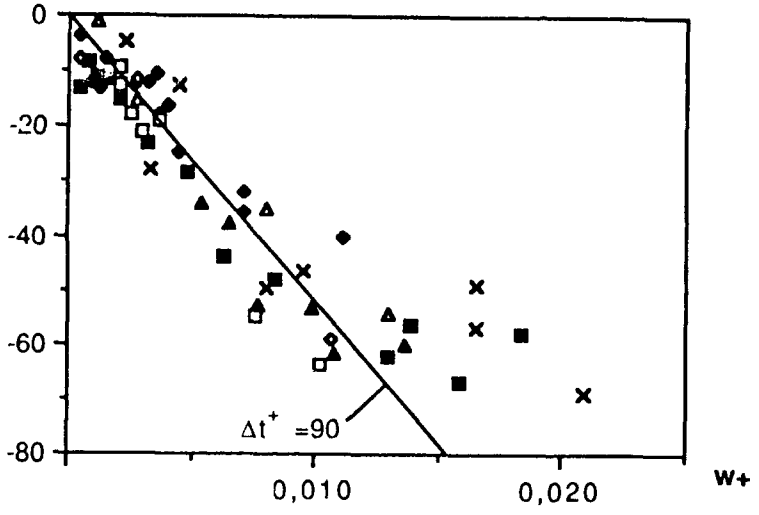

Figure 16 Modulation of the turbulent fluctuations of the wall shear stress. For legend see Table 3

a) Amplitude

b) Phase shift

a)

$a_{\widetilde{u'u'}} / a_{\tilde{u}}$; $a_{\widetilde{\tau'\tau'}} / a_{\tilde{\tau}}$

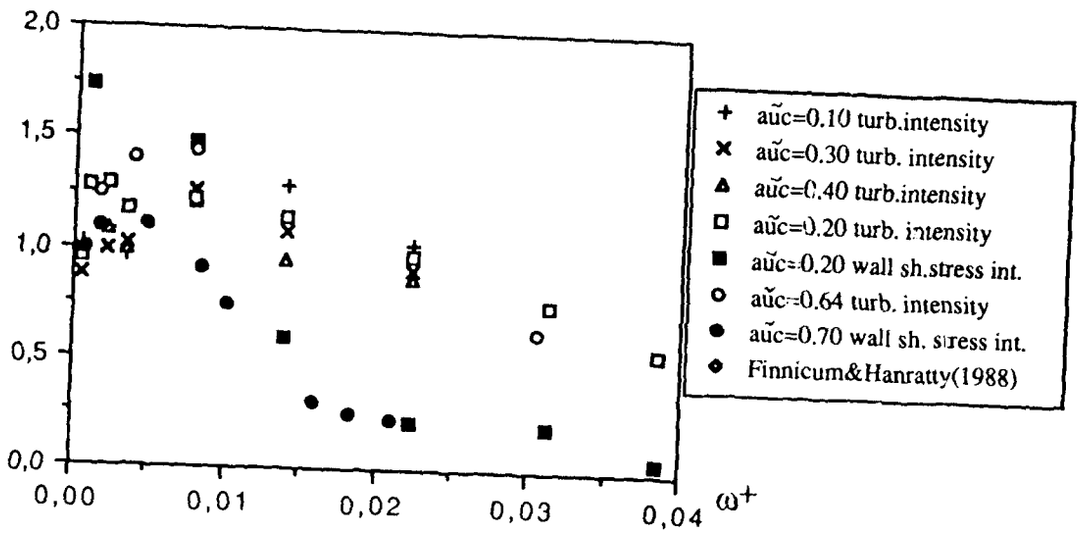

b)

$a_{\widetilde{u'u'}} / a_{\widetilde{u'u'(qs)}}$; $a_{\widetilde{\tau'\tau'}} / a_{\widetilde{\tau'\tau'(qs)}}$

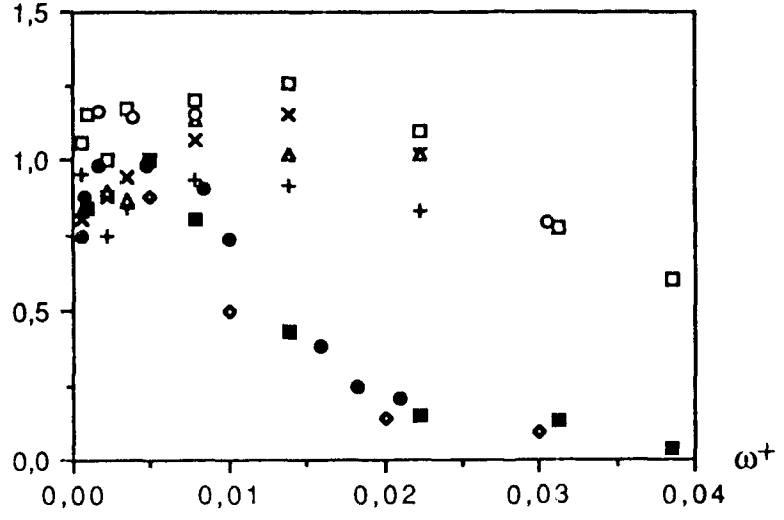

c)

$\Phi_{\widetilde{u'u'}} - \Phi_{\widetilde{u}\,(y+=15)}$; $\Phi_{\widetilde{\tau'\tau'}} - \Phi_{\widetilde{\tau}}$

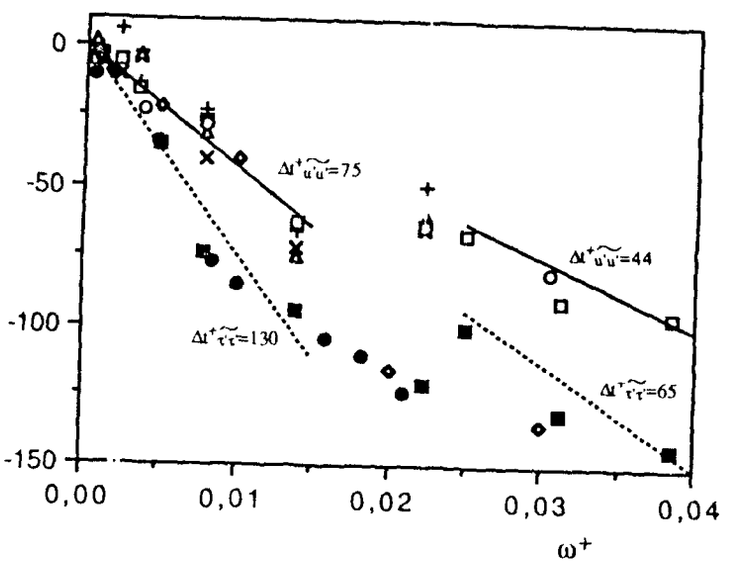

Figure 17 Modulation of the turbulent intensites of the velocity at $y^+=15$ and of the wall shear-stress vs forcing frequency

a) Ratios of relative amplitudes

b) Ratios with respect to the quasi-steady values.

c) Phase shifts

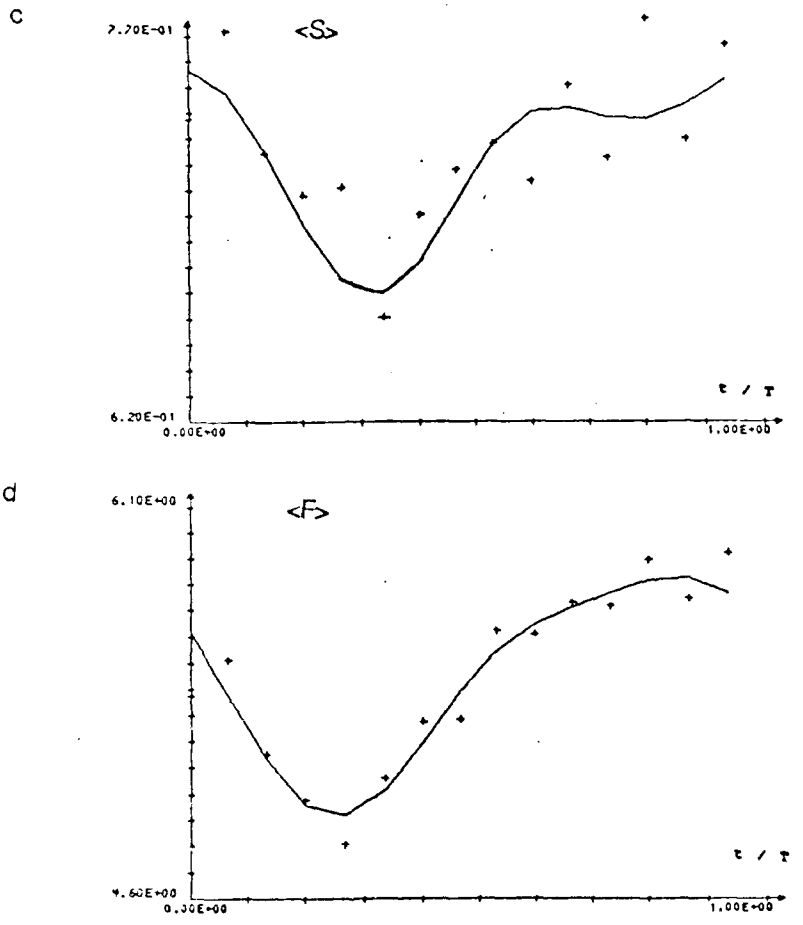

Figure 18

Examples of phase averages $y^+=15$; $a_{uc}^{\sim}=0.20$; $l_s^+=9.5$

a)Taylor time micro-scale; b)Liepmann time-scale; c)Skewness factor of $\partial u'/\partial t$ d) Flatness factor of $\partial u'/\partial t$

$\bar{\Lambda}^+$ and $\bar{\lambda}^+$

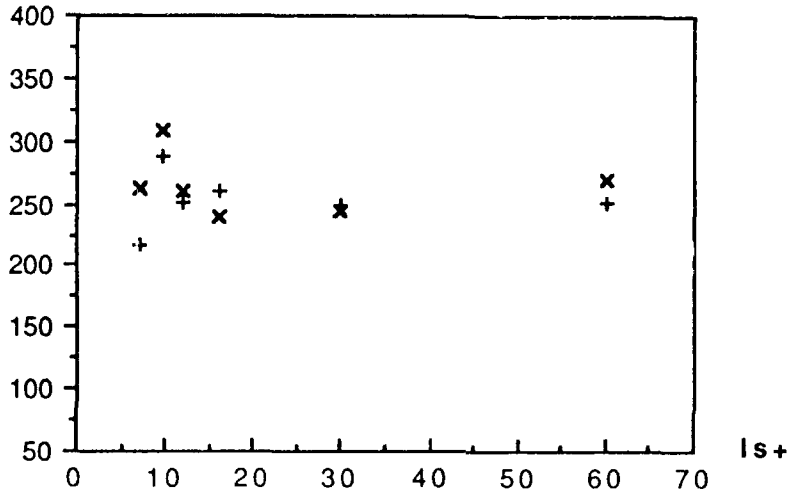

Figure 19 Time mean of the zero crossing period and time mean Taylor scale versus frequency parameter. +: $1/N_0^+$; x : $1 / 2\pi\lambda^+$ ($y^+=15$)

a)

$a_{\tilde{\Lambda}}$ and $a_{\tilde{\lambda}}$

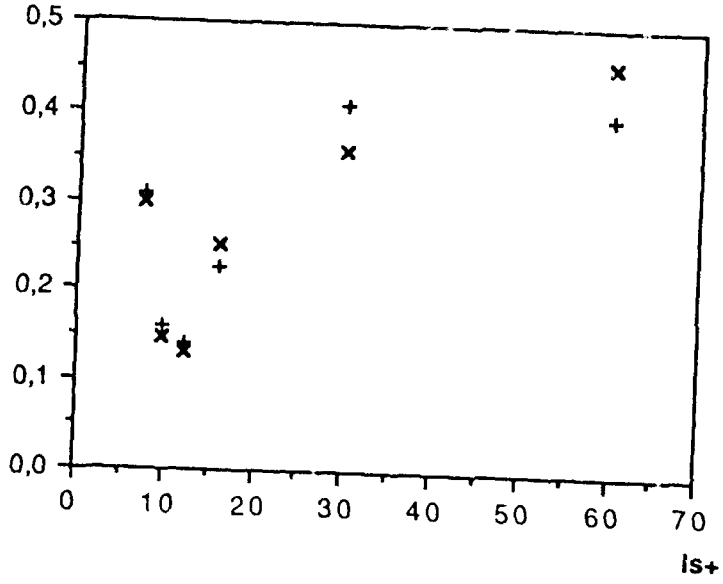

b)

$a_{\tilde{\Lambda}} / a_{\tilde{\tau}}$ and $a_{\tilde{\lambda}} / a_{\tilde{\tau}}$

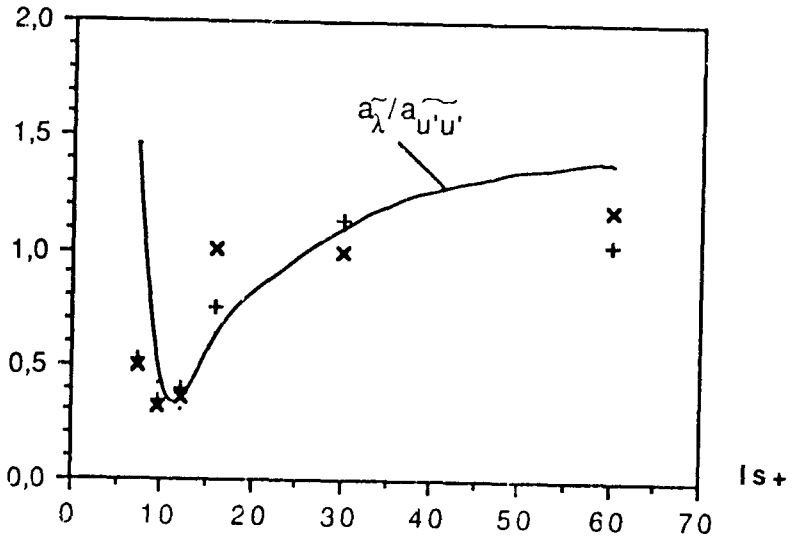

c)

$\Phi_{\tilde{\Lambda}} - \Phi_{\tilde{\tau}}$ and $\Phi_{\tilde{\lambda}} - \Phi_{\tilde{\tau}}$

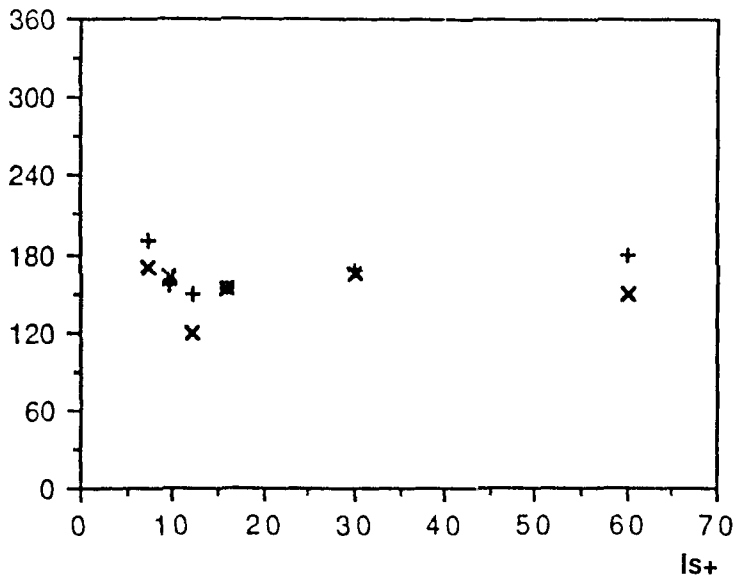

Figure 20 Amplitudes of the modulations of the Liepmann and of the Taylor micro scales vs frequency parameter

a) Relative amplitudes

b) Relative amplitudes scaled with the amplitude of the wall shear stress .

c) Phase shift with respect to the oscillations of the wall shear stress

$\bar{S}(du'/dt)$

$\bar{F}(du'/dt)$

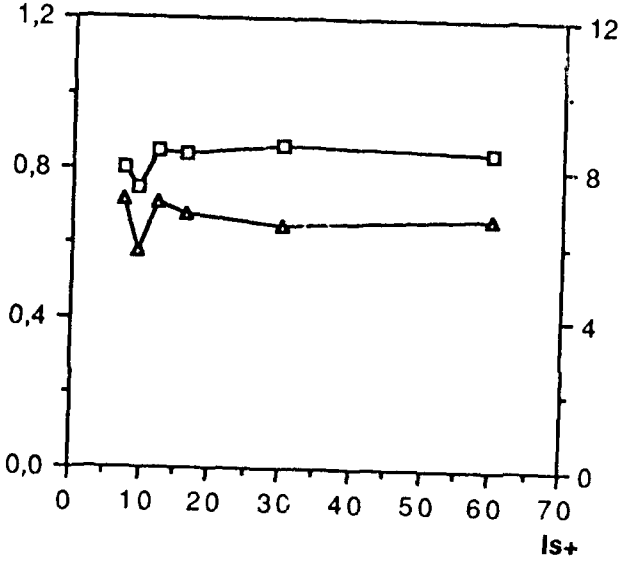

Figure 21 Time mean values of skewness and flatness factors of $\partial u'/\partial t$ vs frequency parameter

Δ: Flatness

$a_{\tilde{S}}(du'/dt)$; $a_{\tilde{F}}(du'/dt)$

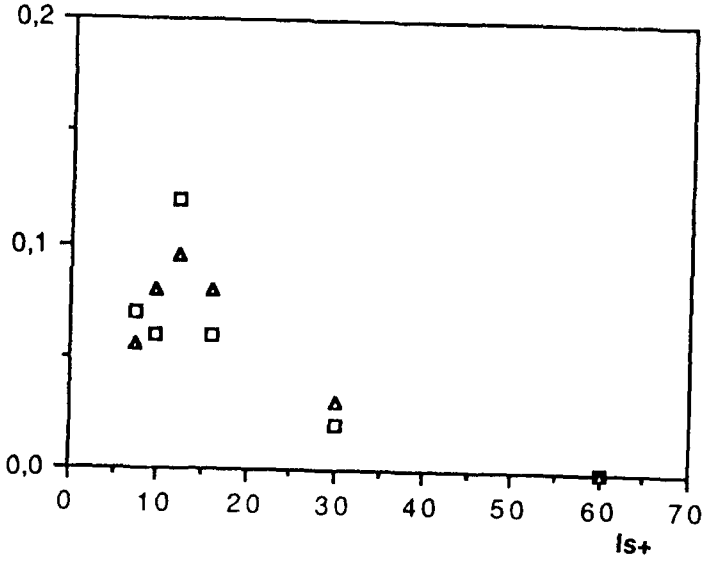

Figure 22 Relative amplitudes of the modulations of the skewness and flatness factors of $\partial u'/\partial t$

Δ: Flatness

PART TWO

WALL SHEAR STRESS MODULATION IN UNSTEADY TURBULENT CHANNEL FLOW WITH HIGH IMPOSED FREQUENCIES

Submitted to Physics of Fluids A March 1991

WALL SHEAR STRESS MODULATION IN UNSTEADY TURBULENT CHANNEL FLOW WITH HIGH IMPOSED FREQUENCIES

F. Sedat TARDU Gilbert BINDER

Institut de Mécanique de Grenoble
BP 53-X
38041, Grenoble, Cédex-France

Abstract

Results concerning the modulation of the wall shear stress in an unsteady channel flow are presented. The imposed frequency is increased up to seven times the mean bursting frequency. The imposed amplitude varies between 10 to 60 times the mean centreline velocity. The characteristics of the modulation of the wall shear stress $\tilde{\tau}$ and of the turbulent wall shear stress intensity $\widetilde{\tau'\tau'}$ are discussed. The time mean flow is insensitive to the forcing. There is a coexistence of viscous Stokes flow with a fully developed turbulent mean flow for imposed frequencies f such that:

$$0.02\ u_\tau^2/\nu < \omega = 2\pi f < 0.045\ u_\tau^2/\nu$$

The flow quits the Stokes regime for $\omega > 0.045\ u_\tau^2/\nu$. The amplitude of the modulation of the turbulent wall shear stress intensity decreases first from the quasi-steady limit but increases again for $\omega > 0.045\ u_\tau^2/\nu$. The time lag of $\widetilde{\tau'\tau'}$ with respect to $\tilde{\tau}$ is constant and 130 in wall units for $\omega < 0.014 u_\tau^2/\nu$ and for higher imposed frequencies it decreases with increasing imposed frequency.

1) INTRODUCTION

Past research on unsteady channel or pipe flows have shown that the modulation characteristics, such as the amplitude and phase shift of several flow quantities depend strongly on the imposed frequency (Binder et al., 1985; Mao and Hanratty, 1986; Tardu et al. 1991). For instance the modulation of the streamwise velocity $\tilde{u}$, of the turbulent intensity $\widetilde{u'u'}$, of the wall shear stress and its turbulent intensity $\tilde{\tau}$ and $\widetilde{\tau'\tau'}$ is much more dependent on the frequency than the amplitude of the imposed unsteadiness. Indeed, it was shown in unsteady channel flow that, the profiles of the oscillating amplitude of these quantities referred to the imposed amplitude -even when it is as large as 70% of the centreline mean velocity- follow roughly a single curve, in means of a properly chosen frequency parameter (Tardu et al. 1991). Another interesting characteristic of these flows is the complete lack of interaction between the mean and the oscillating flow.

One of the most attractive feature of the unsteady flows is the response of the turbulence to the forcing. It is well established now, that the turbulence may no more follow the imposed oscillations, when the imposed period becomes to be of the same order of its mean relaxation time. This behaviour manifests itself by a sharp decrease of the amplitude of $\widetilde{u'u'}$ and $\widetilde{\tau'\tau'}$ and also by large time-lags as the imposed frequency f increases below a given limit. Roughly speaking, at $\omega^+=2\pi f^+$[1] $=0.03$, the modulation of $\widetilde{\tau'\tau'}$ is practically died out (Finnicum and Hanratty, 1988; Tardu et al. 1991). It is quite streaking, by the way, to note that this imposed frequency is far being small, and is comparable to the bursting frequency $\omega_b{}^+=0.038$ (Bogard and Tiederman,1986).

It is worth saying that, on a fundamental basis, it is important to study the response of the turbulence in unsteady flows with imposed frequencies bevond $\omega_b{}^+$. Experimental results published on unsteady flows are generally limited to smaller imposed amplitudes and imposed frequencies and there is only one study in the literature which covers larger range of ω^+ such that $\omega^+ > \omega_b{}^+$ (Finnicum and Hanratty, 1988). These authors reported results on the modulation of the wall shear stress and of the turbulent wall shear stress intensity, for $0.001<\omega^+<0.0915$ with an amplitude of 10% of the centreline velocity in an unsteady turbulent pipe flow together with some comparison with previous results of Mao and Hanratty (1986). They show important modification of the response of $\widetilde{\tau'\tau'}$ for $\omega^+ > \omega_b{}^+$. Indeed, following the sharp decrease of the amplitude $A_{\widetilde{\tau'\tau'}}$ of the $\widetilde{\tau'\tau'}$ modulation from the quasi-steady limit, $A_{\widetilde{\tau'\tau'}}$ was found to increase again immediately after $\omega^+ = \omega_b{}^+$. This would imply, first that the physical interpretation based on the relaxation of the near wall turbulence is no more valid for $\omega^+ > \omega_b{}^+$ and that on the other hand, more data is needed to elucidate the response of the turbulence in the high frequency regime.

The principal aim of the present study is to extend the existing unsteady channel

[1] + denotes scaling with inner variables, i.e friction velocity u_τ and viscosity ν.

flow data for both large imposed amplitudes and frequencies and to compare them with the recent findings of Finnicum and Hanratty (1988). Experimental results on the modulation of $\tilde{\tau}$ and $\tilde{\tau}'\tilde{\tau}'$ in a frequency range going from the quasi-steady limit to $\omega^+=0.25=7*\omega_b{}^+$ and for six imposed amplitudes are reported in this study. Particular attention is paid for the scaling of the modulation of various quantities. The accent is put here on the imposed frequency regime such that $\omega^+>0.02$. The data covering smaller range of ω^+ is discussed in detail by Tardu,Binder and Blackwelder (1991).

2) EXPERIMENTAL FACILITIES

The experiments were performed in a 100 mm wide 2600 mm long channel flow having a span of 1000mm as described by Tardu, Binder and Blackwelder (1991) (TBB hereafter). The generation of the unsteady flow have been done by two ways. In the first case, a cylinder having 24 longitudinal 5*200 mm slots machined in its surface terminating the inflow pipe directly upstream of the settling chamber is used. The end of this cylinder was capped so the water had to exit through the slots. A movable sleeve was tightly fitted around the cylinder so the sleeve covered some, all or none of length of the slots and allowed it to continue into the settling chamber. The oscillation frequency of the sleeve was controlled by a variable speed motor through an eccentric bearing. The eccentricity was adjustable to control the amplitude of the oscillation. The mean flow was controlled by adjusting the length of the connecting arm between the eccentric bearing and the sleeve. These three variables were easily changed in a continuous manner and allowed great flexibility in adjusting flow conditions. The amplitude could be varied from 0 to 80% of the mean flow and the period of the oscillations ranged from 2.5 to infinity. Thus, this apparatus being limited in the range of imposed frequency, higher ω^+ were obtained, either by sufficiently decreasing the Reynolds number and using this pulsating device, or by using a reciprocating piston with adjustable speed and stroke mounted on the caisson upstream of the grids and honeycomb. When the piston was used the Reynolds number based on the half channel height was $Re_h=hU_c/\nu=10000$ and the imposed frequency was increased up to 1.40 Hz. Otherwise, Re_h was decreased until 5000 since the imposed frequency of the pulsating device is limited to 0.4 Hz. These flow regimes were fully developed and turbulent (TBB, 1991).

The flow conditions are shown on Table 1. Five imposed amplitudes are studied going from 10 to 60% of the centreline velocity.

The streamwise velocity in the channel flow was measured by a laser Doppler anemometer as described by TBB,1991. TSI 1268W film probes were used to measure the shear stress on the surface. The dimensions of the sensing element are 127μm in diameter and 1.016 mm in the spanwise ($\Delta x^+=1$ and $\Delta z^+=8.3$ for $U_c=18$ cm/s). The hot films were operated at constant temperature at 2-8% overheat by DISA 55MO1 anemometer unit. A digital

to analog converter was used to suppress the DC anemometer output at zero velocity, so that the signal could be amplified before A/D conversion. These conversions are performed with an Analog-Device RTI-800 board (accuracy 11bit+sign; 8 channel) installed in a PC computer. Simultaneously the pulse delivered by a photocellule installed on the pulsating device marking the beginning of each cycle required for phase averaging was also recorded.

The hot-film gauges were calibrated in situ by operating the channel at different mean velocities. The LDA was used to determine the friction velocity u_τ from the logarithmic layer and the velocity gradient at the wall in steady flow. The mean wall shear τ was aptly correlated by the Blasius formula $\tau = 0.048\ Re^{-1/4} \rho U_c^2/2$. This empirical relation was then used to obtain a least squares fit of the mean output voltage squared and $\tau^{1/3}$.

The classical triple decomposition is used. A quantity q(t) is decomposed into a mean $\bar{q}$,an oscillating $\tilde{q}$ and random q' component:

$$q(t;T)=\bar{q} +\tilde{q}(t/T) + q'(t)$$

< > designates the phase average i.e:

$$<q(t/T)>= \tilde{q}(t/T) + \bar{q}$$

The amplitude and phase of the fundamental of $\tilde{q}$ are respectively noted by $A_{\tilde{q}}$ and $\Phi_{\tilde{q}}$. $a_{\tilde{q}} = A_{\tilde{q}} / \bar{q}$ denotes the relative amplitude of $\tilde{q}$.

3) RESULTS

3.1) Time mean flow

Figure 1a and 1b show respectively the time mean wall shear stress and the time mean wall shear stress intensity versus the imposed frequency ω^+ . In Fig. 1a τ_{unst} is referred to the steady wall shear stress τ_{st}. It is seen that this ratio is close to one within the experimental uncertainty. Note that even with an amplitude of 60% of the centreline velocity and imposed frequency as high as 7 times the bursting frequency, the time mean wall shear stress is insensitive to the forced oscillations.

It has to be remembered that when the imposed frequency and amplitude are high enough, reverse flow occurs near the wall, and the part of the phase average of the wall shear stress $<\tau>$ corresponding to the reversal phase has to be rectified. On the other hand, due to the axial diffusion the measured $<\tau>$ never goes to zero, as shown by Tardu et al. (1985). These authors have also shown the good qualitative and quantitative correspondence between the measured and computed values of $<\tau>$ when reversal occurs. The rectification of $<\tau>$ is thus

done here with respect to $<\tau>=0$ in the same way of TBB (1991). On the other hand, the effect of the conduction into the subsurate is negligible, since the cutoff frequency of the wall element in the present working conditions is well above the maximum imposed frequency here.

Figure 1b shows that $\sqrt{\overline{\tau'\tau'}}$ / $\sqrt{\overline{\tau}}$ is between 0.4 and 0.3, as in steady flow (Alfredson et al., 1989) and, thus the turbulent intensity of the wall shear stress is not affected either. It is seen on Fig.1b that, the points corresponding to the $a_{\widetilde{uc}}=0.1$ and $U_c=10$ cm/s ($Re_h=5000$) case are in a some systematical manner, smaller than 0.4 (around 0.3) and some Re effect may be suspected there.

3.2) Oscillating flow

3.2.1) Oscillating wall shear stress

Previous studies (Binder et al.,1985; Mao and Hanratty, 1986; Finnicum and Hanratty,1988; TBB, 1991) have shown the coexistence of a viscous oscillating flow and a fully developed turbulent mean flow for $\omega^+\approx0.02$. Thus, the amplitude of the modulation of the wall shear stress, becomes to be of the same order of the viscous Stokes solution $A_{\widetilde{\tau}(Stokes)}=\rho A_{\widetilde{uc}}\sqrt{\nu\omega}$, and the phase shift $\Phi_{\widetilde{\tau}}-\Phi_{\widetilde{uc}}=45^0$. On the other hand, in the quasi-steady limit ($\omega^+\text{-->}0$) simple considerations give that :

$$A_{\widetilde{\tau}}/A_{\widetilde{\tau}(Stokes)}=\frac{0.056}{1+\frac{21}{64}a^2_{\widetilde{uc}}}l_s^+$$

and $\Phi_{\widetilde{\tau}}-\Phi_{\widetilde{uc}}=0$ as is shown by TBB(1991).

The set of data presented in this paper confirms these findings as it is shown on Fig. 2 . The Stokes regime is reached at $\omega^+\approx0.02$ since there $\Phi_{\widetilde{\tau}}-\Phi_{\widetilde{uc}}\approx45^0$. The amplitude ratio $A_{\widetilde{\tau}}/A_{\widetilde{\tau}(Stokes)}$ (Fig. 2a) is however systematically smaller than one for $0.02<\omega^+<0.1$ as also was observed by Ronneberger and Ahrens(1977), Mao and Hanratty (1986) and TBB(1991). This behaviour has been explained so far by taking account of a time dependent eddy viscosity which could be phase shifted with respect to the shear. This tendency is not noted however by Finnicum and Hanratty (1988) and the ratio $A_{\widetilde{\tau}}/A_{\widetilde{\tau}(Stokes)}$ deduced from their data stays closer to one until $\omega^+=0.1$.

$A_{\widetilde{\tau}}/A_{\widetilde{\tau}(Stokes)}$ is minimum at $\omega^+=0.04$ increases further and becomes to be close to one for $\omega^+>0.01$. This would alone indicate that the flow characteristics are modified towards high imposed frequency regime.

The behaviour of the phase shift strengthen this last suggestion (Fig. 2b). The

phase shift $\Phi_{\tilde{\tau}}-\Phi_{\tilde{u}c}$ is about 45^0 for $0.02<\omega^+<0.045$, i.e. the wall shear stress modulation follows the Stokes solution only in a limited imposed frequency range. For $0.04<\omega^+<0.1$ the phase shift decreases with a minimum of 25^0, around $\omega^+\approx 0.1$. For higher frequencies, the phase shift is constant but smaller than 45^0 which the viscous Stokes solution would require. This means that the flow modulation does no more follow the viscous solution for $\omega^+>0.045$.

The same tendency of the decrease of $\Phi_{\tilde{\tau}}-\Phi_{\tilde{u}c}$ towards large ω^+ is also noted from the data given by Mao and Hanratty (1986). However the minimum at $\omega^+\approx 0.1$ observed by the data presented here is not confirmed by these authors nor by Finnicum and Hanratty (1988). The first attempt to explain this disagreement would be the experimental scatter. It was pointed out in the previous section that the experimental conditions are such that the frequency response of the thermal boundary layer, nor the effect of the conduction into the substrate of the wall element may play a role that would falsify the data. Yet, if the frequency response was bad, a continuous decrease of the phase shift $\Phi_{\tilde{\tau}}-\Phi_{\tilde{u}c}$ would be observed as ω^+ is increased further, while $\Phi_{\tilde{\tau}}-\Phi_{\tilde{u}c}$ is found to increase slightly at $\omega^+=0.1$ as it is seen in Fig. 2b. The observed trend is thus really physical. To check if the flow is fully developed, and how the data is repetitive, simultaneous measurements were made by means of 4 hot film gauges respectively at x/h=34., 39.6, 45.2, and 50.8 where x is the distance from the entrance of the channel. Figure 2c shows the results for $a_{uc}=0.1$ and $U_c=10$ cm/s. It is seen that the data is coherent and the decrease of the phase shift at $\omega^+=0.1$ is clear independently of the test station x/h. The maximum scatter of the data in Fig. 2c is $+-5^0$.

It is interesting to note that, $\omega^+=0.1$ is close to the ejection frequency $\omega_e^+=0.075$ given by Coughran and Bogard (1987). It is recalled that the ejection frequency is defined as being the frequency of the individual lift up of low momentum fluid near the wall, while the bursts may contain one or more ejections (Bogard and Tiederman, 1986).

The data presented in this paper confirms the results of a direct numerical simulation of unsteady channel flow, recently undertaken by Rida and Tran (1991). Two cases have been investigated so far by these authors. The first case corresponds to an imposed frequency of $\omega^+=0.026$, while the second case is with $\omega^+=0.61$ which is very high indeed. Rida and Tran report a phase shift of the velocity oscillations near the wall of about 45^0 at $\omega^+=0.026$. The phase shift decreases however up to 20^0 at $\omega^+=0.61$. Although their highest frequency is 2.5 times greater than the one investigated here, the direct simulation data shows also that the Stokes solution is no more valid in the high frequency regime.

Rida and Tran (1991) shows also that the amplitude of the velocity oscillations follows better the Stokes solution at $\omega^+=0.61$ than at $\omega^+=0.026$: This point is also confirmed

by the experimental results since in Fig. 2a $A_{\tilde{\tau}}/A_{\tilde{\tau}(Stokes)}$ =0.8 thus nearest to one for $\omega^+>0.1$, while this ratio is about 0.6 for $0.02<\omega^+<0.06$.

3.2.2) Modulation of the turbulent wall shear stress intensity

Fig. 3a shows the relative amplitude of the modulation of the turbulent wall shear stress intensity $a_{\widetilde{\tau'\tau'}}$ related to the relative amplitude that $a_{\widetilde{\tau'\tau'}}$ would have in the quasi-steady limit. $a_{\widetilde{\tau'\tau'}}$ qs has been computed by using the fact that as ω^+-->0, the Blasius relationship is valid at each instant of the oscillation cycle, i.e:

$$<\tau_{qs}>= 0.048 <Re_h U_c^2>\rho/2$$

and that $<\tau'\tau'>_{qs}/<\tau>_{qs}$ =cte=0.35^2 (TBB,1991). This results in $\Phi_{\widetilde{\tau'\tau'}} = \Phi_{\tilde{\tau}} = \Phi_{\widetilde{uc}}$ and for small amplitudes $a_{\widetilde{\tau'\tau'}} \approx 2\, a_{\tilde{\tau}}$ and $a_{\tilde{\tau}} \approx 7/4\, a_{\widetilde{uc}}$, so that $a_{\widetilde{\tau'\tau'}} \approx 7/2\, a_{\widetilde{uc}}$. For imposed amplitudes such that $a_{\widetilde{uc}} > 0.40$ the relative amplitude $a_{\widetilde{\tau'\tau'}}$ qs becomes to be nearly one. Once $<\tau'\tau'>_{qs}$ was computed this way, the Fourier analysis was performed to find $a_{\widetilde{\tau'\tau'}}$ qs.

Figure 3a shows that the ratio $a_{\widetilde{\tau'\tau'}} / a_{\widetilde{\tau'\tau'}}$ qs decreases sharply from the quasi-steady limit until $\omega^+\approx 0.03$. This confirms the previous published results that show that the turbulence may not follow the imposed unsteadiness once the imposed period becomes to be of the same order as the mean relaxation time of the near wall turbulence (Mao and Hanratty,1986; TBB, 1991). For $\omega^+>0.03$ however, $a_{\widetilde{\tau'\tau'}} / a_{\widetilde{\tau'\tau'}}$ qs increases again. At $\omega^+=0.15$ this ratio becomes to be as important as 0.7 and for further higher imposed frequency it becomes to be constant and stays around this value. The imposed frequency range for which this fundamental modification of the response of the near wall turbulence takes place corresponds roughly with the range where the modulation of the wall shear stress quits the Stokes regime. The immediate conclusion deduced from these results is that the relaxation model can no more explain the behaviour of $\widetilde{\tau'\tau'}$ once $\omega^+>0.03$, i.e when the imposed frequency is larger than the mean bursting frequency $\omega_b^+=0.038$.

The data from Mao and Hanratty (1986) and Finnicum and Hanratty (1988) are also shown on Fig. 3a.These authors present their results as $A_{\sqrt{<\tau'\tau'>}} / \bar{\tau}$ versus ω^+. We used the fact that for small imposed amplitudes as is the case for their data (a_{uc}=0.1) this last expression can be written as

$$1/2\, a_{\widetilde{\tau'\tau'}} \frac{\sqrt{\overline{\tau'\tau'}}}{\bar{\tau}} .$$

We then deduced $a_{\widetilde{\tau'\tau'}}$ by taking :

$$\frac{\sqrt{\widetilde{\tau'\tau'}}}{\bar{\tau}} = 0.35$$

The results presented here compare well with the data of Mao and Hanratty (1986), unless one point in the high frequency regime where they report $a_{\widetilde{\tau'\tau'}} / a_{\widetilde{\tau'\tau'}}\,qs = 1$, while we did not measure a ratio as high as one, our maximum being 0.7. On the other hand, there is not a good quantitative agreement between our results nor those of Mao & Hanratty (1986) with the data given by Finnicum and Hanratty (1988). These authors explain this disagreement by the effect of the pipe diameter which in their case is different from the one used by Mao and Hanratty. The hydraulic equivalent diameter of the channel used in this study is D_h=18 cm and is close to D=19.4 cm , the pipe diameter of Mao and Hanratty's experiments (D used by Finnicum and Hanratty is equal to 5.08 cm). It is, however, difficult to argue on the physical significance of the pipe diameter which would play a role on the interaction between the imposed oscillations and the turbulence. That would imply that the size of the largest eddies play a role in the relaxation mechanism near the wall, a point which stays to be proved.

A different scaling of the amplitude of the $\widetilde{\tau'\tau'}$ modulation is used in Fig. 3b. where $a_{\widetilde{\tau'\tau'}}$ is related to $a_{\widetilde{\tau}}$. It is seen that in the small imposed frequency range, $a_{\widetilde{\tau'\tau'}} / a_{\widetilde{\tau}}$ nearly equals 2 if the imposed amplitude is small, as would indicate the quasi-steady solution, since there $\langle\tau'\tau'\rangle/\langle\tau\,\tau\rangle$=constant, and this equality leads to the first order to $a_{\widetilde{\tau'\tau'}} = 2\,a_{\widetilde{\tau}}$. It is noted that for high imposed amplitudes such that $a_{\widetilde{uc}}>0.5$, $a_{\widetilde{\tau'\tau'}} \to 1$ and $a_{\widetilde{\tau}} \to 1$ so that $a_{\widetilde{\tau'\tau'}} / a_{\widetilde{\tau}} = 1$ as is the case for some points in the low frequency regime corresponding to $a_{\widetilde{uc}}$=0.6 shown on Fig. 3b. The sharp decrease of $a_{\widetilde{\tau'\tau'}} / a_{\widetilde{\tau}}$ at $\omega^+ \approx 0.03$ confirms once more the earlier results of TBB, 1991.

For $\omega^+ > 0.03$ an increase of $a_{\widetilde{\tau'\tau'}} / a_{\widetilde{\tau}}$ is noted. This increase is obviously small compared with the increase of $a_{\widetilde{\tau'\tau'}} / a_{\widetilde{\tau'\tau'}}\,qs$, because for a given $a_{\widetilde{uc}}$ $a_{\widetilde{\tau'\tau'}}\,qs$ is constant , while in the ratio $a_{\widetilde{\tau'\tau'}} / a_{\widetilde{\tau}}$ and in the high frequency regime

$$a_{\widetilde{\tau}} = \frac{A_{\widetilde{\tau}}}{\bar{\tau}} = \frac{A_{\widetilde{\tau}}\,\text{Stokes}}{\bar{\tau}}$$

and $a_{\widetilde{\tau}}$ increases with increasing ω^+. Note also that the scatter with this scaling is small compared to $a_{\widetilde{\tau'\tau'}} / a_{\widetilde{\tau'\tau'}}\,qs$ (Fig. 3a) and the data from Mao and Hanratty and from Finnicum and Hanratty are both in agreement with the results presented here.The relatively good collapse of both of the data when the scaling $a_{\widetilde{\tau'\tau'}} / a_{\widetilde{\tau}}$ is used may be understood since in the Finnicum and Hanratty's data $a_{\widetilde{\tau}}$ is found to be systematically larger and this compensates the larger values of $a_{\widetilde{\tau'\tau'}}$.

A second quantity which is important in the study of the response of the turbulence to imposed unsteadiness is the phase shift $\Phi_{\widetilde{\tau'\tau'}} - \Phi_{\widetilde{\tau}}$, because the unsteadiness manifests itself especially through this characteristic. Figure 3c shows the behaviour of $\Phi_{\widetilde{\tau'\tau'}} - \Phi_{\widetilde{\tau}}$ versus ω^+. The scatter is small as is the case generally for the phase shifts. The time lag $\Delta t^+ = (\Phi_{\widetilde{\tau'\tau'}} - \Phi_{\widetilde{\tau}}) / \omega^+$ shown in Fig.3d is even more instructive. Previous measurements have shown that Δt^+ is constant for $\omega^+ < 0.014$ and equals to -130 which is also the mean relaxation time of the near wall turbulence (TBB, 1991). The same authors also report that the time lag $-\Delta t^+$ decreases suddenly to 65 in the range $0.014 < \omega^+ < 0.04$. However, further measurements in the high frequency regime indicate that the time lag $-\Delta t^+$ is not constant and decreases with increasing frequency as shown on fig. 3d for $\omega^+ > 0.014$. This is rather surprising, because the response of the turbulence to forcing has been so far explained under the relaxation mechanism of the near wall turbulence by a linear model which implies a constant time lag (Mao and Hanratty, 1986). Furthermore the present results would indicate that the response of $\widetilde{\tau'\tau'}$ is quite different in the high imposed frequency regime.

The characteristics of the flow has been physically explained by TBB,1991 by the *parameter* $l_s^+ = l_s / l_v = \sqrt{2}/\omega^+$ where l_s is the Stokes length of the viscous oscillating flow. If $l_s^+ < 12$, the oscillating flow is confined in the viscous layer and the interaction between the oscillating and time mean flow becomes weaker. It has to be noted that at $\omega^+ = 0.25$ the value of l_s^+ is 3 which means that the Stokes layer is confined between $0 < y^+ < 3$ i.e the oscillating flow is within a very thin layer and the flow is in the plug regime immediately for $y^+ > 3$. Note also that the range of the departure from a constant value of the time lag Δt^+ corresponds to $12 < l_s^+ < 3$. Since the time lag varies with l_s^+ this would indicate that the relaxation mechanism of the near wall turbulence depends on the length of the viscous layer which is exposed to the unsteadiness: when the oscillating flow is within the buffer or logarithmic layer the turbulence responds linearly and Δt^+ is constant, while once it is confined in the viscous sublayer, $-\Delta t^+$ decreases with decreasing l_s^+ .

The changes in the behaviour of the response of turbulence begin by the apparition of higher harmonics in the phase average of $\langle \tau' \tau' \rangle$ as also was observed by Finnicum and Hanratty,1988. To quantify the importance of the higher harmonics the correlation coefficient defined as:

$$C=\frac{\sum_{t=0}^{t=T}\left(A_{\widetilde{\tau'\tau'}}\cos(\omega t+\Phi_{\widetilde{\tau'\tau'}})\right)^2}{\sum_{t=0}^{t=T}\left(\widetilde{\tau'\tau'}(t/T)\right)^2}$$

was computed. In this relationship $A_{\widetilde{\tau'\tau'}}$ and $\Phi_{\widetilde{\tau'\tau'}}$ are the amplitude and phase of the fundamental. C is, in some way, the goodness of the fit of $<\tau'\tau'>$ with the first harmonic and C=1 indicates that the fundamental is 100% representative of the $<\tau'\tau'>$ modulation. It is seen from Fig. 4 that the correlation coefficient is about one in the quasi-steady regime and that it drops out until 0.7 near ω^+=0.03. This indicates that the response of the turbulence is no more linear for ω^+>0.03 and that a non-linear interaction between the oscillating flow and the turbulent wall shear stress intensity takes place. Recall that ω^+=0.03 denotes the limit of the frequency regime in which $a_{\widetilde{\tau'\tau'}}/a_{\widetilde{\tau'\tau'}}$ qs decreases.For higher imposed frequencies where an increase of $a_{\widetilde{\tau'\tau'}}/a_{\widetilde{\tau'\tau'}}$ qs is noted, the coefficient C increases but is no more near 1 as would necessitate a perfect linear response.

4. CONCLUSION

It is interesting to summarise the results on the response of the wall shear stress and of the turbulent wall shear stress intensity in terms of the imposed frequency compared with the characteristic frequencies of the near wall turbulence. The comparison, here will be made on the following quantities:

a) The ejection frequency ω_e^+: The frequency of the individual lift up of the low momentum fluid near the wall; ω_e^+ equals 0.075 in steady channel flow.

b) The bursting frequency ω_b^+ . A bursting event corresponds to the break up of a single streak; it may contain one (Bursts with single ejection (BSE)) or several (Bursts with Multiple ejections (BME). In steady channel flow the mean frequencies of these categories are respectively ω_{BSE}^+=0.024 and ω_{BME}^+=0.014 (Tardu and Binder,1991) so that the bursting frequency $\omega_b^+ = \omega_{BSE}^+ + \omega_{BME}^+$ =0.038. All of these quantities were found to be insensitive to the forcing (Tardu and Binder, 1991).

The first significant difference of the response of the turbulent wall shear stress intensity takes place at $\omega^+\approx\omega_{BME}^+$ where the time lag $-\Delta t^+$ begins to decrease. ω_{BME}^+ may be commented as the frequency of the large scale bursts. For imposed frequencies higher than this characteristic frequency, the time lag is no more constant and the response of the relaxation mechanism of the near wall turbulence changes of character.

For imposed frequencies smaller than the bursting frequency ω_b^+ the relative amplitude $a_{\widetilde{\tau'\tau'}}$ decreases from its quasi-steady value $a_{\widetilde{\tau'\tau'}}$ qs and this may be explained by a linear response of the relaxation mechanism of the near wall turbulence. Once the imposed frequency increases beyond the mean bursting frequency the ratio $a_{\widetilde{\tau'\tau'}} / a_{\widetilde{\tau'\tau'}}$ qs increases and that shows a basic difference of the $\widetilde{\tau'\tau'}$ reaction in the high frequency regime. The use of the scaling $a_{\widetilde{\tau'\tau'}} / a_{\widetilde{\tau\tau}}$ makes the scatter less important and the data from several authors collapse better.

The time mean flow coexists with a Stokes viscous oscillating flow only in a limited range of imposed frequency. For $\omega^+ \approx \omega_e^+$ the phase shift $\Phi_{\widetilde{\tau}} - \Phi_{\widetilde{uc}}$ is found to be smaller than 45^o which is required for a purely viscous oscillating flow.

The results presented in this paper show that the response of the turbulence to the imposed velocity oscillations is a complex phenomena depending strongly on the imposed frequency. The numerical simulation of this type of flow should, therefore take into account this complexity, especially the dependance of the time lag Δt^+ on ω^+.

Acknowledgment

This work was supported in part by the European Office of the U.S. Army Research Development and Standardisation Group (contract DAJA 45-87-C-001). This support is gratefully acknowledged.

References

BINDER G. ,TARDU S. ,BLACKWELDER R.F., KUENY J.L., 1985 "Large Amplitude Periodic Oscillations in the Wall Region of a Turbulent Channel Flow" Fifth Symposium on Turbulent Shear Flow Août 7-9,1985,Cornell University,Ithaca,New-York -USA

BOGARD,D.G.; TIEDERMAN, W.G., 1986 "Burst Detection with Single Point Velocity Measurements" J. Fluid Mech. 162, 389

COUGHRAN, M.T.; BOGARD, D.G., 1987 "An Experimental Study of the Burst Structure in a LEBU-Modified Boundary-layer" 10th Symposium on Turbulence, Rolla, Missouri. September 1987, 45-1

FINNICUM, D.S.; HANRATTY, T.J., 1988 "Influence of Imposed Flow Oscillations on Turbulence" PCH PhysicoChemical Hydrodynamics, 10, 585

MAO, Z-X.; HANRATTY, T.J., 1986 "Studies of the Wall Shear Stress in a Turbulent Pulsating Pipe Flow" J. Fluid Mech., 170, 545

RIDA, S.; DANG TRAN, K.,1991 "Effects of External Forces on Turbulent Channel Flow" Euromech 272 Symposium on Response of Shear Flows to Imposed Unsteadiness; January 14-17,1991; Aussois-France

RONNEBERGER, D. AHRENS, C.D. , 1977 "Wall Shear Stress Caused by Small Amplitude Perturbations of Turbulent Boundary-Layer Flow:An Experimental Investigation" J. Fluid Mechanics, 83, 433 .

TARDU S.; BINDER G.; BLACKWELDER R.F.,1985 "Wall Shear Stress Measurements in Reversing Oscillatory Turbulent Boundary Layers" Euromech 202 Conference on Measurement Technique in Low-Speed Flows;7-10 Octobre 1985,N.L.R. Netherland

TARDU S. ; BINDER G. ; BLACKWELDER R.F., 1991 "Turbulent Channel Flow Subjected to Large Imposed Velocity Oscillations" Submitted to Journal of Fluid Mechanics

TARDU S.; BINDER G., 1991 "Response of Bursting to Imposed Velocity Oscillations" Submitted to Journal of Fluid Mechanics

	$\overline{U}_c$ (cm/s)	$a_{\widetilde{uc}}$
+	10.0	0.10
×	12.3	0.14
◇	17.5	0.20
□	19.5	0.40
○	20.0	0.60
●	Mao and Hanratty (1986)	
■	Finnicum and Hanratty (1988)	

Table 1) Flow conditions

a)

$\tau_{unst}/\ \tau_{steady}$

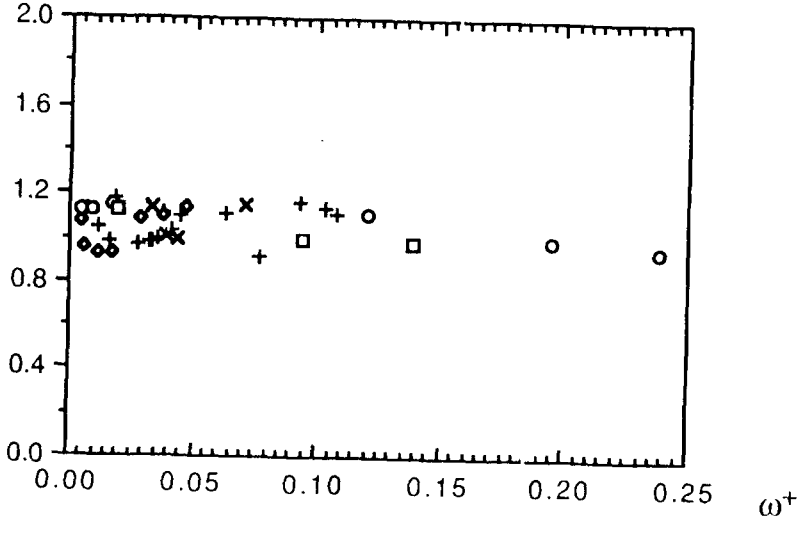

b)

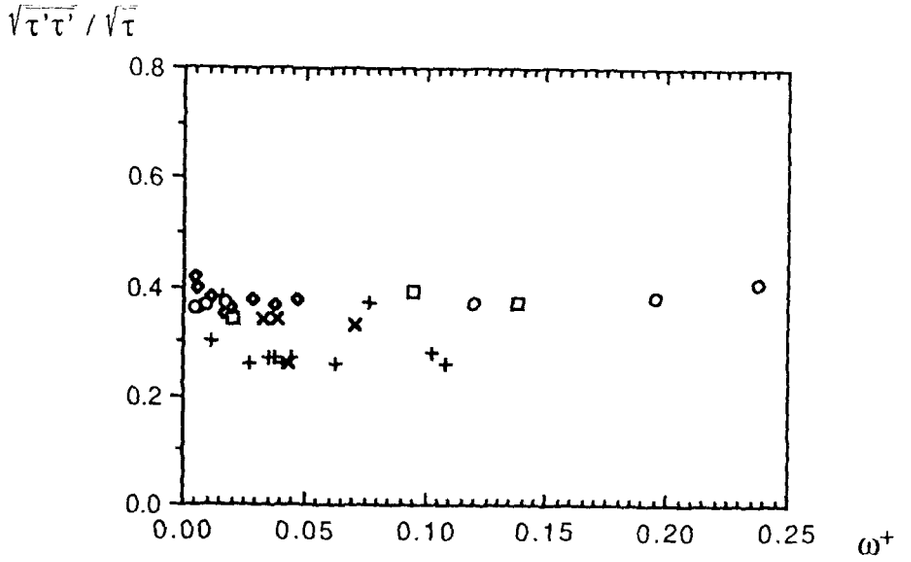

Figure 1) Time mean wall shear stress versus w^+
a)Ratio of the unsteady to the steady time mean wall shear stress
b)Turbulent wall shear stress intensity

a)

$A_{\tilde{\tau}} / A_{\tilde{\tau}\,(\mathrm{Stokes})}$

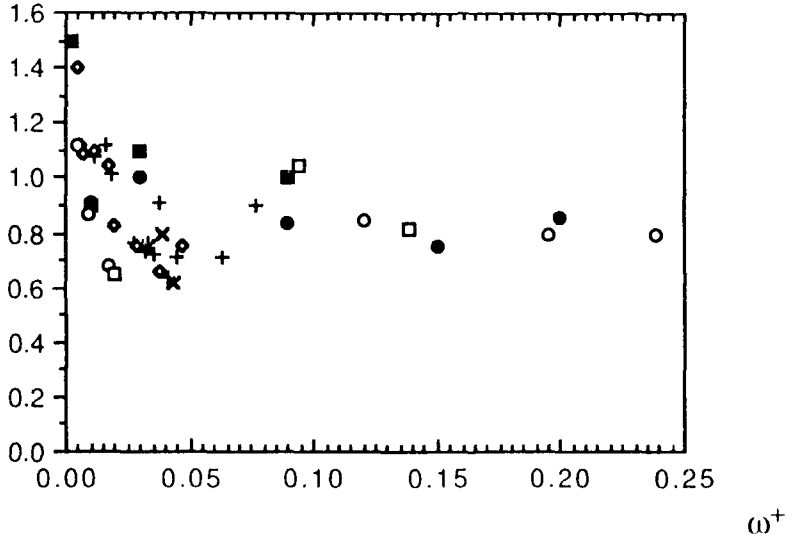

b)

$\Phi\tilde{\tau}$ - $\Phi\tilde{\text{nc}}$

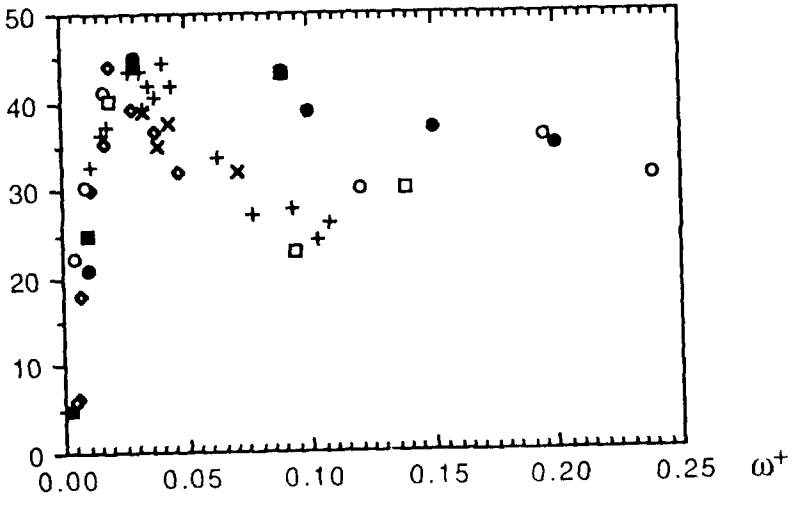

$\Phi_{\tilde{\tau}} - \Phi_{\tilde{u}\tilde{c}}$

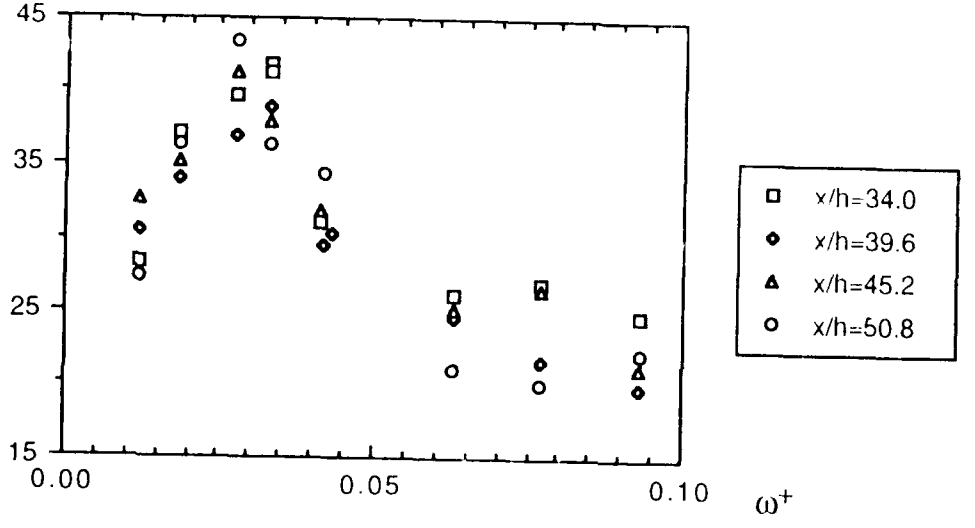

Figure 2) Modulation of the wall shear stress vs imposed frequaency (for legend see Table 1)
a) Amplitude
b) Phase shift
c) Phase shift at several streamwise positions for U_c=10 cm/s; a_{uc}=0.1(Legend on the fig.)

a)

$a_{\tau'\tau'} / a_{\tau'\tau'_{qs}}$

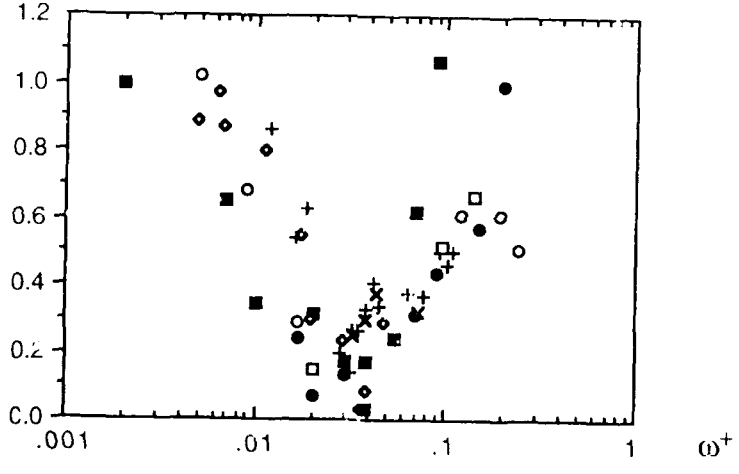

a)

$a_{\widetilde{\tau'\tau'}} / a_{\widetilde{\tau'\tau'}_{qs}}$

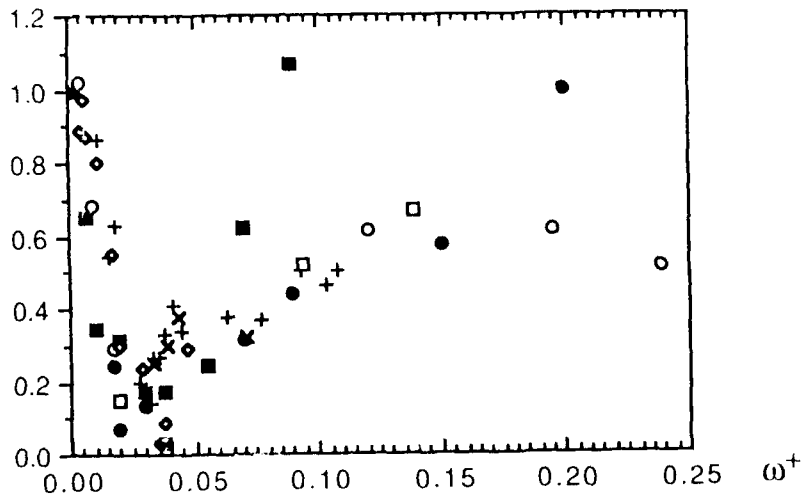

b)

$a_{\widetilde{\tau'\tau'}} / a_{\widetilde{\tau}}$

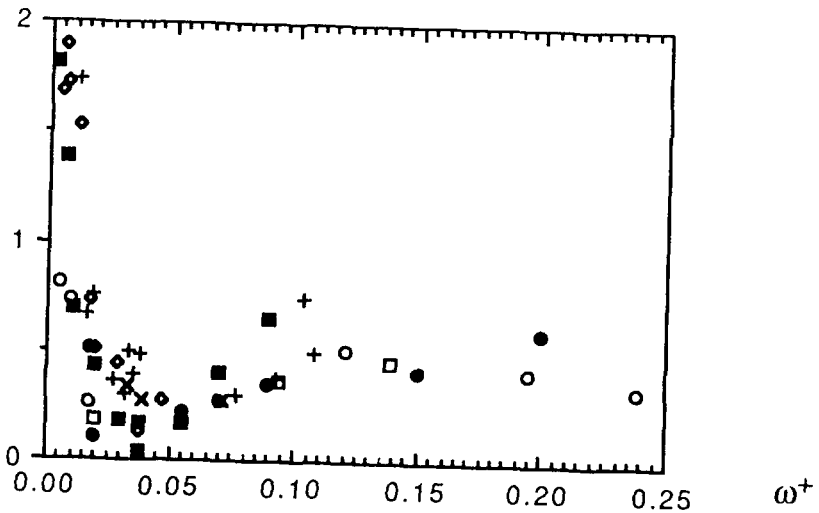

b)

$a_{\widetilde{\tau'\tau'}} / a_{\widetilde{\tau}}$

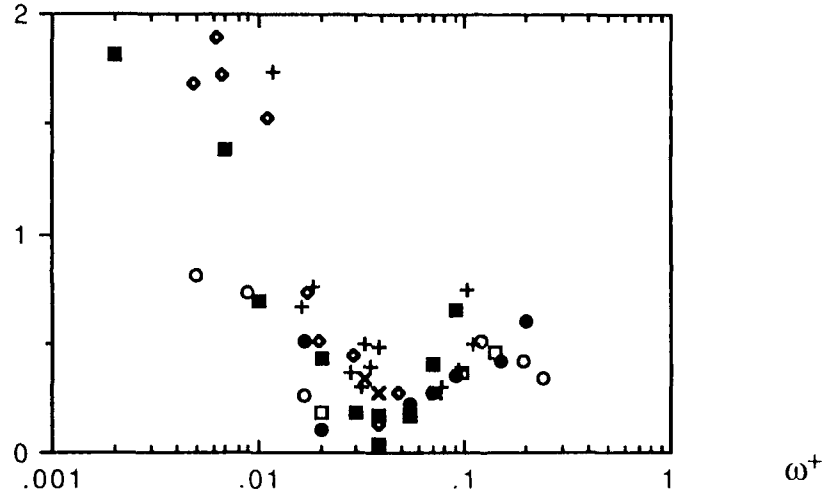

c)

$\Phi_{\widetilde{\tau'\tau'}} - \Phi_{\widetilde{\tau}}$

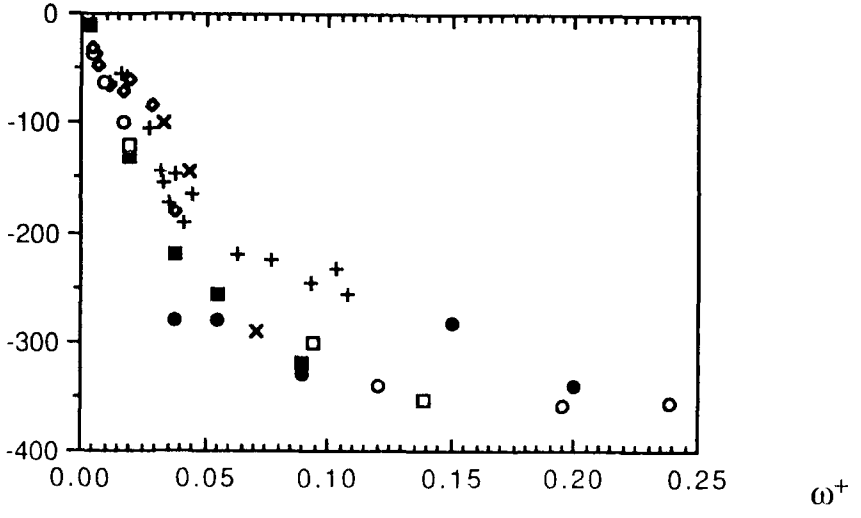

c)

$\Phi_{\widetilde{\tau'\tau'}} - \Phi_{\widetilde{\tau}}$

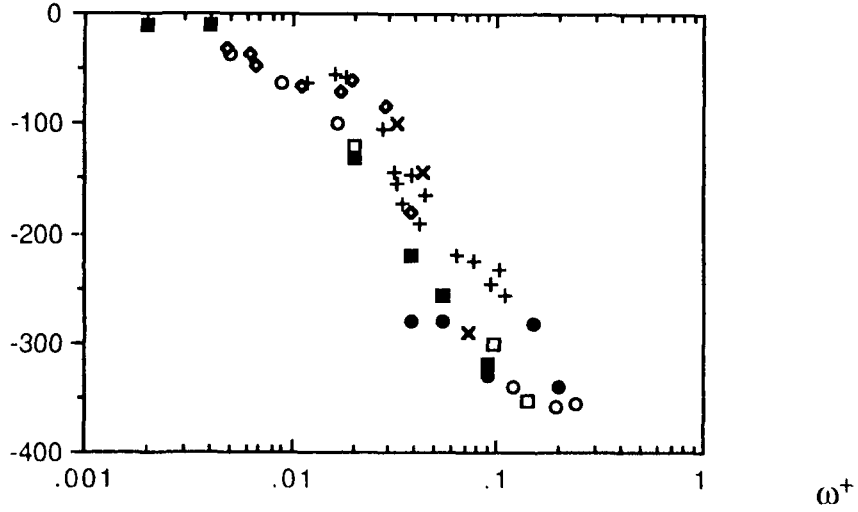

d)

Δt^+

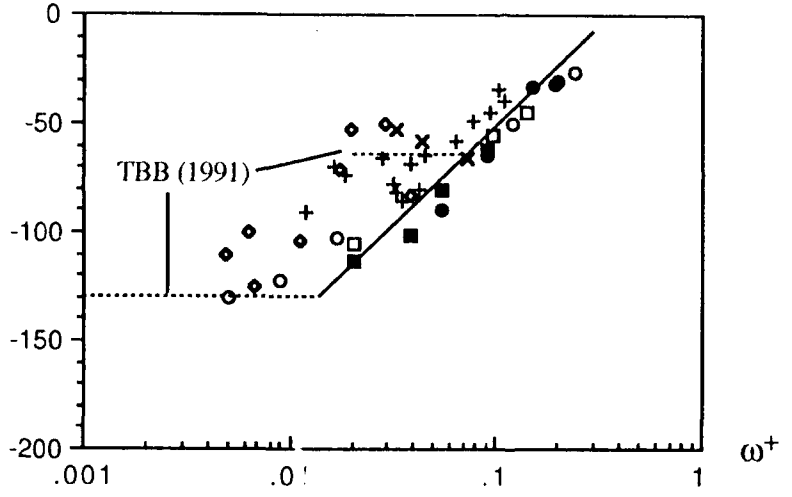

Figure 3) Turbulent wall shear stress intensity modulation. For legend see Table 1
a) Relative amplitude related to the quasi-steady relative amplitude
b) Relative amplitude related to the relative amplitude of the wall shear st
c) Phase shift with respect to the wall shear stress modulation
d) Time lag of the modulation of the turbulent wall shear stress intensity

C

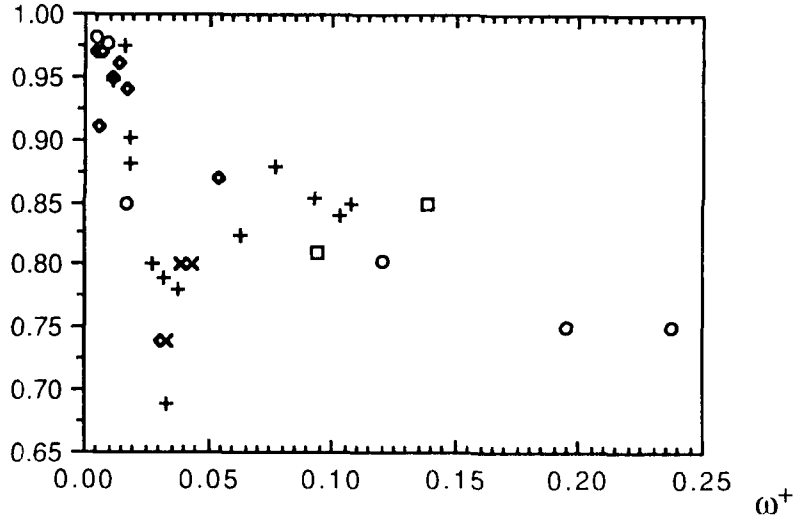

Figure 4) Coefficient of correlation between the phase average of the turbulent wall shear stress intensity and the fundamental.

PART THREE

RESPONSE OF BURSTING TO IMPOSED VELOCITY OSCILLATIONS

Submitted to Journal of Fluid Mechanics

RESPONSE OF BURSTING TO IMPOSED VELOCITY OSCILLATIONS

Sedat F. TARDU Gilbert BINDER

Institut de Mécanique de Grenoble

B.P. 53-X, 38041 Grenoble Cédex France

Abstract

Ejections and bursts in the near wall region in pulsatile channel flow are investigated by means of hot film measurements of the fluctuating velocity u' in the buffer layer and the fluctuating wall shear stress τ'.The forced oscillations have an imposed amplitude of 20% of the centerline velocity and the imposed frequencies are changed from 9.10^{-5} to 6.10^{-3} times the inner frequency.Four single point detection schemes are used and compared.A new technique concerning the grouping of the ejections into bursts is introduced.The modulation characteristics of the detection parameters are discussed.The time mean ejection frequency decreases in the high frequency regime.The amplitude and the phase shift of the ejection frequency depends strongly on the imposed frequency.The modulation of the several characteristics becomes weaker when the imposed frequency is of the same order of the frequency of bursts with multiple ejections. Two independent techniques show that the modulation of the frequency of the bursts with multiple ejections always scales with the modulation of the wall shear stress, while the frequency of the single ejection bursts has modulation characteristics that depend strongly upon the forcing regime. The characteristics of the modulation of the conditionnal averages are also discussed.

1)Introduction

There are two main reasons for interest in unsteady turbulent wall flows. On the one hand such flows occur in a number of practical situations and on the other, forced unsteadiness may be a means of manipulating turbulence. Manipulating turbulence by using forcing velocity oscillations (driven by a periodic pressure gradient on boundary layers or channel flows) has so far been deceptive, because most of the mean flow properties have been remarkably insensitive to such perturbations even when these have large amplitudes (Tardu et al. 1985-1990) . This constancy of the mean characteristics is, however, largely due to the effect of long time averaging because ensemble averages reveal profound changes in the time dependent properties.

Turbulent channel flow with forced periodic oscillations is considered in this investigation.It has been previously found that the the modulation of the turbulent intensities of the streamwise velocity $\langle u'u' \rangle$ and of the wall shear stress $\langle \tau'\tau' \rangle$ vary considerably during the cycle but with decreasing amplitudes when the frequency of the imposed oscillations is high (Tardu et al.1990-Finnicum and Hanratty (1987)). Therefore the fundamental question is how the turbulence production and the coherent structures respond to periodic unsteadiness of sufficiently large amplitude. In various investigations, experimental proofs of the modulation of the bursting process have been given, with sometimes more or sometimes less detail. The published results on this subject are not only very limited but also contradictory.Mizushima et al. (1973-75) have measured an increase in the time mean bursting frequency and they conclude that there is a resonance between the turbulence production mechanism and the forcing when the imposed frequency increases beyond a critical value.However, since their detection technique is based on a weak peak in the auto-correlation function, these results should be considered with caution.The high pass filtered streamwise fluctuating velocity signal used by Richter and Ronneberger (1981) revealed that the rate of occurence is modulated, and it also lags the outer velocity oscillations by the same amount of time as the high turbulent

frequencies.The well established VITA detection technique (Blackwelder & Kaplan 1976) was used by Kobashi & Hayakawa (1981), Cousteix and Houdeville (1983-1985) and by Tardu,Binder and Blackwelder (1987-a). The latter authors paid particular attention to adapt the VITA scheme to the unsteady flow case by taking into account the appropriate modulation of the threshold in phase with the turbulent intensity.The bursting frequency was found to be strongly modulated and in phase with the turbulent intensity, the modulation being strongest when a constant threshold was maintained.Tardu et al. (1987-a) also showed that the characteristics of the conditional averages change considerably during the oscillation cycle.A more systematic study was carried out by Tardu,Binder and Blackwelder (1987-b) who used the streamwise velocity signal at $y^+=15$[1] for four imposed amplitudes going from 10 to 40 % of the free stream velocity and six imposed frequencies ranged from $f^+=3.5*10^{-3}-8.8*10^{-5}$ .VITA with modulated threshold, but constant integration time was used. Although most of the flow properties are unaffected by the imposed oscillations (Tardu et al. 1990) the bursting frequency was found to decrease in the high frequency regime contrary to the increase reported by Mizushima et al.(1975) . The oscilation frequency of $f^+=2.1*10^{-3}$ appeared as a critical value for the modulation characteristics with phase shifts depending more on the imposed frequency than on the amplitude.

Furthermore, recent work on ejections and bursts in steady turbulent wall flows detected with single probes (Bogard and Tiederman, 1986) leads to the question:how much of these modulations of the bursting are really physical and how much are artifacts of the detection schemes? More specifically,if it seems logical to use modulated thresholds proportionnal to <u'u'> (but not to u'u'),for instance,it is not at all obvious what the appropriate integration time should be in the VITA detection scheme.

The second point concerns the rather recent distinction made between ejections and bursts (Bogard & Tiederman (1986)).Indeed every one point detection scheme detects

[1] + designates variables in wall units i.e. normalized by viscosity ν and friction velocity u_τ

ejections and not the bursts, a burst being able to contain more than one ejection (Offen and Kline -1975-). Once the ejections are identified by the single probe, they have to be grouped into bursts. This poses the problem of the adaptation of the existing grouping techniques to the unsteady flow case, in order to study the modulation characteristics of the different groupes of the bursting process.

In this paper the modulation of ejections and bursts is further investigated not only by comparing results obtained through different detection schemes applied to single-probe signals in the buffer layer, but also at the wall using instanteneous wall shear stress signal. Furthermore,every technique used in this study was carefully adapted to the unsteady flow case. It is believed that these results may also have physical insight into the bursting mechanism in steady channel flow.

2)Experimental Conditions; Data Reduction

The experiments were performed in a 100 mm. wide 2600 mm. long channel flow having a span of 1000 mm. as described by Tardu,Binder and Blackwelder,1991(TBB here after). The unsteady flow was generated by a cylinder situated directly upstream of the settling chamber.The amplitude and frequency of the imposed oscillations together with the centerline velocity were changed independently in a continuous manner. The flow was fully developed and turbulent up to $\bar{U}_c$=9 cm/s which corresponds to a Reynolds number based on the channel half width of Re_h=4500. The period of oscillations which ranged from 2.6 s to infinity was repeatable to within 0.2%.

The standard notations are used.A quantity q was decomposed into a mean , $\bar{q}$, oscillating $\tilde{q}$ and a random q' component i.e. $q=\bar{q}+\tilde{q}+q'$; $\langle q\rangle=\bar{q}+\tilde{q}$ designates the phase average. Examples are $\langle f_e\rangle$,$\langle f_b\rangle$, where f_e and f_b are respectively the ejection and bursting frequency. The modulation of several quantities are characterized by the amplitude A and phase Φ of the first Fourier mode of $\tilde{q}$. The relative amplitude is defined

by $a_{\tilde{q}}=A_{\tilde{q}} / \bar{q}$ (ex: $a_{\tilde{fe}}$; $a_{\tilde{fb}}$) . $(+)$ designates the variable normalized with inner scale $\bar{u}_\tau$ $\nu/\ \bar{u}_\tau$, $\bar{u}_\tau^2 / \nu$ velocity ,length and frequency based on the time mean wall shear stress $\bar{\tau}$.

In previous works (Binder et al (1985);TBB (1991)),it was shown that the similarity parameter for the oscillating inner layer is the Stokes length in wall units $l_s^+=l_s/l_\nu$, where $l_s=\sqrt{\nu/\pi f}$, f being the imposed frequency.When the imposed frequency is sufficiently high i.e. for $l_s^+<10$, a viscous Stokes flow coexists with the time mean turbulent flow.The turbulence is then relaxed and the amplitude of the fluctuating quantities such as $a_{\tilde{\tau'\tau'}}$ and $a_{\tilde{u'u'}}$ decreases. However at $l_s^+\cong 8$ a nonlinear interaction between the oscillating flow and $\langle\tau'\tau'\rangle$ takes place and $a_{\tilde{\tau'\tau'}}$ increases again for $l_s^+< 8$ (Finnicum and Hanratty ,1988; Tardu and Binder 1991). This study was carried out for $f^+=1/\pi l_s^{+2}< 0.0073$, where the upper limit roughly corresponds to the end of the relaxation regime.

The measurements were made by means of a DISA 55 R11 single fiber probe located at $y^+=15$ and a TSI 1268W flush mount . hot film gauge.The sensing element of the fiber probe is 70μm in diameter, and 1.25 mm. long (13-9 l_ν depending on the mean flow conditions) .The dimensions of the sensing element of the hot film gauge are 127μm in diameter and 1.016 mm in the spanwise corresponding to $\Delta x^+=1.3$-0.9 and $\Delta z^+=10.5$-7.4. Thus the dimensions remain within the acceptable limit therefore avoiding the spanwise averaging of the detected events (Haritonitis & Blackwelder -1987-)

The calibration was done in situ by operating the channel at different mean velocities.The calibration range covered 0. to 1.6 times the mean centerline velocity. This corresponded to an equivalent imposed amplitude of 60%, while the imposed amplitude was limited to 20% in this investigation. The LDA was used to determine the friction velocity $\bar{u}_\tau$ from the logarithmic layer and the velocity gradient at the wall in steady flow.The mean wall shear stress τ was aptly correlated by the Blasius formula

$\tau=0.048\ Re_h^{-1/4}\ \rho\ U_c^2\ /2$ and this relationship was then used with five centerline velocities to obtain a least square fit of the mean output voltage squared and $\tau^{-1/3}$. The calibration of the hot film at $y^+=15$ was carried out by measuring the velocity at the same point by LDA. At least six calibration points were applied to the least square formula $e^2=A+Bu^n$ where e is the hot-film anemometer output voltage. n was found to be between 0.45 and 0.5 .

The measurements were taken with two time mean flow conditions (Table 1) . In both cases the imposed amplitude at the centerline equalled 20 % . Flow visualizations, by means of the injection of dye by a wall slot showed that no instanteneous reverse flow exists in this case in the range of the imposed frequencies investigated in this study. Since no significant Reynolds number dependency on the ejection and bursting frequency modulation characteristics was observed when the inner scaling is used (the time mean Reynolds number was changed only by a factor of 1.43) the results will be presented in the same group for the sake of clarity of the exposé.

Two systems were used for the data acquisition and reduction.In the first case the analog output signals were digitalized by a Preston A/D converter (15 bit accuracy + sign) stored in digital form and processed on a Nord-100 computer.In this case the sampling frequency was set between $f_s=4.2 \cdot 8.1\ f_v$ depending on the mean Reynolds number. In the second case the acquisition was done by means of Analog Device RTI-800 series acquisition cards with 12 bit accuracy, 8 input channels. The removal of the constant anemometer voltage was carried out by using D/A conversion. The analysis of the data was then performed on a PC. In this case the acquisition frequency equalled $2\ f_v$. The signals were prefiltered by a Krohn-Hite filter with accurate cut-off frequencies.

Once the hot-film signals were stored u and τ were calculated from the calibration curve (calibration was checked before and after each run),then the phase averages $\langle u \rangle$ and $\langle \tau \rangle$ were computed and stored. The phase average of the velocity and of the wall shear

stress was then used to determine the phases and the amplitudes of the Fourier modes by least square analysis.The first two Fourier modes of $<u>$ and $<\tau>$ were found to be representative within 99%.Thus they have been used to determine $u'(t)=u(t)-<u>$ and $\tau'(t)= \tau(t)-<\tau>$ for each acquisition point.

One of the main difficulties that investigation of unsteady flows poses is the need for long record length, because the statistical convergence has to be ensured in each bin of the oscillation cycle.The total record length of the velocity and of the wall shear stress data was $2.2 \cdot 10^5$ T_ν for Re_h=11400 (9300 T_{out} ; $T_{out} = h/\tilde{U}_c$ is the outer time scale) and $1.16 \cdot 10^5$ T_ν (6570 T_{out}) for Re_h=8345. The number of bins alternated between 50 and 25 depending on the quantity investigated.Consequently the minimum record length for each bin was $4.\cdot 10^3$ T_ν (219 T_{out}).

3) Flow characteristics

The present measurements confirm previous results (TBB) that the time mean flow is not affected by the imposed oscillations over the ranges of frequencies tested. In particular $\sqrt{\overline{u'u'}}/u_\tau = 2.6$ a value which is sensibly equal to the steady value at $y^+=15$ and the time mean turbulent wall shear stress intensity is $\sqrt{\overline{\tau'\tau'}}/\bar{\tau}=0.35$-$0.4$ as in steady flow.

The modulation of the wall shear stress also confirms earlier results, namely for $f^+>0.003$, the amplitude of $<\tau>$ is nearly equal to the viscous Stokes amplitude with a phase shift of $\Phi_{\tilde{\tau}} - \Phi_{\tilde{uc}} = 45^0$.

Figure 1 shows the behaviour of the modulation of the turbulent intensity $<u'u'>$ and of the turbulent wall shear stress intensity $<\tau'\tau'>$ versus the imposed frequency f^+. The sharp decrease of the ratios $a_{\tilde{\tau'\tau'}}/a_{\tilde{\tau}}$ and $a_{\tilde{u'u'}}/a_{\tilde{u}}$ is clear from Fig. 1a , in a way similar to TBB. Note, however that at the highest imposed frequency $f^+=0.0073$ investigated here a

difference of the behaviour of <u'u'> and <τ'τ'> is observed. $a_{\widetilde{\tau'\tau'}}/a_{\widetilde{\tau}}$ and $a_{\widetilde{u'u'}}/a_{\widetilde{u}}$ are indeed, increasing again at this imposed frequency. This behaviour is persistant for higher f^+ as it was shown by Finnicum and Hanratty (1988), and more recently by Tardu and Binder (1991).

The phase shifts $\Phi_{\widetilde{u'u'}} - \Phi_{\widetilde{u}}$ at $y^+=15$ and $\Phi_{\widetilde{\tau'\tau'}} - \Phi_{\widetilde{\tau}}$ are shown on Fig. 1b. The corresponding time lags $\Delta t^+ = -(\Phi_{\widetilde{u'u'}} - \Phi_{\widetilde{u}})/2\pi f^+$ and $\Delta t^+_{\tau'\tau'} = -(\Phi_{\widetilde{\tau'\tau'}} - \Phi_{\widetilde{\tau}})/2\pi f^+$ agree well with the values reported by TBB. Note that the time lag is 2 to 3 times larger in the viscous layer than in the buffer layer. Furthermore a difference is again noted at the highest imposed frequency. Indeed, Tardu and Binder (1991) have shown that in this high frequency range the time lag is no more constant but decreases with increasing frequency.

4.)Detection schemes

Three detection schemes were used and compared: u'-level, modified u'-level (Luchik & Tiederman 1987) (here after designated by u'-l and m-u') and VITA (Blackwelder & Kaplan 1976).Each of these methods require a single turbulent signal and they have high detection probabilities of ejections when compared with visual observations or with results from the u'v'-quadrant method (Bogard & Tiederman 1986).

The detector function D(t) of the m-u' and u'-l schemes is defined as follows:

m-u' : $D(t)=1$ if : $-L_1\sqrt{\langle u'u'\rangle} > u'(t) > -L_2\sqrt{\langle u'u'\rangle}$

u'-l: $D(t)=1$ same as m-u' but $L_1=L_2$

where L_1 and L_2 are the detection parameters.The adaptation of these detection methods to the unsteady case poses no problem, if the threshold is carefully chosen. It is important to note that the local value in the cycle <u'u'> (t/T) is used in the threshold rather than the time mean value $\overline{u'u'}$, in the same way as the local value of $\overline{u'u'}$ is taken when these schemes are applied at different y^+ positions in steady flow. The detection parameters L_1

and L_2 were set at their usual values as used in steady channel flow namely:

u'-l : L_1=-1.3 L_2=-1.25

m-u': L_1=-1 and L_2=-0.25

After determining the time of occurrence of the trailing edge ($u'(t) > -L_2\sqrt{<u'u'>}$) and the leading edge ($u'(t) < -L_1\sqrt{<u'u'>}$) of an ejection, the number of events occurring during the opening of a phase-locked bin are then counted, the frequency $<f_e>$ being the total number of events in the bin divided by the time the bin was open. Thus, one can determine the modulation of the ejection frequency based on the trailing and the leading edge of the events. Since no significant difference was observed , only the modulation of $<f_e>$ based on the leading edge will be studied.

The detector function for VITA is:

D(t)=1 if: $\sigma_v > k<u'u'>$ and $du'/dt > 0$

D(t)=0 otherwise

$$( )_v = {}^{1}\!/_{<T_v>} \int_{t-<T_v>/2}^{t+<T_v>/2} ( )\,dt'$$

where $\sigma_v=(u'^2)_v-(u'_v)^2$.

VITA was applied to u'(t) at y^+=15 as well as to the instanteneous wall shear stress $\tau'(t)$.At y^+=15 the threshold was set at k=0.35 as in steady flow also used by Luchik & Tiederman (1987),while at the wall k equalled 0.165. This last value which is smaller than the threshold used at y^+=15 (as was also encountered in the measurements of Chambers et al.,1983), was found in the steady channel flow to give the same time mean ejection frequency at y^+=0 compared with the detection at y^+=15. Note also that k=0.35 is significantly smaller than k=1 used generally to determine the bursting frequency, since the procedure here is to determine first the ejection frequency and then, to group them into bursts which requires a smaller threshold as concluded by Luchik &

Tiederman (1987) in their comparative study of probe detection with visualization results.

The time of occurrence of a VITA ejection was taken as the middle of the D(t) pulse.Note that only the accelerating events were taken into account.The thresholds are set respective to the phase average of $\langle u'u' \rangle$ at $y^+=15$ and $\langle \tau'\tau' \rangle$ at the wall.The methods giving the modulation of the VITA integration time $\langle T_v \rangle$ will be discussed in the next paragraph.

5.)Modulation of the VITA integration time

The adaptation of the VITA detection scheme poses another problem, namely the proper choice of the modulation of the VITA integration time $\langle T_v \rangle$. This is more difficult than setting the modulation of the threshold, since it is generally less easy to have access to the information concerning the modulation of a time scale.On the other hand the proper choice of $\langle T_v \rangle$ is important since the time scale of the detected structures depends strongly on the integration time (Johannson and Alfredson (1982)).

Two methods have been used here to determine $\langle T_v \rangle$.The first one was based on the comparison of individual detected VITA events with u'-level and m-u' level ejections.To this end the VITA analysis is performed for a range of integration times $\overline{T^+}_v$=0-40 in a given phase range (10 bins have been used for this purpose). For each $\overline{T^+}_v$ and each bin the following quantities were computed:

* The ratio <r> equal to number of VITA events divided into the number of u'-level (or m-u') events

**The one to one correspondance probability $\langle P_C \rangle$(probability for one and only one VITA event between two consecutive u'-l events,and same for m-u') ie:

$\langle P_C \rangle = \langle N_C \rangle$ / $\langle N_{u'\text{-level}} \rangle$ where $\langle N_C \rangle$ is the phase average of one-to one corresponding VITA events and $\langle N_{u'\text{-level}} \rangle$ is the corresponding number of detected u'-level ejections.

Other quantities such the multiple correspondance probability (probability that one or

more than one VITA events are found between two consecutive u'-level (m-u') ejections; when they are multiple correspondance, only one of the VITA events is counted as the corresponding event with a specified reference occurrence time),the total correspondance probability (the sum of multiple and one-to one correspondance probabilities), and the false detection probability.Details will not be discussed here and they can be found in Tardu (1988).

The value of $<T_v>$ is then selected such that $<P_C>$ is maximum and $r \equiv 1$. This procedure gives in some way the modulation of the time scale of the high shear layer structure given place (or being to) the high level crossing structures.

Figures 2.a and 2.b show the distribution of the one-to one correspondance probability between VITA and u'-l events as a function of $<T_v^+>$ for two epochs of the oscillation cycle ($l_s^+=9.5$).The maximum value of $<P_C>$ is about 0.4 and it is difficult to correctly define the corresponding value of the integration time since the curves are quite flat.Neverthless, the one to one correspondance probability between m-u' and VITA events is higher (the time mean value is about $\overline{P_C} \equiv 0.7$) with a well defined peak which provides a good definition of $<T_v>$.Some examples corresponding to $l_s^+=9.5$ are shown in Figures 2.c and 2.d and the same behaviour was observed for other flow configurations. The ratio <r> is also given on the same figures.

The good correspondance between m-u' and VITA may be understood by noticing that,with the given parameters,VITA detects events with u'-variation such that: $\Delta u'=\sqrt{0.35<u'u'>}=0.6\sqrt{<u'u'>}$ and m-u' detects events such that $\Delta u' = 0.75\sqrt{<u'u'>}$ (of course,for VITA this $\Delta u'$ must occur over a $\Delta t \equiv T_v$ while for m-u', u' must rise from $u'=-1\sqrt{<u'u'>}$). The u'-l detector on the other hand,is only associated with a large negative value of u', $-1.3\sqrt{<u'u'>}$, and small oscillations about this value will each be counted. Remind also that Luchik & Tiederman (1987) defined the VITA parameters ($k=0.35\ \overline{T^+}_v=13$) ,used also in this study,to have maximum correspondance between the

probe and visually detected events.

The figure 3 shows examples of the VITA integration time obtained by the method of correspondance, for l_s^+=9.5 and 60. The immediate conclusion is the strong dependance of the VITA time scale on the imposed frequency. The part of the subjectivity of determining $<T_v>$ by use of $<P_{CP}>$ may be estimated to be not negligible. In the majority of the cases the maxima of $<P_{CP}>$ was well defined, neverthless when its distribution presented a plateau region, the smallest value of $<T_v^+>$ for which $<r>$=1 was chosen. In all of the cases,the distributions of the probability of false and total correspondance were also taken into account and compared.If,in spite of everything, the choice of $<T_v^+>$ was judged to be not convincing, the corresponding bin was suppressed during the phase averaging.It is not possible to compute $<T_v^+>$ in this way for the wall shear stress fluctuations, since it is not established that the u'-level or the m-u' method may be applied to $\tau'(t)$.

A second method is based on the conditionnal averages $<u'_{cond}>$ and $<\tau'_{cond}>$.In steady flow the characteristic time scale of the conditionnal averages Δt ,defined as the coordinate difference between the minimum and the maximum of u'_{cond} is directly related to $\overline{T_v}$ (Johannson & Alfredson (1982). An iterative method is thus developped.

The conditionnal averages are phase averaged for at least 22 bins.The smallest number of ejections contributing to the ensemble averages was about 50. Examples of $<u'_{cond}>$ and $<\tau'_{cond}>$ at different times of the oscillation cycle are shown in Figure 4. Figure 4 compares well with other published data in steady flow (Johannson & Alfredson (1982); Shah & Antonia (1986). To be consistent with the data published elsewhere the suggestion of Chambers et al. (1983) was adapted to define the characteristic time scale $\Delta t_{\tau'}$: this time scale is defined as being the time interval during which :

$$<\tau'_{cond}> = (1-e^{-1})<\tau'_{cond}>_{max}$$

It has to be noted that the abscissa in figure 4. is normalized with the time mean of

the inner time scale $\overline{t_v}$ and not with its phase average $<t_v>$.The modulation of $<\Delta t^+>$ is then clear especially for $l_s^+=44$, and that if the time abscissa was normalized with $<t_v>$, the conditional averages would completely coincide in the quasi-steady limit .

The iterative procedure begins first by computing the modulation of the VITA ejection frequency with a time mean integration time $T_v^+=13$. The conditional averages are then performed and the modulation of the structure characteristic time scale $<\Delta t^+>$ is computed. The modulation of the integration time is then taken proportional to $<\Delta t^+>$, i.e.

$$<T^+_v> = \frac{\overline{T^+_v}}{\overline{\Delta t^+}} <\Delta t^+>$$

since $\overline{T^+_v} \neq \overline{\Delta t^+}$), and is injected into the VITA ejection computation.The procedure is repeated until $<\Delta t^+>$ and the phase average of the ejection frequency $<f_e^+>$ (time mean,amplitude and phase) are converged.

The VITA filtering detects a dominant band of time scales rather than events with a unique time scale. As a constant T_v is imposed for each epoch of the oscillation cycle at the first stage of the procedure, and if the time scale of the conditional averages was simply proportional to the integration time, any modulation of $<\Delta t^+>$ should be observed. $a_{\widetilde{\Delta t^+}}$ that results from the iterative procedure then indicates tnat the median of the time scales of the contribuing VITA events is shifted with respect to the imposed constant integration time.

Figure 5 shows examples of the modulation characteristics obtained during the iterations. In all of the cases, 3-4 iterations were sufficed to obtain convergence for $<T_v>$ and $<f_e>_{VITA}$. It has to be noted that even at the beginning of the procedure (iteration number $N_i=0$) when a constant integration time is imposed an important modulation of $<T_v^+>$ is obtained. In the quasi-steady limit ($l_s^+=44$) a relative amplitude as important as 0.23 is computed.This behaviour is frequency dependent (see for example the case

concerning $f^+=0.0022$ for which $a_{\widetilde{T_v}}$ is small from the beginning to the end of the procedure).

The phase average of the modulation of the characterisric time $<\Delta t^+>$ was well converged and the fundamental mode was representative to within 90% in all of the cases.

Figure 6 summarizes the characteristics of the modulation of the VITA integration time using the correspondance method and by the computation based on the conditionnal averages. The relative amplitude of $<T_v^+>$ based on $<\Delta t^+>$ is systematically greater than a_{Tv} obtained by the use of $<P_{CP}>$ but the maximum difference does not exceed 20%.It is somewhat surprising that the two methods coincide so well, although they were completely independent.The modulation characteristics of the VITA ejection frequency obtained by the two methods differed by less than 10% (time mean,amplitude and phase shift). The iterative method was preferred to determine $<f_e>_{VITA}$, since it was judged to be more objective.

In the quasi-steady limit the proper choice of $<T_v>$ is such that $<T_v>/<t_v>=<T_v>/<v/\tau>=13$ at each epoch of the oscillation cycle.This implies that $a_{\widetilde{T_v}}$ has to be equal to the relative amplitude of the wall shear stress $a_{\tilde{\tau}}$ and $<T_v>$ should be in opposition of phase with respect to $<\tau>$ i.e $\Phi_{\widetilde{T_v}} - \Phi_{\tilde{\tau}} = 180°$. (supposing the linear approximation is valid which is approximatively the case here). Figures 6-b and 6-c show that, indeed this is the case for $f^+<3.5*10^{-4}$ ($l_s^+>30$). The modulation of the VITA integration time becomes weaker as the imposed frequency is increased not only for the detection at $y^+=15$ but also for the detection at the wall. $a_{\widetilde{T_v}}$ presents a minimum at $f^+=2.2*10^{-3}$ ($l_s^+=12$). That means that even at the wall $<T_v>$ is frequency dependent and does not always scale with $<t_v>$ contrary so would be expected. This behaviour is a real manifestation of the unsteadiness: $l_s^+=12$ corresponds to a particular imposed frequency for which the

behaviour of several characteristics is altered for example the phase shift $\Phi_{\widetilde{u'u'}} - \Phi_{\widetilde{u}}$ at $y^+=15$ (TBB, 1991). For $f^+>2.2*10^{-3}$ the modulation of $<T_v>$ increases again, more rapidly at the wall however than at $y^+=15$, but $a_{\widetilde{T_v}}$ is found to be smaller than its quasi-steady value in a large range of imposed frequencies.

The phase shift $\Phi_{\widetilde{T_v}} - \Phi_{\widetilde{\tau}}$ is also frequency dependent (Fig. 6c). $\Phi_{\widetilde{T_v}} - \Phi_{\widetilde{\tau}}$ obtained at the wall generally coincides well with the phase shift at $y^+=15$. Note a tendency of the VITA integration time to be in phase with the modulation of the wall shear stress in the very high frequency regime i.e. $\Phi_{\widetilde{T_v}} - \Phi_{\widetilde{\tau}}$ reaches values as near as 300°. Thus, the quasi-steady assumption $<T_v>=cte*<v/\tau>$ is only valid in a small range of the imposed frequencies as otherwise real unsteady effects have to be taken into account.

6) Modulation of the ejection frequency

6.1) Modulation of u'-level and modified u'-level ejection frequency

Although some correspondance exists between the level crossing and VITA events it is noteworthy to say that these two categories of events correspond to different parts of the bursting event. First of all, VITA contains a time scale, and detects strong internal shear layers; for the sake of brevity we will call them VITA ejections instead of using the internal shear layer activity. For this reson u'-level and mu' ejection frequency is studied separately from the VITA events.

The evolution of $<f_e>$ obtained with the u'-level and mu' method is shown in figure 7 for $f^+=3.5*10^{-3}$ and $0.09*10^{-3}$. The phase average of $<f_e>$ was generally well defined and the fundamental was representative to within 90%.

The results obtained with the u'-level method generally coincide well with the m-u' method (Figure 8). In spite of slight differences observed in the amplitude, the two

detection schemes give more or less the same results, although they are quite different.The one-to-one correspondance probability between these events is small (40%) but the total correspondance probability is high (70%) and that explains why at the average $<f_e>_{u'\text{-level}}$ coincides with <fe>mu'.

The steady ejection frequency obtained for Re_h=12500 and 8750 is

$$\overline{f_e^+}_{(Steady)} = 0.0123$$

and in unsteady flow we find:

$$\overline{f_e^+}_{(Unsteady)} = 0.0120$$

a value which also compares well to the data given by Coughran&Bogard (1987) -steady channel flow-. A decrease of the time mean ejection frequency of about 20% is observed at $f^+=3.5*10^{-3}$; the same behaviour was also noted for the zero-crossing frequency (TBB-1991). It is difficult to conclude from one point measurement that the level crossing is affected at the mean, but the same tendency is noted with the VITA events, with a time mean $\overline{T^+_v}$ and modulated $<T^+_v>$ integration time. On the other hand the same decrease of the ejection frequency was also reported by Tardu et al. (1986) with VITA events for which the detection was done using a larger threshold (k=1) and the study was enlarged for different imposed amplitudes ranging from 10 to 40%.

It has been shown by TBB (1991) that in the high frequency regime, the unsteady effects are confined into the Stokes layer of thickness $l_s=\sqrt{Tv/\pi}$ with a time mean turbulent flow coexisting with a purely Stokes flow and the scaling with respect to l_s is appropriate. It has to be noted that for the highest frequency investigated in this paragraph, $l_s^+=7.2$, the level crossing detection point $y^+=15$ is in the outer region of the Stokes layer,since $y_s=y/l_s=y^+/l_s^+=2.2$. Thus, if there exists some tendency of the time mean level crossing ejection frequency with increasing imposed frequency (i.e $l_s^+<9.5$) this tendency may be obscured since the detection point is in the plug flow for

$l_s^+<8$. To clarify this point, profiles of $<f_e>$ are needed as a function of y_s.

The u'-level and mu' ejection frequency is strongly modulated in the whole imposed frequency regime investigated in this study (Fig.8b).If it is assumed that $<f_e>$ scales with the inner variables, in the quasi-steady limit one should have:

$<f_e>\nu/<\tau>=(f_e^+)_{steady}$

which implies with the linear approximation:

$a_{fe}=a_\tau$ and $\Phi_{fe}=\Phi_\tau$

Those conditions are well established for $l_s^+>30$ (Figures 8.c and 8.d).The present observations also confirm the inner scaling of the ejection frequency.

The real manifestation of the unsteadiness on the ejection mechanism takes place in the high frequency regime.The relative amplitude again has its minimum value at $f^+=0.0022$ ($l_s^+=12$). Although the amplitude is frequency dependent the phase shift $\Phi_{fe}-\Phi_\tau$ is less sensitive to the imposed unsteadiness and the ejection frequency is almost in phase with the wall shear stress ,even though with a slight phase lag near $f^+=0.0012$ ($l_s^+=16$). The phase shift with respect to the local turbulent intensity $<u'u'>$ increases with increasing frequency f, and $<f_e>$ becomes in quadrature with $<u'u'>$ at high frequency. At $f^+=0.006$ ($l_s^+=7.2$) a_{fe} reaches again its quasi-steady value but $a_{fe}/a_\tau \neq 1$, since for $l_s^+<20$ the wall shear stress follows the viscous solution with $A_{\tau(Stokes)}=\sqrt{2}\,A_{uc}/l_s$, and consequently a_τ increases with increasing frequency.

6.2) Modulation of VITA ejection frequency

The VITA detection scheme is applied to both u'(t) and $\tau'(t)$ and the modulation characteristics of $<f_e>$ is studied in a slightly extended range of imposed frequency compared with the level crossing ejection frequency. Figure 9 compares results obtained in

this way using the modulated VITA integration time as discussed in 5. The VITA ejection frequency obtained by taking a time mean T_v generally compares well with these results, but the time mean ejection frequency is found to be smaller by an amount of 5-8 % smaller and slight differences of a the amplitude and phase shift of $<f_e>$ are noted.

The comparison of the figure 9 with the figure 8 allows us to conclude that the modulation characteristics of the VITA ejection frequency with $<T_v>$ and T_v at $y^+=15$ are similar in every aspect to those of the level crossing ejection frequency (The results obtained with u'-level method are also plotted on fig. 9 to allow comparison). This has to be expected since, it has been shown that the VITA events with $<T_v>$ correspond up to 70% on a one to one basis with m-u' events and the latter have the same modulation characteristics compared with u'-level ejections.

The time mean VITA ejection frequency is shown in fig. 9.a. The sudden decrease of f_e^+ in the range $0.003<f^+<0.005$ is clear, especially from the measurements at the wall. With regards to this point, the effect of the imposed unsteadiness on f_e^+ at the buffer layer is relaxed more rapidly than at the wall, i.e. the mean ejection frequency at $y^+=15$ returns to its quasi-steady value at $f^+=0.005$, earlier than at the wall, where the same phenomena takes place at $f^+=0.006$. The ejection frequency is the only quantity which is found to be affected at the mean, and, in a systematical manner by the imposed oscillations. That would indicate a decrease of the time mean production rate by an amount of 10-20%. A similar conclusion was observed in the numerical simulation of Reddy(1984) who found a decrease of the production rate (of about 20%) around $y^+=12$ for $a_{uc}=0.50$ and $f^+=0.01$,so at a much higher imposed frequency than in our measurements.

The ratio of the relative amplitude of the VITA ejection frequency to a_τ is shown in Fig. 9b. At the wall the ejection frequency has slightly smaller relative amplitudes than at

$y^+=15$ in the high imposed frequency, when omitted this detail has the same modulation amplitude.

Some differences in the behaviour of Φ_{fe}-Φ_τ are noted from Fig. 9c in the range of *imposed frequencies corresponding to* $0.001<f^+<0.002$. The increase of the phase shift begins earlier at the wall than in the buffer layer. This observation is in general agreement with the differences observed in the phase shifts of $\Phi_{\tau'\tau'}$-Φ_τ and $\Phi_{u'u'}$-Φ_u $(y+=15)$ (TSB 1991).

Another interesting point concerns the modulation of the average peak of $\sigma_{u'}$ and $\sigma_{\tau'}$ of the detected events when scaled respectively by $k_{u'}$ <u'u'> and $k_{\tau'}$ <τ'τ'> i.e. $<\sigma_{u'}(t)D(t)_{max}> / k_{u'}$<u'u'> and $<\sigma_{\tau'}(t)D(t)_{max}> / k_{\tau'}$<τ'τ'>. The value of this function is respectively 3. and 2. for the τ' measurements and for u' measurements and the relative amplitude varies from 8 to 3 % being systematically smaller for the fluctuating streamwise velocity. This may be interpreted as a lack of bias of the detection scheme toward the cycle variations of the turbulent fluctuations. It must, however, be recognized that a strong modulation of the detected relative peak values of σ could have meant a true change in the structure of u'(t) and τ'(t) and not necessarily a bias of the detection scheme.

6)Modulation of the bursting frequency

6.1)Grouping of the u'-level ejections

6.1.1)Modulation of the u'-level grouping time

Before the bursts can be counted it is necessary to group ejections which belong to the same burst.This implies the definition of the bursts with multiple ejections (BME) resulting from multiple break-up of the same streak (Bogard & Tiederman (1986) ; Kim et al. (1971)),and bursts with a single ejection (BSE).

The grouping of the u'-level ejections at a given phase is done in much the same way as in steady flow, by use of the cumulative probability distribution of time between ejections P(t/t'>t) (Barlow and Johnston (1985) ; Bogard & Coughran (1987)).This distribution has a break which marks the separation between the two types of ejections belonging to BME and BSE.The phase average of P(t/t'>t) has been generally done using 5 to 4 bins.The minimum ejection number contributing to P(t/t'>t) was 250 for Re_h=8750 and 500 for Re_h=12500.Figure 10 the cumulative probability distribution of u'-level ejection interarrival times at 4 epochs of the oscillation cycle for l_s^+=9.5.P(t/t'>t) was generally well converged and the break point which gives the grouping time $<t_g>$ was well defined.To minimize the part of the subjectivity the regression lines were systematically computed in the ranges $(0;0.6)<t_e>$ and $(0.;2.5)<t_e>$.

$<t_g>$ is another time scale which has been studied in detail in this study.In steady flow the grouping time t_g is related to the ejection period by t_g/t_e=0.6 , which gives t_g^+=49.Figure 11.a shows that the time mean grouping time is sensibly equal to its steady value for l_s^+>9.5.A decrease of about 25% is observed in the high frequency regime for l_s^+=7.2.On the other hand in the quasi-steady regime , the grouping time is related to the ejection period by $<t_g>=0.6<t_e>=0.6/<f_e>$.This implies with the approximation of small amplitudes that:

$$a_{tg}=a_{fe} \text{ and } \Phi_{tg}-\Phi_{fe}=180^\circ$$

Figures 11-c and 11-d show indeed that the above relationships are well established for l_s^+>30.The modulation characteristics are, however, completely different when the imposed frequency increases further.The amplitude decreases by an amount of 30% already at l_s^+=16, and the minimum of a_{tg} is still found to be at l_s^+=12 (figure 11-b).The phase shift for l_s^+> 16 is particullarly interesting since the grouping time is no more in opposition of phase with the ejection frequency but $\Phi_{tg}-\Phi_{fe}$ is about 45° for l_s^+=9.5 and

$<t_g>$ lags $<f_e>$ at $l_s^+=7.2$ (*figure 11.c*)It has to be noted that the particullarly long duration of the data allowed us to find the phase average of all the quantities and parameters involved hereand to clarify the real unsteady effects.It would be more easier ,but not correct to take into account only the time mean of the parameters,for instance t_g since, all of the quantities are strongly modulated ,and more importantly the phase shift is a strong function of the imposed frequency.In order to point out the deviation from the quasi-steadiness $a_{<tg>/<te>}$ is also plotted on figure 11.b.If $a_{<tg>/<te>}\neq 0$,the grouping time modulation behaves differently than in the quasi-steady regime.Indeed $a_{<tg>/<te>}$ is approximatively 0.04 at $l_s^+>30$ but increases up to 0.24 at the highest imposed frequency.

6.1.2) Modulation of the u'-level bursting frequency

Once the grouping is done the modulation of the several parts of the bursting event may be studied separately.It is important for instance to separate the bursts with multiple ejections from the bursts with single ejection, since if these two categories of bursts are result of eventual different mechanism and if they have different modulation characteristics, the mixing of them during the phase average would cause a kind of phase jitter, and the computed results would give a wrong idea of $<f_b>$ modulation.

The reference time of the bursts are reported to the arrival time of the trailing edge of the ejections; the modulation of the

*first ejection of the bursts with multiple ejections

*last ejection of the BME's

*bursts with single ejection

is studied. Generally 25 bins have been used to determine $<f_b>_{BME}$ and $<f_b>_{BSE}$. The phase averages were well converged as it may be seen from figure 12 where examples are shown for $l_s^+=9.5$.How the modulation of the BME's is different from the BSE's modulation

for this imposed frequency is already evinced from figure 12, and this justify the separated study of the BME's and BSE's.

The time mean of the frequency of the bursts with multiple ejections $(f_b^+)_{BME}$ and of the single ejection bursts $(f_b^+)_{BSE}$ is shown on figure 13.a,versus the imposed frequency $f^+=1/\pi l_s^{+2}$. In steady flow and at the two Reynolds number investigated in this study the mean frequency of the BME and of the BSE are found to be respectively $(f_b^+{}_{BME})_{st}$ =0.0025 and $(f_b^+{}_{BSE})_{st}$=0.0038.Figure 13.a shows that the BSE's and the BME's are insensitive at the mean to the imposed oscillations , at least for l_s^+>9.5.A slight decrease of $f_b^+{}_{BME}$ of about 16% is systematically observed for l_s^+<9.5 with a slight increase of $f_b^+{}_{BSE}$.

The time mean bursting frequency f_b^+ is the sum of $f_b^+{}_{BME}$ and $f_b^+{}_{BSE}$. f_b^+ is constant and near, even equal to the steady mean bursting frequency $f_b^+{}_{st}$=0.0062. Thus although some slight effects are observed concerning the u'-level ejection frequency the bursting mechanism is not altered at the mean by the forcing.The mean number of ejections per BME (figure 13b) decreases systematically in the high frequency regime.This situation is reminiscent of the observations made with LEBU devices which reveal a decrease in the number of ejections per unit time while the number of bursts remained essentially constant (Coughran & Bogard 1987).

The relative amplitude of the frequency of the first ejection of the BME's is practically equal to the relative amplitude of the last ejection frequency.This shows that the duration of the BME's is essentially not modulated during the oscillation cycle (Figure 14.a).

The bursts with multiple ejections have modulation characteristics which are quite different from those of the bursts with single ejection.The BME's are completely governed

by the wall shear stress :Whatever is the value of the imposed frequency (recall that it has been changed by a factor of 70!) $(a_{fb})_{BME}$ *is nearly equal to the relative amplitude of* the wall shear stress a_τ (Figure 14.b).The phase shift of the first ejection and of the last ejection with respect to $<\tau>$ *is nearly equal to zero, and the difference between the phase* of the first ejection $\Phi_{F(BME)}$ and of the last ejection $\Phi_{L(BME)}$ is due to the duration of the *BME's.The time reference taken at the middle of the BME's is in phase with the wall shear* stress although a slight phase lag is observed at $l_s^+>16$.The duration of the BME's which is equal to:

$$\Delta t^+ = (\Phi_{L(BME)} - \Phi_{F(BME)}) l_s^{+2}/2$$

is betwwen 50-70 and is not affected by the imposed unsteadiness unless for $l_s^+<9.5$ ($f^+>3.5\ 10^{-3}$) where a decrease of about 50% is noted . This observation is consistent with the decrease of the time mean grouping parameter and the number of ejections per BME, and shows again an effect on the time mean parameters in the high frequency regime. These results are spectacular ,since for $l_s^+> 16$, a_τ increases with increasing frequency following the Stokes solution (TBB- 1990) and $(a_{fb})_{BME}$ follows a_τ which increases by a factor of 2 between $f^+=1.24*10^{-3}$ -$6.14*10^{-3}$.

The relative amplitude and the phase shift of the single ejection burst are shown and compared with the BME's characteristics on figures 14 and 15.The BSE's modulation parameters $(a_{fb})_{BSE}$ and $(\Phi_{fb})_{BSE}$ are completely different from the BME's modulation.$(a_{fb})_{BSE}$ *is strongly dependent on the imposed frequency* f^+*:in the quasi-steady* limit $(a_{fb})_{BSE}$ and $(\Phi_{fb})_{BSE}$ are comparable with $(a_{fb})_{BME}$ and $(\Phi_{fb})_{BSE}$ but the amplitude of the BSE's frequency decreases until 7% at $f^+=2.21*10^{-3}$ and increases again towards higher values of f^+.Remark the value of this last imposed frequency : $f^+=2.21*10^{-3}$ ($l_s^+=12$) is near the mean steady frequency of the bursts with multiple ejections

($f^+_{(BME)st}=2.9*10^{-3}$). Thus an interaction takes place between the oscillating flow and the bursts with single ejection when the imposed frequency reaches $f^+_{(BME)}$.Note that the decrease of the amplitude of the several characteristics in the buffer layer takes always place at this imposed frequency.The filtering on the response of the wall shear stress intensity $a_{\tau'\tau'}$ takes also for $f^+=1.24\text{-}2.21\ 10^{-3}$.The phase shift $\Phi_{fb(BSE)}-\Phi_\tau$ is strikingly different from the phase shift of the bursts with multiple ejections.$<f_b^+>_{BSE}$ is in phase with $<\tau>$ in the quasi-steady limit, but ags the wall shear stress for $1.24*10^{-3}<f^+<3.5*10^{-3}$, and even becomes to be in opposition of phase at $l_s^+=12$. Thus although the inner scaling $\nu/<\tau>$ is valid in the whole range of imposed frequency for the BME's it is no more adequate for the u'-level BSE's for $l_s^+<30$.

The study of the interaction with the BSE's and the oscillating flow remains a real chalenge.The important conclusion inferred from this paragraph is that the bursts with multiple ejections and the bursts with single ejections result from different mechanism.The BME's are formed by pockets of ejections with smaller interarrival times, and it is then expected that they are governed by the viscous time scale.The bursts with single ejection have modulation parameters which are comparable to the ejection frequency modulation which however phase lags with respect to the wall shear stress much more important.

6.1.3)A new method for grouping VITA ejections

The cumulative distribution of inter-arrival times between VITA ejections has a purely Poissonian trend and there is no way to extract a grouping parameter from it (the same is found for m-u' ejections).(Tiederman (1987). Tardu (1988)Therefore ,a new procedure has been developped in order to identify VITA bursts.Bogard & Tiederman (1987) have shown that the maximum of u' of the conditionnal averages at the trailing edge of the LAST ejection of a BME ($max(u')_L$) is much greater than that of

the preceding ones ($max(u')_P$).The trailing edge of the single ejections also has a high maximum ($max(u')_S$) when compared with $max(u')_P$.These significant differences between these values of max(u') provide additional conditions for the grouping of VITA ejections into bursts.A similar procedure may be applied to m-u' events.

The new method for determining $<f_b>_{VITA}$ is as follows:Three regions are distinguished in the time distribution of VITA arrivals.For time intervals t separating two consecutive VITA-ejections which are either short or too long with respect to the average interarrival time say:

$$t < <t_{g1}> \quad \text{or} \quad t > <t_{g2}>$$

the grouping poses no problem. For intermediate times:

$$<t_{g1}> <t< <t_{g2}>$$

max(u') provides then an additionnal criteria:

* ***If*** the preceding ejection has been identified as belonging to a BME,one has to decide whether the new one marks the end of the burst.Therefore max(u') is compared with $max(u')_L$ and $max(u')_P$.If

$$max(u') > 1/2 \; (<max(u')_L> + <max(u')_P>)$$

the ejection is considered as the last of the BME.If not,the next ejection belongs to the same burst.

** ***If*** the preceding ejection marks the end of a burst (BME or BSE),one has to decide whether the new one is a BSE or whether it belongs to a new BME.Thus max(u') is compared with 1/2 ($<max(u')_P>+<max(u')_S$).According to whether max(u') is smaller or larger than

$$1/2 \; (<max(u')_P>+<max(u')_S)$$

the ejection is considered as the beginning of a new BME,or it is classified as a BSE.

Since the five parameters of the procedure t_{g1},t_{g2},$max(u')_P$,$max(u')_L$,$max(u')_S$ are interdependent a double iterative procedure is used.

At a first step $<t_{g1}>$ and $<t_{g2}>$ are fixed and the iteration is continued until $max(u')_P$,$max(u')_L$ and $max(u')_S$ are converged.At a second step $<t_{g1}>$ and $<t_{g2}>$ are

computed with the new values of the maximas, and the entire processus starts again.The first step converges to within 5% after 4 to 5 iterations.

The initialisation of the method is done by the grouping time of the u'-level ejections, i.e

$<t_{g1}>_1 = 1/3 <t_g>_{u'\text{-level}}$ $\quad <t_{g2}>_1 = <t_g>_{u'\text{-level}}$

and at the ith step:

$<t_{g1}>_{i+1} = <t_g>_i$ $\quad <t_{g2}>_{i+1} = 3<\Delta t \text{ EJ.BME}>_i$

where $<\Delta t \text{ EJ.BME}>_i$ is the average time between ejections within the same BME; i denotes the number of iteration step --Considering that the interarrival times within the BME's have poissonian distribution the probability that

$P(t/t'>t_{g2}) = 1-e^{-t/(\Delta t \text{ EJ.BME})} = 0.95$

gives $t_{g2} = 3(\Delta t \text{ EJ.BME})$ --

The maxima are computed,for each individual ejections,from the time of occurrence of the ejection to within $0.7<T_v>$.The results have changed by less than 5% by changing *this last parameter from 0.5 to 0.85* $<T_v>$.*It was not necessary to evaluate the time* $<t_{g1}>$ since it was choosen suficiently small at the beginning of the computation such that $t<<t_{g1}>$ denotes without ambiguity an ejection belonging to a BME.A test with other choice of $<t_{g1}>$ *have shown that the final results do not depend significantly on this choice unless of course* if it was choosen too large.Another test performed for $<t_{g2}>_i$ by choosing it such that $<t_{g2}>_{i+1} = <\Delta t \text{ EJ.BME}>_i + 2 <\text{var}(\Delta t \text{ EJ.BME})>_i$ and gave results satisfactorily comparable with *the simple equation* $<t_{g2}>_{i+1} = 3<\Delta t \text{ EJ.BME}>_i$.

The same method has been applied without modification to the VITA events detected at the wall.Note that the above procedure does make any hypothesis on the relative *amplitude of the maximas ,and if it does converge (which is the case) that is only due to* the real physical dynamical characteristics of the bursting event.

The data studied in this paragraph is extended with additionnal points and in particular with one flow corresponding to a slightly higher frequency $f^+ = 0.0073$.

The maximas are reported to the corresponding values of the phase average of the thresholds i.e. $\sqrt{k_u}\cdot\langle u'u'\rangle$ and $\sqrt{k_\tau}\cdot\langle\tau'\tau'\rangle$.Figure 16 shows the time mean of the maxima obtained at the end of the computation.The maxima of the preeceding ejections $\max(u')_P$ is 5 to 10 times smaller than the maxima of the last ejection (fig. 16a). The ratio $\max(u')_L / \max(u')_P$ is about 5 in the quasi-steady limit and this compares well with Bogard & Tiederman(1987).The maxima of the burst with single ejection has the same magnitude as $\max(u')_L$. Bogard & Tiederman(1987) made conditionnal averages of the maxima of the ejections within a burst based on visually detected events and simulraneous probe measurements. The $\max(u')_L$ that they report is about 2 times smaller than the maxima of the VITA events.If this factor is taken into account,the time mean values shown in figure 16a compares also well with their results for the measurements at $y^+=15$.

The method is successufully applied to $\tau'(t)$ signal to determine the modulation of $\langle f_{BME}\rangle$ and $\langle f_{BSE}\rangle$ detected at the wall. Figure 16b shows that the ratio $\max(\tau')_L/\max(\tau')_P$ varies between 2 and 4, thus the difference between previous ejections and the last ejection of the BME's is less pronounced at the wall than in the buffer layer. The time means of the maxima at $y^+=0$ are approximately 3 times greater than maxima of u' at $y^+=15$. This has to be expected because the conditional averages of τ' are skewned towards positive values with maxima greater than the maxima of the conditionnal averages of u' (see for example Fig 3).

The other modulation characteristics of the maxima are believed to give no more information and are not reported here. Let us note however that the maxima of u' of the preceeding ejections reported to the phase averaged threshold is much more strongly modulated than $\max_{u'}$ of the last and single ejections, with relative amplitudes exceeding one in much of the cases. This indicates that $\langle\max(u')_P\rangle$ has even negative values during the oscillation cycle.

6.1.4) Modulation of the VITA bursting frequency

The behaviour of the reaction of the VITA bursts is similar in very aspects to the level crossing bursts.The time mean frequency of the VITA BMEs and BSEs is comparable with their level crossing homologues (Fig. 17.a). Note however that $f^+_{b(BSE)}$ is larger when VITA is used to detect the bursts. Alternaly $f^+_{b(BME)}$ is slightly smaller. Fig. 17b shows that $f_{b(VITA)}{}^+$ is 0.007 (both at y^+=15 and y^+=0) and is slightly larger than the bursting frequency obtained by the u'-level method.

Fig. 17a shows also that, a slight increase of $f^+_{b(BSE)}$ is noted at y^+=15 in the high frequency regime, together with a decrease of $f^+_{b(BME)}$ so that the mean bursting frequency is constant to within 15% in the whole imposed frequency regime investigated here. Both the time mean frequency of the BSE's and BME's are however constant at the wall. Recall once more that an effect on the time mean ejection frequency was found for f^+=0.0035 with four detection schemes. Figures 17.b and 13.a show that although $<f_e>$ was affected at the mean for this particular imposed frequency, the time mean bursting frequency is unaltered.

As the level crossing bursts, the VITA bursts with multiple ejections follow the modulation of the wall shear stress.The relative amplitude of frequency of the first and the last ejection of the BMEs is close to a_τ (Fig. 18.a). Only $a_{f(BME)}$ based on the last ejection is compared with the relative amplitude of the modulation of the bursts with single ejection $a_{f(BSE)}$ on Fig. 18a. The difference of the reaction to the imposed unsteadiness of the single ejection bursts is irrefutable, since $a_{f(BSE)}$ is five times smaller than $a_{f(BME)}$ at f^+=0.002 when the detection is done at y^+=15. This factor increases even up to 9 when the detection is done at the wall. Fig. 18a shows also that the frequency of the bursts with single ejection is systematically less modulated at the wall than in the buffer layer, once

$f^+ > 0.002$. This would indicate that the reaaction of the BSE's to the imposed oscillations differs from this of the BME's in a more pronounced manner at the wall than at $y^+=15$.

The phase shift $\Phi_{f(BME)} - \Phi_\tau$ varies between +- 50^0 at the wall as well as in the buffer layer (Fig. 18b). The phase shift of the modulation of the single ejections bursts depends strongly on the imposed frequency as was also observed with u'-level bursts. $<f_{BSE}>$ is nearly in opposition of phase at $f^+=0.0025$ and at $y^+=0$. Once more, a difference of the behaviour is noted from fig 18b, concerning the BSE's and depending where they are detected. The minimum of $\Phi_{f(BSE)} - \Phi_\tau$ is more pronounced at the wall than in the buffer layer. The comparison of Fig. 18b with Fig. 15 shows on the other hand that VITA applied to $\tau'(t)$ corresponds better to u'-level method. It is recalled that VITA detects strong shear layers while u'-level, when applied near the wall, is similar to u'v'-quadrant technique, these two techniques detecting then different parts of the bursting event.

In conclusion, the multiple ejection bursts have modulation characteristics similar to those of the wall shear stress modulation, and strong differences exist between the response of the BSE's and BME's as it is shown by two independent and quite different techniques . On the other hand, an interaction between the oscillating flow and the bursting modulation takes place at $f^+=0.0025$ where both the amplitude and the phase of $<f_{BSE}>$ differ significantly from the quasi steady behaviour. It is interesting to note that this imposed frequency corresponds to the time mean frequency of the multiple ejection bursts since in steady flow $f^+_{(BME)st}$[2] $=0.0024$ (also in unsteady flow see Fig. 17a). An effect on the time mean ejection frequency is observed at imposed frequencies near $f^+=0.004$ followed by a slight increase of the time mean frequency of the BSEs, and this last imposed frequency compares well with $f^+_{(BSE)st}$.

The last ejection of the BMEs is always in phase with the modulation of the wall shear stress, while the phase shift of the single ejection bursts depends strongly on the

[2] st is for steady flow

imposed frequency.Due to the duration of the BMEs the phase shift of the last ejection is also a function of f^+ as it is shown on Fig. 19a.

The duration of the BMEs is given by $\Delta t^+_{BME}=(\Phi_{first}- \Phi_{last})/2\pi f^+$ and is shown on Fig.19b. $-\Delta t^+_{BME}$ varies between 40 and 80 viscous units in the buffer layer, while it is larger at the wall especially at $f^+=0.002$.

The number of ejections per BME decreases also in the high frequency regime as well as the VITA events are concerned. Although the decrease is not striking, it is systematic as was the case for the u'-level ejections.These observations strengthen the conclusions discussed in the previous paragraph and show that the VITA bursts do not differ from the u'-level bursts , at least in a significant manner.

7.)Modulation of the characteristics of the conditionnal averages

The characteristics of the conditionnal averages are used to determine the VITA integration time, and thus, the results concerning its modulation have already been introduced in 4. Other characteristics of the conditionnal averages of the VITA ejections, which modulation characteristics are also imposed frequency dependent, have interesting future and are introduced here.

Magnitude of the conditional averages

The magnitude $\Delta u'_{cond}$ (and $\Delta \tau'_{cond}$) of the conditional averages is defined as the difference between the maximum and the minimum preceeding the sharp rise which is detected. In steady channel flow, when the conditional averages are non-dimensionalized by the local threshold $\sqrt{ku'u'}$ they collapse quite well independently of the detection point y+ and the Reynolds number (Johannsonn & Alfredsonn 1982). In a similar manner, the

conditionnal averages in unsteady flow <u'cond> and <τ'cond> are reported to their respective phase averaged thresholds $\sqrt{k_{u'}}\,\langle u'u'\rangle$ and $\sqrt{k_{\tau'}}\,\langle \tau'\tau'\rangle$. Some typical examples are shown in figure 3.

The time means of the magnitude of the conditionnal averages $\langle u^{*'}\rangle=\langle u'cond\rangle/\sqrt{k_{u'}}\,\langle u'u'\rangle$ and $\langle \tau^{*'}\rangle=\langle \tau'cond\rangle/\sqrt{k_{\tau'}}\,\langle \tau'\tau'\rangle$ are respectively $\overline{\Delta u'^{*}}=3$ and $\overline{\Delta \tau'^{*}}=4.5$ in the whole imposed freequency range (figure 20a), and these values are close to those found in steady flow (Johannson & Alfredson, 1982; Shah& Antonia, 1986). These results show that the turbulence activity described by VITA averages are unaffected at the mean by the imposed oscillations.

The strong modulation of the magnitude of $\langle u^{*'}\rangle$ and $\langle \tau^{*'}\rangle$ is illustrated in figure 18b. $a_{\widetilde{\Delta u'}}/a_{\widetilde{\tau}}$ and $a_{\widetilde{\Delta \tau'}}/a_{\widetilde{\tau}}$ reache a value as large as 0.8 at $f^{+}=0.001$ and decrease slowly towards high frequency regime . Since in steady flow, the magnitude of $u'cond/\sqrt{k_{u'}}\,u'u'$ is found to be nearly independant of the y+ position and of the Reynolds number, in the quasi-steady regime the magnitude of the conditionnal averages should be such that $\langle \Delta u'\rangle \approx \sqrt{k_{u'}}\,\langle u'u'\rangle$, and this implies that the modulation of $\langle \Delta u'^{*}\rangle$ should decrease towards zero. For similar reasons, one should observe the same behaviour for $\langle \Delta \tau'^{*}\rangle$ modulation. Figure 20b shows indeed that this is the case for $f+\rightarrow 0$. However, note that the quasi-steadiness is hard to be reached for this particular characteristic of the conditionnal averages, since the magnitude of $\Delta u^{*'}$ and especially of $\Delta \tau^{*'}$ is still modulated, even at imposed frequencies as small as $f+=1.6\ 10^{-4}$. Note also that the quasi-steadiness is harder to be reached for $\langle \Delta \tau'_{*}\rangle$ than for $\langle \Delta u'_{*}\rangle$. The departure from the quasi-steadiness becomes to be important as early as at $f^{+}=4\ .10^{-4}$. This strong modulation of the magnitude of the conditionnal averages can not be explained simply by the breathing of the boundary layer and is a real manifestation of the imposed unsteadiness on the energical structures.

The effect of the unsteadiness is also clear on the phase shift of $\langle \Delta u'_{*}\rangle$ and of $\langle \Delta \tau'_{*}\rangle$ with respect to the modulation of the wall shear stress $\langle \tau\rangle$. While $\langle \Delta \tau'_{*}\rangle$ is nearly

in phase with $<\Delta\tau>$ the phase shift $\Phi_{\widetilde{\Delta u'^*}} - \Phi_{\widetilde{\tau}}$ (nearly zero in the quasi-steady regime), becomes -180° when the imposed frequency increases (fig.20c). This observation stresses the strong dependance of the response of the coherent structures to the imposed unsteadiness.

8.)Conclusion

i) Several time scales as VITA integration time,u'-level ejections grouping time, have been investigated in this study.In the quasi-steady limit the modulation characteristics have been found to scale with the inner variables.The modulations become to be weaker when the imposed frequency reaches values near the steady value of the frequency of bursts with multiple ejections.At further higher frequencies, however, the amplitude of the modulation of the time scales increases and a tendancy of scaling with the wall shear stress is noted indicating some kind of return to the quasi-steady behaviour.

ii) Unless slight differences, four detection schemes investigated here gave similar results concerning the modulation of the ejection frequency.An interaction of the modulation of the ejection frequency with the imposed unsteadiness is also noted when the imposed frequency is of the same order of $f^+_{(BME)st}$. The modulation of the ejection frequency is in quadrature with the modulation of the wall shear stress near this imposed frequency ,while at the high frequency regime and in the quasi-steady limit the phase shift are zero.At slightly higher imposed frequency ($f^+=1.5\ f^+_{(BME)st}$) a decrease of about 30% of the time mean ejection frequency is noted and this is the unique flow quantity which is affected at the mean by the imposed unsteadiness.

iii) The mean bursting frequency is not affected by the unsteadiness as it was shown by two independent techniques.The bursts with multiple ejections have the same modulation characteristics as the modulation of the wall shear stress in the whole frequency regime.The reaction of the bursts with single ejections are strongly dependent on the

imposed frequency.On the other hand, the mean number of ejections per burst with multiple ejections decreases in the high frequency regime, together with a decrease of the time mean frequency of the BMEs and an increase of the time mean frequency of the BSEs.These observations allow to conclude that those two categories of bursts result from different mechanisms.More detailed studies are needed in steady flow, particularly by the use of direct numerical simulation data, to determine the causal effects that generate bursts with multiple and single ejections.

ACKNOWLEDGEMENT

Financial support from the European Research Office of the U.S. Army under contract DAJA 45-87-C-0015 is gratefully acknowledged.

Rcferences

(1)BINDER G.,TARDU S.,BLACKWELDER R. 1985 "Large Amplitude Periodic Oscillations in the Wall Region of a Turbulent Channel Flow",Fifth Symposium on Turbulent Shear Flows,Cornell University,pp 16.1-7

(2)FINNICUM D.,HANRATTY T.J 1987 "Effect of Imposed Sinusoidal Oscillations on Turbulent Flow in a Pipe" Sixth Symposium on Turbulent Shear Flows,Toulouse,pp. 4.1-1

(3)KOBASHI,Y.;HARAKAWA,M. 1981 "Structure of a Turbulent Boundary Layer on an Oscillating Flat Plate",IUTAM-Symposium on Unsteady Turbulent Shear Flows,Springer-Verlag pp.67-76

(4)COUSTEIX,J. HOUDEVILLE,R. 1985 "Turbulence and Skin Friction Evolutions in an Oscillating Boundary Layer" Fifth Symposium on Turbulent Shear Flows,Cornell University

(5)RONNEBERGER D. 1985 "Investigation of the Dynamics of a Turbulent Wall Boundary Layer by Introduction of a SmallExternal Perturbation" Fifth Symposium on Turbulent Shear Flows,Cornell University,pp.18.19-24

SHAH;ANTONIA 1986 "Scaling of the wall shear stress fluctuations in a turbulent duct flow" AIAA J.,25,N° 1

(6)TARDU S.,BINDER G.,BLACKWELDER R.1987 "Modulation of Bursting by Periodic Oscillations Imposed on Channel Flow" Sixth Symposium on Turbulent Shear Flows,Toulouse,pp.4.5 1-6

(7)ALFREDSON H.P. , JOHANSSON A.V. 1984 "On the Detection of Turbulence-Generating Events " J.Fluid.Mech. 139,325

(8)BOGARD D.G. ,TIEDERMAN W.G. 1986 "Burst Detection with a Single-Point Velocity Measurements" J.Fluid Mech. 162,389

(9)LUCHIK,T S. ,TIEDERMAN W.G. 1987 "Time Scale and Structure of Ejections and Bursts in Turbulent Channel Flows" J.Fluid Mech.174,529

(10)JOHANSSON A.V.,ALFREDSSON H.P. 1982 "On the Structure of Turbulent Channel Flow" J.Fluid Mech.,122,295

(11)COUGHRAN M.T.,BOGARD D.G. 1987 "An Experimental Study of the Burst Structure in a LEBU-Modified Boundary Layer"Tenth Symposium on Turbulence,Rolla pp.45.1-10

(12)BOGARD D.G.,TIEDERMAN W.G. 1987 "Characteristics of Ejections in Turbulent Channel Flow" J.Fluid Mech.1 79,1

a)

$a_{\widetilde{u}\widetilde{u}} / a_{\widetilde{u}}$; $a_{\widetilde{\tau}\widetilde{\tau}} / a_{\widetilde{\tau}}$

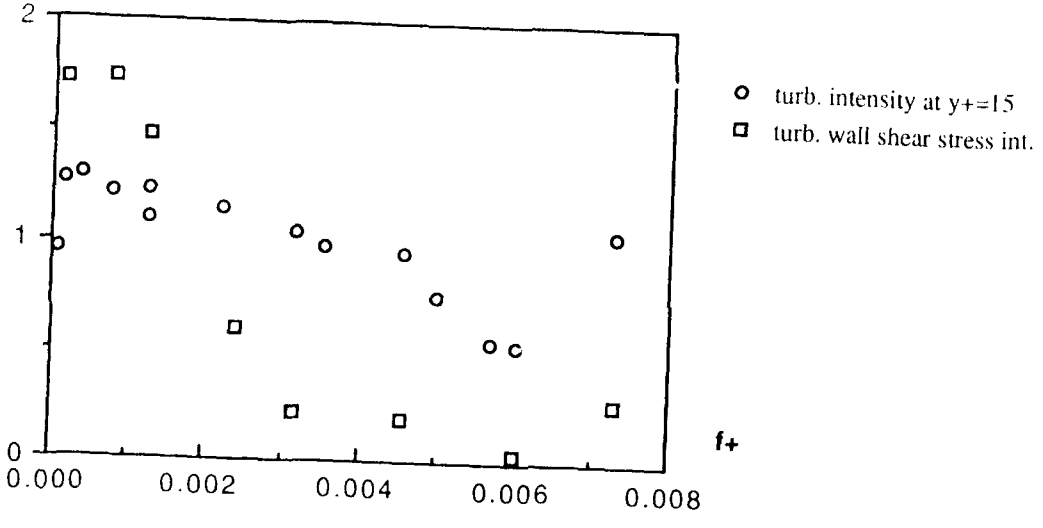

b)

$\Phi_{\widetilde{u'u'}} - \Phi_{\widetilde{u}\,(y+=15)}$; $\Phi_{\widetilde{\tau'\tau'}} - \Phi_{\widetilde{\tau}}$

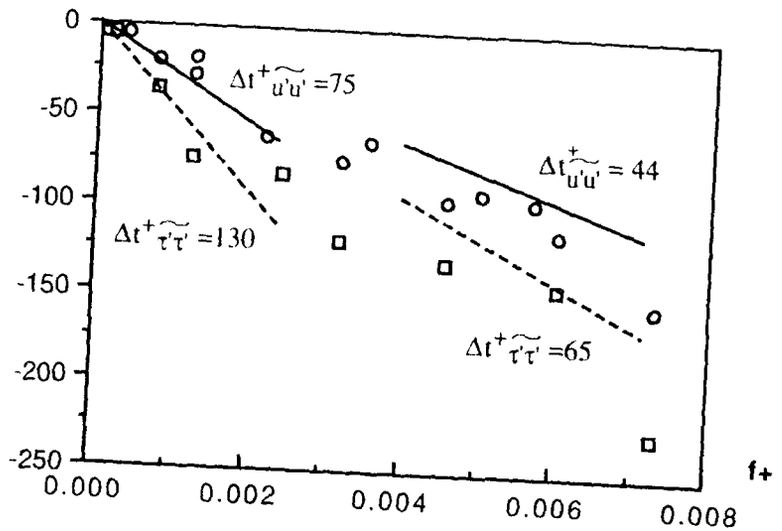

Figure 1) Modulation of the turbulent intensity at y^{+}=15 and of the turbulent wall shear stress intensity
a)Amplitude
b)Phase

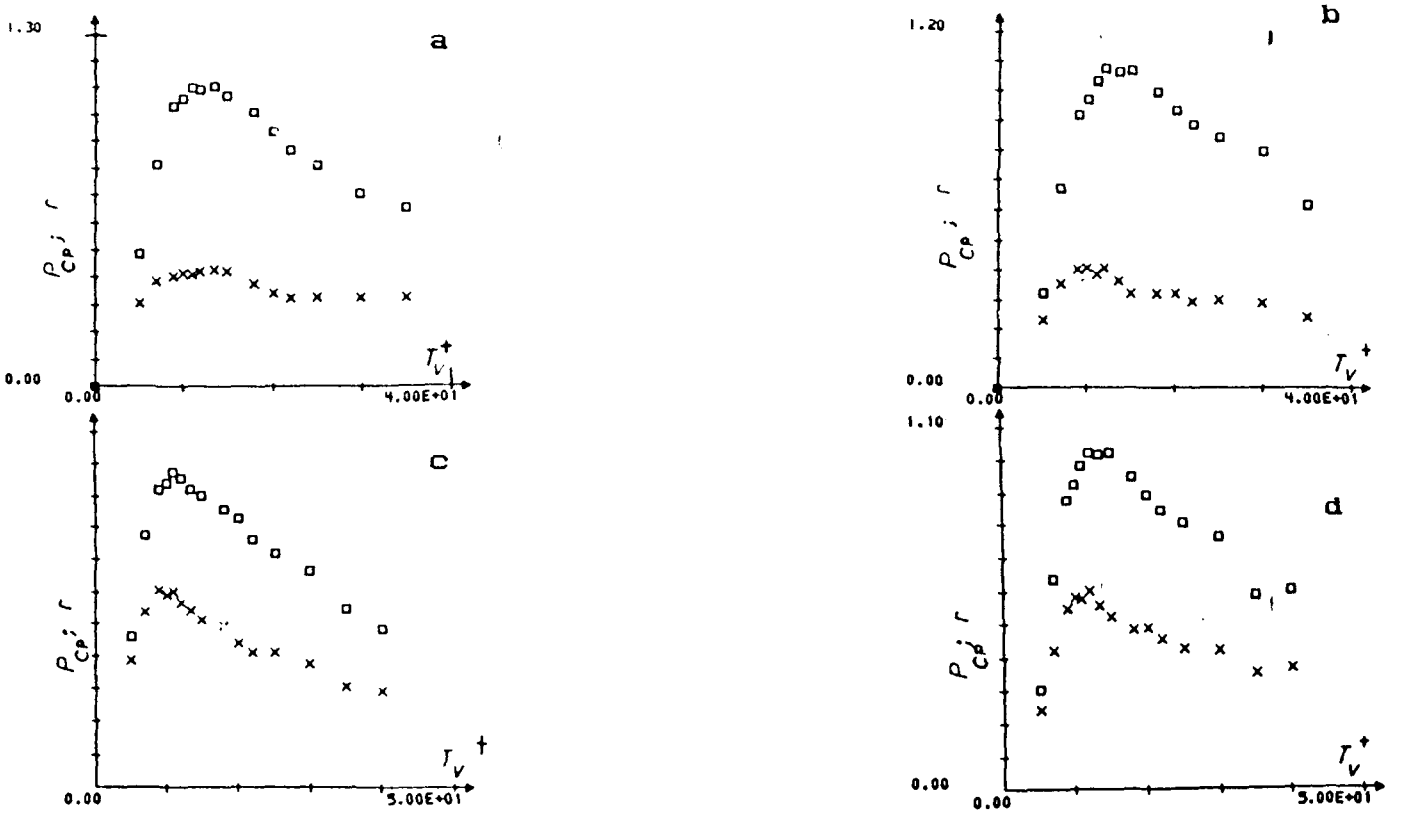

Figure 2-) Distribution of the one to one correspondance probability versus the VITA integration time;VITA and u'-level events:a)t/T=0.3 b)t/T=0.7;VITA and mu' events c)t/T=0.3,d)t/T=0.7

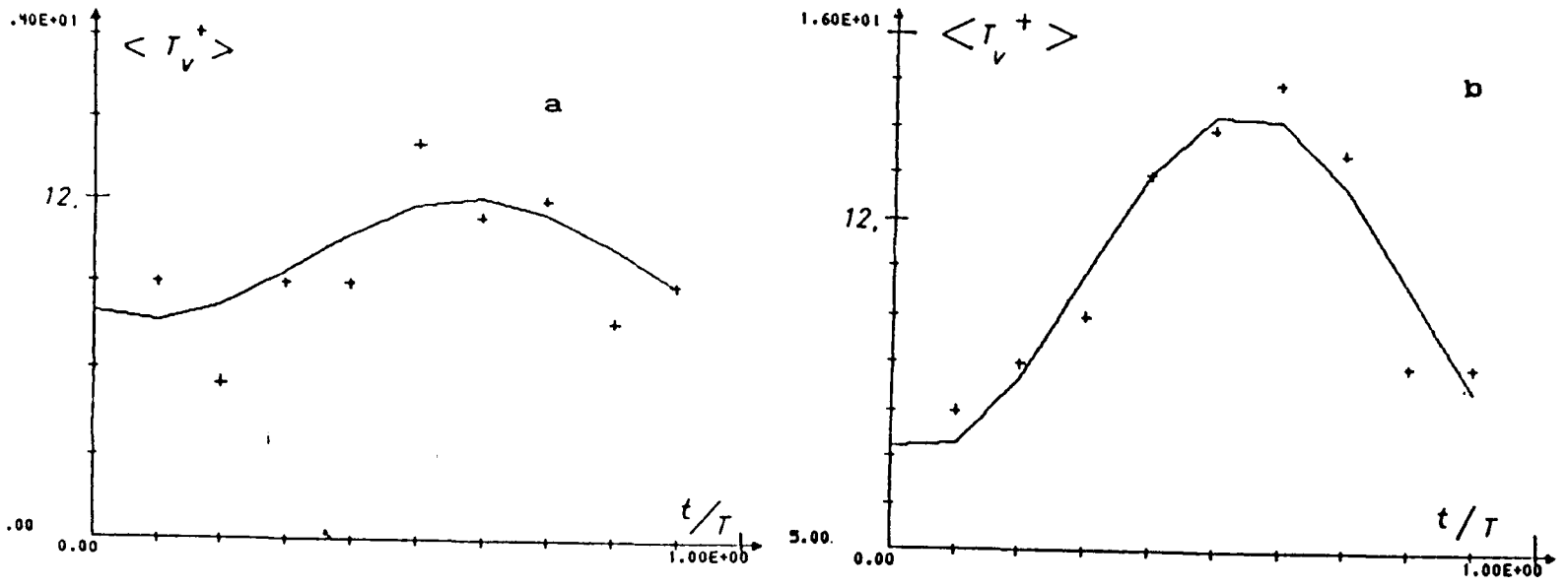

Figure 3.) Examples of the VITA integration time modulation obtained by one to one correspondance a)l_s^+=9.5 b)l_s^+=60

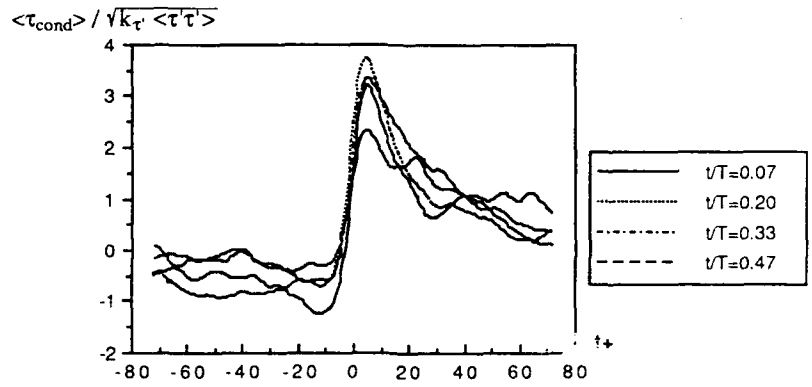

Figure 4.a)Conditional averages of the wall shear stress intensity ls+=9.5

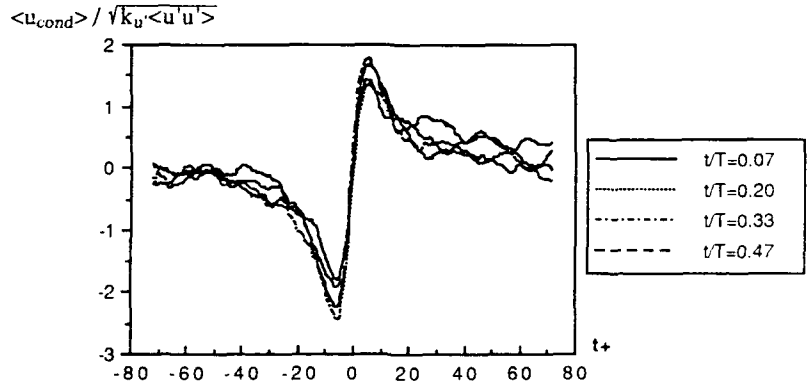

Figure 4.b)Conditional averages of the fluctuating axial velocity at y+=15 ;ls+=9.5

$a_{\tilde{T}v}$

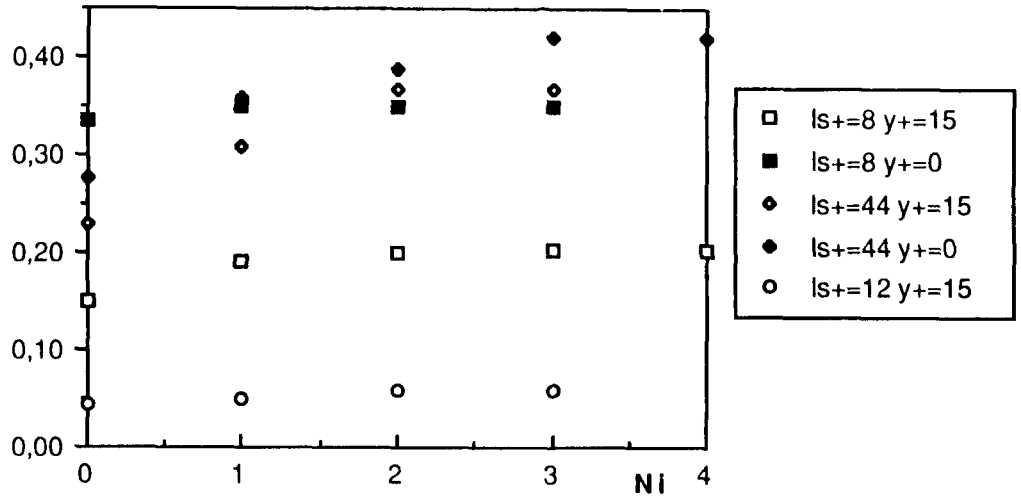

Figure 5.a) Relative amplitude of the VITA integration time versus the iteration number

$a_{\tilde{fe}}$

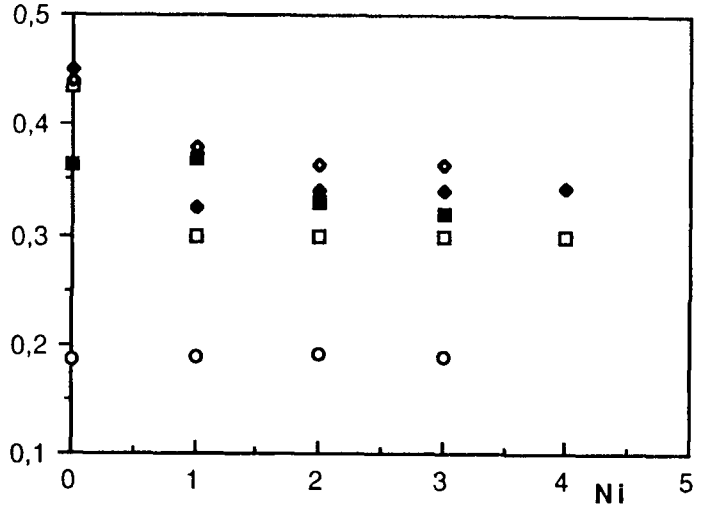

Figure 5.b) Relative amplitude of the VITA ejection frequency versus the iteration number.

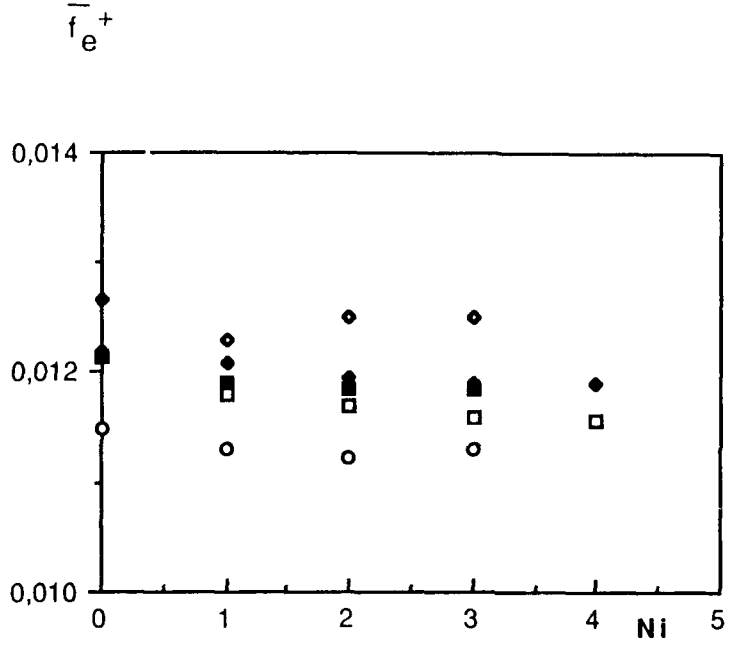

Figure 5.c) Time mean of the VITA ejection frequency versus the iteration number.

$\Phi_{\tilde{T}v} - \Phi_{\tilde{f}e}$

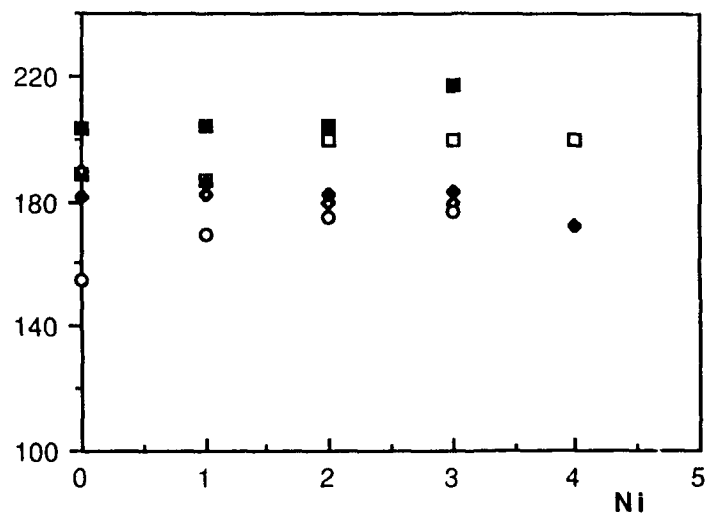

Figure 5.d) Phase shift of the VITA integration time with respect to the VITA ejection frequency.

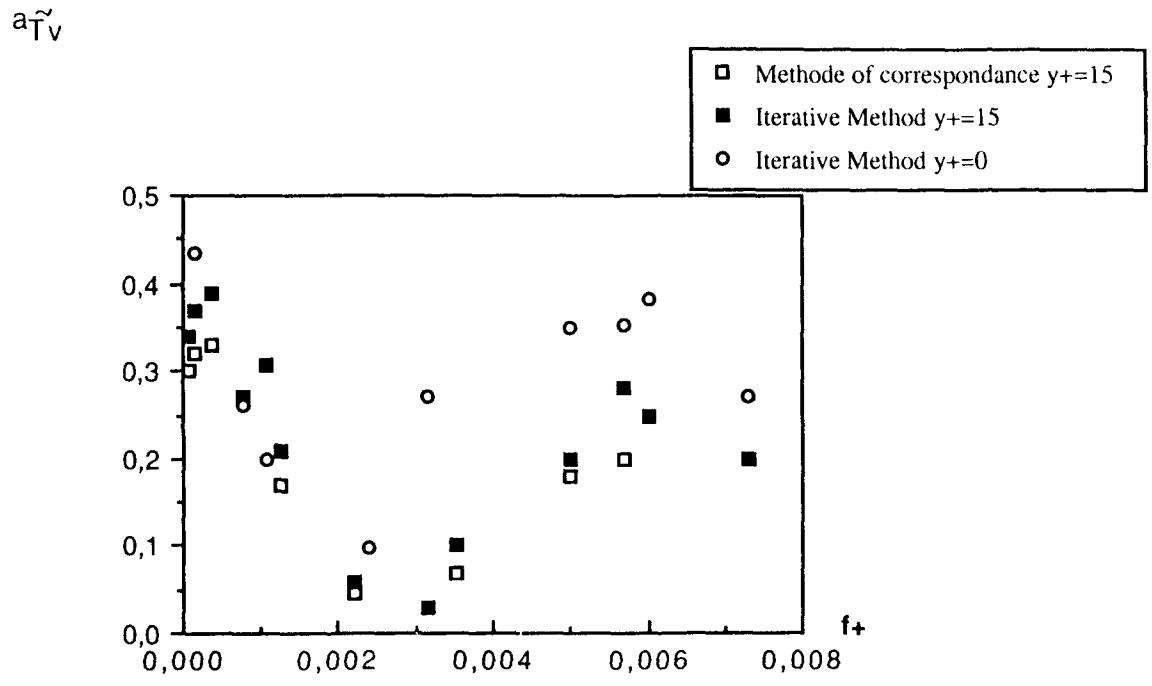

Figure 6.a) Relative amplitude of the VITA integration time versus the imposed frequency. Comparison of two methods.

$a_{\tilde{T}V}/a_{\tilde{\tau}}$

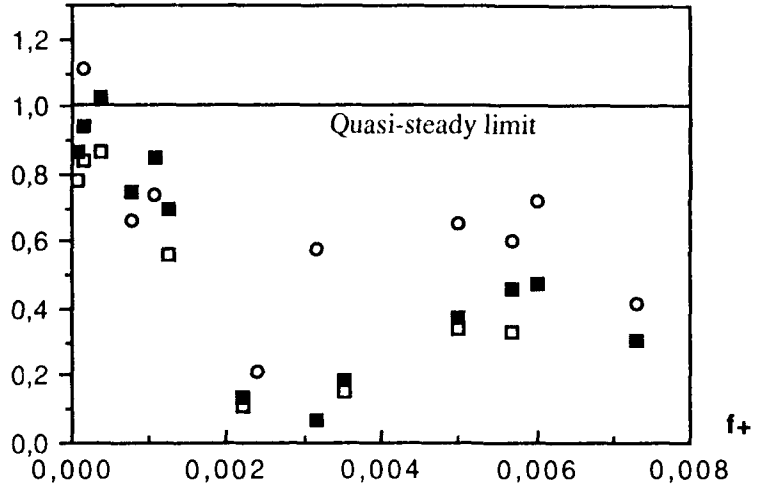

Figure 6.b) Relative amplitude of the VITA integration time repported to the relative amplitude of the wall shear stress.

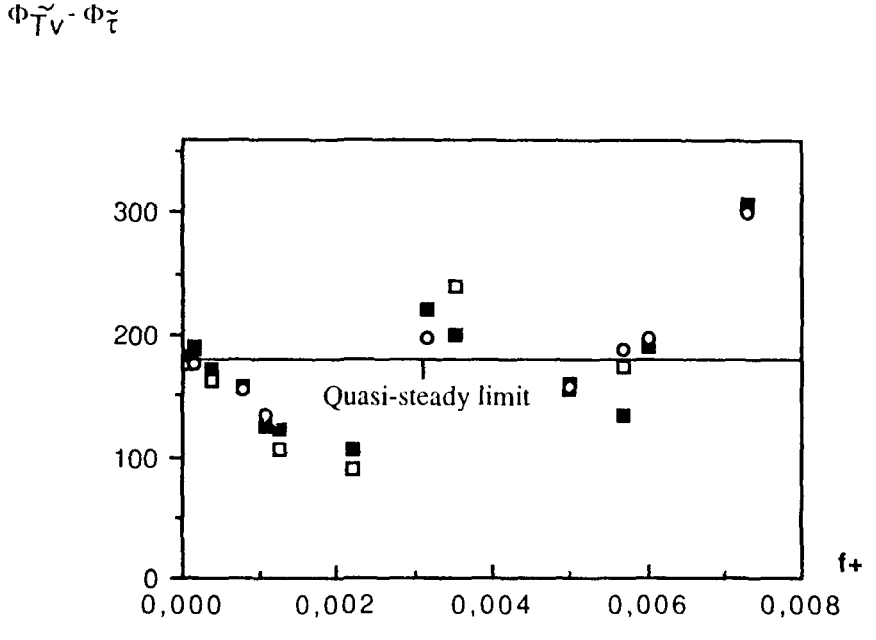

Figure 6.c) Phase shift of the VITA integration time modulation with respect to the wall shear stress modulation.

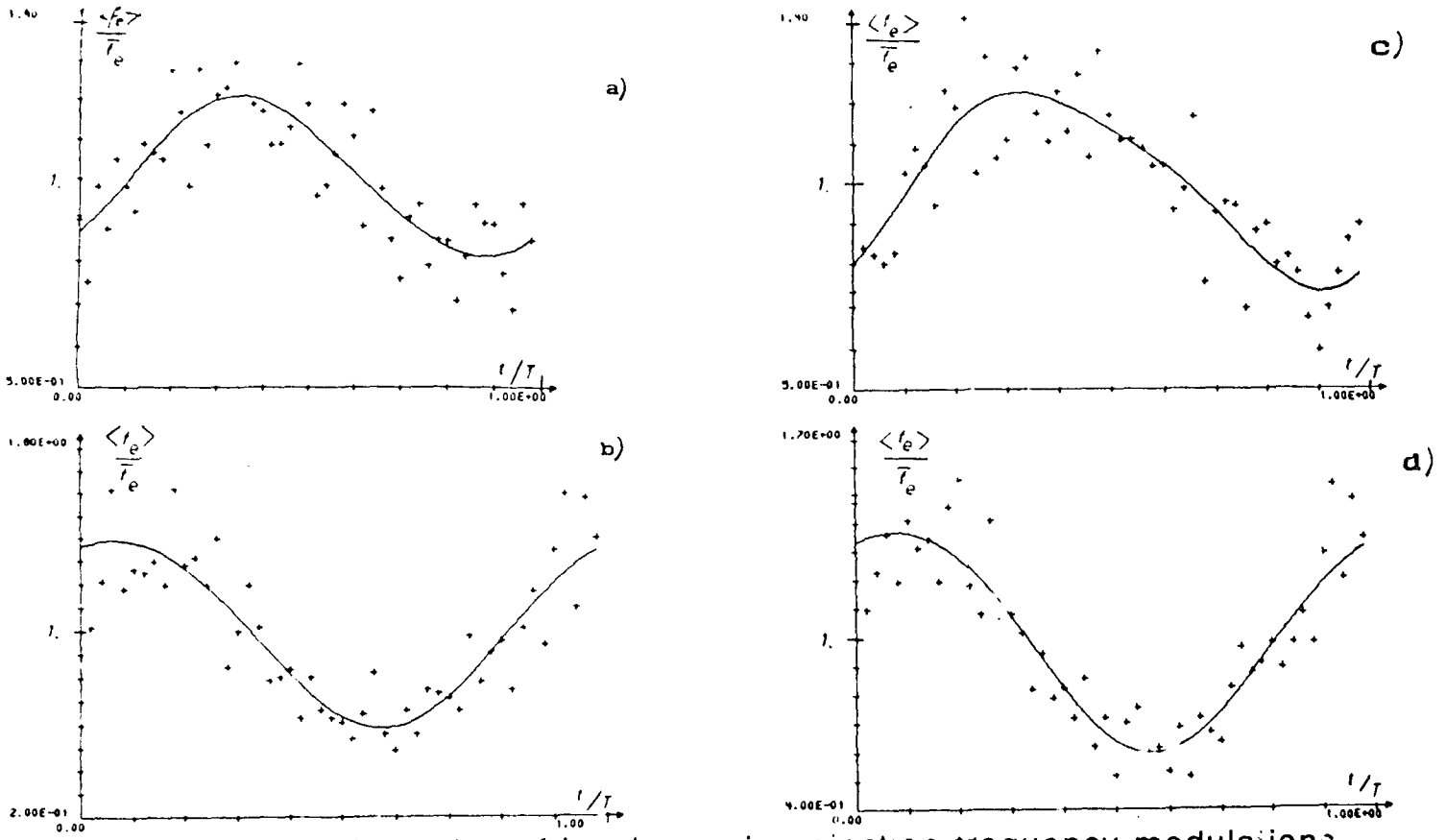

Figure 7) Examples of level crossing ejection frequency modulations a)u'-level ,l_s^+=9.5 b)u'-level ,l_s^+=60. c)mu',l_s^+=9.5 d)mu' ,l_s^+=60.

$\bar{f}_e^+$

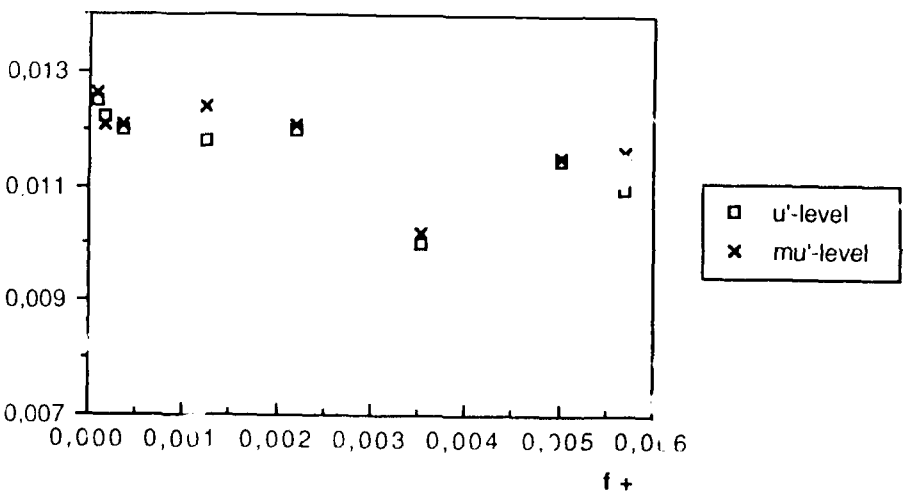

Figure 8.a) Time mean ejection frequency.Comparison with u'-level and modified u'-level methods.

a_{fe} and $a_{u'u'}$

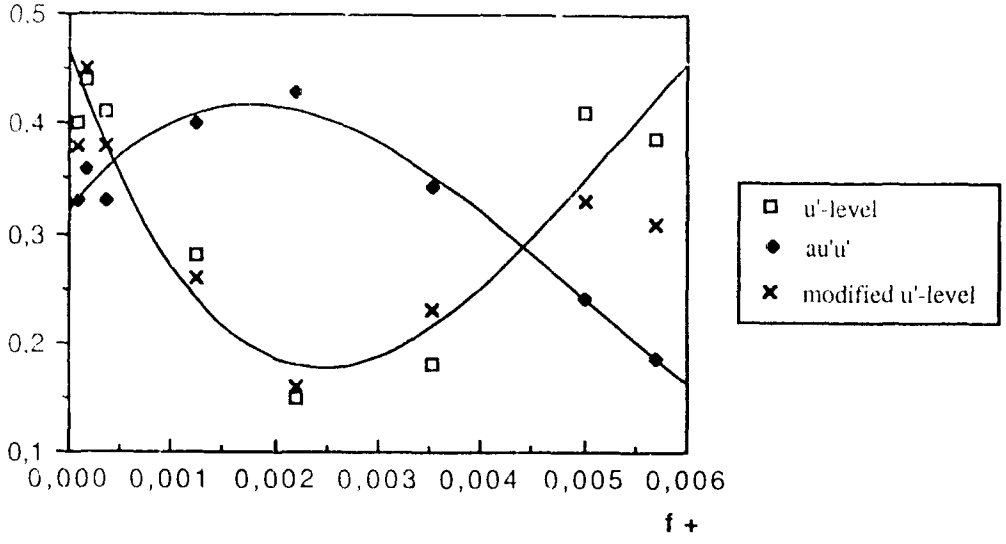

Figure 8.b) Relative amplitude of the level crossing ejection frequency compared with the relative amplitude of the turbulent intensity at $y^+=15$.

$a_{\tilde{fe}} / a_{\tilde{\tau}}$

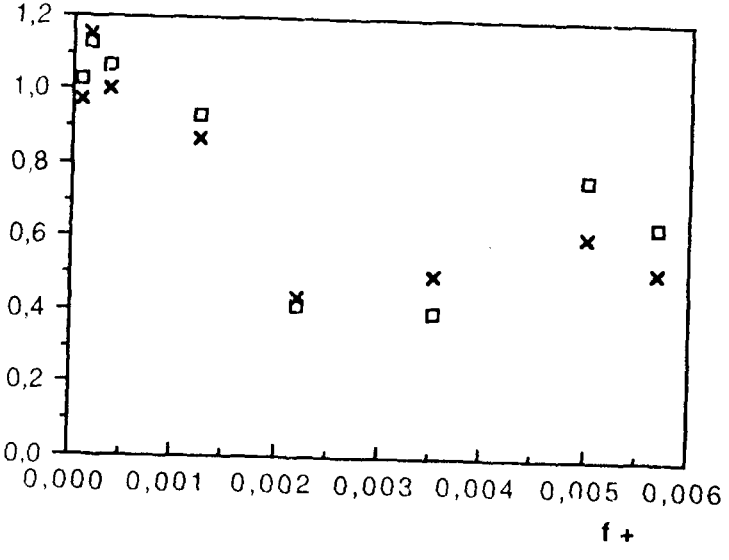

Figure 8.c) Relative amplitude of the modulation of the level crossing ejection frequency reported to the relative amplitude of the modulation of the wall shear stress.

$\Phi_{\tilde{fe}} - \Phi_{\tilde{\tau}}$

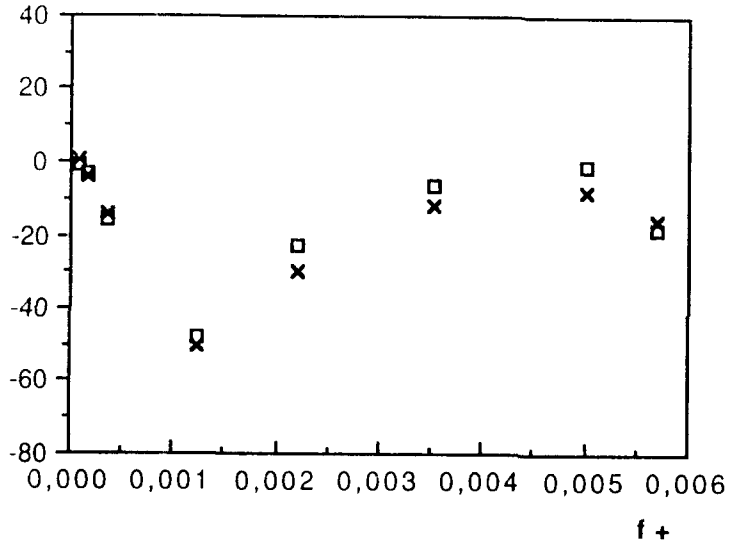

Figure 8.d) Phase shift of the modulation of the level crossing ejection frequency with respect to the modulation of the wall shear stress.

$\bar{f}_e^+$

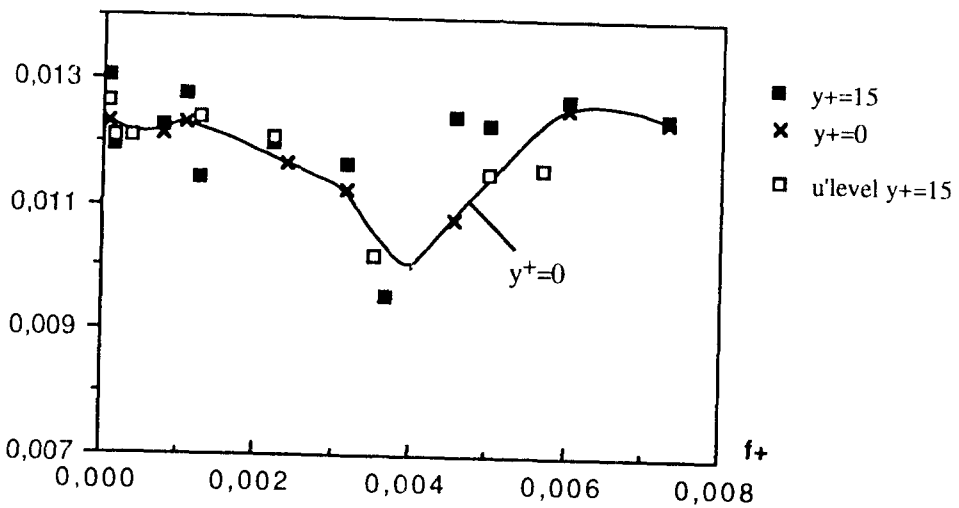

Figure 9.a) Time mean VITA ejection frequency ; detection at $y^+=15$ and at $y^+=0$.

$a_{\tilde{fe}}/a_{\tilde{\tau}}$

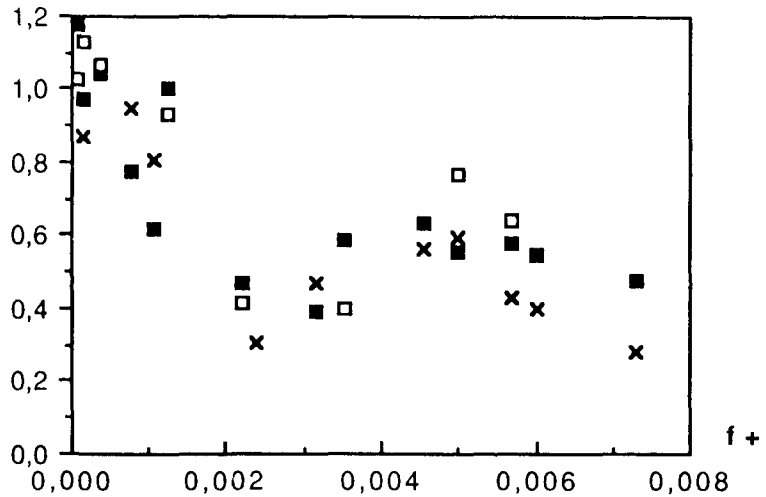

Figure 9.b) Ratio of the relative amplitude of the modulation of the VITA ejection frequency to the relative amplitude of the wall shear stress.For caption see figure 9.a.

$\Phi_{\tilde{fe}} - \Phi_{\tilde{\tau}}$

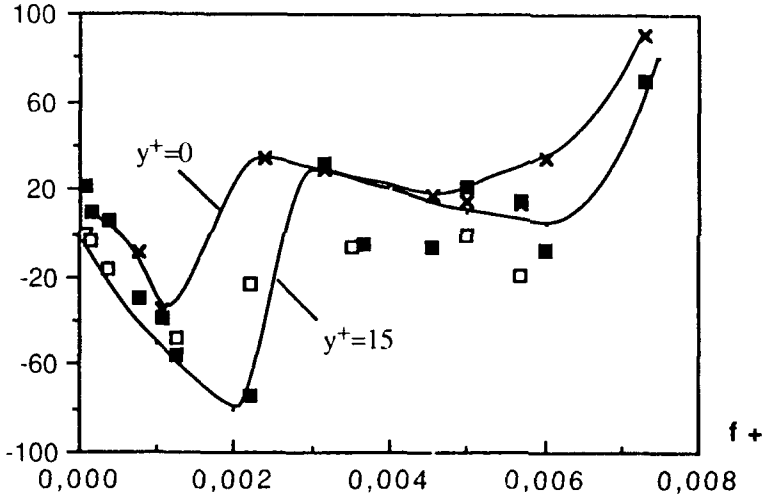

Figure 9.c) Phase shift of the modulation of the VITA ejection frequency with respect to the modulation of the wall shear stress. For caption see figure 9.a.

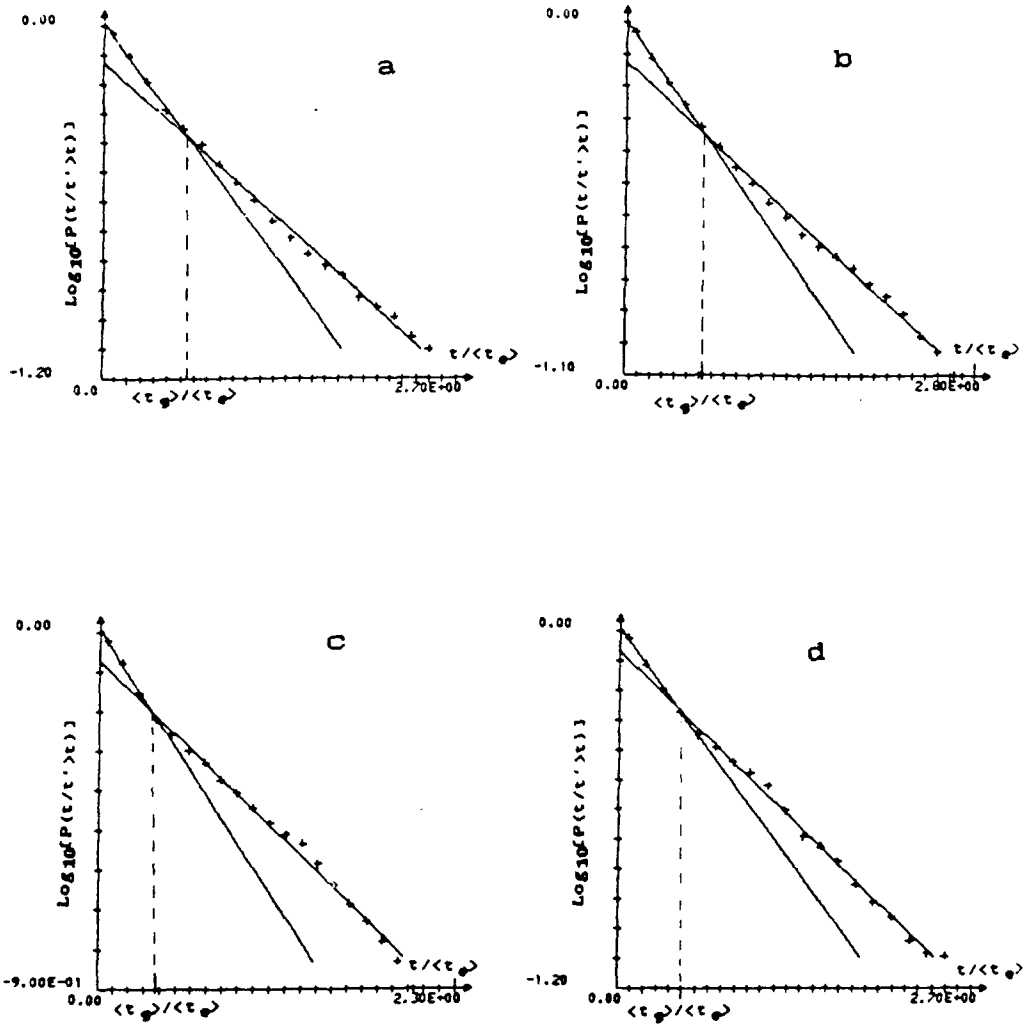

Figure 10)Phase average of the cumulative distribution probabilities of the interarrival times of the u'-level ejections; ls+=9.5; a)t/T=0.25, b)t/T=0.5 c)t/T=0.75,d)t/T=1.

$\overline{t_g}^+$

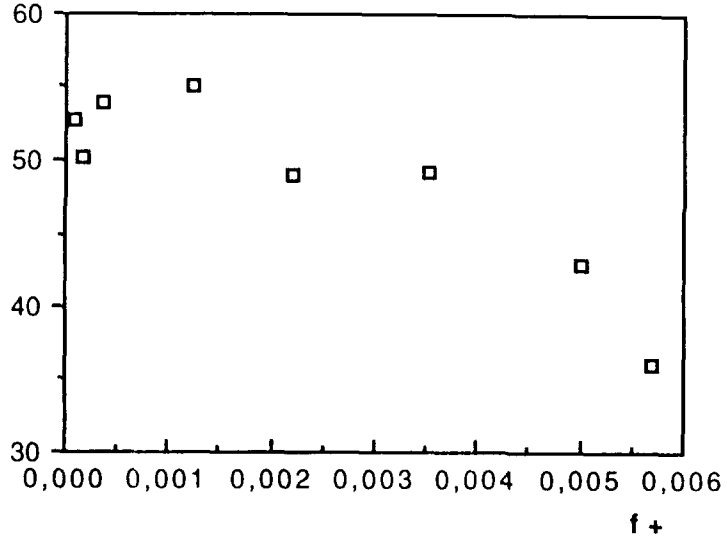

Figure 11.a) Time mean of the u'-level grouping time.

$a_{\tilde{tg}}$ and $a_{(<tg>/<te>)}$

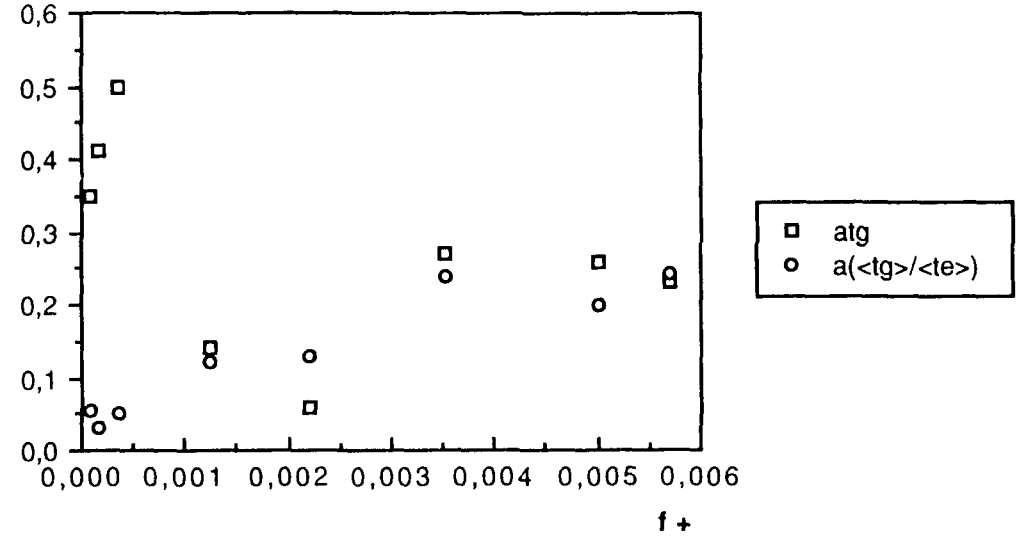

Figure 11.b) Relative amplitude of the grouping time.

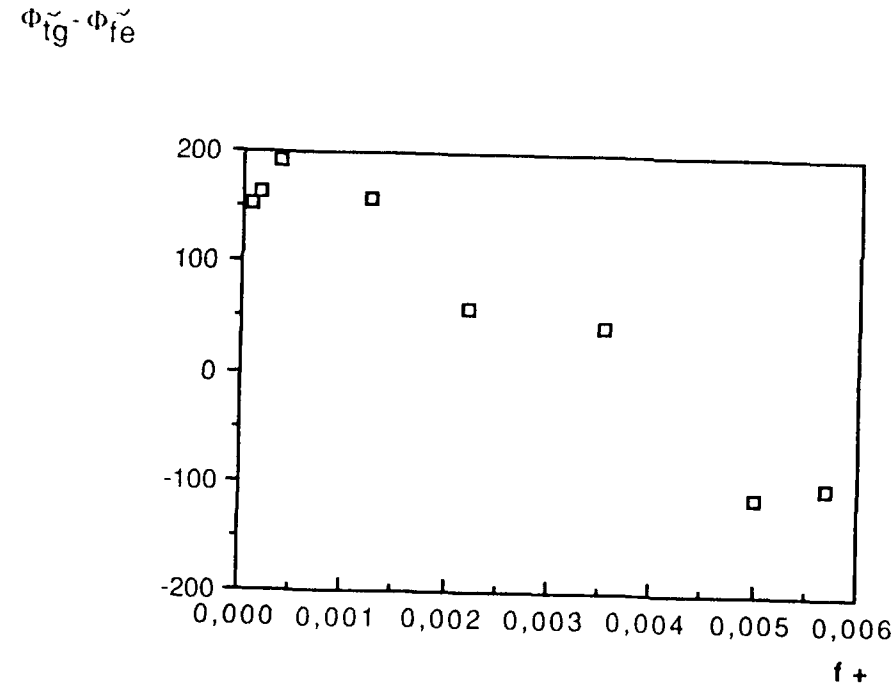

Figure 11.c) Phase shift of the grouping time with respect to the modulation of the u'-level ejection frequency.

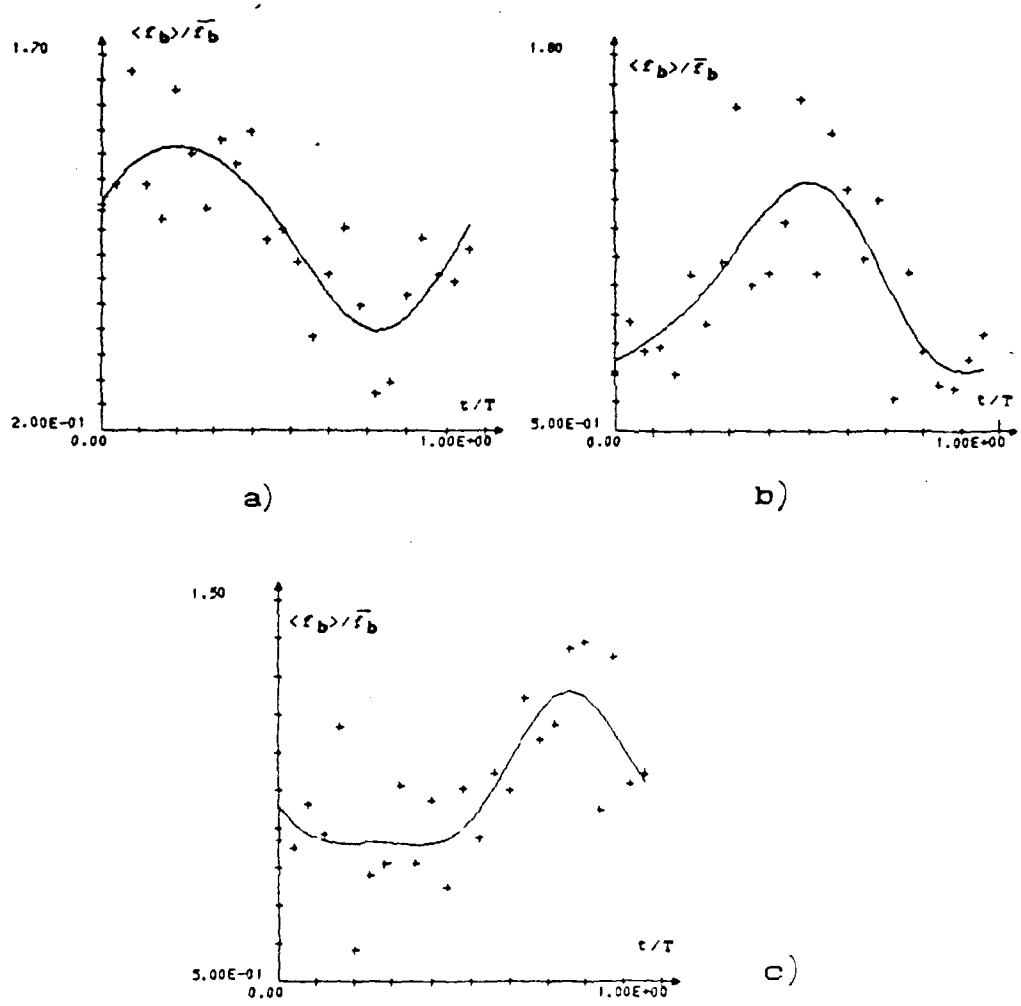

Figure 12) Modulation of the u'-level bursting frequency at ls+=9.5 a)Leading edge of the first ejection of the BMEs; b)Leading edge of the last ejection of the BMEs; c)Leading edge of BSEs.

$\overline{f^+}_b$

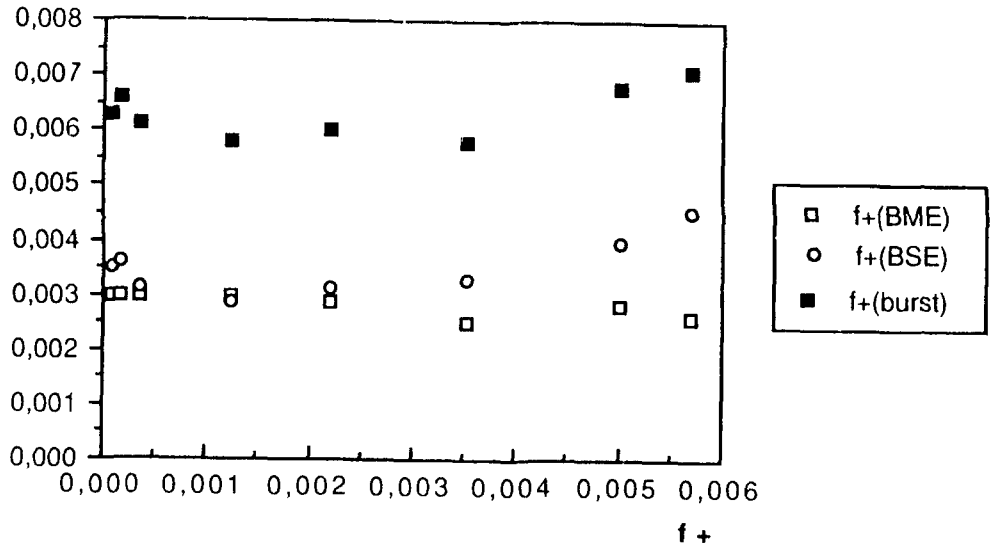

Figure 13.a) Time mean of u'-level bursting frequency

$N_{ej/BME}$

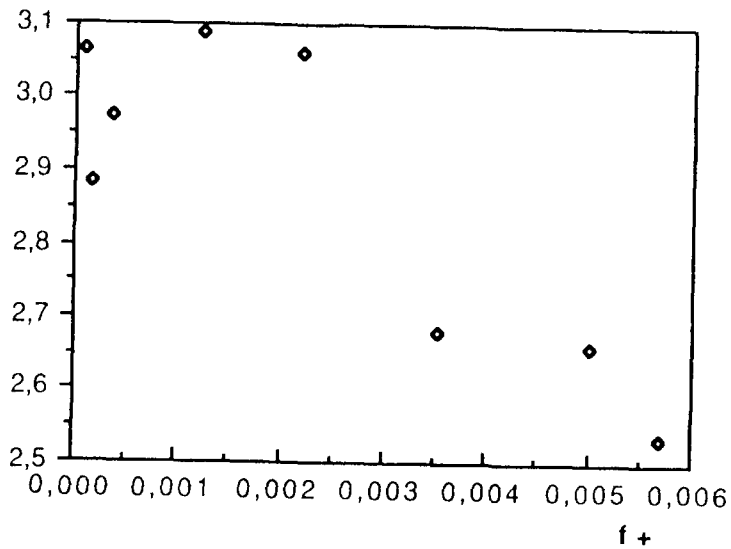

Figure 13.b) Mean number of ejections per u'-level BME versus the imposed frequency.

$a_{\tilde{fb}}$

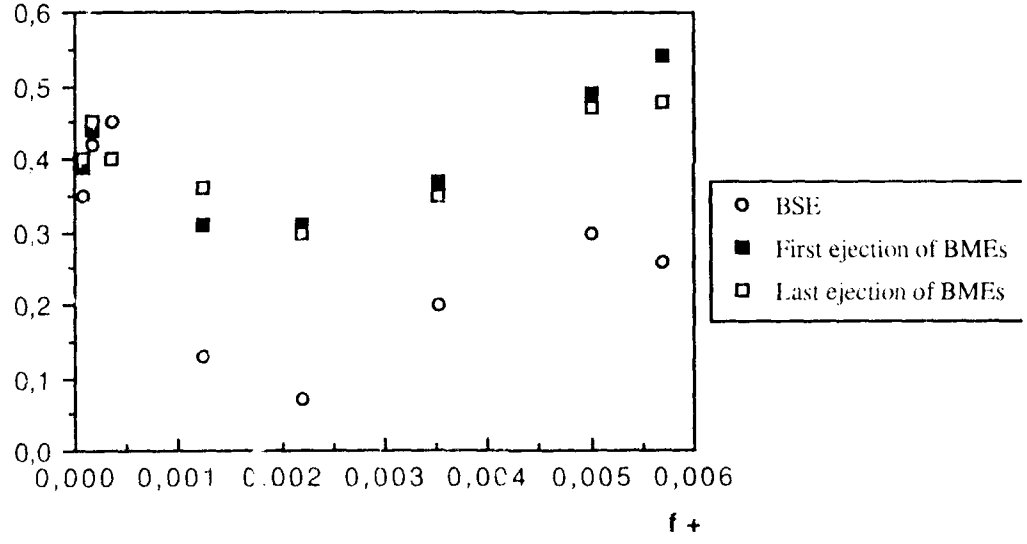

Figure 14.a) Relative amplitude of the frequency modulation of the bursts with single and multiple ejections.

$a_{\tilde{f}b}/a_{\tilde{\tau}}$

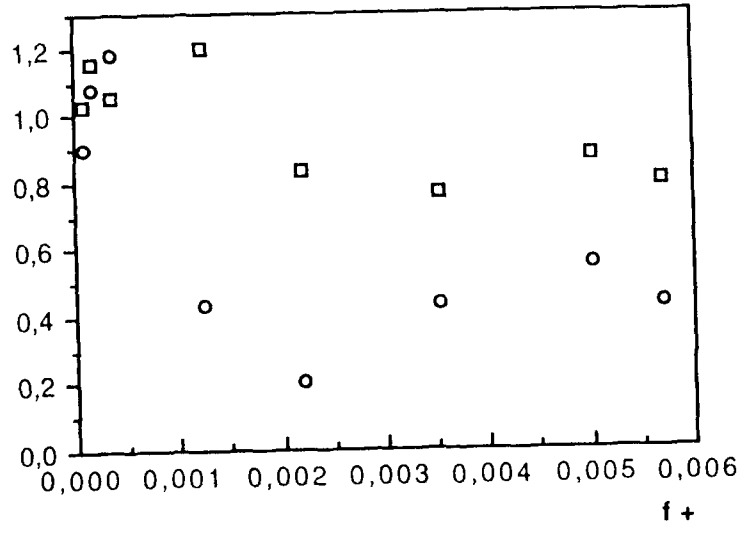

Figure 14.b) Amplitude relative of the modulation of the bursting frequency reported to the amplitude relative of the modulation of the wall shear stress.

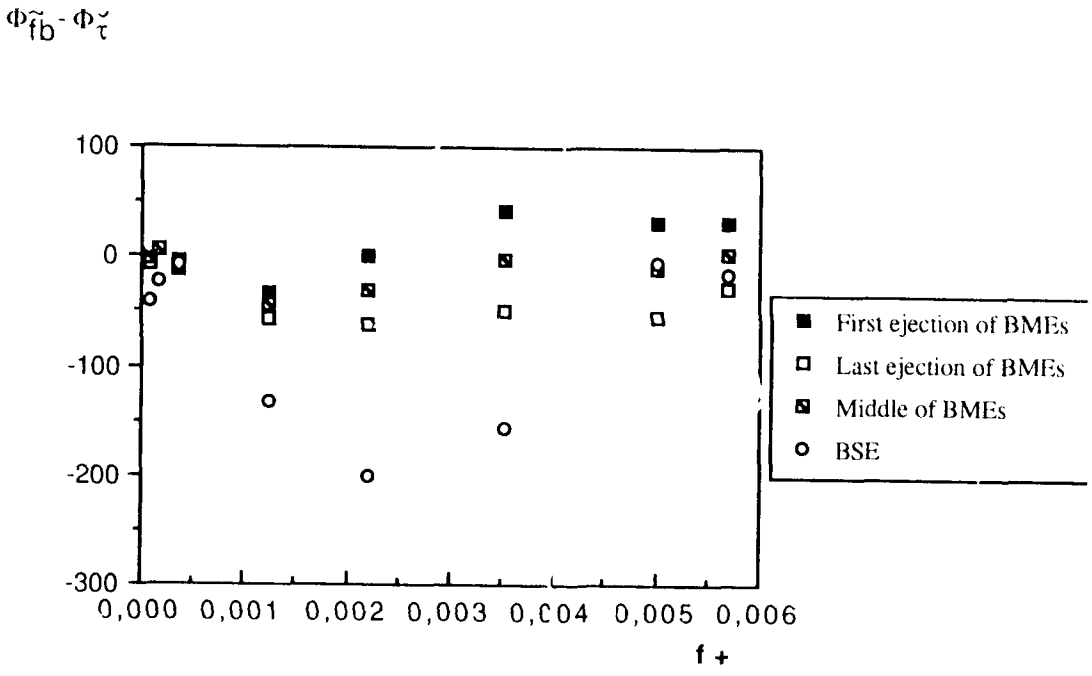

Figure 15.) Phase shift of several parts of the modulation of u'-level bursting frequency.

a)

$$\overline{< \max(u')>/ \sqrt{k_u},\ <u'u'>}$$

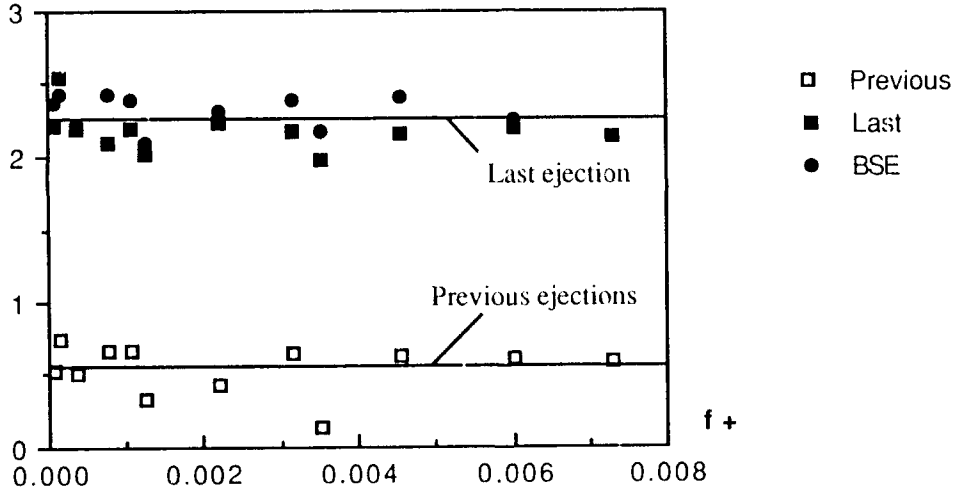

b)

$$\frac{}{< \max(\tau')> / \sqrt{k_{\tau'}}\ <\tau'\,\tau'>}$$

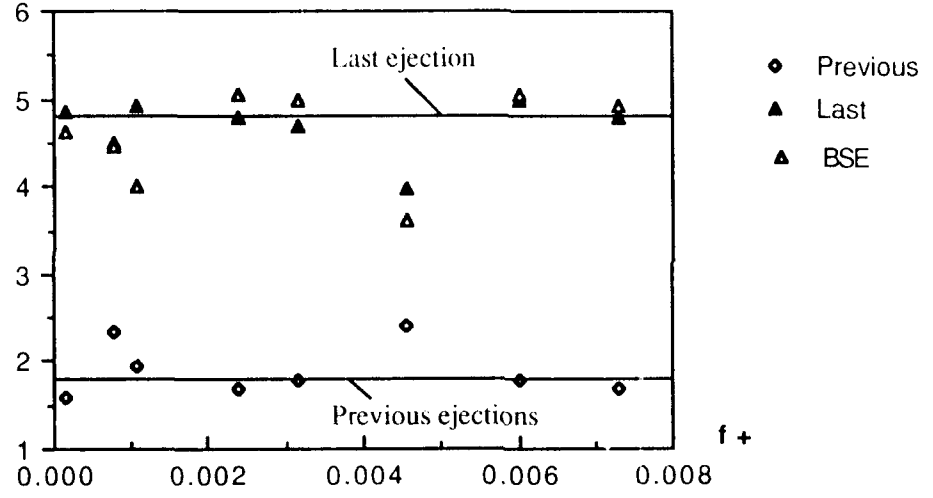

Figure 16.) Time mean of the maximas reported to the phase averaged threshold.

a) Maximas of u' at $y^+=15$

b) Maximas of τ'

a) f^{+}_{BME} ; f^{+}_{BSE}

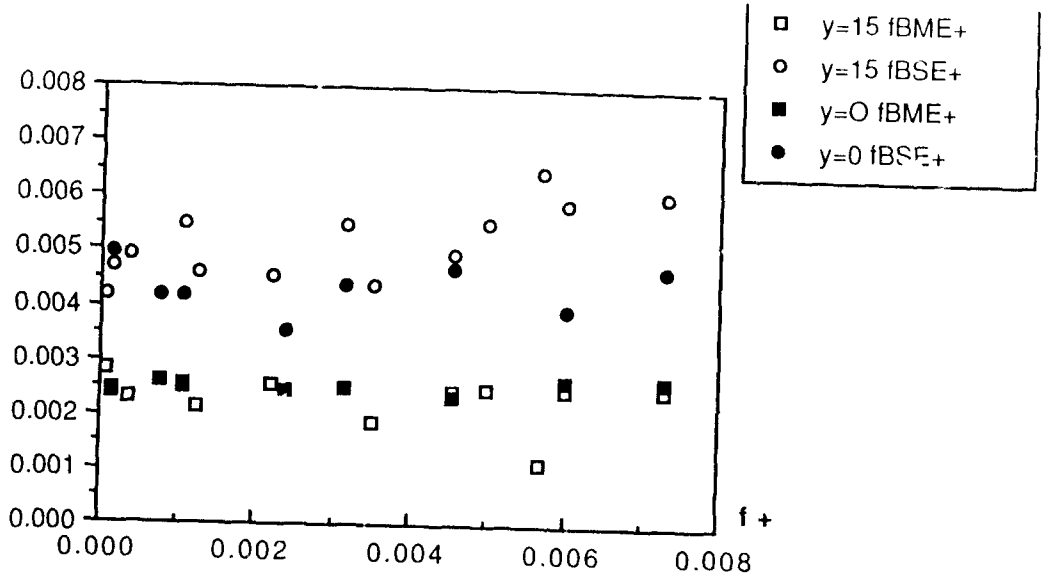
y=15 fBME+
y=15 fBSE+
y=O fBME+
y=0 fBSE+
0.008
0.007
0.006
0.005
0.004
0.003
0.002
0.001
0.000
0.000
0.002
0.004
0.006
0.008
f +

b)

$\bar{f}_b^+$

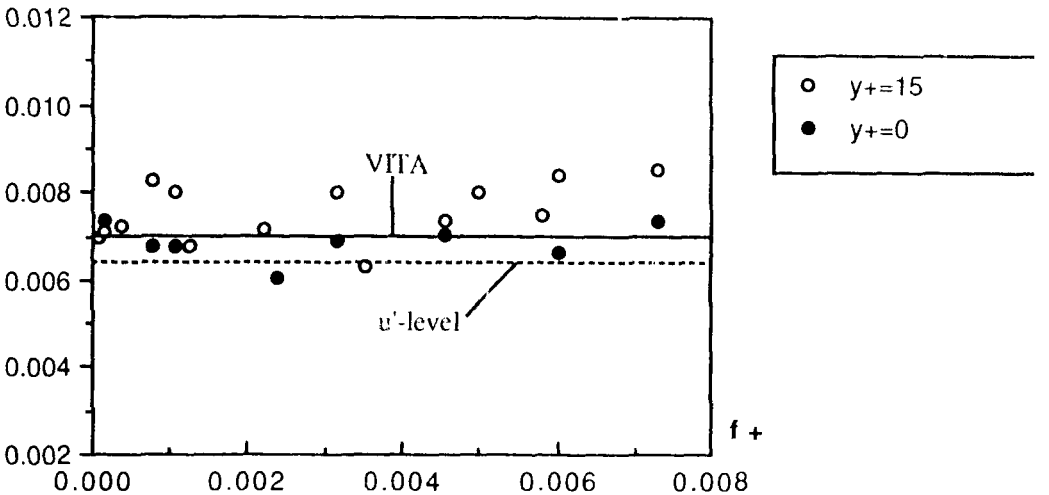

Figure 17.) Time mean of VITA bursting frequency.
a)Time mean frequencies of the BSE's and BME's
b)Time mean VITA bursting frequency compared with u'-level method

$a_{f\tilde{b}} / a_{\tilde{\tau}}$

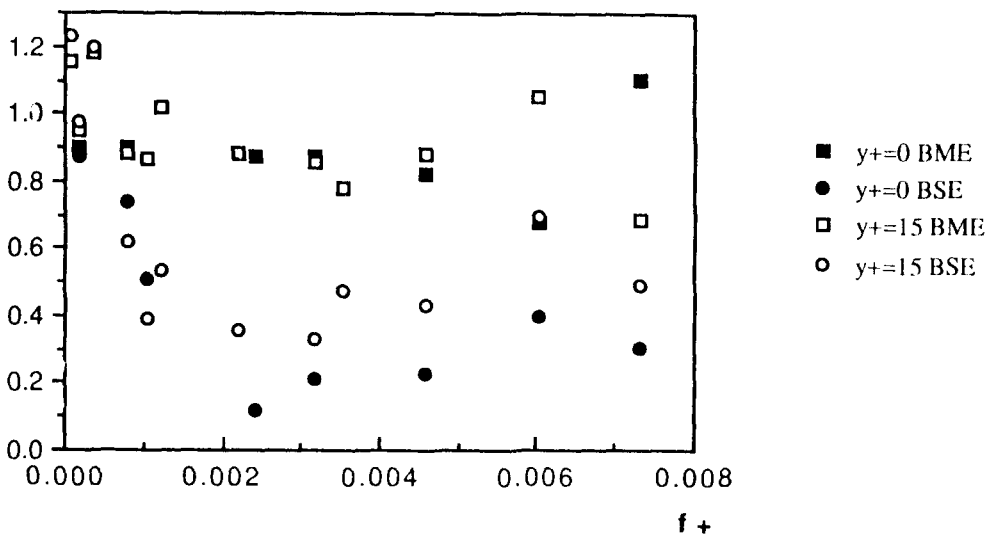

Figure 18.a) Relative amplitude of VITA bursting frequency.Comparison with the detection at the wall and at $y^+=15$.

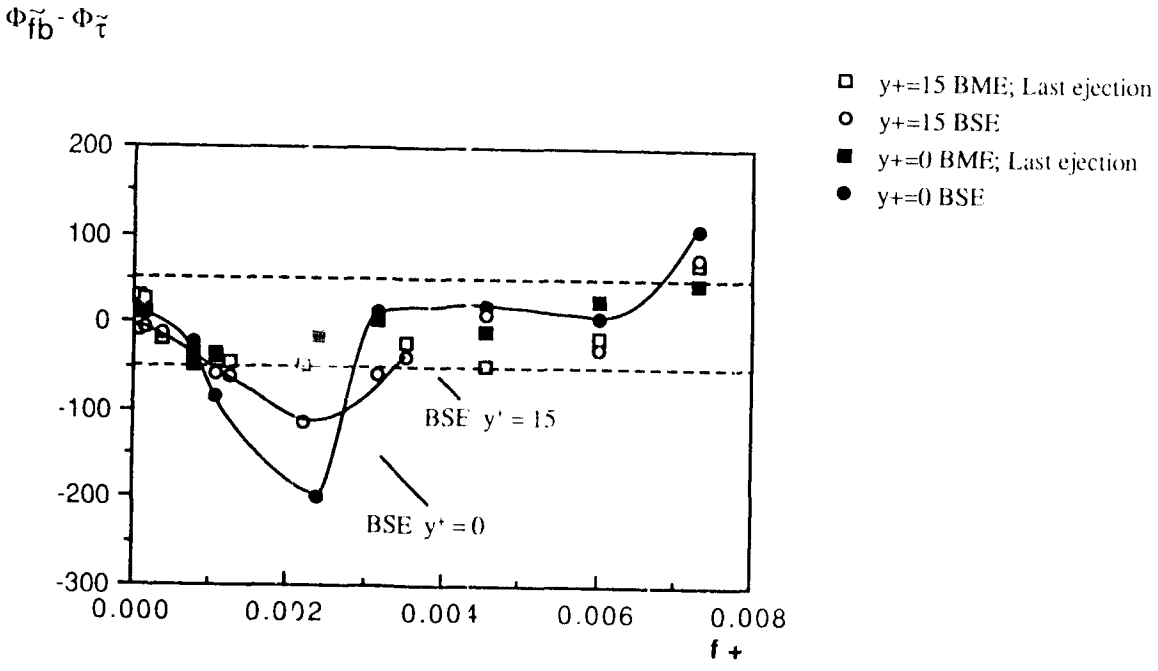

Figure 18.b) Phase shift of VITA bursts with respect to the wall shear stress. Differences of behaviour between BMEs and BSEs.

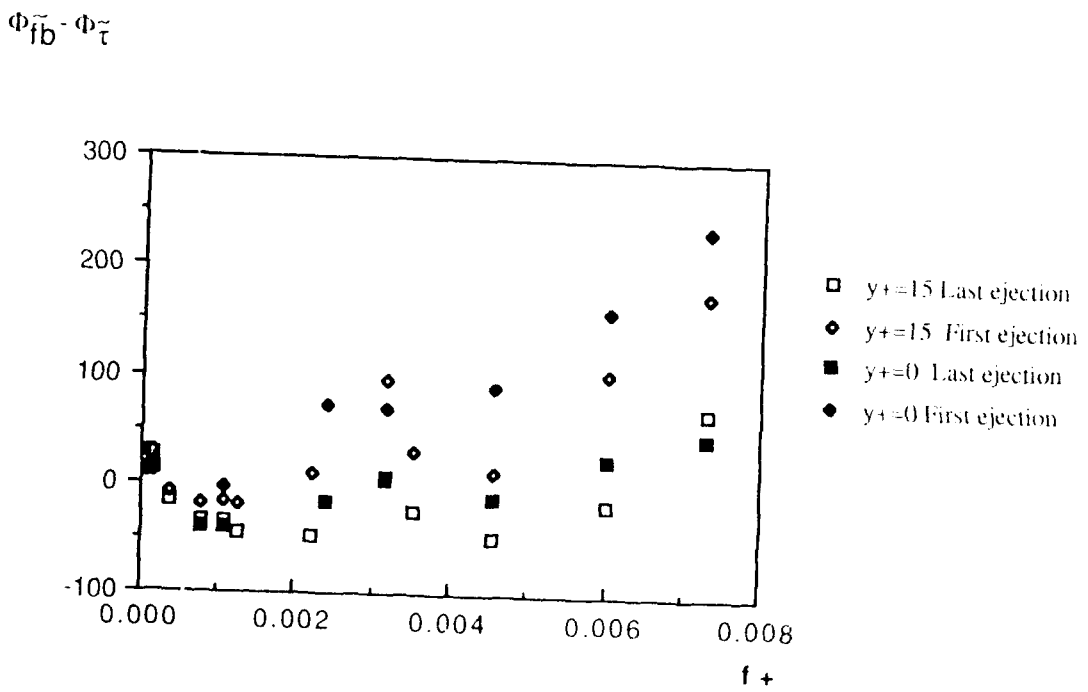

Figure 19.a) Phase shift of several parts of VITA bursts with multiple ejections.

$\overline{\Delta t^+}$(BME)

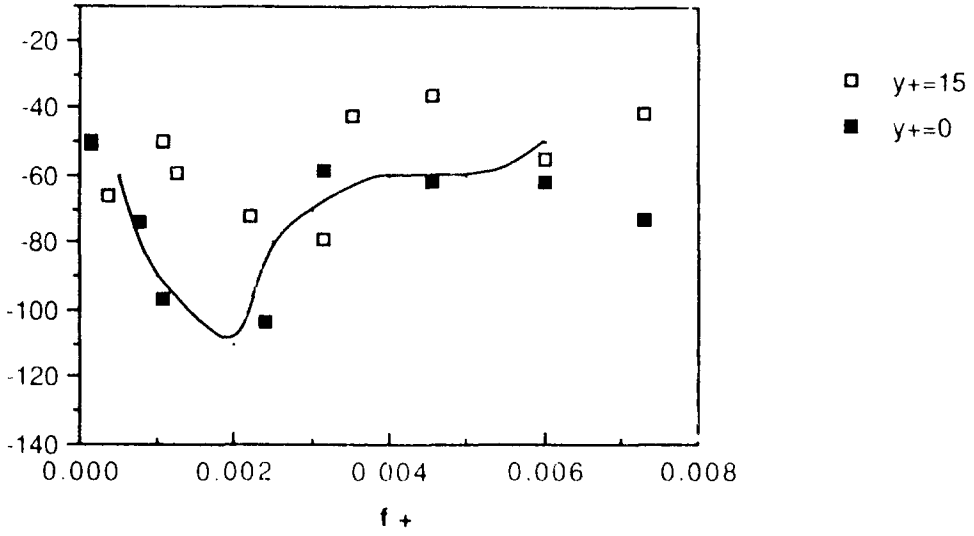

Figure 19b) Duration of the multiple ejection bursts.

Au's and Av's

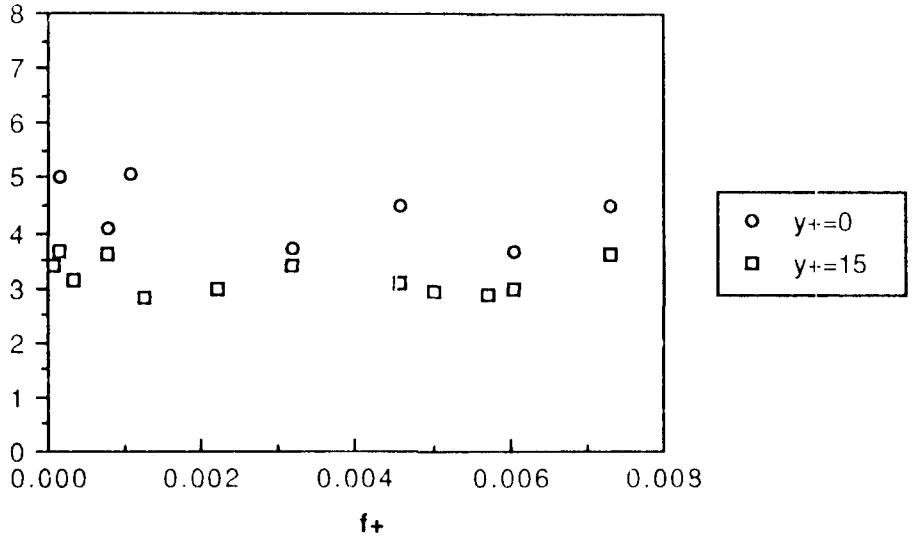

Figure 20 a) Time mean of the magnitude of the conditional averages

$a_{\widehat{\Delta u^+}}/a_{\tilde{\tau}}$ and $a_{\widehat{\Delta \tau^+}}/a_{\tilde{\tau}}$

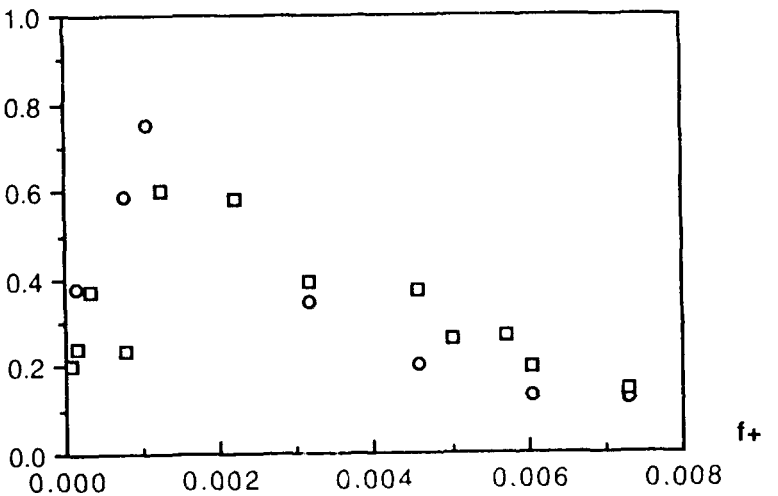

Figure 20b) Amplitude of the modulation of the magnitude of the conditionnal averages

$\Phi_{\widetilde{\Delta u'*}} - \Phi_{\tilde{\tau}}$ and $\Phi_{\widetilde{\Delta \tau'*}} - \Phi_{\tilde{\tau}}$

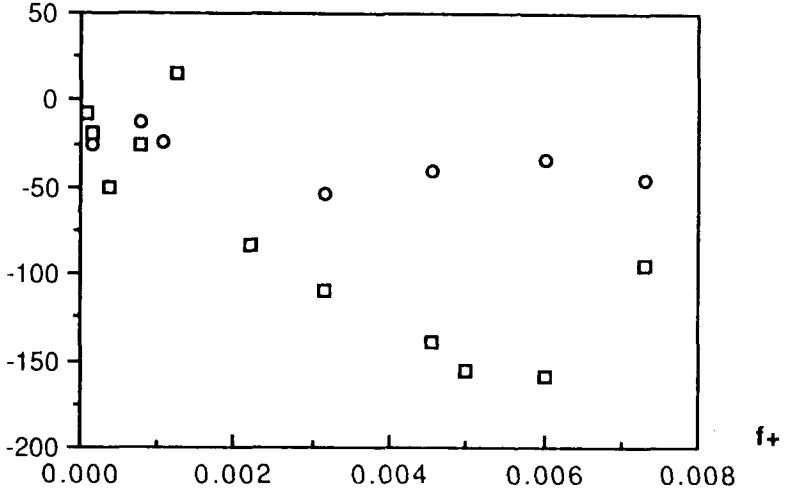

Figure 20c) Phase shift of the modulation of the magnitude of the conditionnal averages

PART FOUR

COHERENT STRUCTURES IN UNSTEADY WALL FLOW VISUALIZATION RESULTS

COHERENT STRUCTURES IN UNSTEADY WALL FLOW VISUALIZATION RESULTS*

M.Q. FENG, S. TARDU, G. BINDER

1. INTRODUCTION

Since coherent structures play an essential role in turbulent momentum transfer and production, it may be expected that the way in which they respond to imposed oscillations in the outer flow will contribute to the understanding of unsteady turbulent wall flows. The reaction of these structures to unsteady forcing may on the other hand, also shed some light on the mechanism which trigger them in steady flow.

The response of coherent structures in unsteady wall flows has only been tackled in a few investigations so far. A review on the subject may be found in the previous section. It is also shown there on the basis of single probe signals from hot films -placed either in the buffer layer or on the wall- that the occurrence of ejections and bursts varies considerably during the cycle. A second important point concerns the response of single and multiple ejection bursts (SEB and MEB): it is shown by means of two independent techniques that these two categories of events respond quite differently to the forcing.

Although several different detection and grouping techniques converged to give similar results as emphasised in the previous section, a basic question which is also encountered in steady flows but is even more crucial in unsteady flows in which both the velocity and the time scales vary during the cycle- is what extent of the results on coherent structures depends upon the detection schemes and what is of true physical significance. Since past work in steady flow (Bogard and Tiederman, 1986) has shown that the detection of structures via visualisations -

* Part of this section is in preparation for paper which will be submitted to Experiments in Fluids

although it gives less quantitative results- was among the least objectionable, it seemed reasonable to assume that results obtained with this technique in unsteady flow would also provide data basis for this complex flow situation.

2. EXPERIMENTAL SET-UP AND FLOW CONDITIONS

The experiments were performed in the unsteady water channel described in I . The centreline velocity was constant (U_c=18 cm/s) through the investigation corresponding to a Reynolds number based on the half width of the channel of Re_h=9000 and a friction velocity of u_τ=0.80 cm/s.

Ten flows corresponding to two imposed amplitudes of 13 and 20 % of the free stream velocity, together with five imposed frequencies are investigated. The imposed frequencies in wall units are $f^+ * 10^4$= 5.0; 10.6; 24.0; 31.7; 73.1 covering a range from the quasi-steady limit to the high frequency regime.

A dye slot mounted at the wall situated at a distance 40h from the entrance of the channel -where the measurements of the wall shear stress are also usually done- is used . The dimensions of the slot are Δx^+=1.5 (in the streamwise direction) and Δz^+=300 (in the spanwise). A solution of fluorescine (5 to 10 gr /lt) is injected at the wall: the flow rate of the dye was controlled to be sure that it does not perturbate the flow in the viscous layer. An argon laser beam (maximum power= 1W) , combined with an oscillating mirror (frequency and amplitude of the displacement can both be controlled) generated a laser sheet of dimensions Δz^+=27 and Δx^+=3000. The width of the laser sheet is small compared with the distance Δz^+=100 of the low speed streaks (Smith and Metzler, 1983). Furthermore it is well aligned in the direction of the mean flow to be sure that at a given instant only one streak is marked.

A colour CCD-Video camera (Sony DXC-102P) is used to record the visualisations with 25 frames/s corresponding to a sampling frequency of f_s^+=0.4. The phase reference is provided by a flash of light (duration 0.1 s) triggered by the pulsator and simultaneously recorded on the video.

3. DETECTION OF EJECTIONS

The intermittent lift-up of the dye is striking and sometimes even spectacular and provides a simple means for the detection of ejections as well as a fairly objective one, considering the small variation (5%) in the counts from two different observers.

The station of the detection of the ejections has to be correctly fixed as it was pointed out by Bogard(1984). The number of detected events depends on the distance from the dye slot and this is essentially due to the diffusion of the dye and to the decay of the structures as they are convected downstream, but also to the fact that a given distance from the slot is needed to assure that the low-speed streaks -formed between the legs of the counter rotating streamwise vortices. It is known that the streamwise extend of the near wall hairpin type vortices is about 1000 l_v (Smith and Metzler, 1983; Wallace, 1982). The distance needed from the dye slot at which all of the ejections are marked is about 800-1000 l_v (Bogard, 1984; Bogard and Tiederman, 1986) . It is interesting to note than that these two values compare quite well. In our previous investigation the detection was made at $X^+ \approx 500$ from the dye slot a distance which revealed not large enough, and some discrepancies have been noted when the flow visualisation results were compared with the probe measurements, in particular in the quasi-steady limit. That is why we repeated here the flow visualisations, and set the detection stations further away from the dye slot.

Bogard and Tiederman (1986) identified the ejections when the element of the fluid marked by dye originates from the region below $y^+=15$, and when an upward movement of at least $\Delta y^+=20$ occurs within a streamwise distance of $\Delta x^+=350$. Later, when they have done simultaneous flow visualisations and probe measurements, they relaxed this last condition by taking into account the events originating within $\Delta x^+=100$ with an upward movement of $\Delta y^+=5$, counting also the ejections in their early stage of development. We proceeded by adopting this last criteria. Thus, the maximum lift-up h_1^+ , h_2^+ and the corresponding times at

two stations located at X_1^+=840 and X_2^+=940 from the dye injection slot are manually recorded. The data was proceeded on a PC using FORTRAN programmes. The number of events was phase averaged in 10 bins covering the cycle . The phase reference triggered by the pulsator allowed the correct arrival time of each event in the oscillation cycle. For each run a record of length $T^+ \approx 20000$ was analysed. This yielded a population of about 200 events. This length resulted from a compromise between the requirements of an acceptable statistical convergence of the phase average and the time to view and analyse the video film. (≈ 40 hours for each run!). In the next future the record length for some flow conditions will be increased in order to have a better statistical convergence.

The same usual notations are used, namely < > for the phase average, A and Φ for the amplitude and phase shift of the fundamental mode. a denotes the relative amplitude. Thus for the ejection frequency:

$$<f_e>= \overline{f_e} + \tilde{f_e}$$

(time mean and modulation), and

$$A_{\tilde{fe}}, \quad \Phi_{\tilde{fe}} \text{ and } a_{\tilde{fe}} = A_{\tilde{fe}} / \overline{f_e}.$$

The detection of ejections is done in two steps:

1) an event is counted when: $h_1^+>15$ **and** $\Delta h^+=h_2^+-h_1^+>5$.

2) $<\Delta h^+>$ is determined and only events with $\Delta h^+>0.9 <\Delta h^+>$ are retained. The factor 0.9 has been chosen so that $\overline{f^+_e}$ in the quasi-steady limit is the same as in steady flow i.e $\overline{f^+_e}$ =0.0125. The purpose of this second step is to take some account of the modulation of the turbulent intensity. Implied is the reasonable assumption that the lift-up is higher when the intensity is larger.

In the probe detection methods (VITA, u'-level, mu'-level) , it is easier to take into account of the modulation of the several characteristics, by taking for example the thresholds proportional to the local turbulent intensity modulations -although some extra efforts have to be paid to determine the modulation of the VITA integration time-. This is however less obvious

in what is concerned with the flow visualisation data. One of the reason that justifies the choice of $<\Delta h^+>$ as detection criteria is that in the quasi-steady limit we noted that $<\Delta h^+>$ computed after the first step of the procedure mentioned above is in phase with $<f_e^+>$ in a way similar to the probe measurements where $<f_e^+>$ is in phase with $<u'u'>$ when $f^+ \to 0$. The second reason is that, although when the first criteria is applied to the steady flow, the time mean ejection frequency is found $f_e^+=0.012$ a value which compares well with Bogard and Coughran (1987), in the unsteady flow, it gave a time mean ejection frequency almost two times larger. It was argued then, that the modulation characteristics should be in some way taken into account. More convincing arguments which justify the choice of $<\Delta h^+>$ will be given later in this section.

Figures 1 to 5 show the phase averages of the ejection frequency for ten flows investigated here. The fundamental of a least square Fourier analysis is also shown on each figure. It may be seen that phase average of $\widetilde{f_e^+}$ is fairly well converged in a majority of the cases, despite the small centreline velocity amplitude and the limited size of the ejection population.

4. RESULTS

Data points from hot film detections (Tardu and Binder,1991-see the previous section) are plotted together with the visualisation results which are capitulated through figures 26 to 28. These detections were made with the VITA method wherein the threshold and the integration time were modulated. The hot film was located at $y^+=15$ and the signal length analysed was six times larger than of the visualisations.

4.1) Time mean ejection frequency

Figure 26 shows that $\overline{f_e^+}$ is independent of forcing frequency and close to the steady flow value 0.012 (Tardu and Binder, 1991). There is good agreement with VITA probe results.

4.2) Modulation of the ejection frequency

Figure 27 shows the ratio of the relative amplitude of the modulation of the ejection frequency to the relative amplitude of the modulation of the wall shear stress, and involves than four quantities. The wall shear stress modulation $<\tau>$ was measured in the same conditions as flow visualisations. The close agreement between the points corresponding to the two amplitudes proves that the scaling with a_τ is appropriate. The characteristics of the modulation of $<f_e>$ depends more on the imposed frequency than on the imposed amplitude. The choice of this scaling is also based on the hypothesis that in the quasi-steady limit the inner scaling is valid i.e. $<f_e><\nu / u_\tau^2>$ =cons. This relationship leads to the first order (see the previous section of this report) to $a_{fe}=a_\tau$ and $\Phi_{fe}- \Phi_\tau=0$. Figures 27 and 28 show that these two conditions are approximately fulfilled when f^+-->0. It is seen on Fig. 27 that at the smallest imposed frequency a_{fe}/a_τ is about 1.2 for a_{uc}=0.20 and 1.35 for a_{uc}=0.13 so larger than one. The same behaviour is also observed in probe measurements, showing that the quasi-steady limit is hard to be reached.In other respects it is noteworthy that the probe measurements agree well with the flow visualisations. That strengthens the validity of the analysis given in the previous section. Consequently the same discussion done there is valid here, namely the sharp decrease of the amplitude a_{fe} in the high frequency regime showing that the turbulence structures respond less to high frequency forcing as was previously observed with the turbulent intensity (Tardu, Binder and Blackwelder, 1991)

In what is concerned with the phase shift $\Phi_{fe}- \Phi_\tau$ and despite the larger scatter, one may distinguish a common trend: first a decrease from zero (expected value in the quasi-steady limit) to about -100º and then a jump to positive values (Fig. 28). The first part implies a roughly constant time delay (Δt^+=140) between the ejections and the wall shear stress. This is logical if it is thought that the ejections require a finite time to react to the additional stretching

imposed by the oscillating shear $\partial\tilde{u}/\partial y$ i.e $\tilde{\tau}$. The sudden increase of $\Delta\Phi$ when $f^+>0.003$ must then result from a quite different hitherto unexplained mechanism. As a first attempt, recall that $f^+=0.003$ corresponds to $l_s^+=10$ and marks the beginning of a regime where the oscillating layer is confined within $y^+<10$. That means that, only the part corresponding to $\Delta h^+<10$ of the vortical structures are interacting with the oscillating layer, and their outer part is within the plug flow. Furthermore at $f^+=0.007$ where $\Delta\Phi$ is practically zero and a_{fe} is closer to its quasi-steady value (i.e. 2 a_{uc}), the part of the layer where an interaction is expected is limited only to $\Delta h^+<7$, a region where there are less active and smaller structures. That may explain why the modulation of the ejection frequency becomes less sensitive to the imposed frequency.

4.3) Ejection heights

The phase averages of the maximum heights at station 1, are shown on figures 6 to 11. The time mean $h_{1(max)}{}^+$ varies between 30 to 40. Perry and Chong (1982) suggested that the turbulent boundary layer has a hierarchy of the hairpins, which, after the cross-stream amalgamation result in a larger but more disperse hairpins. They suggest a probability distribution of hairpin scales which is inversely proportional to the distance from the wall. Lu and Smith (1988) have shown that the probability of identifying a structure of scale $h^+\approx40$ is maximum and that the probability distribution is skewed for smaller values of h^+. The time mean of ejection heights agrees well with these findings.

Since $<h_{1(max)}{}^+>$ is found to modulate slightly (the relative amplitude is smaller than 0.06) so that their modulation characteristics are judged to not be significant.

4.4) Modulation of the lift-up

The phase averages of the lift-up $<\Delta h^+>$ are shown on figures 11 through 15. The time mean of Δh^+ is about 16 independently of the imposed frequency. Recall that the first step of

the detection criteria requires $\Delta h^+ > 5$ and the high time mean found for Δh^+ indicates that there is only a small contribution of the prematurated ejections to $<f_e>$.

In quasi-steady limit one should have $<\Delta h>/<l_v>$ which implies that for $f^+ \rightarrow 0$, $a_{\Delta h} \approx a_{u\tau} \approx 0.5\ a_\tau$ and $\Phi_{fe} - \Phi_{u\tau} \approx \Phi_{fe} - \Phi_\tau \approx 0$. That is why $a_{\Delta h}$ is related to $a_{u\tau}$ in Fig. 29. It is seen from figures 29 and 30 that these two conditions are satisfied in the quasi-steady limit. On the same figures, the modulation of the wall shear stress fluctuations are also plotted (the normalisation with $a_{\tau'\tau'}$ "quasi-steady" is based on $a_{\tau'\tau'\,(qs)} = 2\ a_\tau$ when the amplitude is small). This allows comparison between the modulation of $<\Delta h>$ and the modulation of $<\tau'\tau'>$ which is used as modulated threshold in probe detection techniques (at the wall; see the previous section). The phase shift of $<\Delta h^+>$ follows also the turbulence response quite well. Note the remarkably small scatter on these values of $\Delta\Phi$. These results may be a posterion justification for the second step in the detection scheme.

4.5) Modulation of the bursting frequency

It was shown in the previous section that the grouping of ejections into bursts from velocity signal detections may be based on a break in the cumulative probability distribution curve of the ejection interarrival times or more objectively through an elaborated iterative procedure based on the u'-max value just after the ejection -this last technique is also successfully applied to τ' signal-. None of these methods work with the visualisation data. It has to be recalled that only visualisations in the x-y plane are realised in this study. The most objective way to detect ejections belonging to the same burst (MEB) is to use simultaneous visualisations in the x-z plane in a way similar to Bogard and Tiederman (1986) and to detect the ejections belonging to the same streaks. This will be part of research in the next future. In order to use the existing data, however, several attempts to detect single and multiple ejection bursts (SEB and MEB) were tried. Finally the following iterative method gave the most representative results:

step 1: group ejections satisfying: $\Delta t < 0.2\ t_e$ where t_e is the mean interarrival time. From this grouping, determine $<t_e>_1$ interarrival time of ejections belonging to MEB's.

step 2: recalculate grouping with criteria $\Delta t < 0.7<t_e>_1$

step 3: from the previous grouping determine Δt_{ep} time between last ejection and previous one in MEB's and Δt_{en} time between last ejection of burst and next ejection. Recalculate grouping on criteria for last ejection in a burst if:

$\Delta t > 0.5\ (<\Delta t_{ep}>+<\Delta t_{en}>)$. Iterate step 3 till convergence (10 to 20 iterations).

The phase average of the modulation of frequency of the single ejection and multiple ejection bursts are shown on figures 16 to 25. Seven bins are used to compute the phase averages. The statistical convergence is less satisfactory compared with the phase averages of the ejection frequency. This is to be expected because of the limited size of the averaged populations : there are only 10 events (i.e. MEB or SEB) in each bin on the average. It is recalled that in unsteady flow the record lengths have to be 30 to 50 times larger than the steady flow in order to have a good statistical convergence. Altough in probe measurements this condition can be easily fulfilled, it is more difficult to analyse the flow visualisation data: for instance that would require about 240 hours for each flow configuration!! Nevertheless the record length will be increased by a factor of two in the next future.

Figures 31 and 32 show the amplitude and phase shift with respect to $<\tau>$ of the MEB's and SEB's as well as the VITA hot-film results. The agreement between the results obtained with the two different methods is really encouraging. It is seen on these figures that the amplitude and phase shift of the MEB's vary little with the forcing frequency while for the SEB's the amplitude drops by a factor 3 to 5 and the phase lag with respect to $<\tau>$ increases to about 250^0 when the forcing frequency increases from 0 to 0.002.

The two types of burst do clearly not react in the same way to the forcing in this frequency range. It is also seen that the amplitude and the phase shift of the two families take on similar values when $f^+ > 0.006$.

5. CONCLUSION

The visualisation data presented in this section confirm the previous results obtained from hot film signals on the response of ejections and bursts to forced oscillations. The cyclic variations of the frequency of ejection and of the single ejection bursts go through a definite change in behaviour (in amplitude and phase shift) when the forcing frequency is about 1/4 of the mean ejection frequency. In these conditions the amplitude of the ejection frequency has dropped by a factor four to five from the quasi-steady value and the amplitude of the SEB's by nearly as much. The response of the MEB's on the contrary varies relatively little with the forcing frequency. The difference in the response of the MEB's and SEB's suggests that they result from different mechanisms.

References

1. Bogard, D.(1982) PhD Thesis, Purdue Un. U.S.A

2. Bogard D. ; Tiederman W.G.(1986) J. Fluid Mech. vol.179, p.1

3. Bogard D. , Coughran (1987) , 6th Symp. Turbulent Shear Flow , Toulouse, France

4. Lu L.J.; Smith C.R. (1988) Rep. FM-14 Lehigh Un. Dept. Mech. Engn. Bethlehem U.S.A

5. Perry A.E.; Chong M.S.(1982) J.Fluid Mech. vol.119 p.173

7 Smith C.R.; Metzler S.P.(1983) J. Fluid Mech. vol.129, p.27

6 Tardu S., Binder G., Blackwelder R.(1991) Submitted to J. Fluid Mech.

7 Tardu S., Binder G.(1991) Submitted to J. Fluid Mech.

8.Wallace J.M. (1982) Development in Theoretical and Applied Mech., Un. Allabama in Huntville p. 509

a)

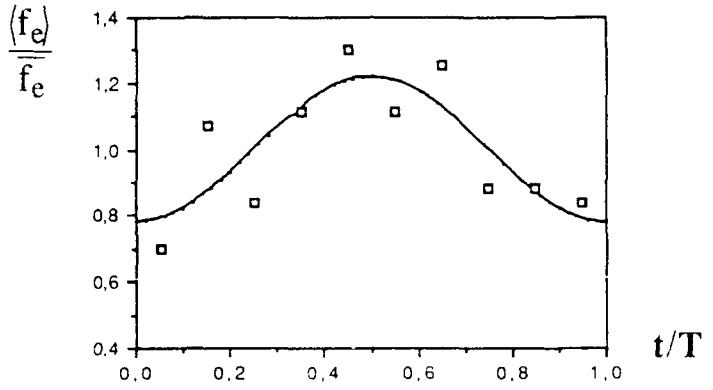

b)

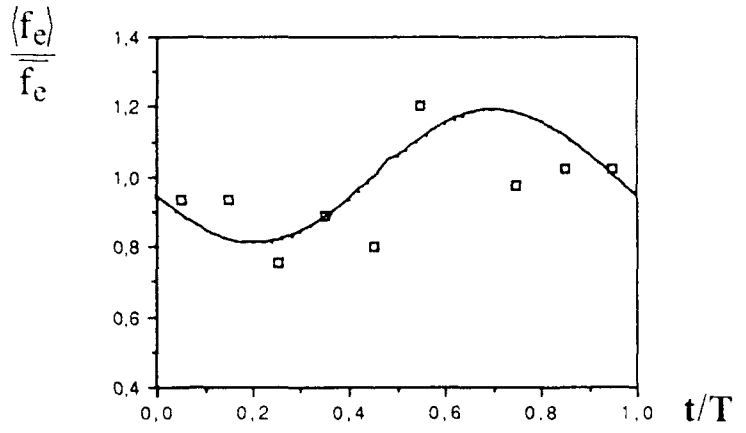

Figure 1. Phase average of ejection frequency. T=2.6s.
a) a_{uc}=0.20; b) a_{uc}=0.13

a)

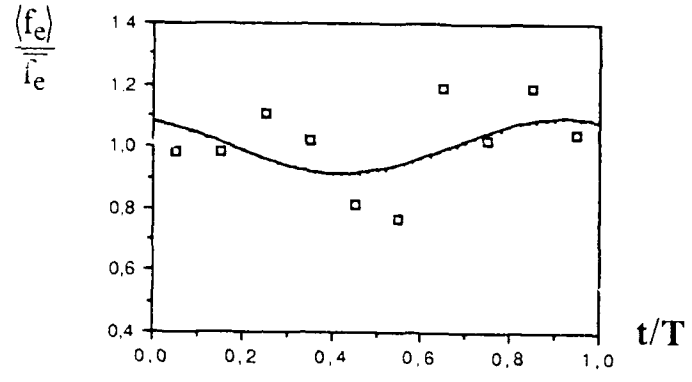

b)

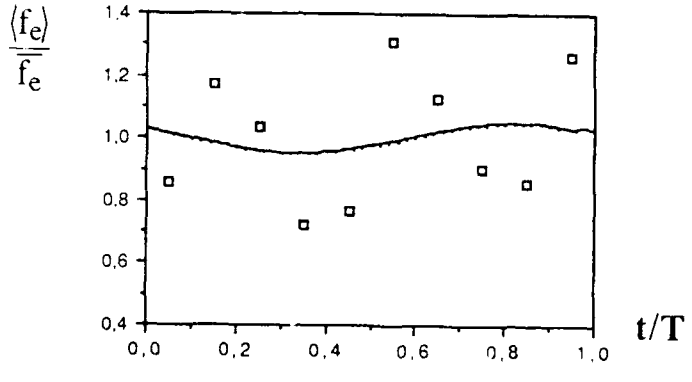

Figure 2. Phase average of ejection frequency. T=5.3s.
a) a_{uc}=0.20; b) a_{uc}=0.13

a)

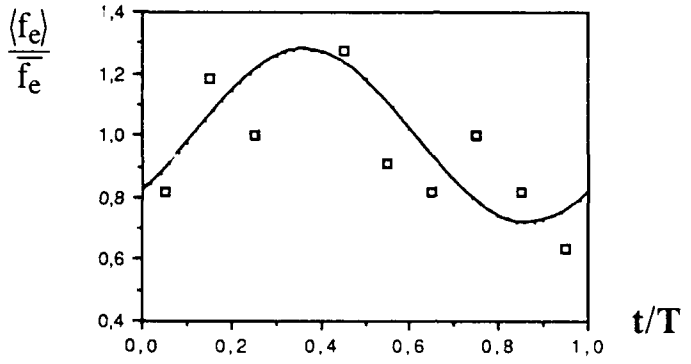

b)

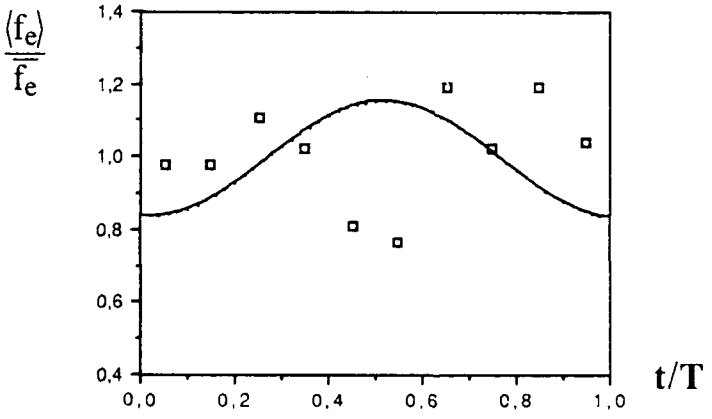

Figure 3. Phase average of ejection frequency.T=7.0s.
a) a_{uc}=0.20; b) a_{uc}=0.13

a)

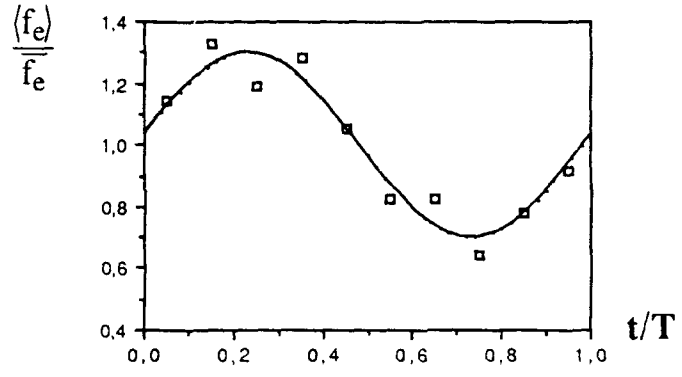

b)

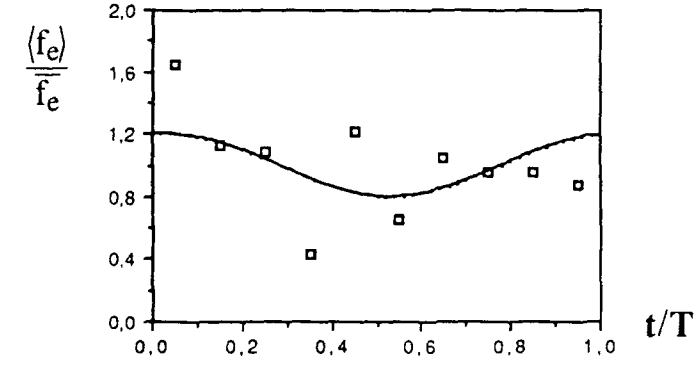

Figure 4. Phase average of ejection frequency.T=16.0s.
a) a_{uc}=0.20; b) a_{uc}=0.13

a)

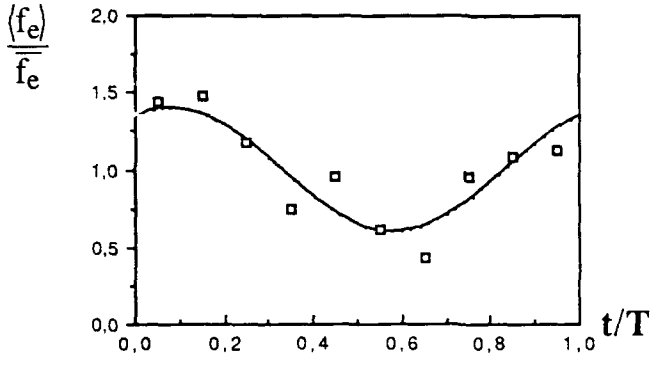

b)

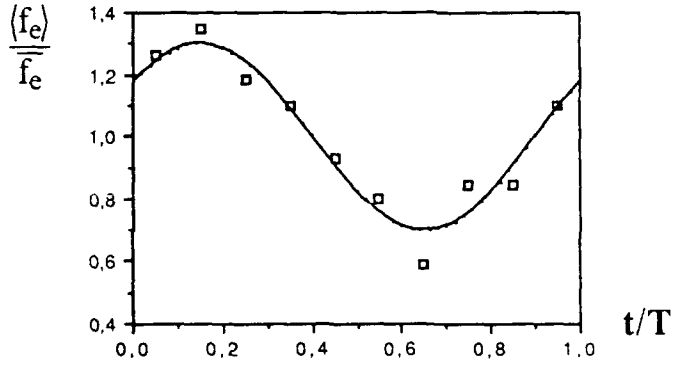

Figure 5. Phase average of ejection frequency.T=34.0s.
a) a_{uc}=0.20; b) a_{uc}=0.13

a)

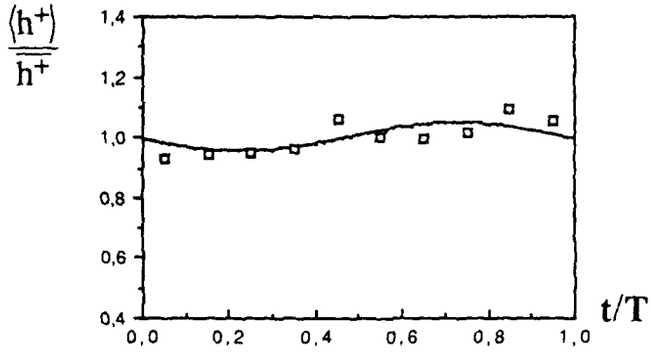

b)

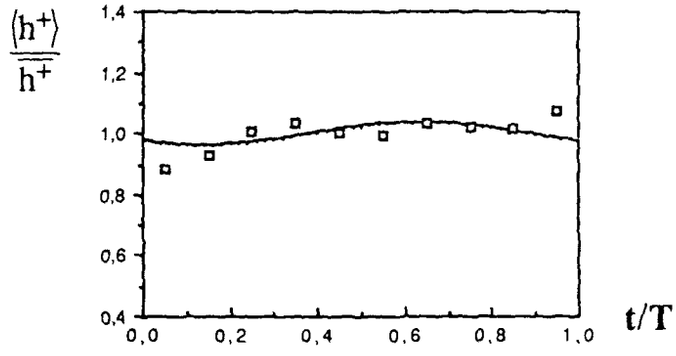

Figure 6. Phase average of ejection height.T=2.6s.
a) a_{uc}=0.20; b) a_{uc}=0.13

a)

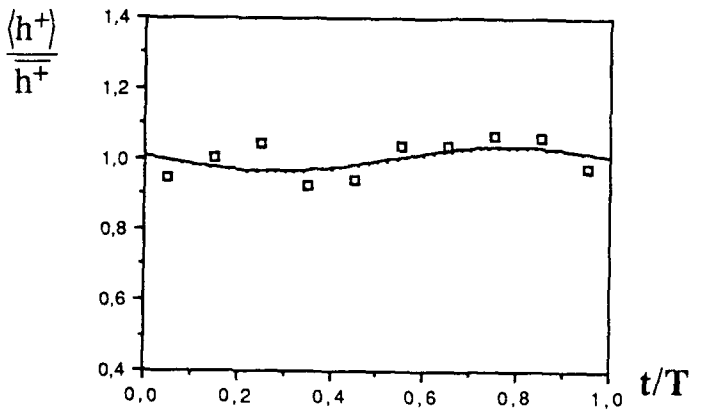

b)

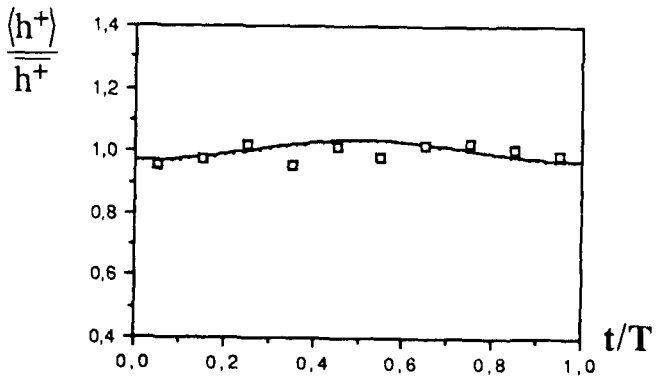

Figure 7. Phase average of ejection height T=5.3s.
a) a_{uc}=0.20; b) a_{uc}=0.13

a)

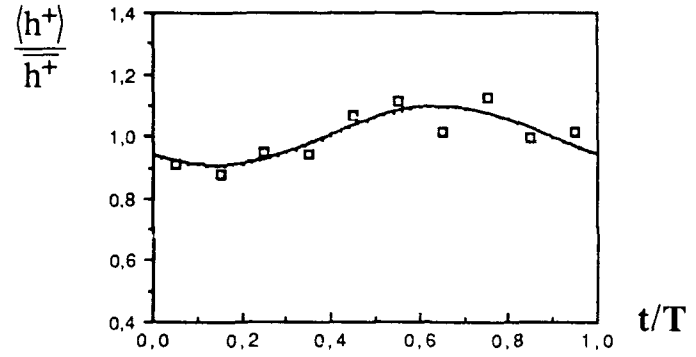

b)

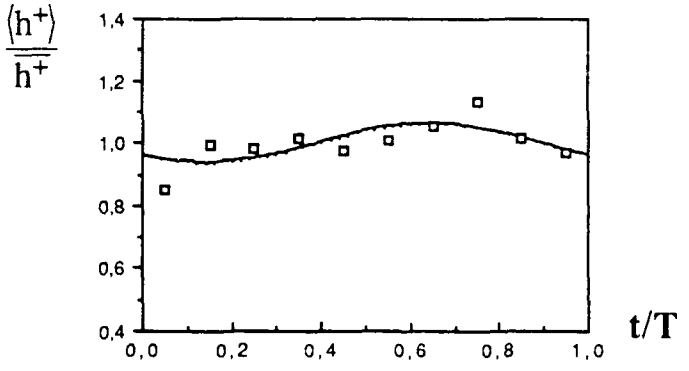

Figure 8. Phase average of ejection height.T=7.0s.
a) a_{uc}=0.20; b) a_{uc}=0.13

a)

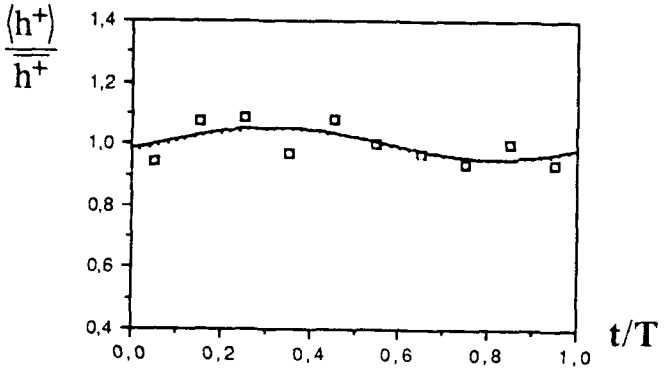

b)

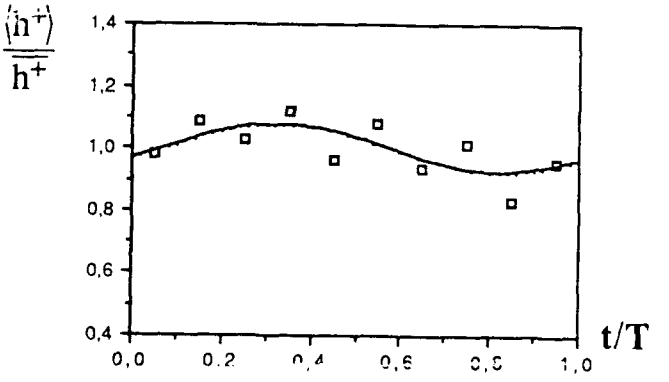

Figure 9. Phase average of ejection height.T=16.0s.
a) a_{uc}=0.20; b) a_{uc}=0.13

a)

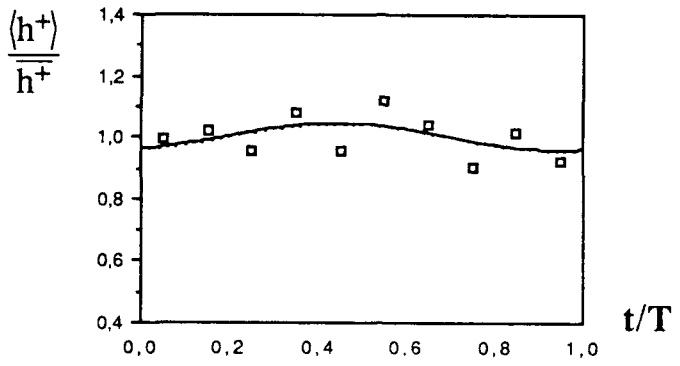

b)

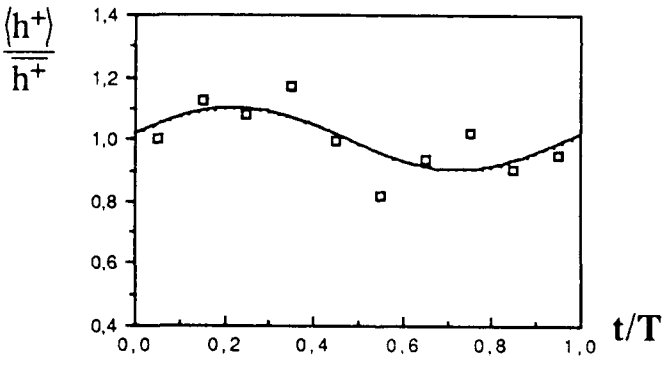

Figure 10. Phase average of ejection height. T=34.0s.
a) a_{uc}=0.20; b) a_{uc}=0.13

a)

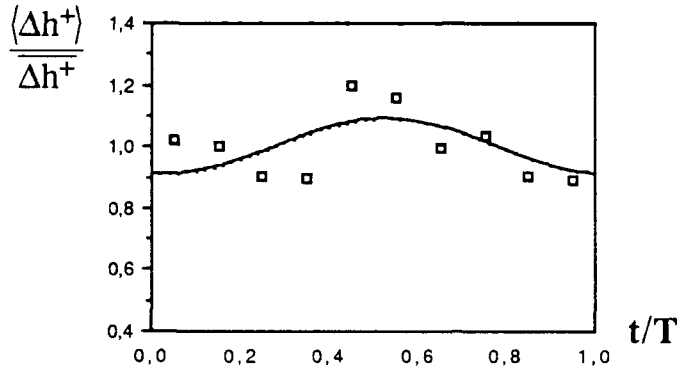

b)

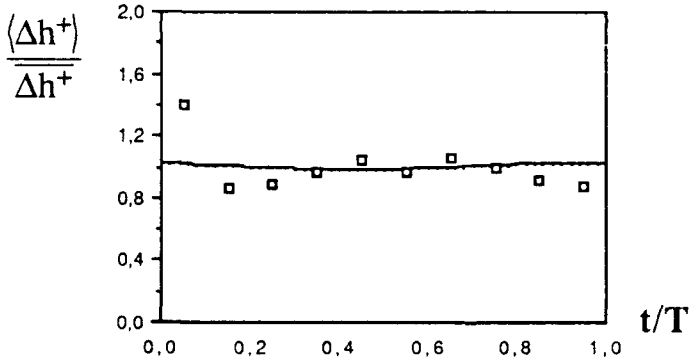

Figure 11. Phase average of ejection lift-up over distance $\Delta X^+=100$. T=2.6s. a) $a_{uc}=0.2$; b) $a_{uc}=0.13$

a)

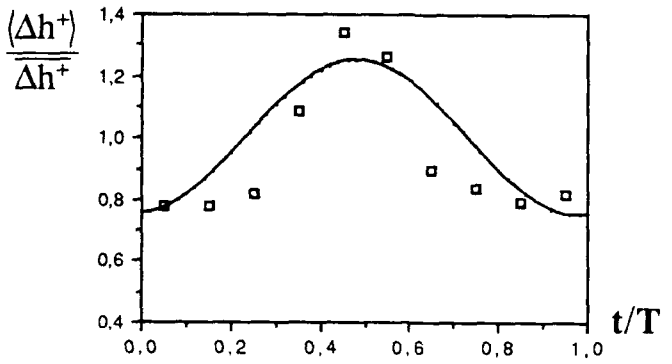

b)

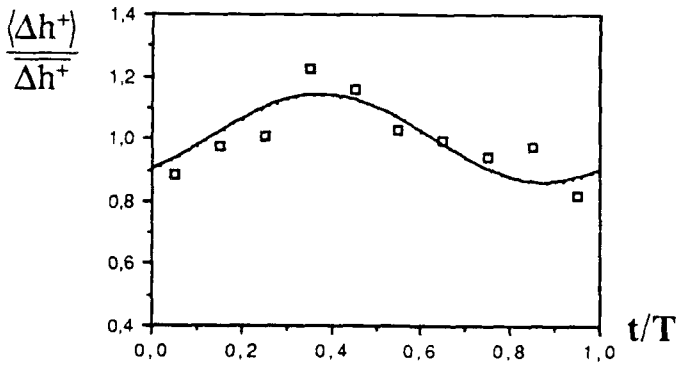

Figure 12. Phase average of ejection lift-up over distance $\Delta X^+ = 100.T = 5.3s$. a) $a_{uc}=0.20$; b) $a_{uc}=0.13$

a)

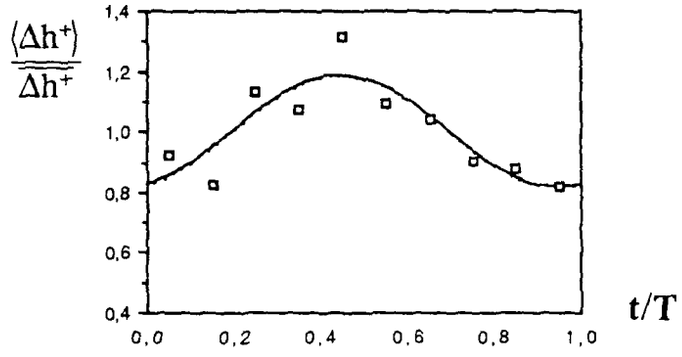

b)

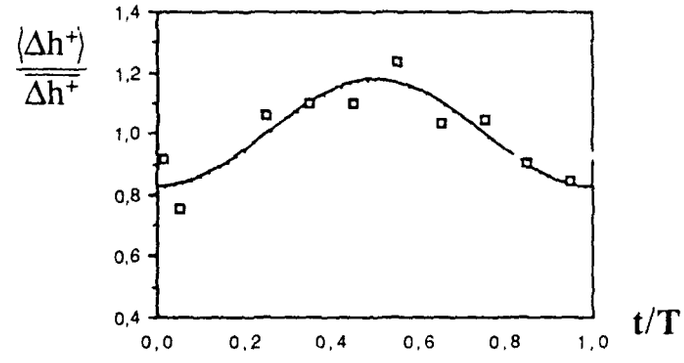

Figure 13. Phase average of ejection lift-up over distance $\Delta X^+=100$. T=7.0s. a) $a_{uc}=0.20$; b) $a_{uc}=0.13$

a)

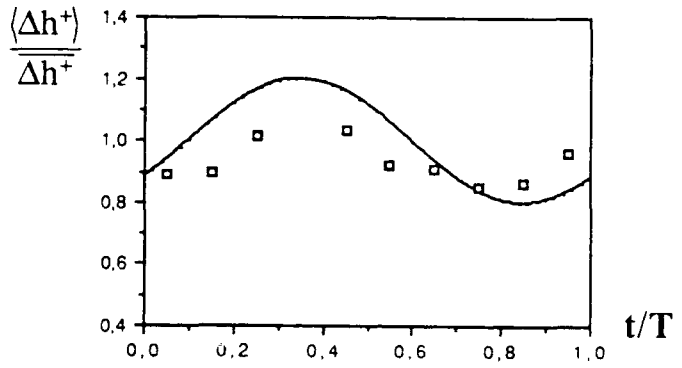

b)

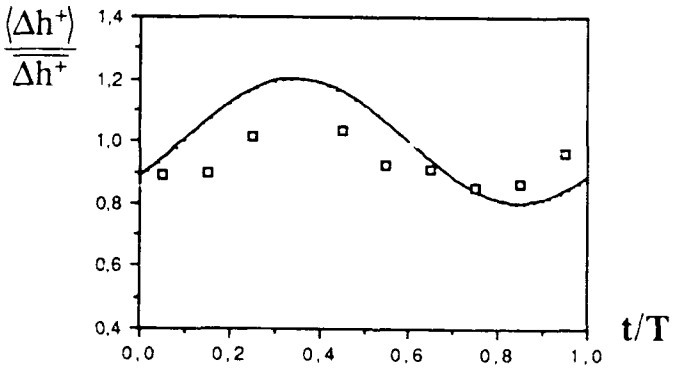

Figure 14. Phase average of ejection lift-up over distance $\Delta X^+=100$. a) a_{uc}=0.20; b) a_{uc}=0.13

a)

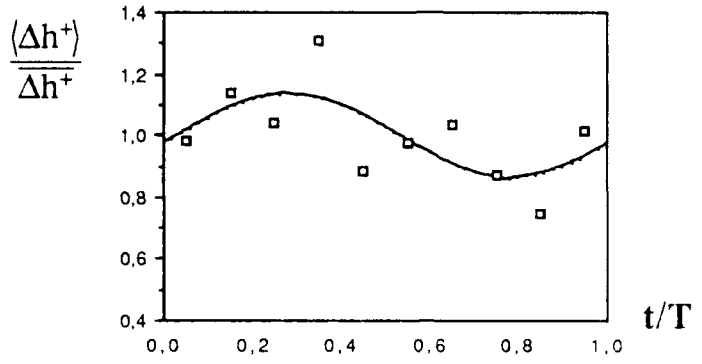

b)

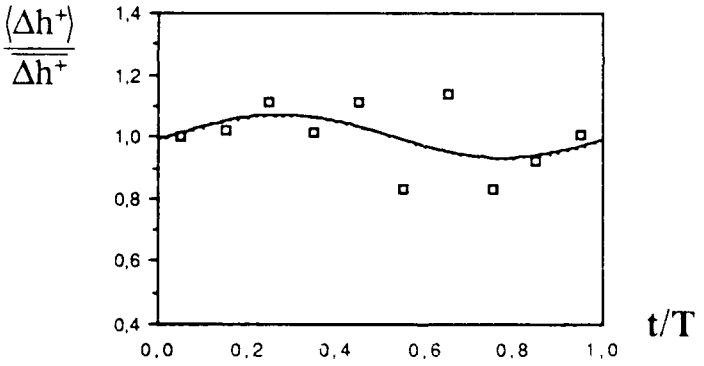

Figure 15. Phase average of ejection lift-up over distance $\Delta X^+=100$. T=34.0s. a) $a_{uc}=0.20$; b) $a_{uc}=0.13$

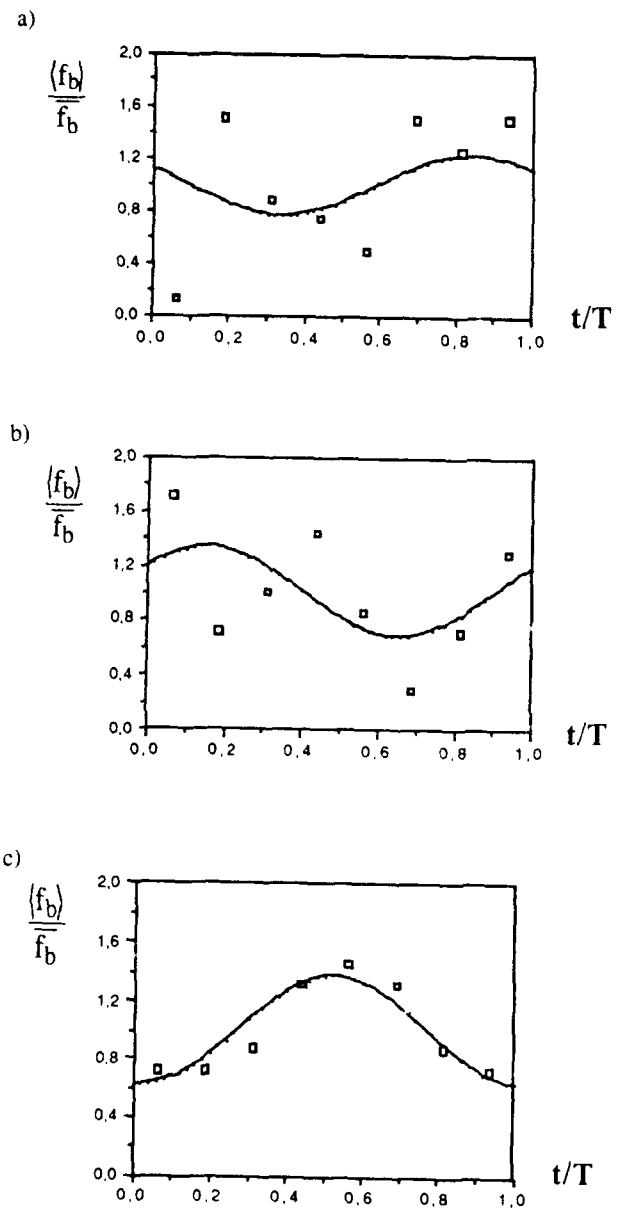

Figure 16. Phase average of burst frequency. T=2.6s, auc=0.20.
a) single ejection bursts; b) multipl ejection bursts. Time of occurence based on first ejection; c) multipl ejection bursts. Time of occurence based on last ejection.

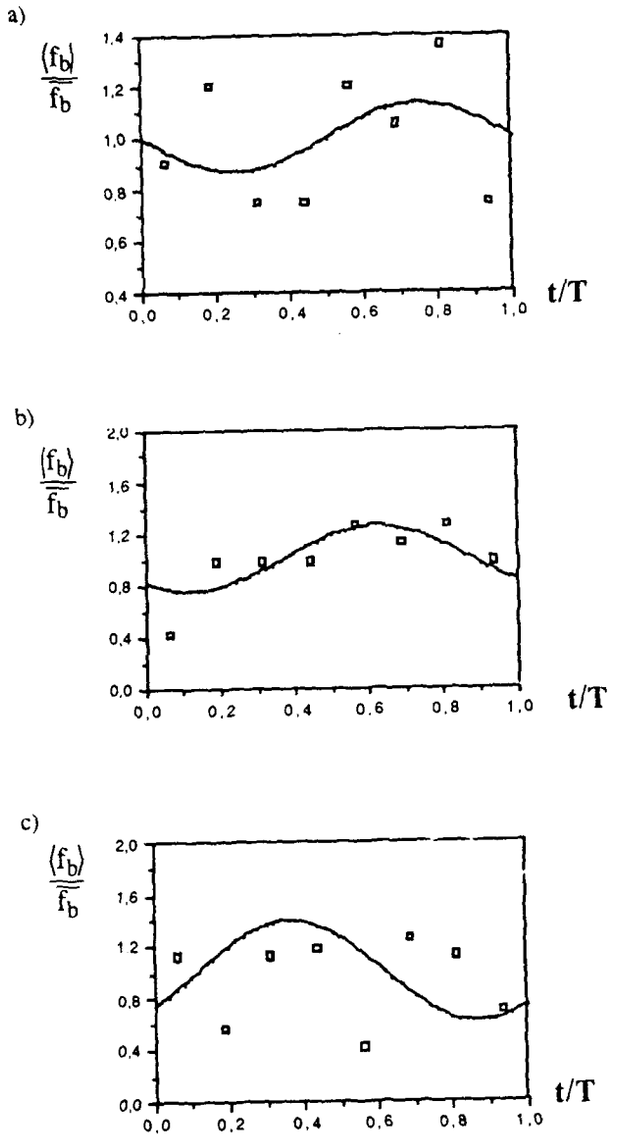

Figure 17. Phase average of burst frequency. T=5.3s, a_{uc}=0.20.
a) single ejection bursts; b) multipl ejection bursts. Time of occurence based on first ejection; c) multipl ejection bursts. Time of occurence based on last ejection.

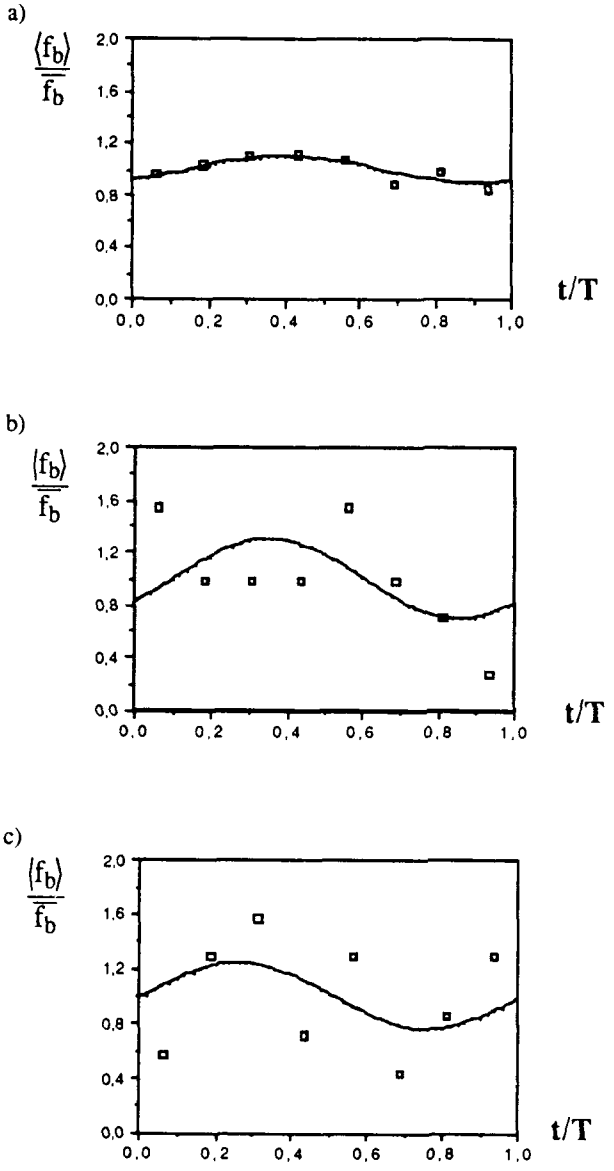

Figure 18. Phase average of burst frequency. T=7.0s, a_{uc}=0.20.
a) single ejection bursts; b) multipl ejection bursts. Time of occurence based on first ejection; c) multipl ejection bursts. Time of occurence based on last ejection.

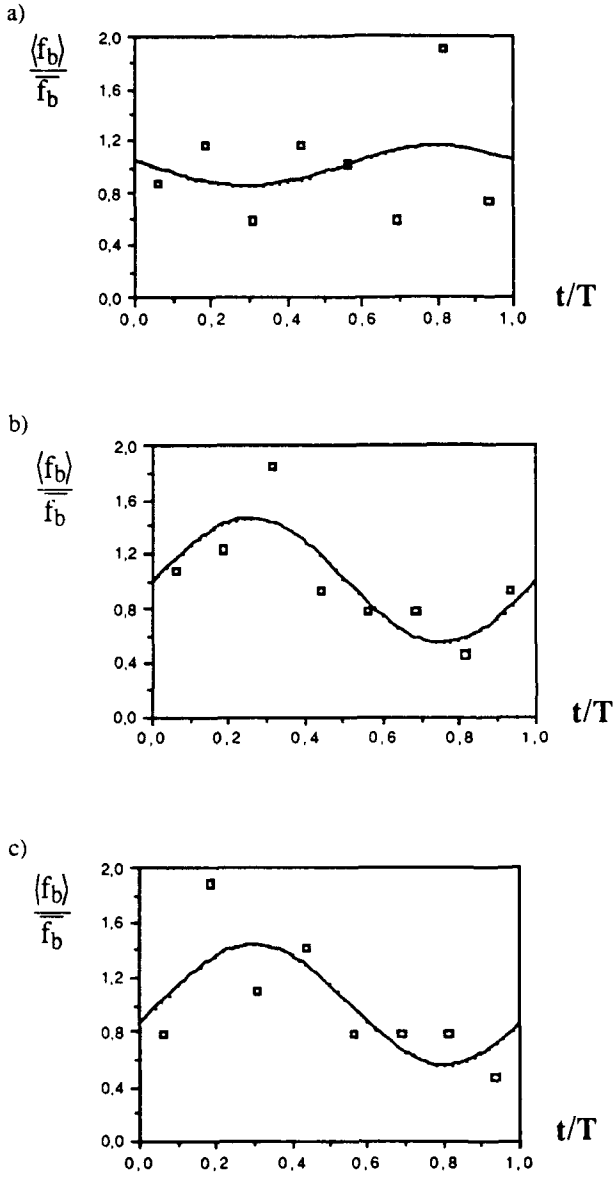

Figure 19. Phase average of burst frequency. T=16.0s, a_{uc}=0.20.
a) single ejection bursts; b) multipl ejection bursts. Time of occurence based on first ejection;c) multipl ejection bursts. Time of occurence based on last ejection.

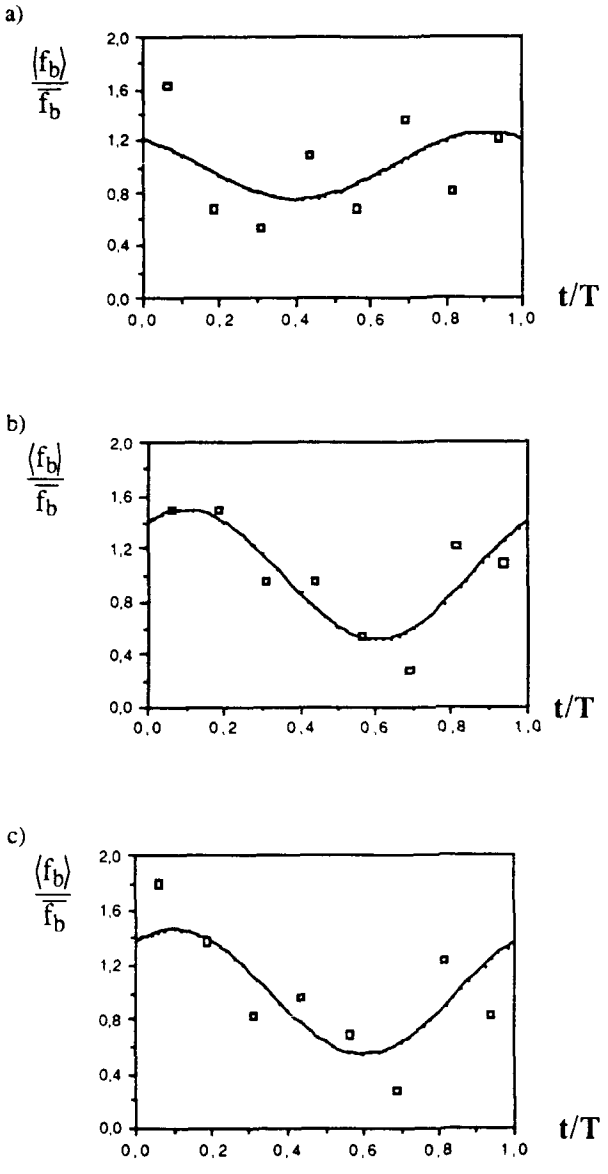

Figure 20. Phase average of burst frequency. T=34.0s, a_{uc}=0.20.
a) single ejection bursts; b) multipl ejection bursts. Time of occurence based on first ejection;c) multipl ejection bursts. Time of occurence based on last ejection.

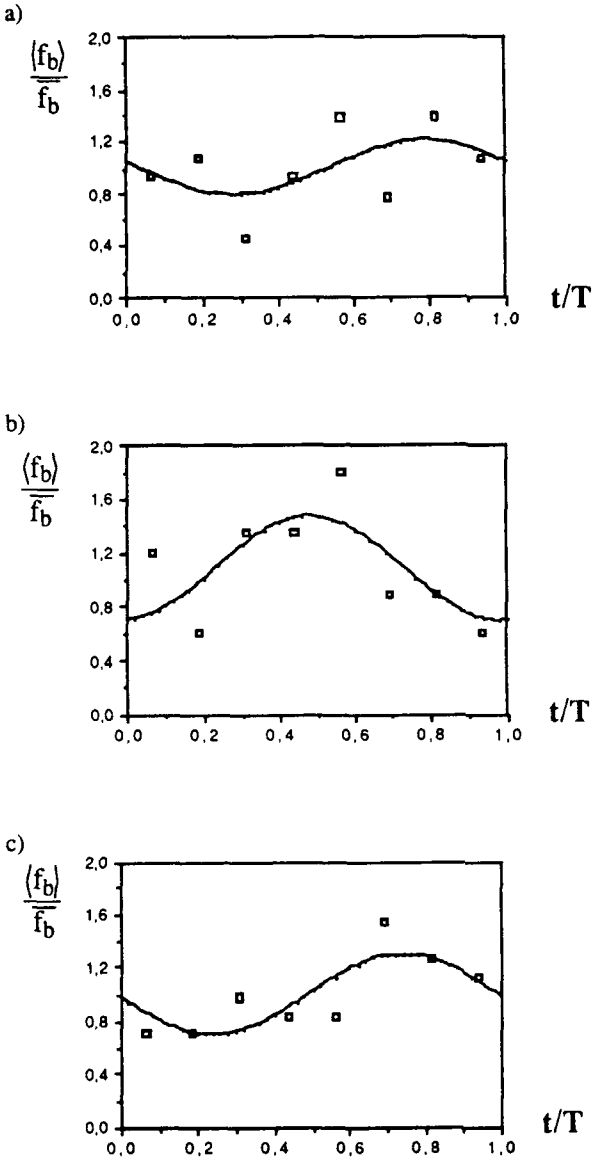

Figure 21. Phase average of burst frequency. T=2.6s, a_{uc}=0.13.
a) single ejection bursts; b) multipl ejection bursts. Time of occurence based on first ejection;c) multipl ejection bursts. Time of occurence based on last ejection.

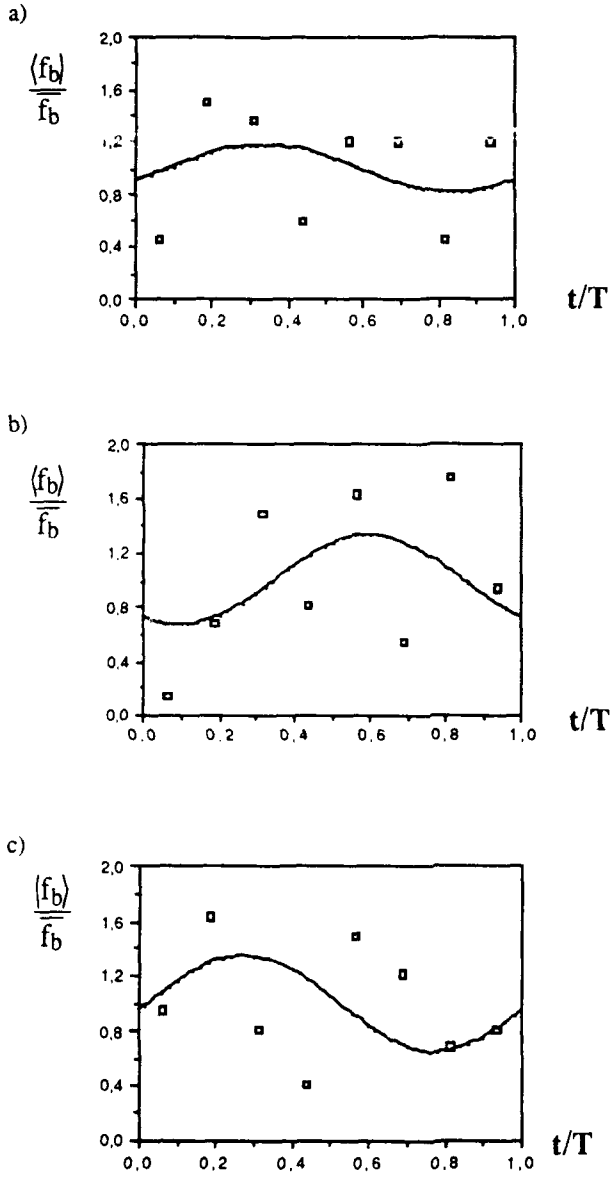

Figure 22. Phase average of burst frequency. T=5.3s, a_{uc}=0.13.
a) single ejection bursts; b) multipl ejection bursts. Time of occurence based on first ejection;c) multipl ejection bursts. Time of occurence based on last ejection.

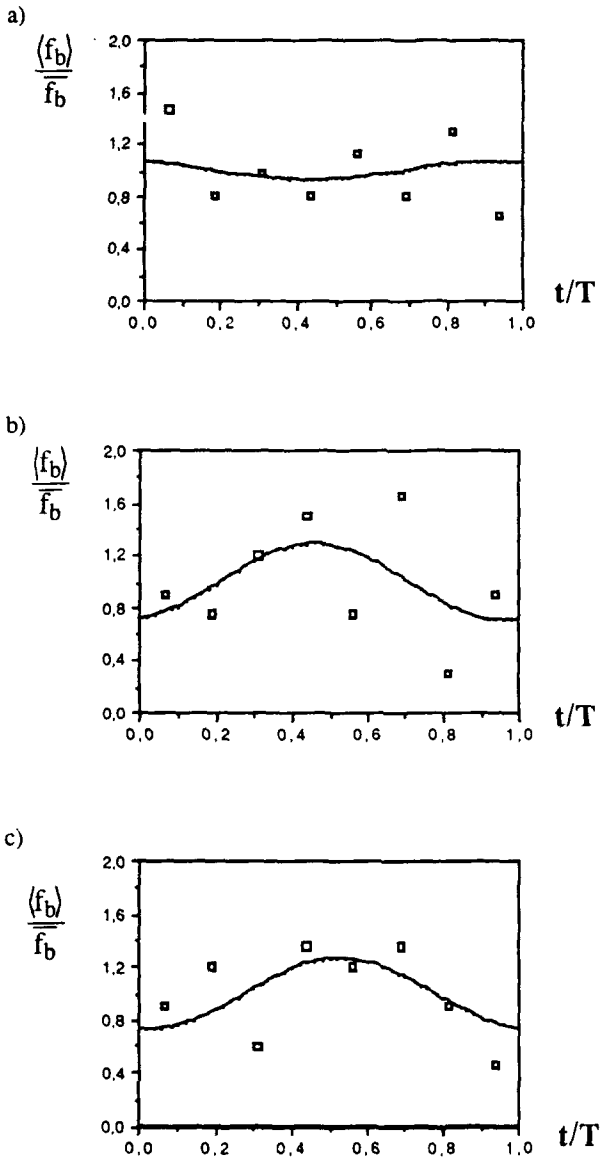

Figure 23. Phase average of burst frequency. T=7.0s, a_{uc}=0.13.
a) single ejection bursts; b) multipl ejection bursts. Time of occurence based on first ejection;c) multipl ejection bursts. Time of occurence based on last ejection.

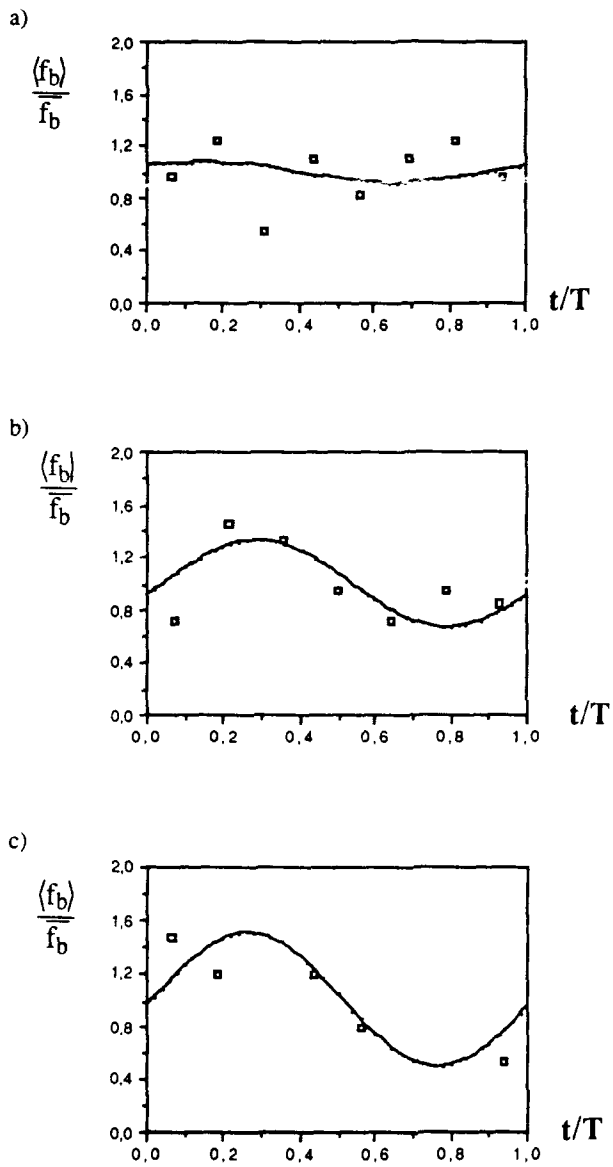

Figure 24. Phase average of burst frequency. T=16.0s, a_{uc}=0.13.
a) single ejection bursts; b) multipl ejection bursts. Time of occurence based on first ejection;c) multipl ejection bursts. Time of occurence based on last ejection.

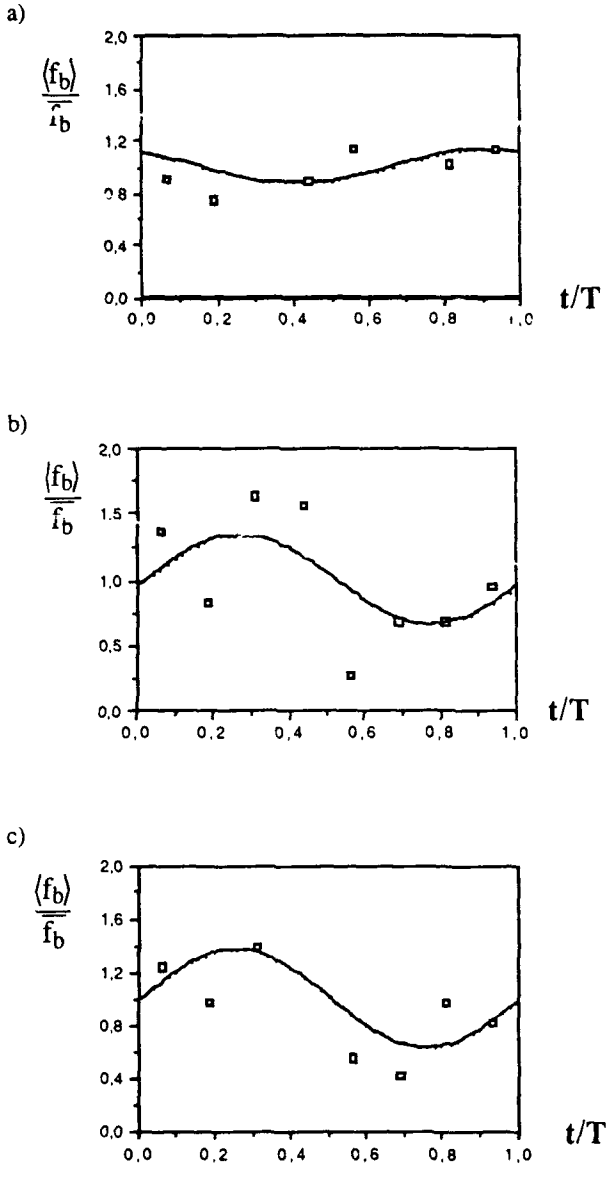

Figure 25. Phase average of burst frequency. T=34.0s, a_{uc}=0.13.
a) single ejection bursts; b) multipl ejection bursts. Time of occurence based on first ejection;c) multipl ejection bursts. Time of occurence based on last ejection.

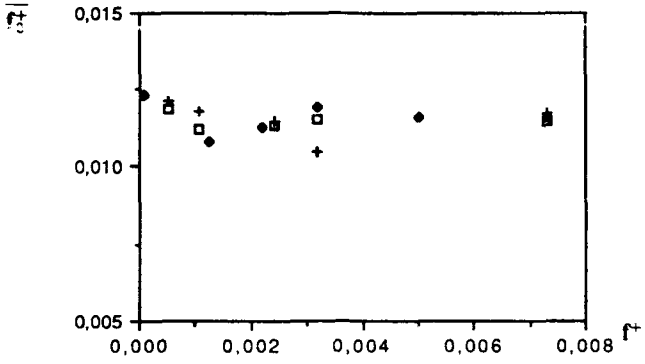

Figure 26. Time mean ejection frequency vs forcing frequency.
□ a_{uc}=0.20; + a_{uc}=0.13; ◆ Tardu&Binder

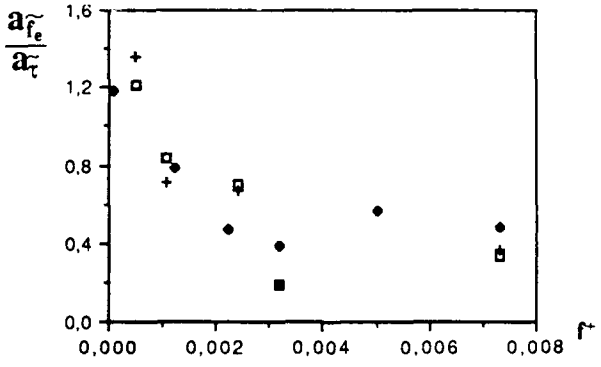

Figure 27. Relative amplitude of ejection frequency modulation vs forcing frequency.
□ a_{uc}=0.20; + a_{uc}=0.13; ◆ Tardu&Binder

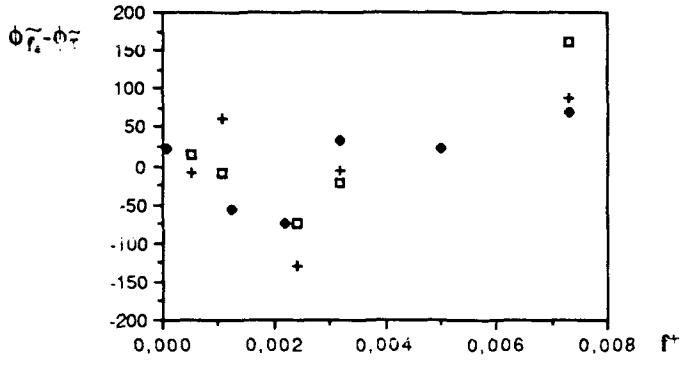

Figure 28. Phase shift of ejection frequency modulation vs forcing frequency.
▫ a_{uc}=0.20; + a_{uc}=0.13; ◆ Tardu&Binder

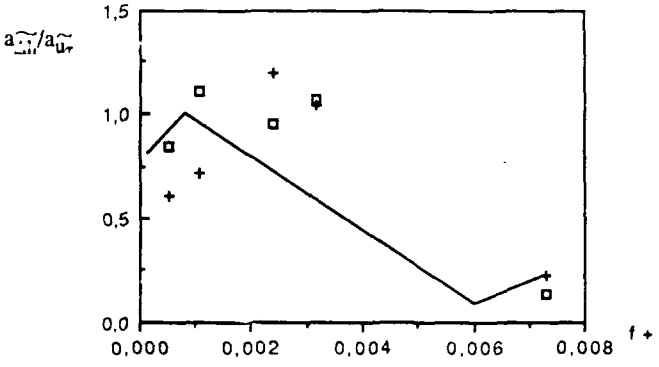

Figure 29. Relative amplitude of ejection lift-up modulation vs forcing frequency.
▫ a_{uc}=0.20; + a_{uc}=0.13; - $a_{\tau'\tau'}/a_{\tau'\tau'(qs)}$

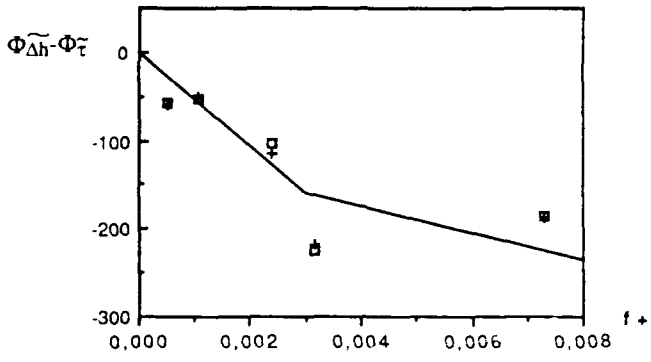

Figure 30. Phase shift of ejection lift-up modulation vs forcing frequency.
▫ a_{uc}=0.20; + a_{uc}=0.13; - $a_{\tau'\tau'}/a_{\tau'\tau'(qs)}$

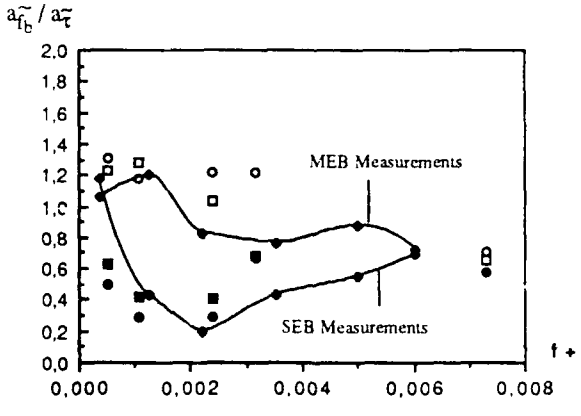

Figure 31. Relative amplitude of burst frequency modulation vs forcing frequency.
○ MEB a_{uc}=0.13; ▫ MEB a_{uc}=0.20; • SEB a_{uc}=0.13;
■ SEB a_{uc}=0.20; ◦ MEB Tardu&Binder; ◆ SEB Tardu&Binder

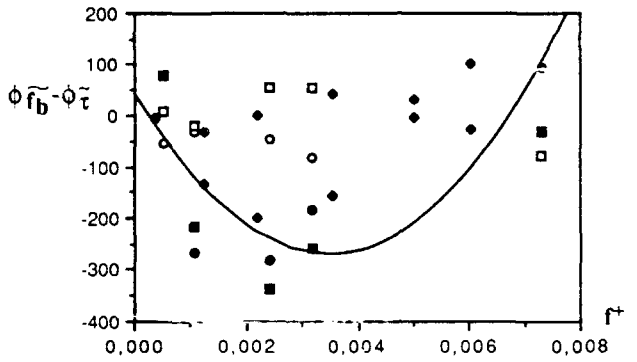

Figure 32. Phase shift of burst frequency modulation vs forcing frequency.
○ MEB a_{uc}=0.13; □ MEB a_{uc}=0.20; • SEB a_{uc}=0.13;
■ SEB a_{uc}=0.20; ◦ MEB Tardu&Binder; ◆ SEB Tardu&Binder

PART FIVE

WALL SHEAR-STRESS MEASUREMENTS IN UNSTEADY TURBULENT FLOWS IN DIVERGING CHANNELS

WALL SHEAR-STRESS MEASUREMENTS IN UNSTEADY TURBULENT FLOWS IN DIVERGING CHANNELS (*)

R.D. MAESTRI, S. TARDU, G. BINDER

1. INTRODUCTION

The aim of the investigation is to determine to which extend time mean adverse pressure gradients affect the features of unsteady turbulent wall flows. Owing to the progress made in the past decade in the knowledge on the simpler flows such as pipe or channel flows or flats plate boundary layers and despite the fact that there are still many unanswered questions especially on the unsteady behaviour of turbulence in these flows, there exists a data basis with which the pressure gradient measurements may be compared to.

In previous adverse pressure gradient experiments (1-5) only a few different cases could be explored so that, despite their interest, it is not possible to infer some general trends in unsteady flow features from them. Such a picture could only emerge from a set of data covering a significant range of the flow parameters.The purpose of the present work is to attempt to obtain such a general --although in no sense complete-- picture of this flow family. A major difficulty for systematic measurements is the complexity of these flows since, besides the Reynolds number, they depend upon four additional parameters, namely the amplitude and the frequency of the imposed oscillations (when the unsteadiness is periodic), the pressure gradient and its

---

(*) accepted for presentation at the EIGHTHS SYMPOSIUM ON TURBULENT SHEAR FLOWS, Munich, Germany, Sept. 9-11, 1991

streamwise variations. Detailed measurement being obviously out of question, it seemed that the wall shear stress would be the most revealing single quantity on which a first diagnosis could be based on.

The measurements reported in this paper pertain to nearly one hundred an fifty different flows: imposed oscillations with three amplitudes and six frequencies, two different diverging channels and four streamwise positions.

Divergence angles θ =2.4° and 6° were selected in order to have a mild and a step adverse pressure gradient, not too steep, however, so as to avoid separation in the channel which would have even further complicated the problem right from the start.

2. APPARATUS

The flow facility is the same as the one described in I.2.1 except for the test section which in the present experiments was diverging. After the first 1.6m of the channel the wall can be inclined up to 20 ° with respect to the channel axis.

The fixed and inclined walls are articuled via a short section where the thickness is reduced to about 1.5 mm which permits bending. The 1m long test section (= 20 h_0) can thus be transformed in a diffusor with a total divergence angle that can be set at any value between 0° and 40°.

3. MEASUREMENT TECHNIQUES

The measurement techniques are also the same as those described in previous parts (see specially I.3). The velocities were measured whit the LDA or with hot film probes. The former

was used for the mean velocity measurements while this latter was used for the determination of the oscillating flow characteristics on the channel axis. The wall shear-stress was measured with flush mounted hot-film gages at four different stations along the test section (see Fig. 1).

The **calibration procedure** of the wall hot film gages (WHFG) was similar to the one used in the constant area channel (I.3.1).

It is recalled that the procedure consists in determining first the relationship between the centerline velocity $\overline{U}_c$ and the wall shear stress $\overline{\tau}$, the latter being obtained from the measurement of $\partial\overline{u}/\partial y$ near the wall with the LDA. Once the $\overline{\tau}$ vs. $\overline{U}_c$ relationship is known, the WHFG calibration curve $\overline{e}$ vs. $\overline{\tau}$ can be obtained from the simpler and much faster measurement of $\overline{e}$ vs. $\overline{U}_c$ (e being the output of the hot wire anemometer). Indeed the LDA measurements of u in the immediate neighbourhood of the wall are long and tedious because the rate of validated Doppler bursts is low owing to the smaller rate of particles crossing the probe volume and to the deterioration of the signal to noise ratio from the PM caused by light reflections from the wall and by the high turbulence intensity which slows down the statistical convergence. In water, moreover, the calibration of the WHFG has to be checked frequently in order to correct for drifts from various sources - mainly from temperature changes - which may have a considerably effect on the output because of the low overheat ratio. Calibration was actually checked every hour when data was taken.

It must further be recalled that the heat transfer law from the WHFG is: $Q - Q_0 \propto \overline{\tau}^{1/3}$ i.e. $E^2 - E_0^2 \propto \overline{\tau}^{1/3}$. Because of the exponents involved and because of the low velocities near the wall the sensitivity of the WHFG is poor specially in comparison to the offset caused by parasitic non-convective heat losses.

With the overheat ratios of 10%, the voltage variations were typically of the order of 100 to 200 mV compared to the offsets of about 1 to 2 V. A change in the water temperature of 0.5°C would in this circumstances produce an error of 8% on τ. For these reasons, the temperature changes of the water were maintained as much as possible to less than 0.1°C/hr.

In the present case of diffusor flow the wall shear stress varies not only with $\overline{U}_c$ but also with X and with the divergence angle of the channel. The above procedure had, therefore to be carried out at each measuring station. This preliminary work has been very time consuming.

A few examples of the $\overline{u}$ vs. y measurements near the wall are shown on Fig.5. It is seen that there are at the least 5 points in the region where u varies linearly with y. When the velocity gradient is steep, i.e. when the viscous length ν / u_τ is small, the point closed to the wall had to be at about a distance of 0.4 mm. In order to appreciate the difficulty of such measurements it must be remembered that the channel is one meter wide.

The relations u_τ vs. $\overline{U}_c$ obtained from the previous measurements are displayed on Fig.6. Since $\overline{\tau} = \rho\, u_\tau^2$, the variations of τ from one station to another are, of course larger than those displayed on the Figure.

Some τ measurements were repeated several times to check the reproducibility. This has in all circumstances been better than $\pm$ 15%. On the average the reproducibility is about $\pm$ 7%.

Data acquisition and phase averaging was made on an OLIVETTI M 240 PC computer equipped with an ANALOG DEVICE board which performs multiplexing, amplification and A/D conversion (12 bit accuracy). Another ANALOG DEVICE board provided the bucking voltages necessary to cancel the DC-offsets of the anemometers so as to permit amplification of the signals before A/D conversion.

4. EXPERIMENTAL CONDITIONS

4.1 - The steady flow conditions.

The time-mean entrance conditions for all flows investigated were

$$\overline{U}_{c\,0} = 17{,}5 \text{ cm/s} \quad Re_{h\,0} = 8\,750$$

Since there is a section with constant area of length 1.6m (= 32 h_0) upstream of the diffusor, the entrance flow into the latter is nearly fully developed channel flow (see discussion in I.2.2) as may be seen on the velocity profiles of Fig. 2 measured at station 1 which is close to the entrance (the entrance section itself is not accessible by the LDA). The different profiles have been measured with the pulsator set on fixed positions corresponding to minimum, mean and maximum flow.

The evolution of the mean velocity on the mean velocity on the diffusor axis for the two angles used in this study and for five fixed positions of the pulsator are show on Fig. 3. If the mean flow in the diverging channel would remain similar in the downstream direction than on should have from continuity :

$$\frac{\overline{U_C}}{\overline{U_{C0}}} = \frac{1}{1+\frac{X}{h_0}\tan\frac{\theta}{2}}$$

i.e. for $\theta = 2.40°$

$$\frac{\overline{U_C}}{\overline{U_{C0}}} = \frac{1}{1+0.021\,\frac{X}{h_0}}$$

for $\theta = 6°$

$$\frac{\overline{U_C}}{\overline{U_{C0}}} = \frac{1}{1+0.0524\,\frac{X}{h_0}}$$

Therefore, if the flow would remain similar the centerline velocity should respectively be reduced by a factor 1.35 and 1.88 between stations 1 and 4. Figure 3 shows that the reduction is in both

cases about 1.2 which demonstrates that **the mean flow is far form similarity**, in other words, these are not equilibrium flows. This conclusions is, of course, not surprising since there is nowhere potential flow in the diverging duct and since the walls have not been tailored to maintain the similarity parameter $\beta = (\delta^*/\tau)\ (\partial p/\partial x)$ constant. The flow undergoes also considerable reorganisation as it moves downstream specially in the $\theta = 6°$ case.

It follows from the previous remarks that the time mean pressure gradient cannot be obtained from $\overline{U}_c\ d\overline{U}_c / dx$. It was consequently measured from the momentum balance at each station in the $\theta = 6°$ diffusor. This requires careful measurements of the velocity profiles in two neighbouring sections located upstream and downstream of each stations. The distance between the sections was $\Delta X = h_0$. This again was a time consuming job and could not be carried out for the $\theta = 2.4°$ diffusor. In the future, it is planned to try to measure $\partial p/\partial x$ directly from the static pressure of a Pitot tube and a pressure transducer with high sensitivity.

The measured pressure gradients are shown on Fig. 4. If the flow were fully potential with uniform velocity profiles then :

$$\frac{h}{\frac{1}{2}\rho U_C^2}\left(\frac{dp}{dx}\right)_{pot} = 2\frac{dh}{dx} = 2\tan\frac{\theta}{2} = 0.104$$

By taking into account the ratio δ^*/h (see table below) it is seen that the actual pressure gradient is about one third of the maximum potential flow gradient.

From these measurements the displacement and momentum thickness, the shape factor and the Clauser parameter were also determined. The values are give in table 1.

Station	h_{mm}	δ^*_{mm}	θ	$H=\delta^*/\theta$	β
S1	59	9.04	6.27	1.44	3.4
S2	74	13.1	8.91	1.47	4.9
S3	83	19.7	11.3	1.75	6.4
S4	99	23.6	15.0	1.6	12.7

The evolution of H and β in downstream direction illustrate the changes in the mean flow characteristics mentioned earlier. Since β is the ratio of the pressure forces to the wall shear stress and since β increases in the downstream direction, it seen that the flow encounters increasingly steeper pressure gradients as it proceeds downstream . It is known that when $\beta \sim 10$ the flow approaches separation.

Finally it was checked that the mean flow remains approximately symmetrical by measuring the profile across the whole channel at station 4 where unsymmetrical behaviour is most likely. The symmetry is satisfied to within about 10%. The absence of reverse flow in the diverging channel was checked by injecting dye at the wall.

4.2 - Oscillating flow conditions.

Oscillations of three different amplitudes and six frequencies were imposed on the mean flow. The three nominal amplitudes at the entrance were : 10, 20 and 40%.

The six forcing periods were : 2.7; 4; 8; 16; 32; 60s.

The corresponding values of the l_s^+ parameter at the entrance were :

$(l_s^+)_0 = 7; 9; 13; 18; 27$ and 36.

The mean position of the pulsator was kept the same throughout these tests. This means that mean flow rate and hence the mean entrance conditions to the diffusor were always the same **in steady flow**. The eccentricity of the driving mechanism of the pulsator was adjusted so as to produce either ±10, ±20 or ±40% velocity variations with respect to the mean in the **steady regime**, i.e. with the pulsator maintained in the fixed position giving the maximum or the minimum velocity. The numbers $(a_{uc})_0$ = 10, 20 or 40% must therefore, be understood as "nominal amplitudes" at the diffusor entrance. The actual amplitudes at the entrance dependent somewhat upon the forcing frequency and on the geometry. This is equivalent to saying that the impedance of the system depends somewhat upon the frequency and geometry. (It is recalled that the flow is driven by a constant head). In short, for a given nominal amplitude **all** the geometrical parameters were kept constant and **only** the frequency of oscillation was changed. This does not insure neither an invariable time-mean flow nor an invariable oscillating flow when the frequency is changed. The changes in the mean flow rate were, however, quite small since the headloss through the diffusor is small compared to the total headloss. This way of proceeding is, of course, not ideal. It would have been preferable to make runs in keeping the actual amplitude at the entrance constant. But this would have required lengthy adjustments by trial and error. For this study it seemed more important to cover a wide frequency range than to maintain the amplitude strictly constant.

The amplitude and phase of $\tilde{u}_C$ (as of any other quantity) are obtained from Fourier analysis of the phase averaged velocity $\langle u_C \rangle$ (for details see I.1 and 3). "Amplitude " and "phase" will hereafter be used to designate the parameters of the fundamental mode.

The measured centreline amplitudes vs. the forcing period are given on Figures 7 and 8 for the 2.4° and 6° channels respectively. It is seen that the actual amplitudes are, but for a few exceptions, smaller than the nominal values which are roughly reduced by the value 0.75 . The 10, 20 and 40% amplitudes cases correspond than qualitatively to small, medium and large amplitudes. Figures 7 and 8 reveal considerable variations of the amplitudes along the channel especially in the 6° diffusor when the nominal amplitude is 20 or 40%. Because of the continuity requirement this is only possible if there are considerable changes in the amplitude (and phase) profiles from one station to the other. This is a strong incentive to complete the present wall measurements with complete amplitude (and phase) profiles : a difficult and arduous but almost certainly rewarding task planed for the future.

The phase shifts of $\tilde{u}_C$ with respect to the phase at station 1 vs. T are shown on Figures 9 and 10. It is seen that the flow nearly oscillates in phase throughout the 2.4° diffusor as in a channel with parallel walls. But large shifts are observed in the 6° diffusor and surprisingly enough the largest ones occurs with the 10 and 20% amplitudes. These phase-shifts reveal again important changes in the shapes of the <u> profiles.

It may be added that the measured phases are repeatable with good accuracy (relative error less 5%), much better than for the amplitudes because less dependent in errors due to temperature drifts or calibration defects.

5. RESULTS

The results at different stations are plotted versus the local value of l_s^+ (or versus ω^+)

particular for τ. It is called that : $l_s^+ = \frac{u_\tau}{\nu}\sqrt{\frac{\nu}{2\omega}}$

and that l_s^+ varies with u_τ. Since u_τ varies with X-position in the diverging channels the local values have been used for plotting the data (and not $(l_s^+)_0$) with the aim of trying to bring out similarities or differences with parallel wall channel flow. Owing to these variations of l_s^+ with X-position the data points for a given frequency do not fall on the same vertical line.

The results of the wall shear-stress measurements (Fig. 11 to 26) are systematically presented with the three amplitude cases for a given geometry on the same page in order to facilitate comparison between the different forcing conditions.

In the subsequent discussion we shall designate for the sake of brevity by "channel" without qualifier the channel with parallel walls.

5.1 - Time-mean properties

5.1.1 - Time mean wall shear stress (Fig. 11-12)

The ratio $\overline{\tau}$ in unsteady flow with respect to the steady steady value (at the same station, of course) is plotted. The most striking feature of these two Figures is the large increase of the ratio in both geometries in the high amplitude and high frequency forcing regime. In the 6° channel the ratio reaches the value two. Worth nothing on Fig. 11 c and 12 c is that the highest ratios are reached at the most downstream station where non-dimensional pressure gradient is the largest. These results are high lighted by the fact that this ratio remains equal to one in the constant area channel (except for an amplitude correction factor equal to $(1 + 21/64\ a^2_{\tilde{uc}})$ which would be 1.05 for $a_{\tilde{uc}} = 0.4$; see I.4.1.3). Clearly there is a remarkable difference between these

forced flows in diverging channels and those in the constant area channel.

One may also observe some values of the shear stress ratio which are appreciably smaller than one in the 6° channel at station 3 and 4 with the medium amplitude and at station 1 with the strong amplitude forcing.

There is, of course, some scatter in the data (incidentally, remarkably small in the θ = 2.4°, 20% amplitude flows) but it should be remembered that these are not easy measurements. But even the pessimistic estimate of 15% error quoted earlier can certainly not account for the measured increase in τ in the flows forced at 40% in the diverging channels.

5.1.2 - Time-mean RMS-value of the turbulent wall shear stress fluctuations (Fig. 13-14)

It is first recalled that the ratio $\sqrt{\overline{\tau'\tau'}}/\bar{\tau}$ in steady turbulent wall flows is about 0.36 . After some controversy and measurements which span a range from 0.06 to more than 0.4! This value based on recent data and direct numerical simulations is now considered the most likely. It was found (see I.4.1.4) that this value is not appreciably modified by forced oscillations in channel flow even when their amplitude near the wall is so large as to produce periodic flow reversal.

With the reference level 0.36 drawn on the graphs of Figures 13 and 14, it is immediately apparent that turbulence level of τ in the adverse pressure gradients flows is almost systematically larger than in steady or unsteady channel flows. Experimental uncertainty can account for the values falling below this level but not for values larger than 0.5 which are quite frequent on these graphs. Turbulence levels of 0.6 which represent more than a 50% increase

with respect to the standard reference value are actually not uncommon in these adverse pressure gradient unsteady flows.

These are not only large increases but very high absolute turbulent intensities. A relative RMS-turbulent intensity of 0.60 implies the existence of frequent instantaneous values larger than one, i.e. of instantaneous reverse flow. Since the hot film rectifies the velocity signal, the present measurements are on the conservative side.

Finally, it is worth noting the relatively small scatter in the 40% amplitudes cases, actually remarkably small in the small angle diffusor.

5.2 - The oscillating flow properties

5.2.1 - The oscillating of the wall shear-stress (Fig. 15 to 18)

It was shown that the amplitude of viscous Stokes solution ($A_{\tilde{\tau}\ Stokes} = \sqrt{2}\ A_{\tilde{u}c}/l_s$ see I.4.2.3) was a useful reference quantity for the amplitude the wall shear stress oscillation in the channel flow since it does involve the centreline amplitude (in all rigour this should be the amplitude at infinity) and a frequency dependence. The same scaling is adopted here. The mean curve from the channel experiments (Fig. 12 a from I, with $a_{uc} = 0$) will serve as reference for discussion . It is the solid line drawn on Figures 15 and 16.

It is seen that in the 2.4°diffusor (Fig. 15) the variations of the amplitude ratio with l_s^+ is roughly the same as in the constant area channel : at high frequencies the values are of order one and at lower frequencies the values increase with l_s^+ due to progressively larger effect of the turbulence on the oscillating wall shear-stress. The amplitude ratio in this geometry is, however, systematically larger than in the channel. There is no explanation for the fairly large scatter of

data points at the present time.

The amplitude behaviour in 6° diffusor displayed on Figure 16 contrasts sharply with that of the previous Figure. First of all, the amplitude ratios are almost systematically smaller than one and values as low as 0.2 have been measured. Values of order 0.8 may be explained (see I.4.2.3) by destructive interference of the shear wave with the strongly damped wave reflected by the buffer-layer where the effective viscosity suddenly increases. In order to account for values of order 0.2 , the same reasoning would require that shear wave suffers nearly no damping which is rather unlikely. Quite a different mechanism should, therefore, be operating.

Secondly, the increase of the ratio with l_s^+ when $l_s^+ > 15$ does no longer seem to occur. This statement is only conditional because the l_s^+ values in the wide angle diffusor are smaller than in the small angle diffusor owning to the smaller values of u_τ.

In any case it is clear that, under the same forcing conditions, the wall shear stress oscillations are considerably smaller in strong mean adverse pressure gradient than in a mild or favourable pressure gradient.

The results concerning the phase shift of $\tilde{\tau}$ with respect to the phase of the centerline velocity are shown on Figures 17 and 18. The full line on these graphs is again a schematic representation of the channel data. It is recalled that in this case the phase shift data is remarkably well correlated by the l_s^+ parameter. As for the amplitude, it is seen that measurements from the 2.4 ° diffusor follow the same trend as those from the channel with notably larger values, however, at high frequencies and larger values at low frequencies when $l_s^+ \geq 20$.

The first impression from the phase-shift results of the 6 ° diffusor (Fig. 18) is large

scatter among the data points. There are large differences from one station to the other and in some instances also from one frequency to the next at the same station. One part of this scatter is certainly due to experimental uncertainties which are lowered by the added effects of tow factors. Firstly the relatively small value of the maximum phase shift of $\tilde{\tau}$ which is only 1/8 or 1/6 of the cycle and, secondly, the small amplitudes of τ in this geometry which slows down the statistical convergence of $<\tau>$ the much the more so that the turbulent intensity is high as observed in 5.1.2 . Despite these irregularities it is possible to guess a general trend when following the points corresponding to the same measuring station : at small l_s^+ values the phase shift is only about 20 to 30 °, it increases with l_s^+, reaches a maximum value between 45 and 60 ° when l_s^+ = 15 to 25 and finally decreases to zero as may be expected.

From the amplitude as well as the phase shift data it is also quite clear that a strong adverse pressure gradient has a large effect on the oscillating wall shear stress.

5.2.2 - Modulation of the turbulent wall shear stress fluctuation intensity

(Fig. 19 to 22)

The modulation $\widetilde{\tau'\tau'}$ of the phase averaged wall shear stress intensity is defined by : $\widetilde{\tau'\tau'} = <\tau'\tau'> - \overline{\tau'\tau'}$ where $<\tau'\tau'> = <\tau^2> - (<\tau>)^2$. $\widetilde{\tau'\tau'}$ is also the response of the turbulence to the forcing. Since the turbulence production is driven the mean shear via the production and since the shear scales with wall shear stress, $\widetilde{\tau'\tau'}$ may be considered as the result of the $\tilde{\tau}$-oscillation. The ratio of relative amplitudes $a_{\widetilde{\tau'\tau'}} / a_{\tilde{\tau}}$ may be interpreted us the response function of the turbulent wall shear stress fluctuations to the periodic forcing. If the system were

linear, this ratio would be independent of forcing amplitude. It should be stresses than this ratio involves four independent quantities. this fact must be kept in mind in judging the importance of the experimental scatter.

The results are presented in tow different ways versus l_s^+ and versus ω^+. It is recalled that $\omega^+ = 2 / l_s^{+2}$. The first representation (Fig. 19 - 20) facilitates the discussion with the other quantities and the second representation (Fig. 21 - 22) is more logical for the discussion of the frequency response of the turbulence. Again, the full line is a schematic indication of the channel flow results (I; Fig. 17a).

Tow features are immediately apparent on these figures. Firstly, the turbulence response in the diverging channels follows the same trend as in channel with parallel walls, in particular the amplitude ratio $a_{\tilde{\tau}\tilde{\tau}'} / a_{\tilde{\tau}}$ starts decreasing when $\omega^+ \sim 0.005$ and stays at a roughly constant low level. It is also confirmed in a variety of situations that the turbulence modulation decreases with increasing frequency once $\omega^+ > \sim 0.005$. Secondly, the ratio $a_{\tilde{\tau}\tilde{\tau}'} / a_{\tilde{\tau}}$ is systematically higher in the diverging ducts than in the channel with parallel walls. the increase of the turbulence response is particularly large in the 6 °diffusor, nearly a factor two in the case of 10% forcing. It is recalled that in the quasi-steady linear approximation limit (I.4.2.6): $a_{\tilde{\tau}\tilde{\tau}'} / a_{\tilde{\tau}} \approx 2$. It is that values of this order are reached in the 6 ° diffusor. From the quasi-steady linear approximation limit, saturation effects have to be expected at large forcing amplitudes, so that $a_{\tilde{\tau}\tilde{\tau}'} / a_{\tilde{\tau}}$ cannot remain independent of amplitude under these conditions.

It is not sure that the ratio $a_{\tilde{\tau}\tilde{\tau}'} / a_{\tilde{\tau}}$ is the best way to account for the effect of the channel divergence on the turbulence modulation since its variations incorporate those of $a_{\tilde{\tau}}$. It has, in particular, been observed in the previous section that the shear stress oscillation is

considerably reduced in the strong adverse pressure gradient. The increase in $a_{\tau'\tau'} / a_{\tau}$ in the diffusors as compared to the values in the channel are, therefore, at least partly, if not essentially, due to the changes in the shear stress oscillations. The amplitude of turbulence modulation can be non-dimensionalized in various ways but it is not sure that the present which is the best or the most physical sealing.

In order to give another view of the modulation of the turbulent shear stress fluctuations, the data have been reploted on Figures 23 to 26 by normalising $a_{\tau'\tau'}$ with the local centerline velocity amplitude a_{uc}. In order to have a feeling for the values of the ratio $a_{\tau'\tau'} / a_{uc}$, it should be remembered that in the quasi-steady small amplitude limit in channel flow (see I.4.2.5) the value should be 7/2 (the amplitude correction factor $(1 + 21/64\ a^2_{uc})$ being neglected). Values around 4 are, therefore, "normal" in case of small amplitude forcing. The large scatter among the data points of Figures 23 - 26 makes difficult to draw any definite conclusions.

The decrease of $a_{\tau'\tau'} / a_{uc}$ with increasing frequency is clear for the 2.4 ° diffusor flows but not for the 6 ° diffusor flows because of the scatter especially at the high forcing frequencies. One does, however, observe many values of this ratio around 4 or above - even as large as 6 - which reveal quite strong modulations of the turbulence. Such values in the case of 40% amplitude forcing may be absent. Indeed $<\tau'\tau'>$ is strictly positive so that $a_{\tau'\tau'} \leq 1$. How is then $a_{\tau'\tau'} / a_{uc} \geq 4$ possible when $(a_{uc})_0 = 0.4$? The answer lies in the fact that the local a_{uc} can be appreciably smaller than $(a_{uc})_0$ as shown in section 4. Some particularly large values of $a_{\tau'\tau'} / a_{uc}$ may, of course, be due to underevaluations of the centerline amplitude.

6. CONCLUSION

From the measurements of the wall shear stress in unsteady turbulent flows in diverging channels, it may be concluded that imposed oscillations :

- modify the mean flow to the wall to considerable extend if their amplitude is large and their frequency is high ;
- increase the time mean turbulent intensity by as much as 50% ;
- produce smaller shear stress oscillations than in channels with parallel walls when the adverse pressure gradient is steep and modifies their phase shift ;
- produce larger modulations of the turbulent shear stress fluctuations with respect to the centerline velocity oscillations.

These effects are, in general, more important when the adverse pressure gradient is steeper. Since an increase in the wall shear stress and in the turbulent intensity delay separation, these conclusions are in agreement with the observations of airfoil stall retardation by imposed mustcadiness.

The results presented here should, of course, be confirmed by other tests and especially by more detailed explorations of the entire flow field.

7 . REFERENCES

[1] JAYARAMAN , R., PAPIKH , P., REYNOLDS , W.C., 1982 "An experimental study of the dynamics of unsteady turbulent boundary layers", technical report number TF-18, Thermosciences Div., Dept. Mech. Eng. Stanford University, Stanford, California.

[2] SIMPSON , R.L., SHIVAPRASAD , B.G., CHEN , Y.T., 1983 "The structure of separating turbulent boundary layer - Effects of periodic free-stream understeadyness", J. Fluid Mech. 127, 219-62 and "Frequency effects of periodic unsteady free-stream flows", J. Fluid Mech. 131, 319-40.

[3] COUSTEIX , J., HOUDEVILLE , R., JAVELLE , J., 1977 "Structure and development of a turbulent boundary layer in an oscillatory external flow", Proceedings of Symposium on Turbulent Shear Flows, Pennsylvania State University.

[4] BRERETON , G.J., REYNOLDS , W.C., 1987 "Experimental study of fluid mechanics of boundary layers", technical report number TF-29, Thermosciences Div., Dept. Mech. Eng. Stanford University, Stanford, California.

[5] MENENDEZ , A.N., RAMPRIAN , B.R., 1983 "Study of unsteady turbulent boundary layers", IIHR report n°270, University of Iowa, Iowa City.

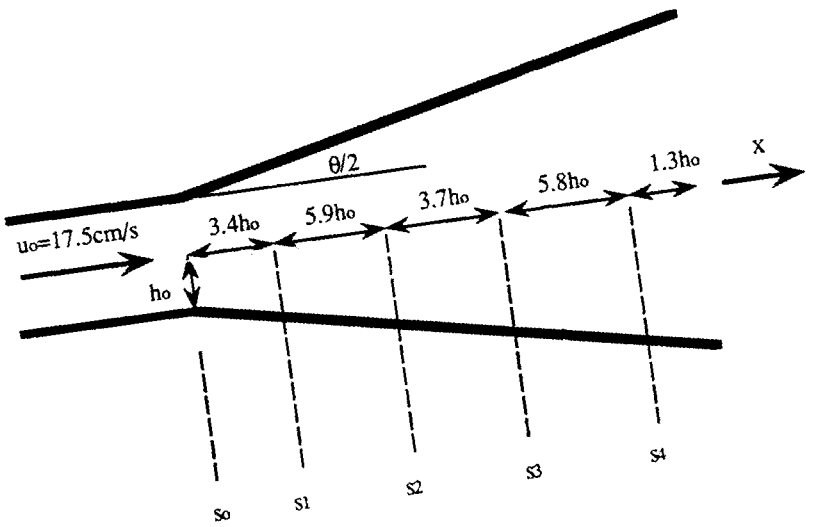

Figure 1. Definition sketch

a)

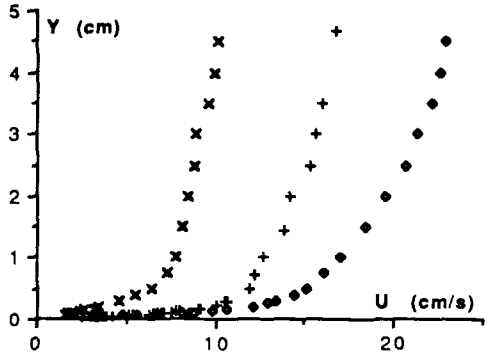

b)

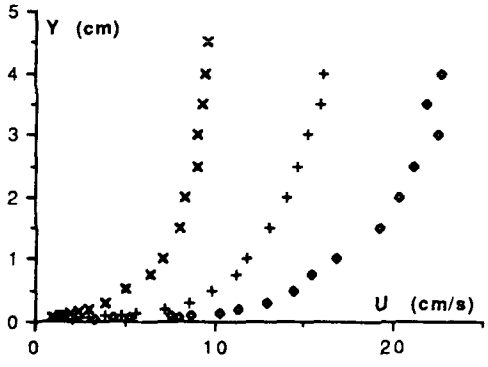

Figure 2. Velocity profils in steady flow at station 1.Pulator set for 40% centerline amplitude at inlet.
◆, + , ×: maximum,mean,minimum velocity.
a) θ=2.4°; b) θ=6.0°

a)

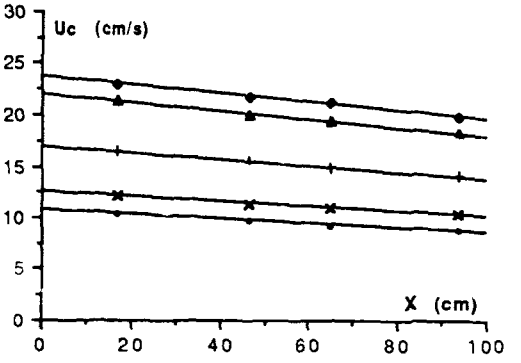

b)

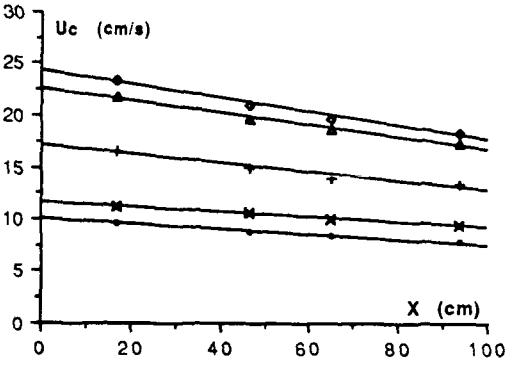

Figure 3. Streamwise variation of velocity on channel axis in steady flow. Pulsator set for 40% centerline amplitude at inlet. Pulsator position spaced by $\pi/4$ between maximum and minimum opening.
a) $\theta=2.4°$; b) $\theta=6.0°$

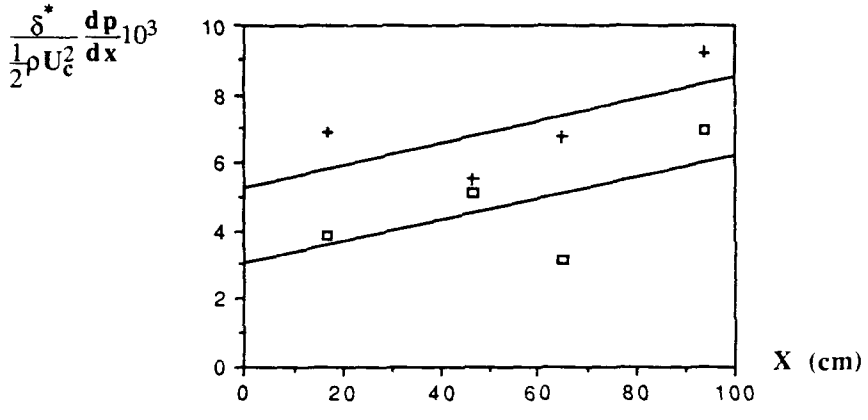

Figure 4. Pressure gradient $(\delta^*/ 0.5\rho U_e^2)(dp/ dx)$.

+ : dp/ dx from momentum balance; ɔ : $dp/ dx=-U_e(dU_e/ dx)$

a)

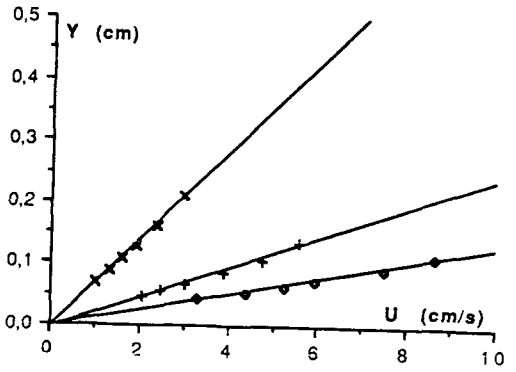

b)

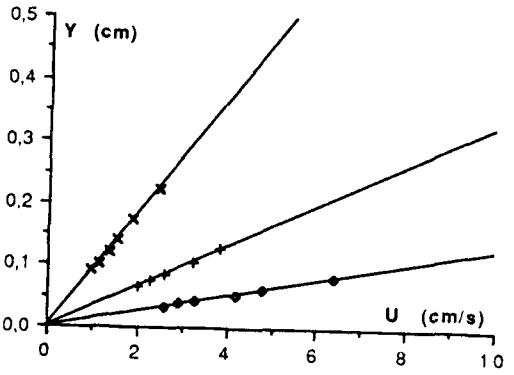

For caption see next page

c)

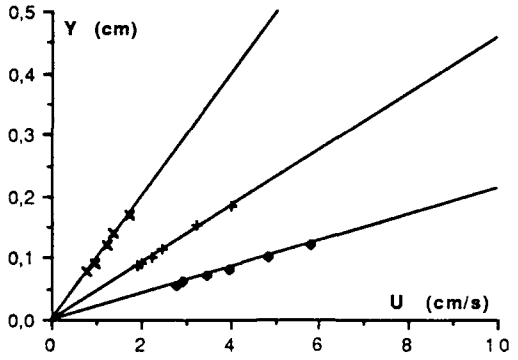

d)

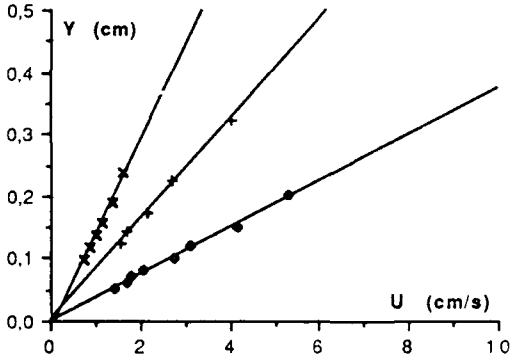

Figure 5. Velocity profils near the wall in steady flow. Pulsator set for 40% centerline amplitude at inlet. $\theta=6.0°$. ∘, +, × : maximum,mean, minimum velocity.
a) station 1; b) station 2; c) station 3; d) station 4

a)

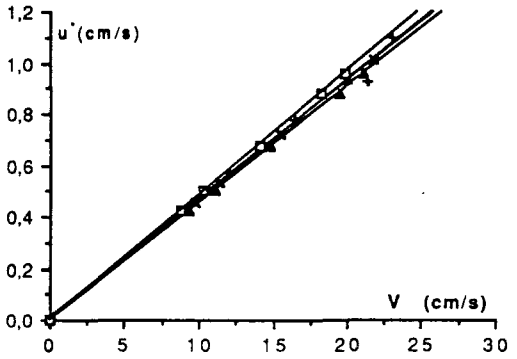

b)

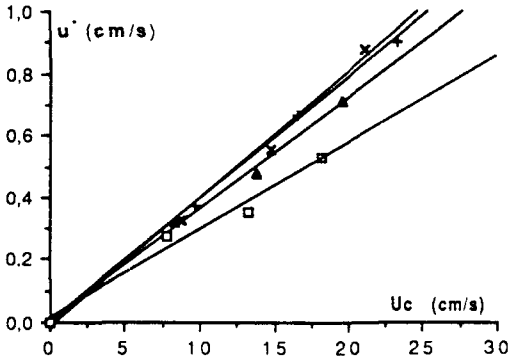

Figure 6 Shear velocity vs centerline velocity.
+ : station 1; × : station 2; △ : station 3; □ : station 4.
a) θ=2.4°; b) θ=6.0°

a)

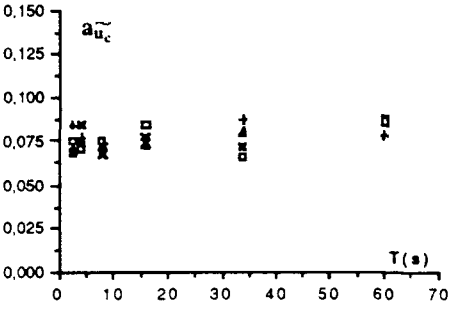

b)

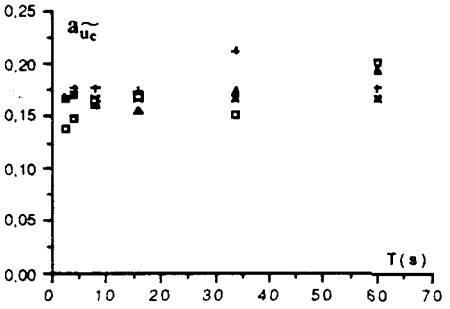

c)

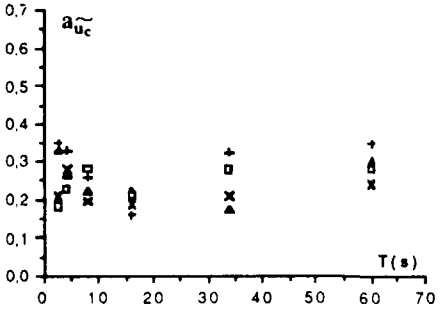

Figure 7. Relative amplitude of centerline velocity vs forcing period.θ=2.4°.
+ : station 1; × : station 2; ▲ : station 3; □ : station 4.
a) $(a_{uc})_o$=0.10; b) 0.20; c) 0.40

a)

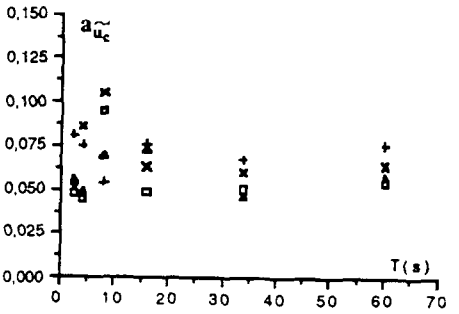

b)

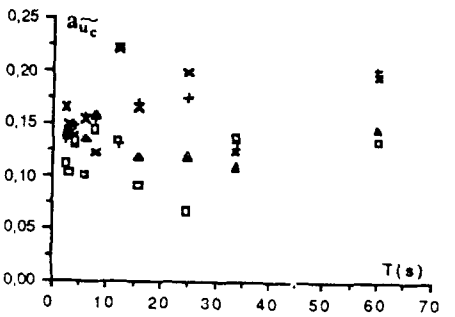

c)

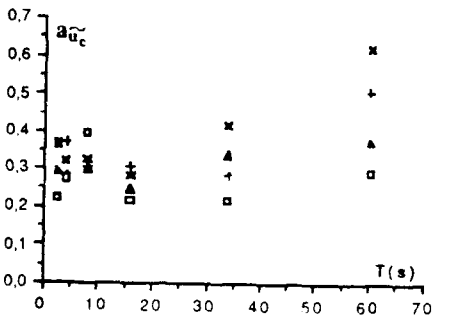

Figure 8. Relative amplitude of centerline velocity vs forcing period.θ=6.0°. + : station 1; × : station 2; ▲ : station 3; □ : station 4.
a) $(a_{uc})_0$=0.10; b) 0.20; c) 0.40

a)

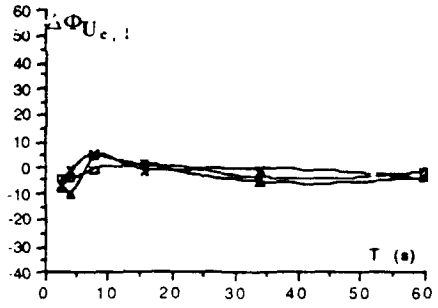

b)

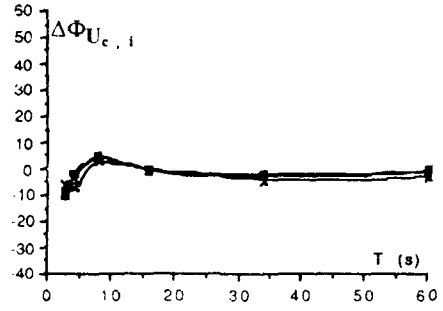

c)

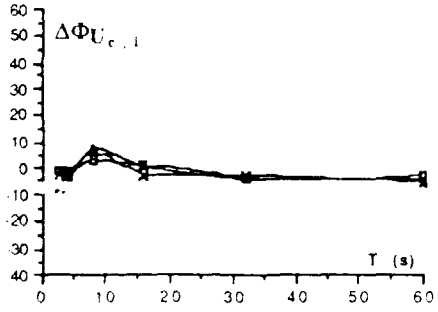

Fig 9. Phase shift of centerline velocity oscillation with respect to station 1 vs focing period.

$\Delta\Phi_{Uc,1}=\Phi_{Uc,s1}-\Phi_{Uc,s1}$; θ=2.4°.

a) $(a_{uc})_0$=0.10; b) 0.20; c) 0.40

a)

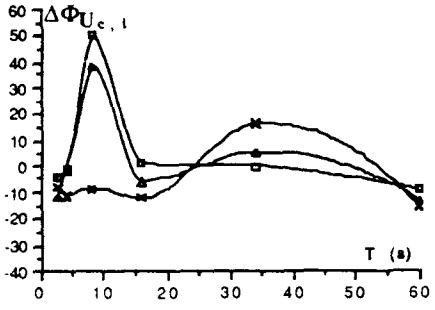

b)

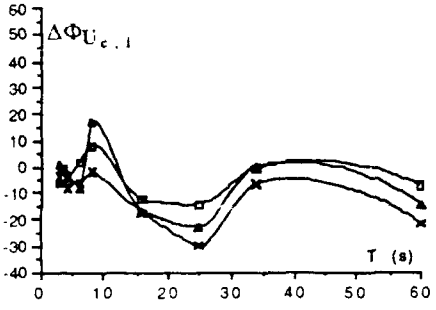

c)

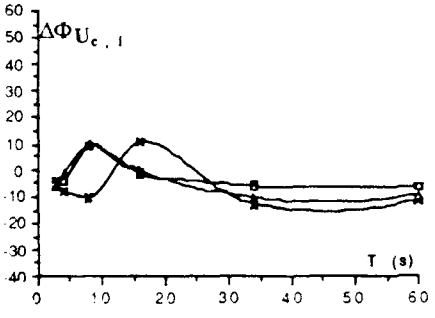

Figure 10. Phase shift of centerline velocity oscillation with respect to station 1 vs focing period.

$\Delta\Phi_{Uc,1}=\Phi_{Uc,s1}-\Phi_{Uc,s1}$; $\theta=6.0°$.

a) $(a_{uc})_0=0.10$; **b) 0.20; c) 0.40**

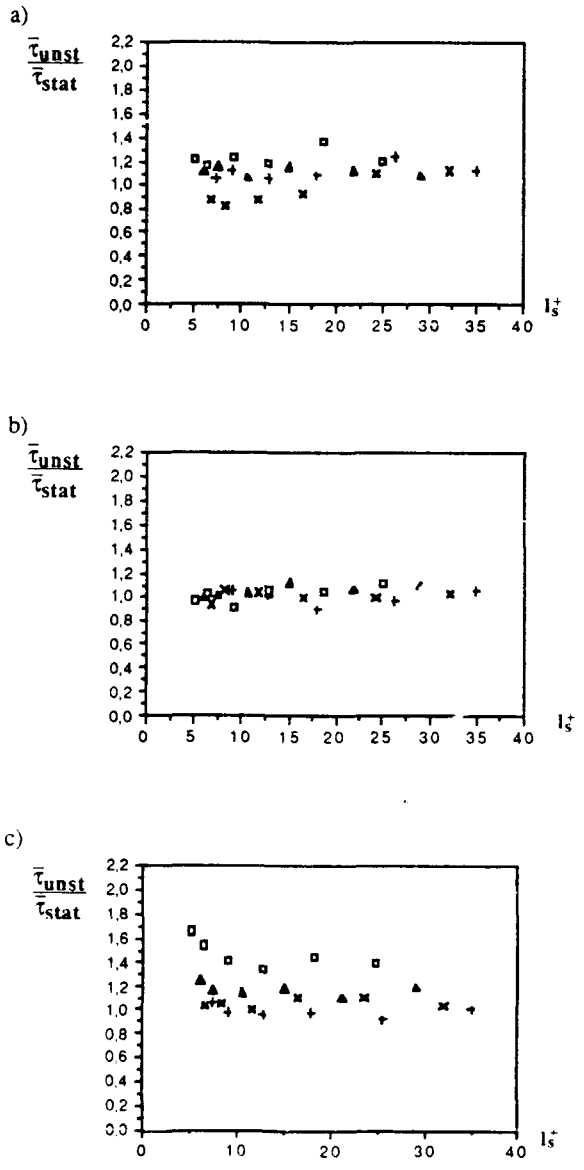

Figure 11. Ratio of unsteady/ steady time-mean wall shear stress vs l_s^+. θ=2.4°.
+ : station 1; × : station 2; ▲ : station 3; □ : station 4.
a) $(a_{uc})_o$=0.10; b) 0.20; c) 0.40

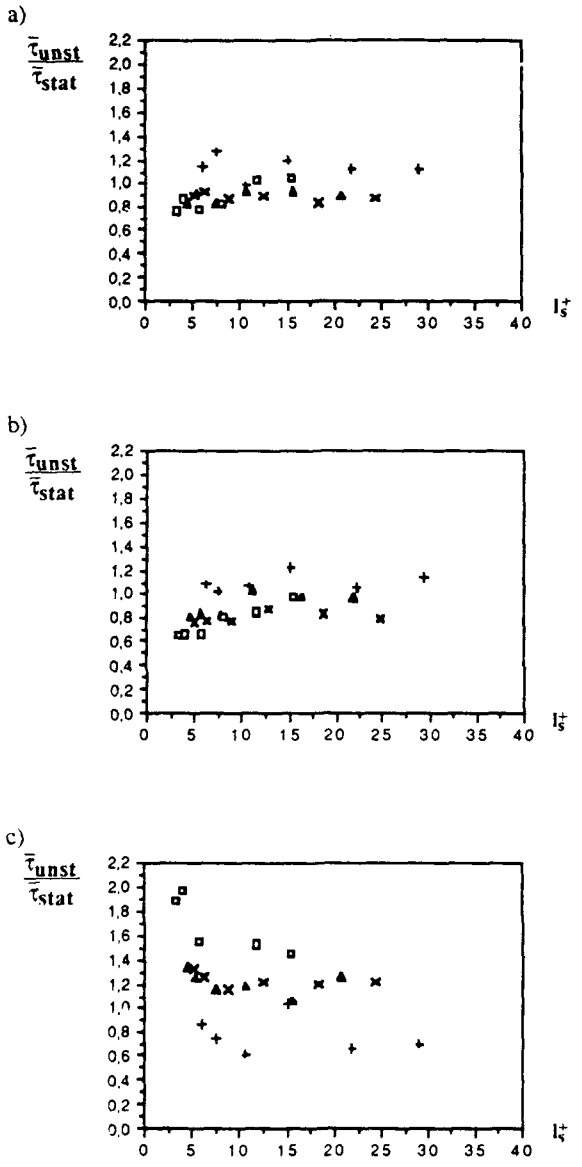

Figure 12. Ratio of unsteady/ steady time-mean wall shear stress vs l_s^+. $\theta=6.^\circ$.
+ : station 1; × : station 2; ▲ : station 3; □ : station 4.
a) $(a_{uc})_o=0.10$; b) 0.20; c) 0.40

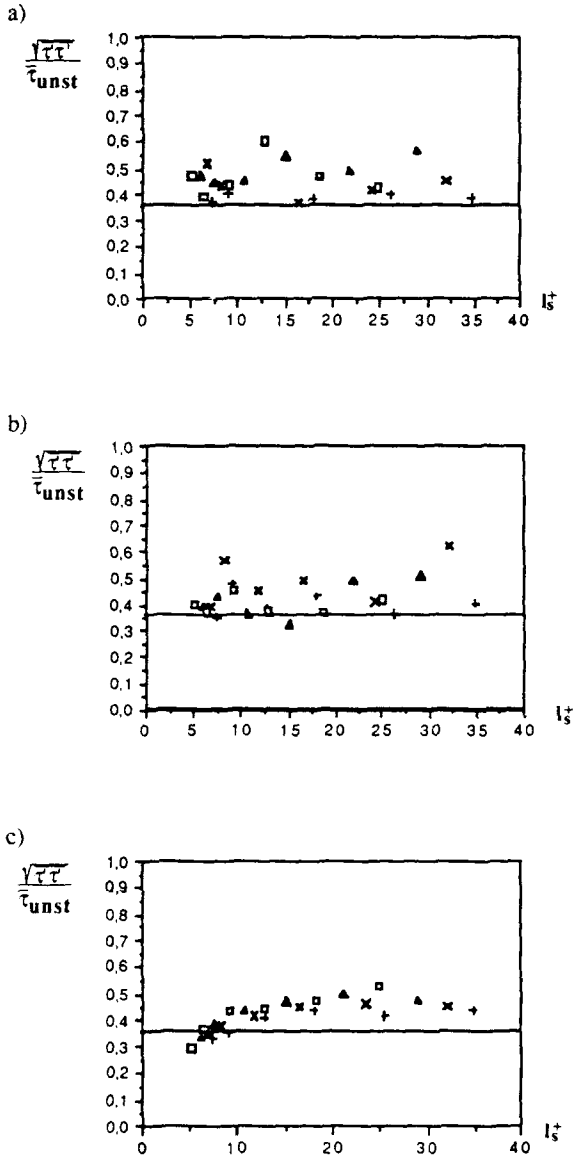

Figure 13.Time mean turbulent intensity of the wall shear stress vs l_s^+. θ=2.4°.

+ : station 1; × : station 2; ▲ : station 3; □ : station 4.

a) $(a_{uc})_o$=0.10; b) 0.20; c) 0.40

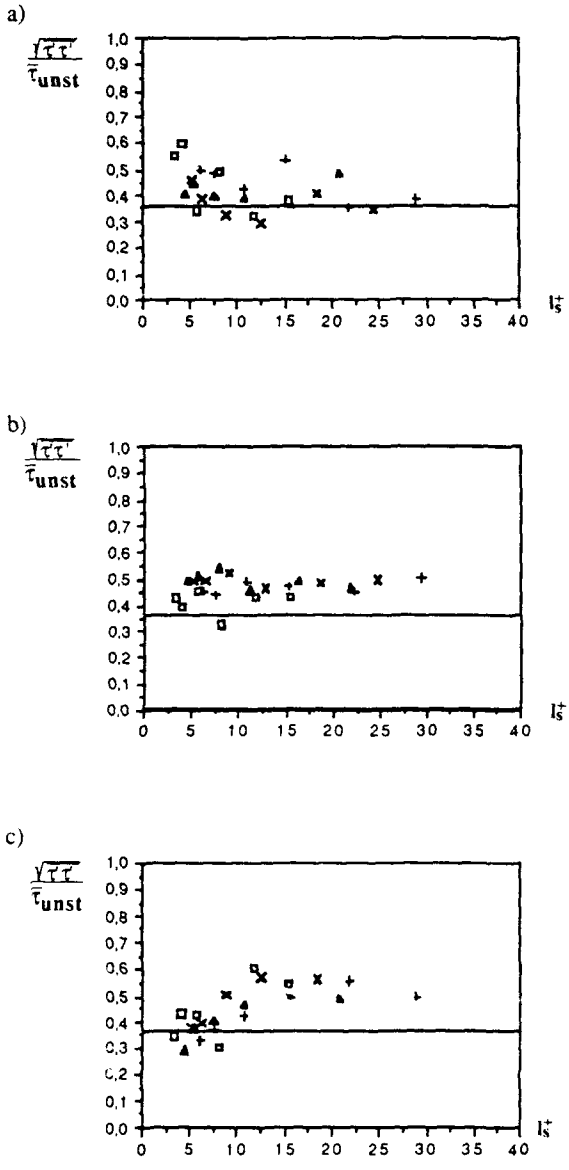

Figure 14.Time mean turbulent intensity of the wall shear stress vs l_s^+. θ=6.0°.

+ : station 1; × : station 2; ▲ : station 3; □ : station 4.

a) $(a_{uc})_0$=0.10; b) 0.20; c) 0.40

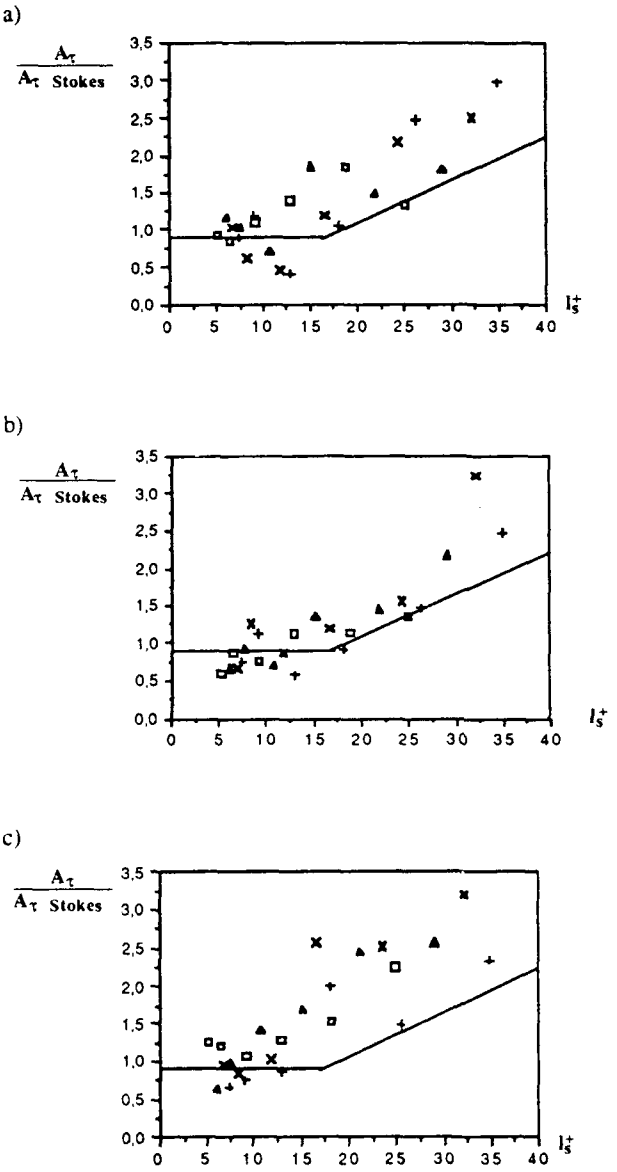

Figure 15.Amplitude of the wall shear-stress with respect to the Stokes value vs l_s^+.θ=2.4°.
+ : station 1; × : station 2; ▲ : station 3; □ : station 4.
a) $(a_{uc})_o$=0.10; b) 0.20; c) 0.40

a)

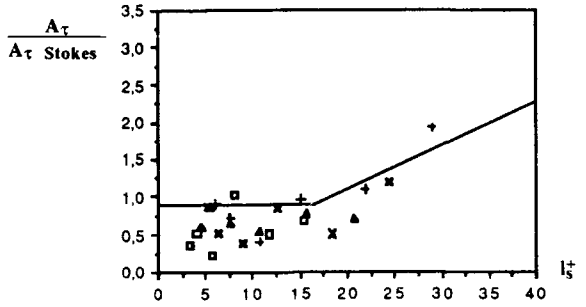

b)

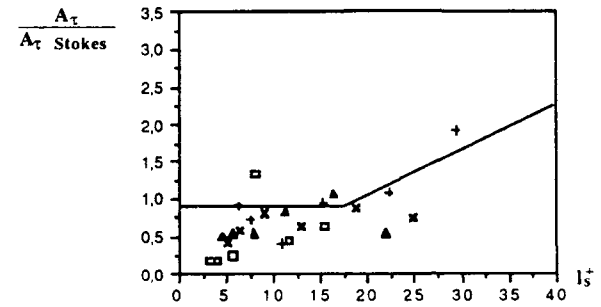

c)

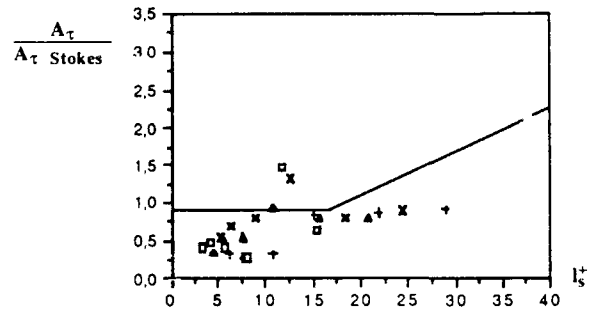

Figure 16.Amplitude of the wall shear-stress with respect to the Stokes value vs l_s^+. $\theta=6.0°$.
+ : station 1; × : station 2; ▲ : station 3; □ : station 4.
a) $(a_{uc})_0=0.10$; b) 0.20; c) 0.40

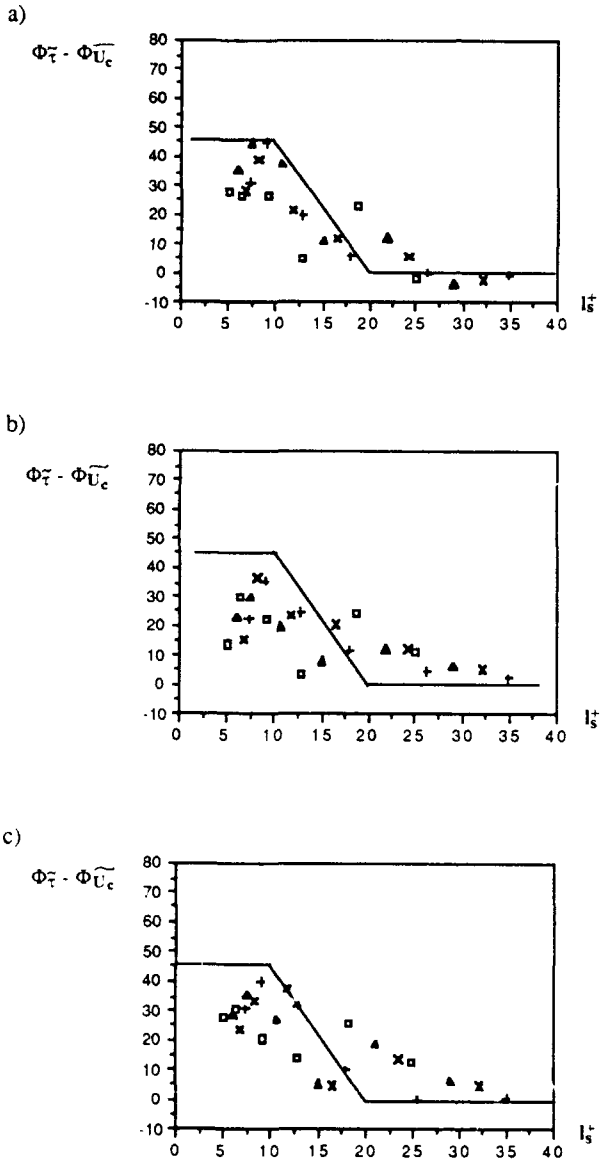

Figure 17. Phase shift of wall shear-stress oscillation with respect to centerline velocity oscillation. $\theta=2.4°$.

+ : station 1; × : station 2; ▲ : station 3; □ : station 4.

a) $(a_{uc})_o=0.10$; b) 0.20; c) 0.40

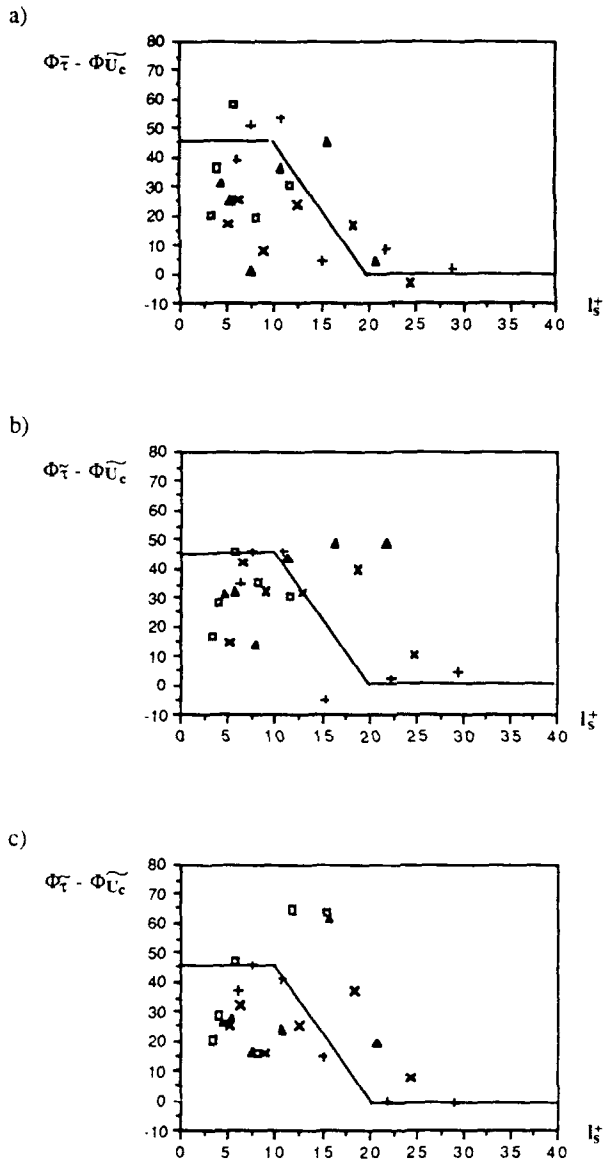

Figure 18. Phase shift of wall shear-stress oscillation with respect to centerline velocity oscillation. $\theta=6.0°$.
+ : station 1; × : station 2; ▲ : station 3; □ : station 4.
a) $(a_{uc})_o=0.10$; b) 0.20; c) 0.40

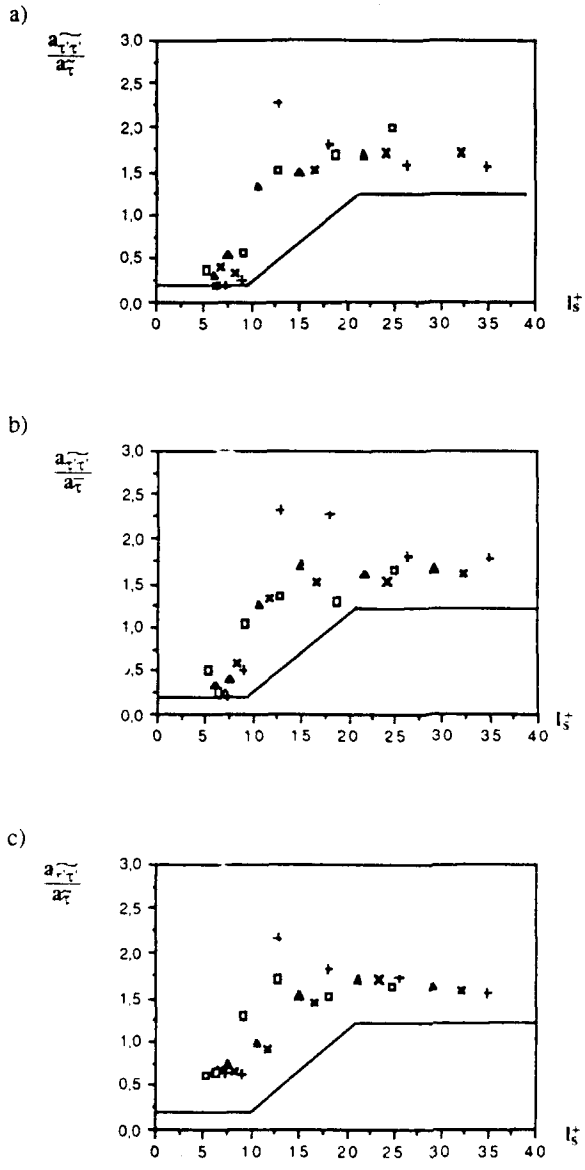

Figure 19. Relative amplitude of the modulation of the turbulent fluctuation intensity referred to the relative amplitude of the oscillation of the wall shear stress vs l_s^+. θ=2.4°.
+ : station 1; × : station 2; ▲ : station 3; □ : station 4.
a) $(a_{uc})_o$=0.10; b) 0.20; c) 0.40

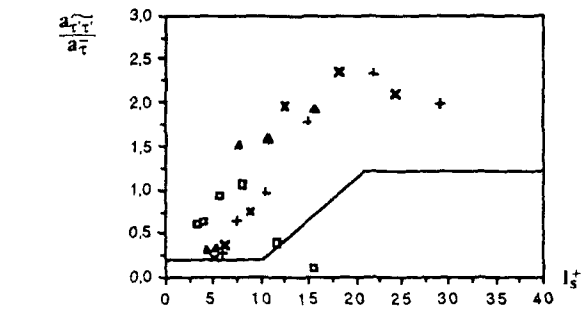

b)

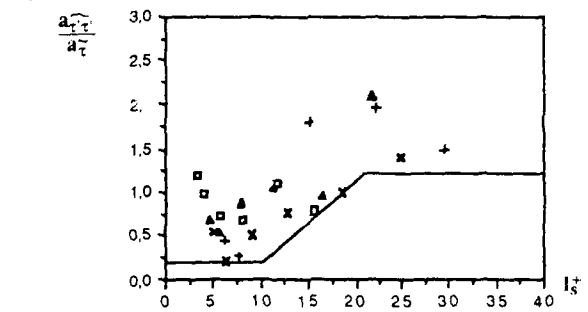

c)

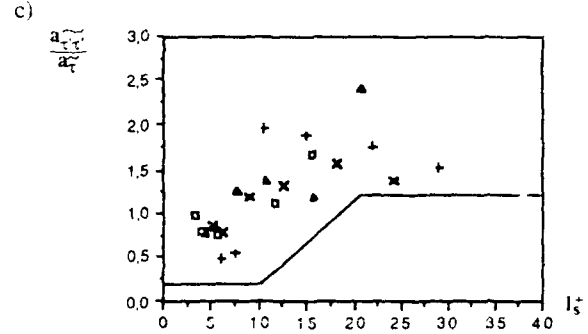

Figure 20. Relative amplitude of the modulation of the turbulent fluctuation intensity referred to the relative amplitude of the oscillation of the wall shear stress vs l_s^+. θ=6.0°.
+ : station 1; × : station 2; ▲ : station 3; □ : station 4.
a) $(a_{uc})_o$=0.10; b) 0.20; c) 0.40

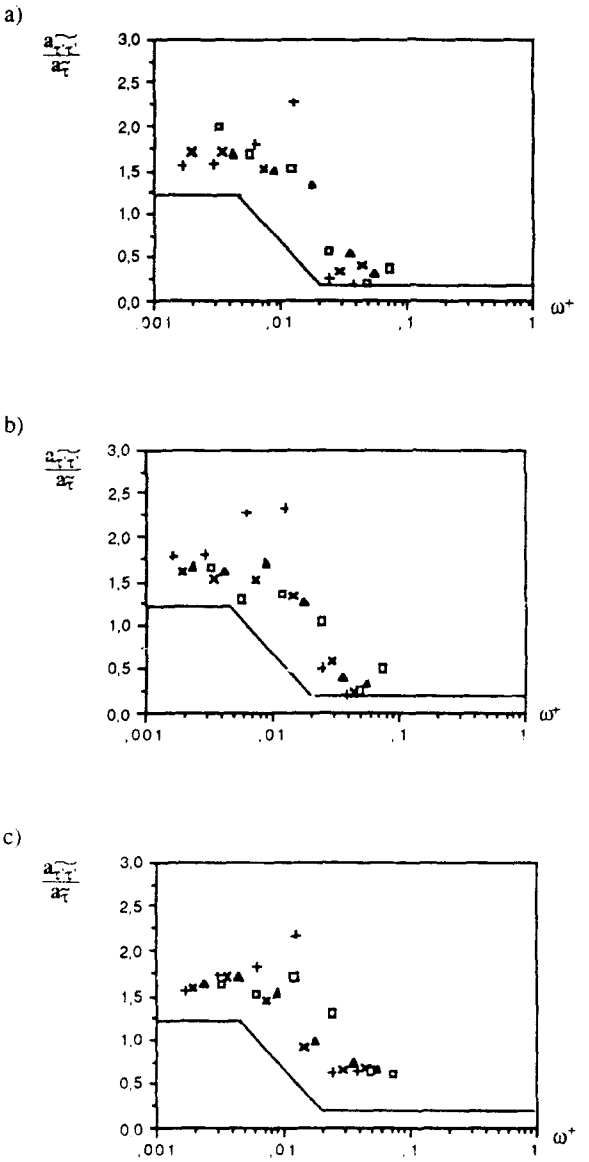

Figure 21. Relative amplitude of the modulation of the turbulent fluctuation intensity referred to the relative amplitude of the oscillation of the wall shear stress vs ω^+. $\theta=2.4°$.
+ : station 1; × : station 2; ▲ : station 3; □ : station 4.
a) $(a_{uc})_0=0.10$; b) 0.20; c) 0.40

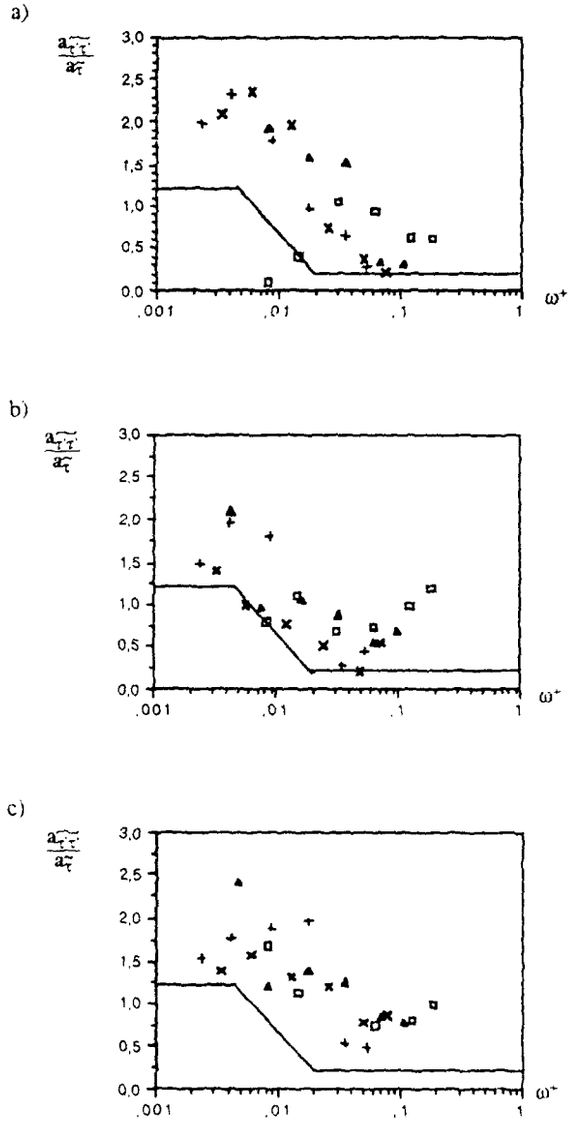

Figure 22. Relative amplitude of the modulation of the turbulent fluctuation intensity referred to the relative amplitude of the oscillation of the wall shear stress vs ω^+. θ=6.0°.
+ : station 1; × : station 2; ▲ : station 3; □ : station 4.
a) $(a_{uc})_0$=0.10; b) 0.20; c) 0.40

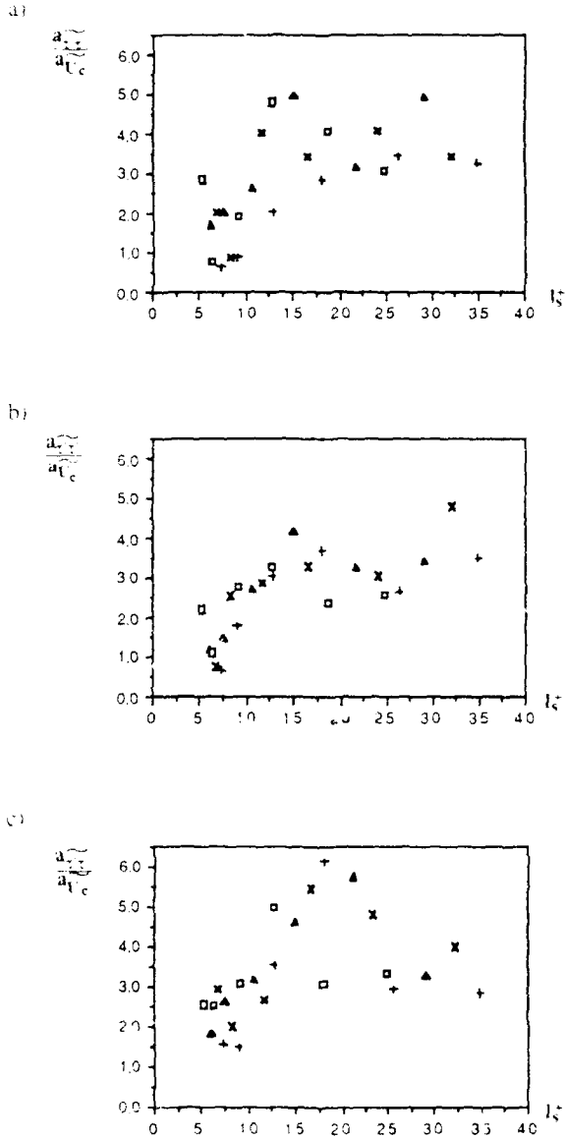

Figure 23.Relative amplitude of turbulent wall shear stress fluctuation modulation referred to the relative amplitude of velocity oscillation in the centerline vs $l_s^+ . \theta = 2.4°$.
+ : station 1; × : station 2; ▲ : station 3; □ : station 4.
a) $(a_{uc})_o = 0.10$; b) 0.20; c) 0.40

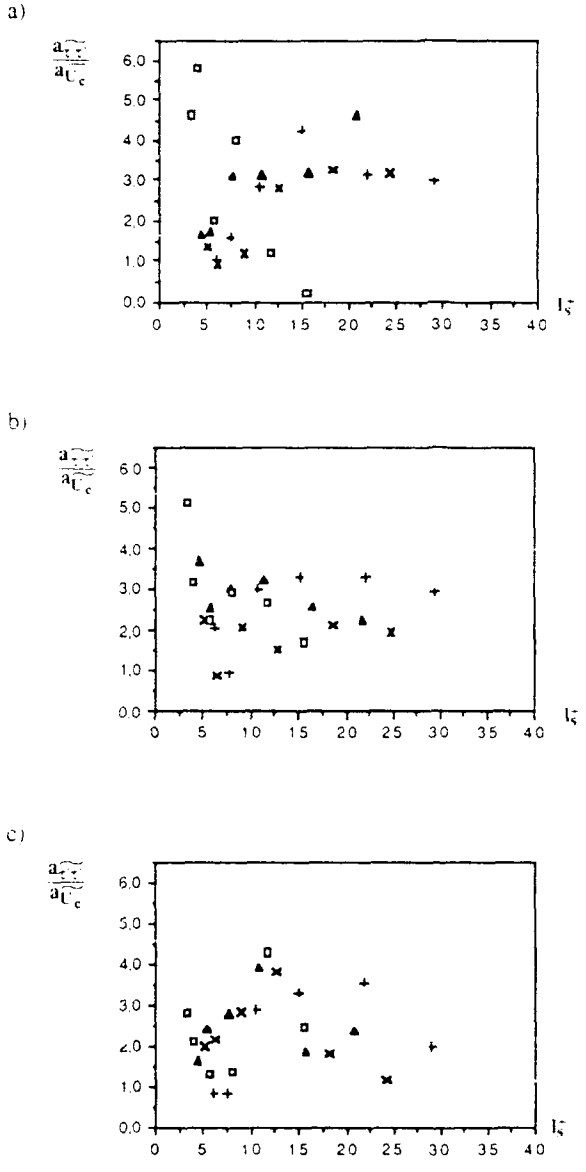

Figure 24.Relative amplitude of turbulent wall shear stress fluctuation modulation referred to the relative amplitude of velocity oscillation in the centerline vs l_s^+. θ=6.0.
+ : station 1; × : station 2; ▲ : station 3; □ : station 4.
a) $(a_{uc})_o$=0.10; b) 0.20; c) 0.40

a)

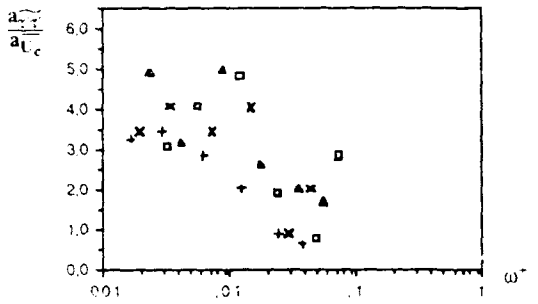

b)

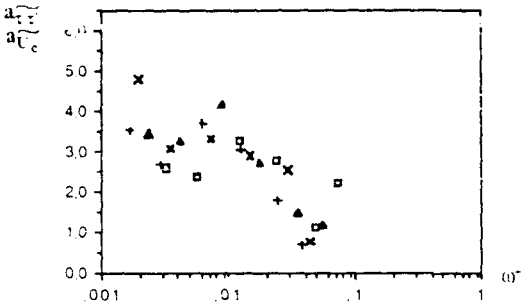

c)

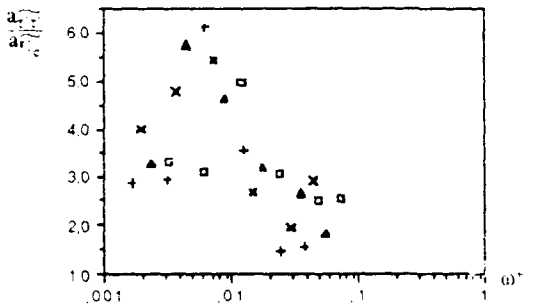

Figure 25.Relative amplitude of turbulent wall shear stress fluctuation modulation referred to the relative amplitude of velocity oscillation in the centerline vs ω^+. θ=2.4°.
+ : station 1; × : station 2; ▲ : station 3; □ : station 4.
a) $(a_{uc})_o$=0.10; b) 0.20; c) 0.40

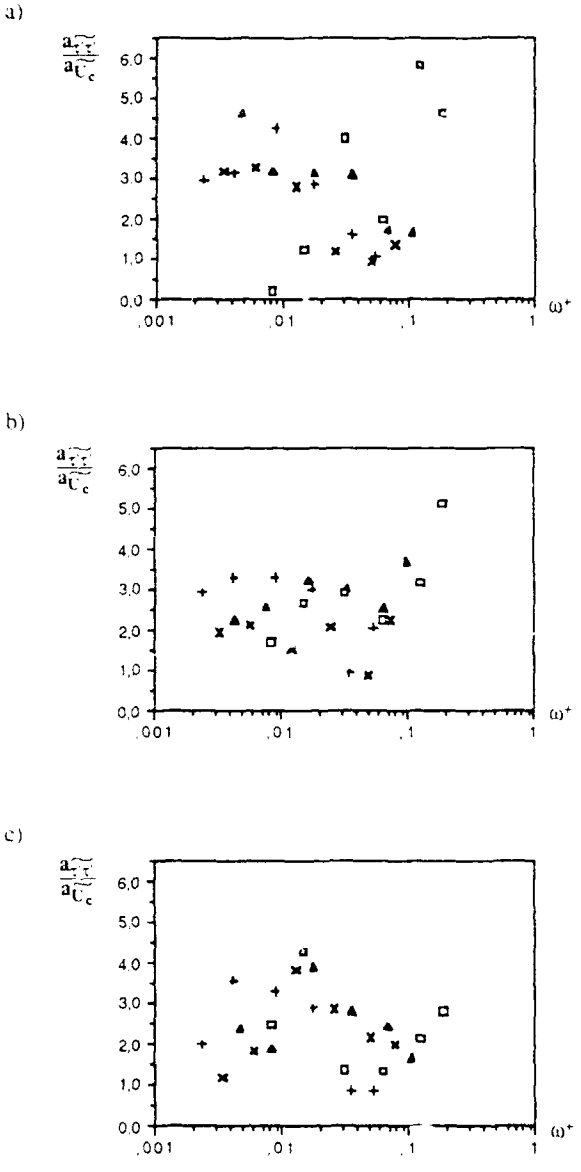

Figure 26. Relative amplitude of turbulent wall shear stress fluctuation modulation referred to the relative amplitude of velocity oscillation in the centerline vs ω^+. $\theta=6.0°$.
+ : station 1; × : station 2; ▲ : station 3; □ : station 4.
a) $(a_{uc})_o=0.10$; b) 0.20; c) 0.40